FATIGUE BEHAVIOUR OF COLD-FORMED STEEL

SECTIONS IN TRANSMISSION TOWERS

By

Sherif Kamal Hassan

A Thesis

Submitted to the Faculty of Graduate Studies

in Partial Fulfillment of the Requirements

for the Degree of

Doctor of Philosophy

Department of Civil and Geological Engineering

The University of Manitoba

Winnipeg, Manitoba, Canada, January 1995

Canada

Name _____

Dissertation Abstracts International is arranged by broad, general subject categories. Please select the one subject which most nearly describes the content of your dissertation. Enter the corresponding four-digit code in the spaces provided.

Civil Engineering
SUBJECT TERM

0 5 4 3
SUBJECT CODE

U·M·I

Subject Categories

THE HUMANITIES AND SOCIAL SCIENCES

COMMUNICATIONS AND THE ARTS
Architecture	0729
Art History	0377
Cinema	0900
Dance	0378
Fine Arts	0357
Information Science	0723
Journalism	0391
Library Science	0399
Mass Communications	0708
Music	0413
Speech Communication	0459
Theater	0465

EDUCATION
General	0515
Administration	0514
Adult and Continuing	0516
Agricultural	0517
Art	0273
Bilingual and Multicultural	0282
Business	0688
Community College	0275
Curriculum and Instruction	0727
Early Childhood	0518
Elementary	0524
Finance	0277
Guidance and Counseling	0519
Health	0680
Higher	0745
History of	0520
Home Economics	0278
Industrial	0521
Language and Literature	0279
Mathematics	0280
Music	0522
Philosophy of	0998
Physical	0523

Psychology	0525
Reading	0535
Religious	0527
Sciences	0714
Secondary	0533
Social Sciences	0534
Sociology of	0340
Special	0529
Teacher Training	0530
Technology	0710
Tests and Measurements	0288
Vocational	0747

LANGUAGE, LITERATURE AND LINGUISTICS
Language	
General	0679
Ancient	0289
Linguistics	0290
Modern	0291
Literature	
General	0401
Classical	0294
Comparative	0295
Medieval	0297
Modern	0298
African	0316
American	0591
Asian	0305
Canadian (English)	0352
Canadian (French)	0355
English	0593
Germanic	0311
Latin American	0312
Middle Eastern	0315
Romance	0313
Slavic and East European	0314

PHILOSOPHY, RELIGION AND THEOLOGY
Philosophy	0422
Religion	
General	0318
Biblical Studies	0321
Clergy	0319
History of	0320
Philosophy of	0322
Theology	0469

SOCIAL SCIENCES
American Studies	0323
Anthropology	
Archaeology	0324
Cultural	0326
Physical	0327
Business Administration	
General	0310
Accounting	0272
Banking	0770
Management	0454
Marketing	0338
Canadian Studies	0385
Economics	
General	0501
Agricultural	0503
Commerce-Business	0505
Finance	0508
History	0509
Labor	0510
Theory	0511
Folklore	0358
Geography	0366
Gerontology	0351
History	
General	0578

Ancient	0579
Medieval	0581
Modern	0582
Black	0328
African	0331
Asia, Australia and Oceania	0332
Canadian	0334
European	0335
Latin American	0336
Middle Eastern	0333
United States	0337
History of Science	0585
Law	0398
Political Science	
General	0615
International Law and Relations	0616
Public Administration	0617
Recreation	0814
Social Work	0452
Sociology	
General	0626
Criminology and Penology	0627
Demography	0938
Ethnic and Racial Studies	0631
Individual and Family Studies	0628
Industrial and Labor Relations	0629
Public and Social Welfare	0630
Social Structure and Development	0700
Theory and Methods	0344
Transportation	0709
Urban and Regional Planning	0999
Women's Studies	0453

THE SCIENCES AND ENGINEERING

BIOLOGICAL SCIENCES
Agriculture	
General	0473
Agronomy	0285
Animal Culture and Nutrition	0475
Animal Pathology	0476
Food Science and Technology	0359
Forestry and Wildlife	0478
Plant Culture	0479
Plant Pathology	0480
Plant Physiology	0817
Range Management	0777
Wood Technology	0746
Biology	
General	0306
Anatomy	0287
Biostatistics	0308
Botany	0309
Cell	0379
Ecology	0329
Entomology	0353
Genetics	0369
Limnology	0793
Microbiology	0410
Molecular	0307
Neuroscience	0317
Oceanography	0416
Physiology	0433
Radiation	0821
Veterinary Science	0778
Zoology	0472
Biophysics	
General	0786
Medical	0760

EARTH SCIENCES
Biogeochemistry	0425
Geochemistry	0996

Geodesy	0370
Geology	0372
Geophysics	0373
Hydrology	0388
Mineralogy	0411
Paleobotany	0345
Paleoecology	0426
Paleontology	0418
Paleozoology	0985
Palynology	0427
Physical Geography	0368
Physical Oceanography	0415

HEALTH AND ENVIRONMENTAL SCIENCES
Environmental Sciences	0768
Health Sciences	
General	0566
Audiology	0300
Chemotherapy	0992
Dentistry	0567
Education	0350
Hospital Management	0769
Human Development	0758
Immunology	0982
Medicine and Surgery	0564
Mental Health	0347
Nursing	0569
Nutrition	0570
Obstetrics and Gynecology	0380
Occupational Health and Therapy	0354
Ophthalmology	0381
Pathology	0571
Pharmacology	0419
Pharmacy	0572
Physical Therapy	0382
Public Health	0573
Radiology	0574
Recreation	0575

Speech Pathology	0460
Toxicology	0383
Home Economics	0386

PHYSICAL SCIENCES
Pure Sciences
Chemistry	
General	0485
Agricultural	0749
Analytical	0486
Biochemistry	0487
Inorganic	0488
Nuclear	0738
Organic	0490
Pharmaceutical	0491
Physical	0494
Polymer	0495
Radiation	0754
Mathematics	0405
Physics	
General	0605
Acoustics	0986
Astronomy and Astrophysics	0606
Atmospheric Science	0608
Atomic	0748
Electronics and Electricity	0607
Elementary Particles and High Energy	0798
Fluid and Plasma	0759
Molecular	0609
Nuclear	0610
Optics	0752
Radiation	0756
Solid State	0611
Statistics	0463

Applied Sciences
Applied Mechanics	0346
Computer Science	0984

Engineering	
General	0537
Aerospace	0538
Agricultural	0539
Automotive	0540
Biomedical	0541
Chemical	0542
Civil	0543
Electronics and Electrical	0544
Heat and Thermodynamics	0348
Hydraulic	0545
Industrial	0546
Marine	0547
Materials Science	0794
Mechanical	0548
Metallurgy	0743
Mining	0551
Nuclear	0552
Packaging	0549
Petroleum	0765
Sanitary and Municipal	0554
System Science	0790
Geotechnology	0428
Operations Research	0796
Plastics Technology	0795
Textile Technology	0994

PSYCHOLOGY
General	0621
Behavioral	0384
Clinical	0622
Developmental	0620
Experimental	0623
Industrial	0624
Personality	0625
Physiological	0989
Psychobiology	0349
Psychometrics	0632
Social	0451

FATIGURE BEHAVIOUR OF COLD-FORMED STEEL SECTIONS

IN TRANSMISSION TOWERS

BY

SHERIF KAMAL HASSAN

A Thesis submitted to the Faculty of Graduate Studies of the University of Manitoba in partial fulfillment of the requirements of the degree of

DOCTOR OF PHILOSOPHY

© 1995

I hereby declare that I am the sole author of this thesis.

I authorize the University of Manitoba to lend this thesis to other institutions or individuals for the purpose of scholarly research.

Abstract

In the expected life span of a transmission tower, the members are subjected to a large number of alternating wind applications. Fatigue behaviour due to repeated loading must therefore be considered in design. This study presents the fatigue-test results of 52 cold-formed steel members. The experimental program involved the use of five cross sectional shapes, two test temperatures (-50°C and 25°C), and two different steel types, ASTM A715 grade 60 steel, and CAN/CSA-G40.21-M 300W. A series of constant amplitude axial fatigue load tests were conducted for each cross sectional shape under a loading frequency that ranged from 1 Hz to 2.5 Hz. All specimens were supported at the ends through bolted connections and were tested under load-controlled condition with a load ratio equal to -1 (fully reversed cycle). Cyclic stress-strain behaviour was monitored at different stages of the test until failure. A group of S-N and Load-N curves were developed for the purpose of determining the safe endurance limit. For each test series, a log-log linear relationship between the stress range and the number of cycles was given. Moreover, similar relationships were defined for the alternating fatigue loads and the total fatigue life for different cross sectional shapes, temperatures, and type of steel involved in the study. The results obtained could be used to establish guidelines for fatigue design of cold-formed steel sections.

A finite element model was designed to simulate adequately the behaviour of

90°-angle sections connected through one leg. Both geometric and material non-linearities were incorporated in the analytical problem. The computed strains and translations were found to be in good agreement with those recorded in the experimental program. In addition, stress concentration factors determined from the finite element analysis were used to obtain fatigue life estimates based on Palmgren-Miner's rule for cumulative damage.

Acknowledgments

The author wishes to express his deepest appreciation and gratitude to his advisor, Dr. Dimos Polyzois, for his continuous guidance and support at all stages of the research investigation. The author is also grateful to his committee members, Drs. Glenn Morris and Sami Rizkalla, Professors in the Department of Civil and Geological Engineering and Dr. Kadar Tandon, professor in the Department of Mechanical and Industrial Engineering at The University of Manitoba, as well as Dr. Murty Madugula, professor in the Department of Civil and Environmental Engineering, University of Windsor, Ontario, for their guidance and insightful comments throughout the research work.

The assistance provided by the technical staff of the Structural Engineering and Construction Research and Development Facility, of the Department of Civil and Geological Engineering at The University of Manitoba throughout the experimental program is highly appreciated.

This research project was made possible through the financial support provided by the Canadian Electrical Association (CEA - Project No. 340 T 844), Manitoba Hydro, and the Natural Sciences and Engineering Research Council of Canada.

vi

TABLE OF CONTENTS

LIST OF TABLES

LIST OF FIGURES

xvii

LIST OF SYMBOLS

A   Gross cross sectional area.

a   Constant to provide a best fit line to the fatigue data.

b   Slope of the mean regression line of the fatigue data.

C_w Warping torsional constant.

D   Diameter of the end hole.

da/dN Fatigue crack growth rate.

E   Modulus of elasticity.

$\{F^a\}$ Vector of applied loads.

$\{F^{nr}\}$ Vector of restoring loads.

FS   Fatigue safety factor.

F_u Tensile strength.

F_y Yield strength.

I_x Moment of inertia about axis x-x.

I_y Moment of inertia about axis y-y.

J   St. Venant's torsion constant.

K_e Strain distribution factor used in the elastic-plasic fatigue calculations (ASME Boiler and Pressure Vessel Code , 1989).

K_f Fatigue notch factor.

K_I Stress intensity factor.

K_t Stress concentration factor.

$[K_T]$ Tangent stiffness matrix.

L   Total length of specimen.

LS   Number of load steps in a particular loading event.

l Unbraced length of the compression member.

$m,\ n^*$ Strain hardening exponents used in fatigue calculations

         (ASME Boiler and Pressure Vessel Code, 1989).

N   Number of cycles to failure   (total fatigue life).

N_{used} Specified number of repetitions for a particular loading event.

$N_{allowable}$ Number of allowable cycles calculated by the ANSYS

         finite element program for a given stress amplitude.

n   Number of data points in a statistical analysis.

P   Alternating fatigue load.

R   Load ratio $(R = P_{min}\ /\ P_{max})$.

r_1 Radius of gyration of the I-section (back-to-back

         channel section) about the axis perpendicular to the

         direction in which buckling would occur.

$r_{critical}$ Minimum radius of gyration.

r_{cy} Radius of gyration of one channel about its centroidal

         axis parallel to the web.

r_x	Radius of gyration with respect to axis x-x.
r_y	Radius of gyration with respect to axis y-y.
S_b	Standard deviation of the slope of the regression line.
S_e	Standard error of estimate in a statistical analysis.
S_{max}	Maximum permissible longitudinal spacing of the connectors joining the back-to-back channels.
t	Value obtained from a significance t-test in a statistical analysis.
x_i	The ith value of the independent variable x.
$\bar{x}$	Mean value of the independent variable x.
y_i	The ith value of the dependent variable $log\,N$.
$\bar{y}$	Mean value of the dependent variable $log\,N$.
$\hat{y}$	Value of $log\,N$ from the regression line.
X,Y,Z	Global coordinate system.
α	Chosen level of significance in a statistical analysis.
ΔK_I	Stress intensity factor range.
$\{\Delta u\}$	Nodal displacement increment vector.
δ	Percent elongation of the material (standard tension tests).
ϵ'_f	Fatigue ductility coefficient.
ϵ_i	Error term in a statistical analysis.

μ	Poisson's ratio.
$\sigma_1, \sigma_2, \sigma_3$	Principal stresses.
σ_a	Alternating stress amplitude.
σ_d	Design level stress.
σ_e	Endurance stress (fatigue limit stress).
σ_f	Average fatigue stress at failure.
σ_f'	Fatigue strength coefficient.
σ_I	Stress intensity.
$\{\sigma\}_i$	Stress vector for loading i.
$\{\sigma\}_j$	Stress vector for loading j.
$\sigma_{i,j}{}^a$	Alternating shear stress.
$\sigma_{i,j}{}^c$	Maximum alternating shear stress.
σ_m	Mean stress $\left(\sigma_m = \dfrac{\sigma_{max} + \sigma_{min}}{2}\right)$.
σ_r	Stress range $\left(\sigma_r = \sigma_{max} - \sigma_{min}\right)$.

CHAPTER 1

Introduction

1.1 General

Metal fatigue is a process which causes failure or damage of a component subjected to repeated loading. It is a complicated metallurgical process which is difficult to describe accurately and to model precisely on a microscopic level. Despite these complexities, fatigue damage assessment for design of components and structures must be performed. If a structure is subjected to cyclic or repeated loading, it may fracture at a stress level less than that required to cause failure under static conditions. Fatigue failures are characterized by the progressive growth of cracks initiated from micro-flaws, in areas of tensile stress. This crack growth may continue to develop until the member cross section is so reduced in area that a fracture occurs.

Fatigue failures can be classified into two main groups, namely, simple and compound. Simple failures result when fatigue starts from a single crack and propagates through the member. A compound fatigue failure occurs when the fatigue crack

originates from two or more locations and propagates through the member. The fatigue life of a structure is significantly influenced by a number of variables. These include the yield point of the material, the crystal structure, environmental effects, the presence of flaws, inclusions and residual stresses, detail type, and load effects such as: stress range, stress ratio, random or constant load cycling, and number of cycles of the applied load.

There are three methods of analysis for fatigue behaviour of metal structures. The first method is known as the stress-life approach. It is used mainly for long-life applications where stresses and strains are elastic. It does not distinguish between initiation and propagation stages of a crack growth, but deals with the total life, or the life to failure of a component. The second method is the strain-life approach which was developed in the 1960's. It is considered an initiation approach, and used mainly when the strain is no longer totally elastic, but has a plastic component. Low cycle fatigue lives generally occur under these conditions. An alternate method of predicting fatigue strength is through the use of linear elastic fracture mechanics (LEFM) principles which are adapted for cyclic loading. This method is used to predict propagation life from an initial crack or defect. If combined with the strain-life approach, it can predict the total fatigue life (i.e. initiation and propagation). All the previously mentioned methods require knowledge of material fatigue properties, flaw sizes, and stress distribution.

Depending on the type of application, fatigue design criteria can be classified into four types; infinite-life design, safe-life design, fail-safe design, and damage tolerant design (Fuchs and Stephens, 1980). The safe-life design is of great interest for civil engineering applications as it includes a margin of safety for the scatter of fatigue results and for other unknown factors. The margin of safety may be taken in terms of life or load, or by specifying that both margins must be satisfied. In general, fatigue testing for design verification is far more demanding than that for research purposes because it forces the engineer to make the test conditions representative of actual conditions of use. The prime requirements for a testing program are to simulate loading and environmental conditions encountered in service.

1.2 Statement of the problem

Tradionally, transmission towers have been constructed using hot rolled steel sections. However, due to recent advances in steel-making technology and the development of new design methods, a serious consideration of the use of cold-formed steel sections in transmission structures was observed. The first transmission tower built entirely from cold-formed members was designed by the SAE Research Center, Milan, Italy, in 1980. It was a self-supporting suspension tower for a 500-kV single circuit line. Since then, some significant advances in fabrication technolo-

3

gy have made the use of cold-formed steel not only feasible but also economical. Other transmission towers consisting of cold-formed steel members have been built in Sweden, Florida, and Texas (Madugula, 1990).

1.2.1 Advantages of cold-formed steel construction

Recently, there has been a noticeable increase in the use of cold-formed steel in the construction of transmission latticed towers. Thus, more slender and lighter towers are now being built utilizing a wide range of sections. The development of such towers became possible through improved understanding of the behaviour of cold-formed steel and the introduction of reliable design standards and specifications. Other factors that have contributed to the increased popularity of cold-formed steel as a construction material in transmission tower structures are as follows:

1. High strength-to-weight ratio.

2. Ease of fabrication: beside the traditional angle shape, other optimal shapes such as the 60°-angles, lipped angles, lipped channels, hat, and T-shaped sections can be easily fabricated.

3. Ease of transportation and erection.

4. Cold-formed shapes usually have higher radii of gyration than hot rolled sections with equivalent cross sectional area, therefore, they can be used with

longer unsupported length. This results in a reduction of the number of members used in a transmission tower.

5. Improvement in the quality of material as a result of the developments in the automation of manufacturing machines due to increased productivity.

1.2.2 Fabrication of cold-formed steel sections

There are two different fabrication methods for cold-formed sections. Roll forming and press braking. In the first method the steel sheet passes through successive rolls until the desired shape is obtained. The shapes are afterwards cut to the required lengths. This method has the advantage of fast production rates but requires large capital investment. In the press braking method, the required shape is produced by feeding the steel sheet with the specified length into a press brake and making one bend at a time. This method offers fast setups and low-cost tooling yet the production rates are not high (Madugula, 1990).

1.2.3 Cold-formed steel and transmission towers

The first systematic research work in the area of cold-formed steel was sponsored by the American Iron and Steel Institute (AISI) at Cornell University under the supervision of Professor G.Winter. This work formed the basis for the first cold-formed steel specification in 1946. Since then, this specification has been revised five times, the 1993 edition being the latest. The Canadian Standard Associ-

5

ation CAN/CSA-S136-M94 (1995), "Cold formed Steel Structural Members", is the corresponding standard in Canada. In 1971 the American Society of Civil Engineers (ASCE) published the *Guide for Design of Steel Transmission Towers*, "Manuals and Reports on Engineering Practice-No.52". This Manual was developed to serve as a uniform basis for the structural design of self-supporting steel transmission towers. Manual 52 has been used extensively in the United States and abroad as the basis for design specifications. An updated edition of Manual 52 (ANSI/ASCE 10-90, 1992) was introduced to reflect new design procedures, availability of new shapes and materials, changes in loading criteria, and results of new test data. In dealing with loads on a transmission tower, the Canadian Standard Association CAN/CSA-S37-M94 (1995), "Antennas, Towers, and Antenna-Supporting Structures", is the first edition to use full limit states design procedures.

The economic advantages resulting from the use of cold-formed steel for the construction of transmission towers prompted Vattenfall, the Swedish State Power Board, to adopt a new design for the construction of a 420-kV network. This involved T-towers built entirely of cold-formed steel. Vatenfall conducted a comprehensive review of traditional types of transmission towers and compared the cost of these towers with the new proposed T-type tower (Gidlund et al. 1988). The results indicated that, for spans longer than 200 m limit of wooden pole structures, the most economical design is the guyed T-type tower with the legs formed to a V.

6

Moreover, the investigation included a cost comparison between an M-type tower designed according to traditional methods and a T-type tower utilizing cold-formed steel. The latter employed 60° cold-formed angles for which there is no hot rolled equivalent. It required 770 bolts, compared to 2,500 bolts used in the M-type tower. As a result, The Swedish State Power Board decided to adopt the T-tower design as a standard for future extensions, and for the reconstruction of the 420-kV network. The first line, 220 km long, was completed in 1989. However, the second stage is to be completed in 1996.

A similar study was conducted by the American Electric Power Research Institute (Catenacci et al. 1989), where four tower types were analyzed and designed using cold-formed steel. It was concluded that the use of cold-formed sections resulted in weight savings of 3-11%, a reduction in the number of members of 31-55%, and savings in bolts of 17-18%.

1.3   Overview of the Research Investigation

1.3.1   Background

The economic considerations of using cold-formed steel in transmission towers, have not always been unchallenged. In 1963, Manitoba Hydro built 282 towers for the

138-kV line between Kelsey and Thompson in Northern Manitoba. Recent inspection of the towers revealed that many members were badly buckled, cracked or bowed. These observations prompted Manitoba Hydro to sponsor two experimental research projects, at The University of Manitoba, to gain an improved understanding of the behaviour of cold-formed angles used in transmission towers.

The first project involved the testing of 10 galvanized and 10 ungalvanized cold-formed angles at temperatures ranging from -40°C to 24°C (Serrette et al. 1987). Two lengths were chosen, 800 mm and 2000 mm, in order to evaluate the performance of the angles in the elastic and inelastic ranges. The angles were $55 \times 55 \times 4$ mm.

The second project involved the testing of 20 cold-formed angles similar in size to those tested in Phase 1 except that all angles were 800 mm long (Polyzois et al. 1990). The specific objectives were to study the influence of temperature, cold work, and galvanization on the mechanical properties of the material. All tested specimens had a slenderness ratio of approximately 70. Moreover, equal numbers of galvanized and ungalvanized angles were tested at various temperatures ranging from -45°C to 25°C. The mechanical properties were obtained through 48 standard tension coupon tests conducted over the same temperature range.

The load was applied through gusset plates attached directly to one of the legs of the angles with a single bolt. This support configuration simulates closely the type of connection used by Manitoba Hydro in prototype structures.

Based on the results obtained from the work conducted at The University of Manitoba, a number of questions were raised regarding the structural performance of cold-formed members with shapes other than those used in the investigation. In addition, points that required further studies included, the effect of galvanization and subfreezing temperatures on the mechanical properties of the material, the fatigue behaviour of the cold-formed steel sections, the level and distribution of residual stresses in galvanized sections, and the effect of various types of corrosion coatings on the strength of the cold-formed steel members.

1.3.2   Overall experimental investigation

Studying the fatigue behaviour of cold-formed steel sections was one part of a comprehensive research investigation conducted at The University of Manitoba over the last two years. The prime objective of the overall research program was to develop a guide covering the design and fabrication of cold-formed steel sections used for the construction of transmission tower structures. The objective was accomplished through a comprehensive experimental program which involved:

- Material properties tests.

- Static compression tests.

- Tests to determine residual stresses.

- Fatigue tests.

Test variables included in the overall research investigation are summarized in Table 1.1. These included five cross-sectional shapes, two steel materials ASTM A715 Grade 60 steel of Italy, and CAN/CSA-G40.21-M 300W steel fabricated in Canada. The specimens were tested at temperatures ranging from -50°C to room temperature ($\simeq 25°C$).

In addition to the experimental program, two exploratory studies were conducted. The first study investigated the protective coating effects on the mechanical properties of cold-formed steel. The second study was concerned with a cost-effectiveness comparison of different corrosion resistance coating methods. A brief description of the work conducted in each of the previously mentioned tasks will be given in the following sections.

1.3.2.1 Material Properties Tests

A proper evaluation of the mechanical properties of the material is essential in understanding its behaviour. As such, the effect of galvanization, temperature, and

cold-forming on the mechanical properties of the steel material types involved were examined. As a part of the overall project, three types of material properties tests were conducted by Abdel-Rahim and Polyzois (1994). These included, standard tension coupon tests, semi-guided bend test for formability, and impact tests to determine the fracture toughness of the two steel types. A short description of each type is given below.

- **Standard tension coupon tests**

A series of 144 standard tension coupons cut from steel members type ASTM A715 Grade 60, and another series of 48 standard tension coupons cut from steel members type CAN/CSA-G40.21-M 300W, were tested. Coupons cut from flat and curved portions of both galvanized and ungalvanized members were tested at various temperatures ranging from -50°C to room temperature ($\simeq$ 25°C).

Typical stress-strain curves for coupons cut from the 90°-angle section of steel type ASTM A715 Grade 60, are shown in Figures 1.1 and 1.2 for tests performed at room temperature, and -50°C respectively. A summary of the mechanical properties is presented in Table 1.2 for steel type ASTM A715 Grade 60, and in Table 1.3 for steel type CAN/CSA-G40.21-M 300W. In general, the results indicated that the hot-dip galvanization process, as well as the cold-forming process, and subfreezing temperatures significantly increased the yield and tensile strengths, as well as

11

the modulus of elasticity, but caused a reduction in the ductility of the materials. Tables 1.4, and 1.5 summarize these effects for the two steel types involved in the study.

- ## Semi-guided bend tests

Semi-guided bend tests were used to evaluate the formability of the materials as evidenced by their ability to resist cracking during bending. Formability can be expressed by the minimum bend radius, and is affected by the thickness of the specimen and the width-to-thickness ratio.

Bend tests were conducted on 13 specimens cut from flat portions of ungalvanized members of the two types of steel. Tests were performed according to ASTM Standard (ASTM E 290-87 1987). Test specimens were simply supported at the ends using roller bearings as shown in Figure 1.3. The load was applied at the mid-span till 5 mm deflection was reached. A vice was then used to bend the specimen to 180° as shown in Figure 1.4. The convex side of each specimen was examined during and after testing. Test results showed that both steel types were ductile enough to bend to 180° without any noticeable cracking.

- ## Cold temperature fracture toughness tests

Charpy V-notch impact tests were performed on 28 subsized specimens cut from

the two types of steel members. The tests were conducted according to ASTM Standard (ASTM E 23-91 1991). Specimens were tested in various temperature levels ranging from -70°C to room temperature. Test results indicated that the low temperature had almost no effect on the absorbed energy of both galvanized and ungalvanized specimens. In addition, both steel types were observed to be ductile in the specified temperature range as illustrated in Figure 1.5.

1.3.2.2 Static Compression Tests

A series of tests to determine the resistance of galvanized cold-formed steel sections subjected to static compressive loading to failure was carried out by Odaisky (1994). In total, 189 tests were conducted using the parametric variations shown in Table 1.1. Test results are summarized in Table 1.6.

The specimens were tested in temperature-controlled chambers designed and built in the Structural Engineering and Construction Research and Development Facility of The University of Manitoba. The results were compared to ultimate loads obtained from Canadian Standards and American Specifications as well as the European Convention Constructional Steelwork (ECCS, 1985) Recommendations for Angles in Lattice Transmission Towers.

13

In general, the design methods used in evaluating the ultimate compressive capacity of the sections provided acceptable results and appeared to be generally adequate for design of cold-formed sections in transmission towers.

1.3.2.3 Tests to determine residual stresses

In cold-formed steel sections, residual stresses are developed during the forming process. The presence of these stresses in structural members could be detrimental or beneficial, depending on the magnitude, sign, and distribution of the stresses with respect to the load-induced stresses. Therefore, the design of such members requires knowledge of the residual stresses. Previous studies on hot rolled shapes (Yang et al. 1952, Huber and Beedle, 1954, and Tebedge et al. 1973), showed that the magnitude of the maximum residual stress was approximately 30% of the yield stress of the material, and was assumed to be uniformly distributed through the plate thickness.

A study for determining the magnitude and distribution of surface and subsurface residual stresses in cold-formed steel sections for the present investigation, was conducted at the Metals Technology Laboratories (MTL), of the Canada Center for Mineral and Energy Technology (CANMET) in Ottawa by Roy et al. (1994). This study formed an important part of the comprehensive experimental program conducted at The University of Manitoba, on The Use of Cold-Formed Steel Sections

14

in Transmission Towers in Canada. (CEA Report 340 T 844, 1994)

The study involved 83 tests on cold-formed specimens for both steel types used. A total of four testing methods were employed to determine the magnitude and distribution of longitudinal and transverse residual stresses. These included, Sectioning method, Hole-Drilling method, X-Ray Diffraction technique, and the Magnetic Barkhausen Noise method (MBN).

The minimum and maximum residual stresses for steel type ASTM A715 Grade 60 are given in Table 1.7. These stresses were presented as percentages of the yield strength of corners obtained from tension coupon tests. It could be concluded that residual stresses recorded in the longitudinal direction were more critical than those developed in the transverse direction. The highest recorded tensile residual stresses were for the 90°-angle section (BA-section). Residual stresses up to 50% of the yield strength were recorded for that section.

For steel type CAN/CSA-G40.21-M 300W, Figure 1.6 shows the variation of the residual stresses in both longitudinal and transverse directions determined by the hole drilling method. The hole was drilled in the center of the specimen and was located at 12 mm below the apex.

1.3.3 Protective coating effects on cold-formed steel

As a part of the overall research investigation on the use of cold-formed steel for the construction of transmission towers, a study was conducted at The University of Manitoba (Mohamedien and Polyzois 1994) to examine the effect of coating types on the strength of cold-formed steel sections. Two types of coatings against corrosion were included in the research, hot-dip galvanizing, and thermal spray metallizing.

The coating layer for 24 standard tension test coupons cut from steel type CAN/CSA-G40.21-M 300W was examined. The thickness of the galvanized coating was measured before and after the standard tension test to examine the presence of cracks and flaking. Table 1.8 gives the percentage of overthickness of the galvanizing layer and the corresponding coating failure mode. The coating thicknesses were compared to 0.086 mm (3.4 mils) based on 50 years service life for a transmission tower in a rural environment as shown in Figure 1.7.

Test results indicated that increasing the thickness of the coating for more than 55% of the required thickness caused early flaking and cracking of the coating layer under tension loads.

1.4 Objectives and Scope of the Present Research

Fatigue failures in transmission tower members are mainly caused by wind-induced vibrations. As reported by Goel (1994), some redundant angle members which were used to support a long compression strut in a lattice tower failed soon after erection. In 1984, Thrasher studied redundant member failures on 765-kV transmission towers. The study concluded that the main strut was oscillating in a torsion mode, and that such oscillation cold worked the end of the redundant member until fatigue failure occurred. Incidents of similar failures were also reported for slender tension hanger members of the tower cross arms.

In the design process, empirical rules are based on specifying limiting values for the slenderness ratios of tower members. However, wind-induced fatigue failures suggest that these empirical rules are not fully satisfactory (Goel, 1994). Obviously, there is an essential need to gain better understanding of the failure phenomenon by conducting a series of fatigue tests on tower members.

The present study is concerned with investigating the fatigue behaviour of cold-formed steel members used for transmission tower construction. The objectives of this study were :

1. To quantify the strength and stiffness reduction of cold-formed steel members

17

under constant amplitude cyclic loading;

2. to develop a series of S-N curves (stress versus number of cycles) for the different cross sections involved in the study;

3. to determine the safe endurance limit for the sections (fatigue limit below which fatigue failure would not occur);

4. to investigate the effect of two test temperatures (-50°C and 25°C) on the fatigue behaviour of cold-formed steel members;

5. to establish guidelines for fatigue design of cold-formed steel sections; and

6. to make recommendations for further work.

The objectives were accomplished through an extensive experimental program that involved fatigue testing of 52 cold-formed steel members for five cross sectional shapes.

1.5 Format of Thesis

Chapter 1 gives an introduction to the overall research investigation. This includes material property tests, static compression tests, and tests to determine residual stresses.

Chapter 2 outlines the state of the knowledge on fatigue design criteria, methods of fatigue analysis, and factors affecting the fatigue strength. An overview

on Standards and Specifications regarding fatigue of steel structures is also high-lighted. Finally, fatigue test data on welded details and on cold-formed steel are presented.

Chapter 3 describes the experimental program. This includes a description of the test specimens, connection configurations, test setups, instrumentation, and test procedures.

Chapter 4 gives a detailed discussion of the test results. The discussion addresses crack initiation and growth patterns, the stress-strain response, and the hysteresis behaviour of the various cross sections. Fatigue strength relationships are also presented.

Chapter 5 presents the results obtained from a finite element analysis performed to investigate the behaviour of the 90°-angle section connected through one leg.

Chapter 6 gives a summary of conclusions, and formulates the findings of the study into a set of general design recommendations.

Finally, **Appendices A** and **B** give the results of the regression analysis performed on the test data.

Table 1.1

Test Variables Included in The Overall Research Investigation

Sections	BA	BC	BB	BG	BN
	Th.= 4 mm	Th.= 4 mm	Th.= 4 mm	Th.= 4 mm	Th.= 5 mm
Nominal Slenderness Ratio (L/r)	40 , 100 , and 200				
Test Temperature° C	-50°C , 0°C, and 25°C				
Type of Steel	ASTM A715 Grade 60 (F_y = 415 MPa) CAN/CSA-G40.21-M 300W (F_y = 300 MPa)				
Surface Condition	Galvanized and Ungalvanizd				

Table 1.2

Material Properties For Steel Type ASTM A715 Grade 60 (Abdel-Rahim and Polyzois, 1994)

Material Properties	Specified Minimum Values [a]	Ungalvanized				Galvanized			
		Flat		Corner		Flat		Corner	
		25°C	-50°C	25°C	-50°C	25°C	-50°C	25°C	-50°C
F_y (MPa)	415	434	485	537	577	462	507	575	617
F_u (MPa)	485	526	584	580	621	540	599	614	675
E (10^3 MPa)	(-)[b]	212	232	226	243	211	232	243	2512
δ (%)	20	27	19	15	11	24	18	13	10
μ	(-)[b]	0.26	0.27	(-)[c]	(-)[c]	0.26	0.25	(-)[c]	(-)[c]

[a] According to ASTM A715-90 (ASTM 1990).

[b] ASTM standard does not specify minimum values for the elastic modulus and the Poisson's ratio.

[c] The Poisson's ratio was not computed for corner coupons.

F_y = Yield strength

F_u = Tensile strength

E = Elastic modulus

δ = Percent elongation

μ = Poisson's ratio

Table 1.3

Material Properties For Steel Type CAN/CSA-G40.21-M 300W (Abdel-Rahim and Polyzois, 1994)

Material Properties	Specified Minimum Values [a]	Ungalvanized				Galvanized			
		Flat		Corner		Flat		Corner	
		25°C	-50°C	25°C	-50°C	25°C	-50°C	25°C	-50°C
F_y (MPa)	300	301	341	544	571	411	454	574	586
F_u (MPa)	450	454	501	589	634	532	601	643	660
E (10^3 MPa)	(-)[b]	182	186	171	209	239	258	173	186
δ (%)	23	37	24	12	11	32	20	13	9
μ	(-)[b]	0.26	0.25	(-)[c]	(-)[c]	0.27	0.25	(-)[c]	(-)[c]

[a] According to CAN/CSA-G40.21-M92 (CAN/CSA-G40.21-M92 1992).

[b] CAN/CSA standard does not specify minimum values for the elastic modulus and the poisson's ratio.

[c] The Poisson's ratio was not computed for corner coupons.

F_y = Yield strength

F_u = Tensile strength

E = Elastic modulus

δ = Percent elongation

μ = Poisson's ratio

22

Table 1.4

Effect of Galvanizing, Cold-Forming, and Subfreezing Temperature
on The Mechanical Properties of Steel Type ASTM A715 Grade 60
(Abdel-Rahim and Polyzois, 1994)

Material Properties		Effect of Galvanizing				Effect of Cold-Forming				Effect of Subfreezing Temperature			
		% Difference Between Galvanized and Ungalvanized				% Difference Between Corner and Flat				% Difference Between Results at -50°C and at 25°C			
		Flat		Corner		Ungalvanized		Galvanized		Ungalvanized		Galvanized	
		25°C	-50°C	25°C	-50°C	25°C	-50°C	25°C	-50°C	Flat	Corner	Flat	Corner
F_y	(%)	6.5	4.5	7.1	6.9	23.7	24.5	24.5	21.7	11.8	7.4	9.7	7.3
F_u	(%)	2.7	2.4	5.9	8.7	10.3	6.3	13.7	12.7	11.0	7.1	10.9	9.9
E	(%)	-0.3	0.0	7.8	3.5	6.6	5.0	15.2	8.7	9.4	7.8	9.7	3.5
δ	(%)	-11.1	-5.3	-13.3	-9.1	-44.4	-42.1	-45.8	-44.4	-29.6	-26.7	-25.0	-23.1
μ	(%)	0.0	-7.4							3.8		-3.8	

Table 1.5

Effect of Galvanizing, Cold-Forming, and Subfreezing Temperature
on The Mechanical Properties of Steel Type CAN/CSA-G40.21-M 300W
(Abdel-Rahim and Polyzois, 1994)

Material Properties		Effect of Galvanizing				Effect of Cold-Forming				Effect of Subfreezing Temperature			
		% Difference Between Galvanized and Ungalvanized				% Difference Between Corner and Flat				% Difference Between Results at -50°C and at 25°C			
		Flat		Corner		Ungalvanized		Galvanized		Ungalvanized		Galvanized	
		25°C	-50°C	25°C	-50°C	25°C	-50°C	25°C	-50°C	Flat	Corner	Flat	Corner
F_y	(%)	36.5	33.2	4.6	2.8	82.0	67.9	39.7	29.7	13.3	4.2	10.6	2.2
F_u	(%)	17.1	20.5	9.1	4.1	29.7	26.6	20.9	9.8	10.4	7.6	14.0	2.6
E	(%)	31.6	39.1	1.8	-9.7	-5.3	11.8	-27.5	-27.7	2.4	24.1	8.0	8.4
δ	(%)	-14.0	-14.7	9.6	-6.5	-67.6	-56.4	-58.9	-53.5	-33.5	-10.7	-35.1	-26.9
μ	(%)	3.0	1.4							3.4		-5.6	

Table 1.6
Static Compression Tests (Odaisky, 1994)

Section	Type of Steel	Nominal Slenderness Ratio (L/r)	Length (mm)	Exp. Failure Load (kN) -50°C	0°C	25°C	Number of Tests for Each Shape	Number of Tests for Each Steel Type
BA		40	552	121	119	119	27	
		100	1380	103	100	99		
		200	2760	28	30	30		
BC		40	736	119	121	118	27	
		100	1840	96	96	93		
		200	3680	32	33	34		
BB	ASTM A715 Grade 60	40	855	226	213	205	27	123
		100	1950	138	133	132		
		200	4240	47	46	46		
BG		40	1640	846	782	731	21	
		100	4120	485	462	467		
		200	8245	-	-	94		
BN		40	1640	1113	1092	1017	21	
		100	4105	401	403	428		
		200	8210	-	-	80		
HBA		40	552	128	-	118	18	
		100	1380	118	-	114		
		200	2760	31	-	29		
HBC		40	736	122	-	115	18	
		100	1840	108	-	102		
	CAN/CSA G40.21-M 300W	200	3680	41	-	37		66
HBB		40	780	204	-	190	18	
		100	1950	129	-	125		
		200	3900	47	-	45		
HBN		40	1580	825	-	761	12	
		100	3950	317	-	358		
	Total							189

Table 1.7

Minimum and Maximum Residual Stresses at The Apex (MPa)
(Roy et al. 1994)
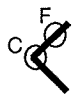
Section	ASTM A715 Grade 60 Steel[a]	Transverse Direction (% of Yield Strength)	Longitudinal Direction (% of Yield Strength)
$\langle$	**BA** (F_y = 596 MPa)[b]	-50 to 50 (8% Comp. to 8% Tens.)	100 to 300 (17% Tens. to 50% Tens.)
$\langle$	**BC** (F_y = 540 MPa)[b]	-150 to 0 (28% Comp. to 0%)	-50 to 120 (9% Comp. to 23% Tens.)
$\langle$	**BB** (F_y = 569 MPa)[b]	-400 to 50 (67% Comp. to 9% Comp.)	-190 to 10 (30% Comp. to 1.7% Tens.)
⌐L	**BG** (F_y = 646 MPa)[b]	-50 to 50 (10% Comp. to 10% Tens.)	0 to 130 (0% to 27% Tens.)
]Γ[	**BN** (F_y = 540 MPa)[b]	-110 to 20 (15% Comp. to 3% Tens.)	-100 to 40 (13% Comp. to 6% Tens.)

[a] For Steel Type CAN/CSA-G40.21-M 300W, F_y = 290 - 320 MPa.
The compressive and tensile residual stresses did not exceed
48% and 50% of the yield strength, respectively.

[b] Yield strength of corners obtained from tension coupon tests.

Table 1.8

Thickness of Galvanized Coating For Coupons Tested at -50 $^{\circ}$C
(Steel Type CAN/CSA-G40.21-M 300W) (Mohamedien and Polyzois, 1994)

Section	Coupon Location	Th. Before Testing [a] (mils) [c]	Th. After Testing [a] (mils) [c]	% Over Thickness [b]	Coating Failure
HBA					
	Flat	4.8	4.8	55 %	Cracks
	Corner	3.7	3.7	15 %	No Cracks
HBC					
	Flat	4.6	4.6	35 %	No Cracks
	Corner	7.9	7.9	130 %	Cracks
HBB					
	Flat	5.1	5.1	50 %	No Cracks
	Corner	4.6	4.6	35 %	No Cracks
HBN [b]					
	Flat	7.6	0.0	123 %	Cracks
	Corner	4.8	0.0	115 %	Flacking and Cracks

[a] The Thickness was measured using a digital magnetic gauge. (Posi Tector 2000)

[b] Thicknesses were compared to a value of 3.4 mils (0.086 mm) given by the AGA standard (1986) for 50 years service life of a transmission tower in a rural environment.

[c] 1 mils = 0.001 inch = 0.025 mm
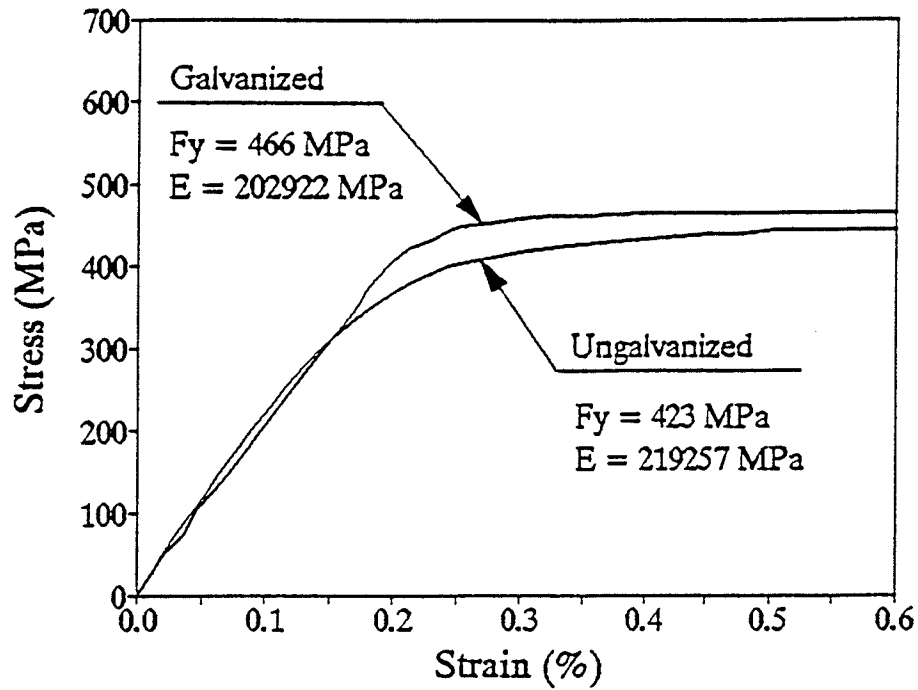
(a) Flat Coupons Tested at Room Temperature (25°C)
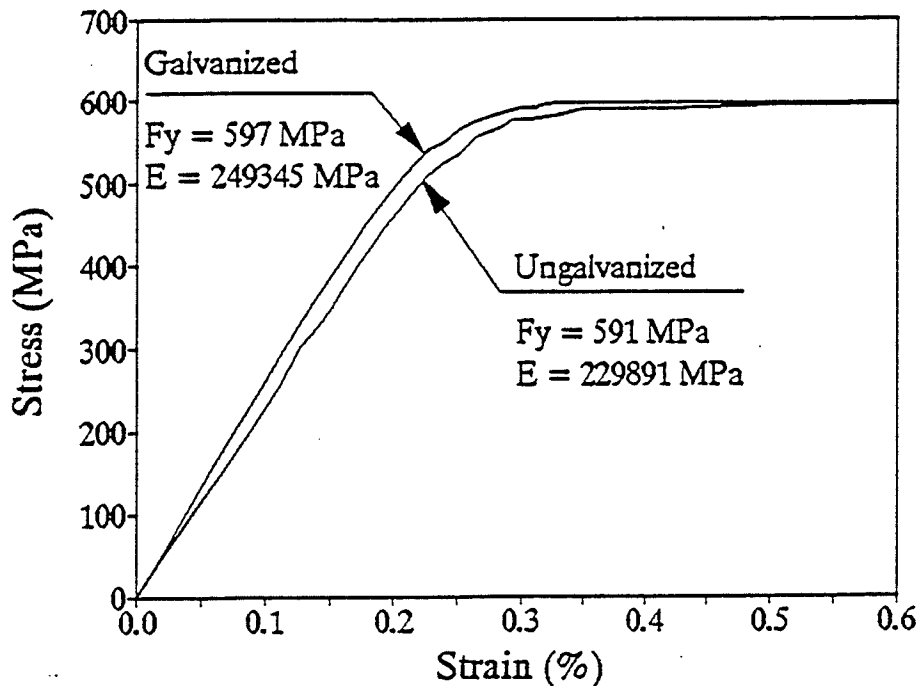
(b) Corner Coupons Tested at Room Temperature (25°C)

Figure 1.1: Typical Stress-Strain Curves for Coupons Cut from the 90° angle section.

(Steel Type ASTM A715 Grade 60). (Abdel-Rahim and Polyzois, 1994)

28
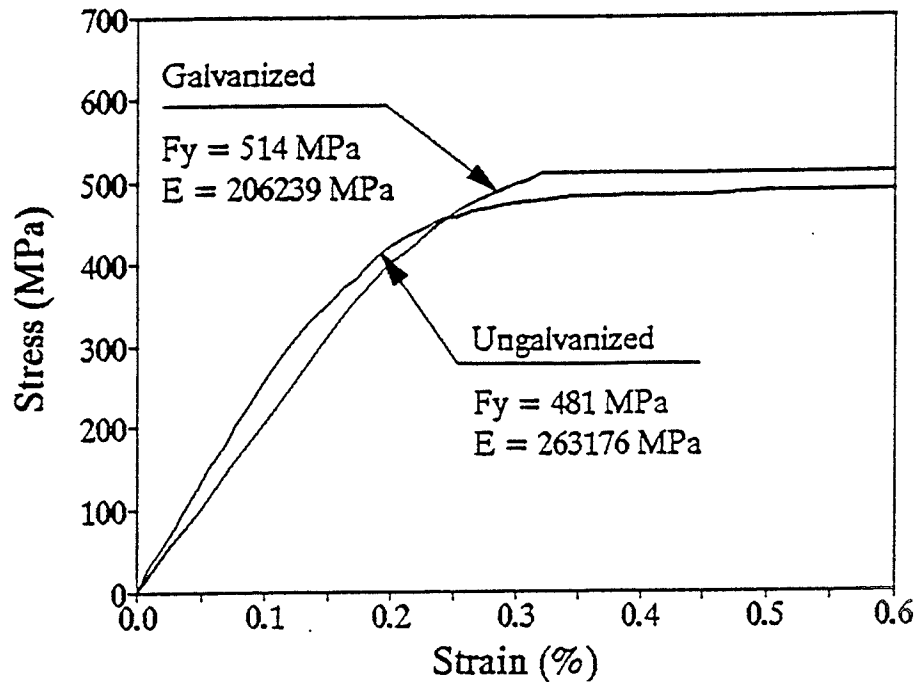
(a) Flat Coupons Tested at -50°C
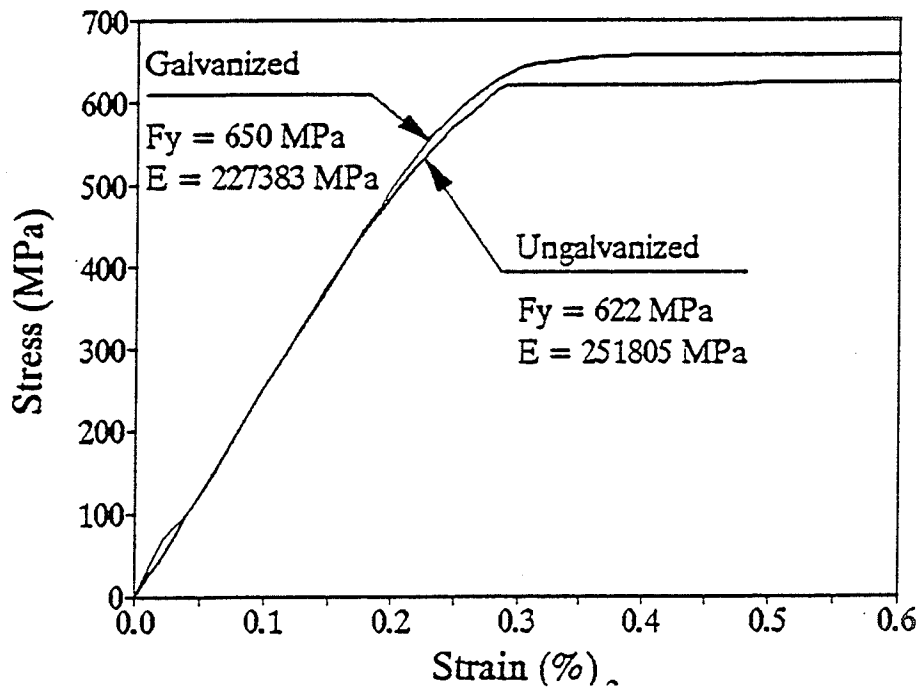
(b) Corner Coupons Tested at -50°C

Figure 1.2: Typical Stress-Strain Curves for Coupons Cut from the 90° angle section.

(Steel Type ASTM A715 Grade 60). (Abdel-Rahim and Polyzois, 1994)
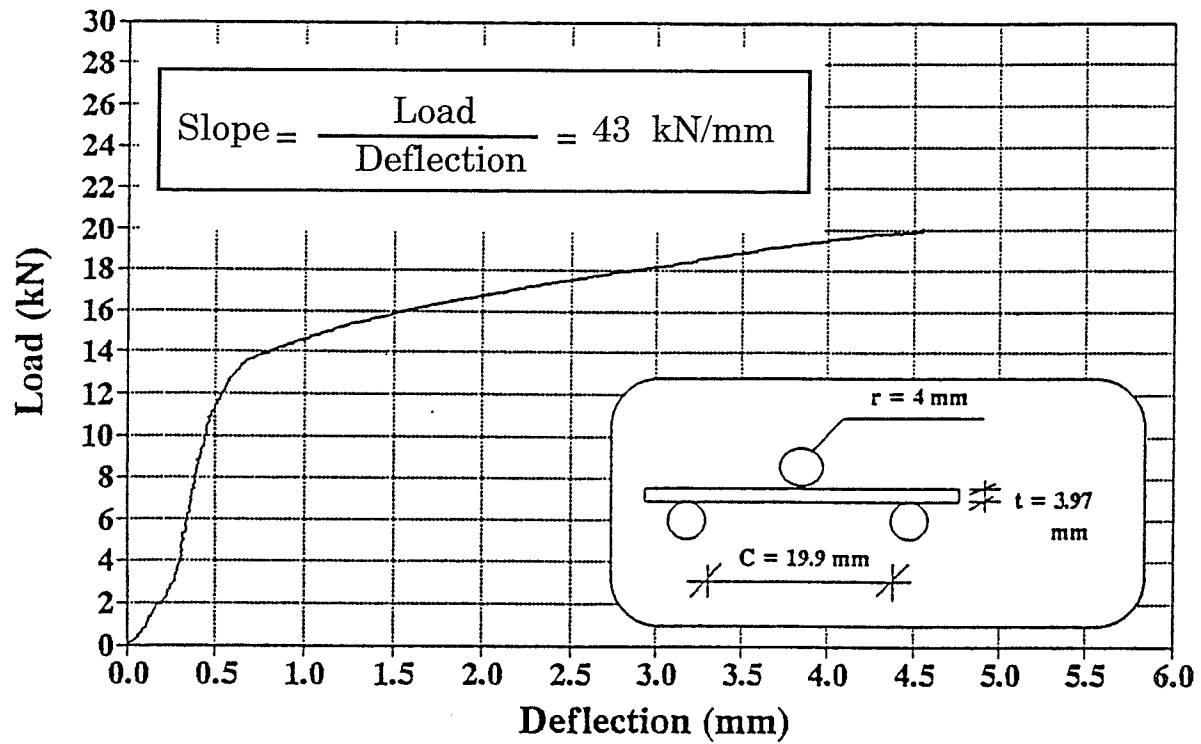
Figure 1.3: Semi-Guided Bend Test for Ungalvanized Specimen Cut from the 90° angle section. (Steel Type ASTM A715 Grade 60). (Abdel-Rahim, 1993)
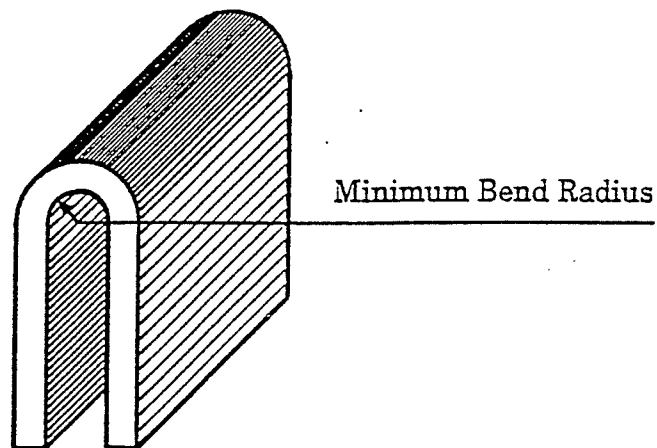
Figure 1.4: Semi-Guided Bend Test Specimen Bent to 180°. (Abdel-Rahim, 1993)
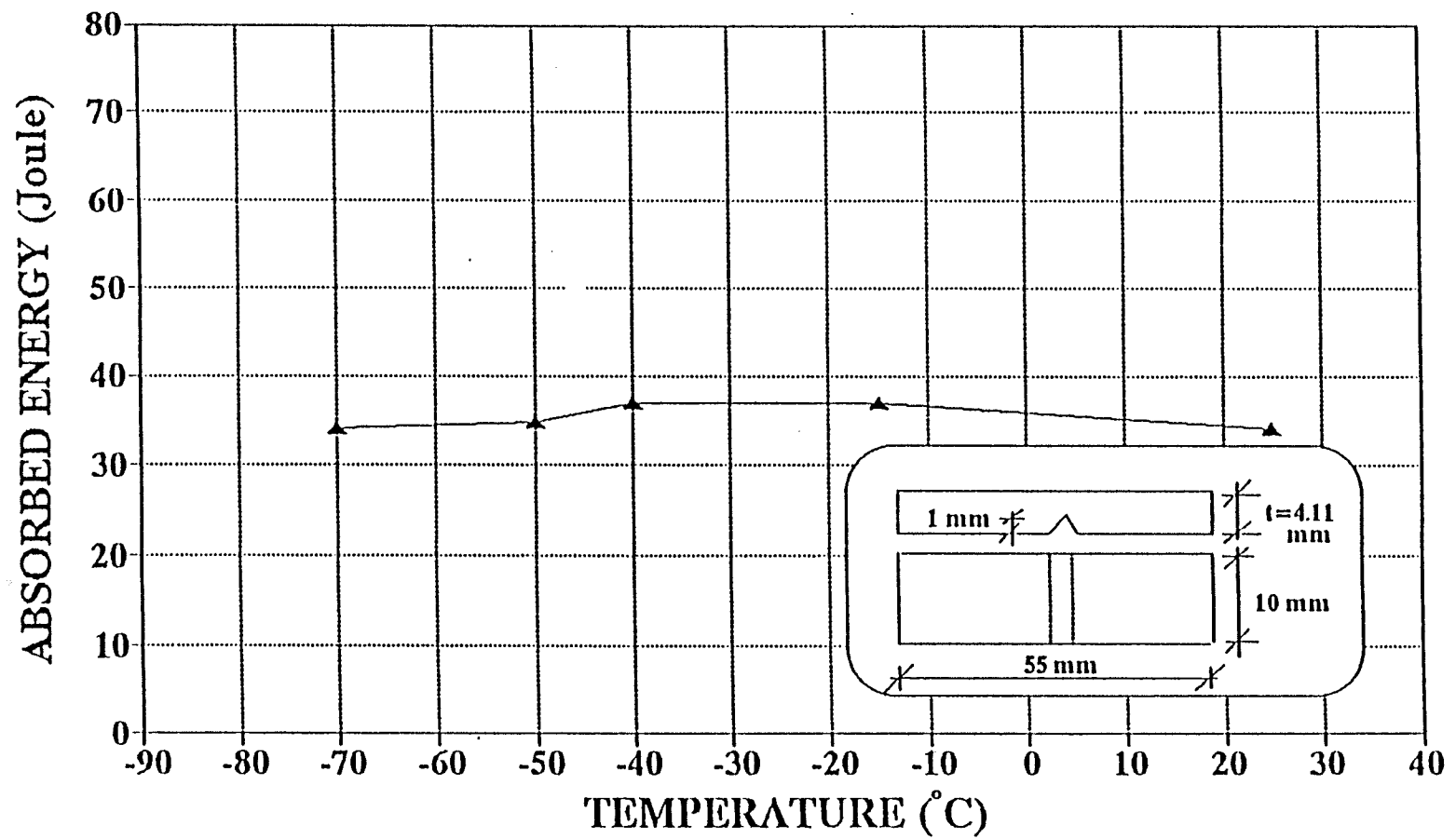
Figure 1.5 : Impact Test for Ungalvanized Specimen Cut from the Lipped-angle Section.
(Steel Type : ASTM A715 Grade 60)   (Abdel-Rahim, 1993)
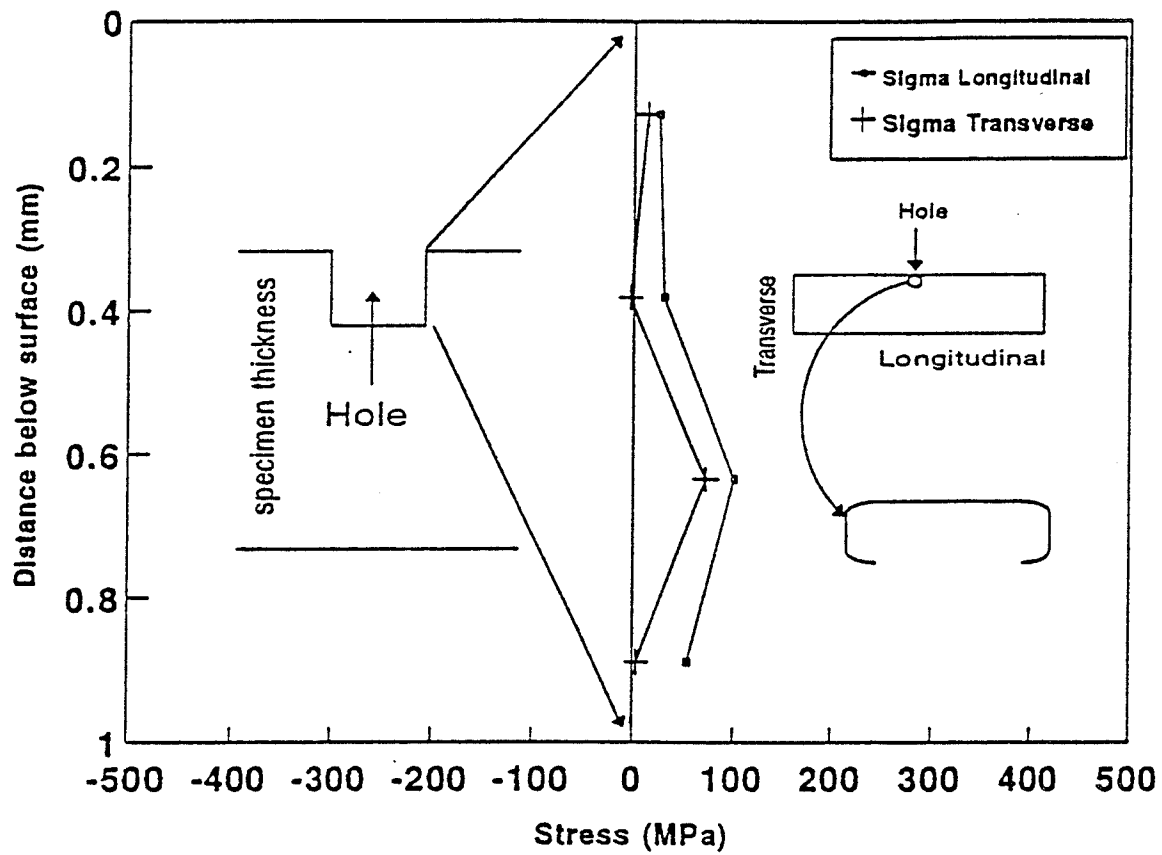
Figure 1.6: Variation of Residual Stresses in the Longitudinal and Transverse Directions for Channel Specimen HBN-37-5 Determined By the Hole Drilling Method. (Steel Type CAN/CSA-G40.21-M 300W) (Roy et al. 1994)

Figure 1.7: Life of Protection Coating Versus Thickness of Zinc and Type of Atmosphere. (AGA, 1986)

CHAPTER 2

Literature Survey

2.1 General

Hydroelectric transmission towers are one example of structures which must not only be designed to withstand a wide range of loading conditions, but also be lightweight and maintenance free. The high strength-to-weight ratio, the simplicity of fabrication, and the ease of erection have made cold-formed steel an attractive material for the construction of such structures. During the expected service life of a transmission tower (50 years), it is subjected to hundreds of thousands of fluctuating wind applications. In addition, these towers are severely exposed to a large range of temperature change and other environmental and climatic conditions. As such, the need for studying the fatigue behaviour of cold-formed steel members under the previously mentioned conditions is now becoming a growing concern.

A thorough review of the available literature showed that there has been a lack of systematic investigation of the axial fatigue behaviour of cold-formed steel members. Fatigue problems were first encountered in the design of machine components

subject to cyclic or repeated stresses. Following that stage, a large body of research concerned with fatigue has grown up in the areas of mechanical and aeronautical engineering. However, it was only recently that fatigue became important to the context of civil engineering practices.

2.2 Historical Overview

The word "fatigue" was introduced in 1829 to describe failures occurring from repeated stresses. In Germany, Albert subjected mine-hoist chains to repeated proof loadings in tension before they were put into service (Hoppe, 1896). During the period from 1850 to 1875, August Wöhler (1867), conducted laboratory fatigue tests concerned with railway axle failures to establish a safe alternating stress below which failure would not occur. Thus Wöhler introduced the concept of the S-N diagram (stress versus number of cycles) and the fatigue limit. For the next twenty years, more researchers expanded Wöhler's classical work. Gerber along with others investigated the influence of mean stress, and Goodman proposed a simplified theory regarding mean stress. Their names are still associated with diagrams involving alternating and mean stresses. In 1885, Bauschinger developed a mirror extensometer with the sensitivity to measure one microstrain and for many years studied the relationship between small inelastic strains and the safe stress in fatigue.

In the 1900's the optical microscope was used to pursue the study of fatigue mechanism. Localized slip lines and slip bands leading to the formation of microcracks were observed by Ewing and Humphery in testing flat fatigue specimens made from high quality Swedish steel. Gough (1924), and other researchers heavily contributed to the understanding of multiaxial fatigue (bending and torsion effects). In 1923, Jenkin used a model for simulating stress-strain behaviour of metals. The importance of cyclic deformations was clearly established in 1923, but largely ignored until forty years later. During the same period, Griffith (1920), published his classical paper on fracture mechanics. He showed that the last cycle of fatigue was nothing more than a brittle fracture caused by cyclic growth of a fatigue crack to an unstable length. The crack propagation problem was then addressed in the 1960's by Paris. Moore and Kommers, published the first comprehensive American book on fatigue of metals in 1927. Moore was responsible for organizing an ASTM Committee on Fatigue Research which later grew into Committee E-9 on Fatigue.

During the 1930's and 1940's, research in fatigue was mainly directed to experimentally establishing the effects of many factors that influence the fatigue strength of metals. Haigh (1930), presented his rational explanation of the difference in the response of high tensile strength steel and of mild steel to fatigue when notches are present. He employed concepts of notch strain analysis and self-stresses that

were later more fully developed by others. In 1937, Neuber introduced the stress gradient effect at notches and the elementary block concept. He then concluded that the average stress over a small volume at the root of the notch is more critical than the peak stress at the notch. In 1945, Miner formulated a linear cumulative fatigue damage criterion previously introduced by Palmgren in 1924. Despite its shortcomings, the Palmgren-Miner rule still remains an important tool in fatigue life predictions.

Major contributions to the subject of fatigue in the 1950's were revealed through the introduction of the electron microscope which opened new horizons to better understanding of basic fatigue mechanisms. Irwin (1957), introduced the stress intensity factor K_I, which is considered the basis of linear elastic fracture mechanics (LEFM) and of fatigue crack growth life predictions.

Coffin and Manson (1962), began their work in the early 1960's studying the low cycle strain-controlled fatigue behaviour. They introduced the Manson-Coffin relationship between plastic strain amplitude and fatigue life. In 1963, Paris showed that the fatigue crack growth rate da/dN could best be described using the stress intensity factor range ΔK_I. Much of this work was made possible by the introduction of the closed-loop materials testing systems and digital computers for solving engineering problems. In the last thirty years, the highly progressive amount of

testing and research has made the fatigue analysis an established engineering tool in many industrial applications.

2.3 Fatigue Design Criteria

In order to guard against fatigue failures, two major design approaches have been devised. One is a fatigue analysis that attempts to establish a "safe-life" for the structure under the assumed loading conditions. This approach implies that the fatigue life of a component can be predicted and that before the end of this specified time, the structure can be repaired, replaced, or retired. It is highly recommended that this analysis be accomplished sufficiently early in the design schedule in order to eliminate the deficiencies and to achieve the desired life. The second design procedure adopts a "damage-tolerant" or "fail-safe" design in which the damage of failed components could be temporarily tolerated by providing alternate load-carrying members and sizing them to reasonably sustain the load levels. The real goals for a damage-tolerant design are somewhere between two extremes, one indicates that the structure will be tolerant of any damage that may be inflicted. The opposite opinion implies that such a structure cannot be successfully configured to carry the service load once major failures or damage has occurred.

2.3.1 Safe-life design

Recently, safe-life has been falsely thought to describe results of fatigue tests and analyses particularly performed to prove that a structure is free of fatigue cracks. However, the initiation of a fatigue crack does not indicate the end of the useful or safe-life of a structure. The safe-life is defined as the time period for operation in a known environment with a known probability of exposure to ultimate loads. Proper inspection and maintenance coupled with a damage-tolerant design could lead to an infinite safe-life.

This design approach is directly related to those types of structures which do not receive inspection and maintenance during their operating period or service life. Recent developments in fracture mechanics especially in its treatment of crack propagation has made the damage-tolerant design approach more superior than the safe-life approach.

2.3.2 Fail-safe or damage-tolerant design

Possibilities of failure or overloads exist from errors in design, manufacturing, maintenance, and corrosion during the service life of a structure. The recognition of such possibilities requires the provision of sufficient residual strength and stiffness in the remaining members of a structure for continued operation under reasonably

normal loading until failure can be repaired (Osgood, 1982). The primary goal of the fail-safe design approach can only be achieved when supplemented by suitable inspection and maintenance. For cases when such inspection is impossible, the fail-safe design still provides the best probability of sufficient survival to continue performance of the mission, but at a degraded level. Aspects to be considered in the damage-tolerant design approach are as follows:

1. The design must include adequate residual strength after cracking.

2. The structure must have a crack-free period, or one during which the crack growth rate is sufficiently low to allow for crack detection using adequate inspection procedures.

3. Critical areas must be visually inspected during the service life of a structure.

4. Redundant load paths are to be designed with some extra capacity above its theoretical share of the ultimate load in order to allow for the possibility of overloading upon failure of one path.

5. Damaged elements are to be repaired or replaced.

The establishment of a proper level of residual strength is important not only for safety but also from the stand point of structural efficiency. In applying the fail-safe design for aircraft wings, the British Air Registry Board (Troughton et al. 1963), required that the number of individual elements be chosen such that at least

67% of the design ultimate load can be met with any one element failed.

One major conclusion may be that the safe-life design approach is implied for individual elements going into a structural assembly, whereas fail-safe or damage-tolerant design approach is usually applied when considering the complete structural assembly.

2.3.3 Factors of safety in fatigue design

In any fatigue design approach a safety factor is included. A simple procedure is implied for static design, where the limit load which is normally expected to occur only once or at most a few times during service life, is multiplied by one factor to account for a number of uncertainties and various kinds of scatter. This procedure cannot be applied for fatigue design because of the differences in material behaviour when subjected to static or fatigue loads. The factor of safety used for fatigue design must be sufficiently large to reduce the probability of failure to an acceptable level (Osgood, 1982). It is often obtained by traditional methods (1.15 on yield or 1.50 on ultimate), or by considering the statistical properties of the fatigue test data.

The fatigue safety factor intended to cover the scatter in fatigue properties could be applied on the load (stress), or on the life. Albrecht (1962), has considered the

factor of safety approach based on the average fatigue stress from a limited number of full-scale test specimens. The factor of safety is defined as $FS = \sigma_f / \sigma_d$, where σ_f is the average fatigue stress at failure, and σ_d is the design level stress. In his study, a value of σ_d was determined for a 90% confidence level on the mean test results, and 99.9% probability of survival. The relationship between the design stress and the fatigue limit is a function of the number of specimens tested. The Civil Aeronautics Manual No. 6, of the Federal Aviation Agency (1959), gives the factor of safety values corresponding to the minimum number of fatigue test specimens. This Manual uses the lowest failure stress level as a design fatigue limit instead of a mean fatigue limit reduced for a given confidence and survival limits as was proposed by Albrecht (1962). Table 2.1 lists the factor of safety values given in The Civil Aeronautics Manual.

2.3.4 Structural reliability

Structural reliability must be considered in structural design. In this manner, the factor of safety is defined as the ratio of the probable strength to the probable critical force, and is a function of the desired reliability and the variations in the loads and strengths. If the applied and ultimate loads are sharply defined (insignificant variability), then a factor of safety as low as 1.01 could result in an extremely high reliability. On the other hand, if the variability is high, a large factor of safety would

be required to provide a small probability of failure. Recently, there has been very high pressure to generate numerical reliability numbers, instead of a factor of safety in representing structural integrity (reliability). However, this would require more fatigue test data, new methodology incorporating the effects of different fatigue design approaches, and new maintenance and inspection provisions. All these factors have to be developed before structural reliability numbers could be considered as valuable end results.

2.4 Methods of Fatigue Analysis

The prime objective of all fatigue analysis, calculations, and testing is to develop an acceptable combination of load and fatigue life. In comparing the different techniques of fatigue analysis, their relative strengths and limitations can be pointed out as follows:

- Any particular method of fatigue analysis is chosen on the basis of its level of acceptance. Such level is related to the amount of confidence the designer has in the method. The stress-life (S-N) approach was introduced from over 100 years compared to 40 years for the strain-life (ϵ-N) approach and 30 years for the linear elastic fracture mechanics approach. Thus, designers have had many more years of experience with the S-N approach, and with this experience a

43

greater level of confidence was gained.

- The S-N approach may be used more intelligently when associated with the insights offered by other techniques for the purpose of providing a universal picture of the fatigue behaviour.

- For design purposes, the standard provisions regarding fatigue testing of structural details, are expressed in the form of S-N curves relating the allowable stress range to the fatigue life of a structural detail.

- The choice between using the stress-life approach or the strain-life approach is dependent upon the life range. In the low cycle region, the total strain-life method is more sensitive than the stress-life method. In addition, mean stresses do not exist. However, for the intermediate to high cycle region, mean stresses can exist, and therefore, the stress-life approach is probably more convenient to use.

- The strain-life approach can only be used in high strain, low cycle fatigue situations where plastic strains are significant. This may involve materials with low yield points (< 200 MPa). The method accounts only for initiation life and cannot be used to predict the propagation life. Moreover, the strain-life constants relate to the condition of the specimen tested and there is no defined way other than additional testing to account for differences in surface finish and surface treatment. For the stress-life approach, there are reams of

data available to account for almost any variation in surface finish, surface treatment, and load configuration.

- The strain-life approach is very useful for applications involving variable amplitude load histories where the load sequence effect on the residual mean stresses is important.

- The linear elastic fracture mechanics approach (LEFM) is essentially a propagation approach which generates problems when used to deal with crack initiation where the assumptions of linear elastic fracture mechanics are not valid. The method requires an estimate of the stress intensity factor which may be difficult to determine for complicated geometries. In general, the LEFM approach could be used in conjunction with the strain-life approach (initiation approach) to predict the total fatigue life.

2.5 Factors Affecting the Fatigue Strength

There are several factors that can highly influence the fatigue strength of a material. A discussion of some of these factors and their effects is given in the following sub-sections.

2.5.1 Effect of stress concentration

An optimum way of minimizing fatigue failures is through the reduction of avoidable stress raisers by careful design, machining, and fabrication. Fatigue strength is significantly reduced by the introduction of a stress raiser such as a notch or a hole. Fatigue cracks in structural parts usually initiate at such geometric irregularities.

The effect of stress concentration on fatigue is generally studied by performing uniaxial fatigue tests on typical fatigue test specimens containing a V-notch or a U-notch at the middle of the reduced cross section zone. The presence of a notch introduces three effects: (1) an increase or concentration of stress at the root of the notch, (2) a stress gradient is set up from the root of the notch toward the center of the specimen, and (3) a triaxial state of stress is produced at the notch root. The ratio of the maximum stress in the region of the notch to the corresponding nominal stress is the stress concentration factor (K_t) which can be calculated using the theory of elasticity, or from a refined stress analysis using the finite element method.

The effectiveness of the notch in decreasing the fatigue limit is expressed by the fatigue-notch factor (K_f). This factor is the ratio of the fatigue limit of unnotched specimens to that of notched specimens. For materials that do not exhibit a fatigue

limit, the fatigue-notch factor is based on the fatigue strength at a specified number of cycles. In general, the effect of notches on the fatigue strength is determined by comparing the S-N curves of notched and unnotched specimens.

2.5.2 Effect of test specimen size

Fatigue performance of laboratory tests on small specimens cannot be used to directly predict the fatigue behaviour of actual components. The fatigue strength of large members is significantly lower than that of small specimens. Moreover, changing the size of a fatigue specimen usually results in variations of two factors. First, increasing the surface area of the specimen reduces the fatigue performance as fatigue cracks usually initiate at the surface. Secondly, for specimens loaded in bending or in torsion, an increase in diameter usually decreases the stress gradient across the specimen, and increases the volume of material that is highly stressed.

2.5.3 Effect of surface finish and surface treatment

All fatigue cracks initiate at the surface except in special cases where internal defects are involved in a material. As such, fatigue properties are very sensitive to surface conditions. In general, fatigue life increases as the magnitude of surface roughness decreases. Figure 2.1 shows the effect of several degrees of surface finish on the

fatigue strength. As evident from the figure, decreasing the surface roughness minimizes local stress raisers and improves the fatigue strength.

Surface treatments that improve the fatigue strength are cold-rolling and shot peening. The cold-rolling process produces surface compressive residual stresses which are beneficial in retarding crack initiation. In addition, the process of blasting the surface of a component with high velocity steel or glass beads (shot peening) simply puts the core of the material in residual tension and the skin in residual compression thus improving the fatigue strength.

On the other hand, chrome and nickel plating reduce the fatigue strength due to the formation of high residual tensile stresses associated with the plating process. Such a process is beneficial only for fatigue testing in a corrosive environment. Hot rolling and forging can cause surface decarburization. This process involves loss of carbon atoms from the surface of the material causing it to have lower strength. A considerable amount of data concerned with the effect of surface coatings on the fatigue performance of various materials can be found in the Atlas of Fatigue Curves (Boyer, 1986).

2.5.4 Effect of mean stress

For design purposes, it is essentially useful to determine the mean stress effect on the allowable alternating stress amplitude for a given number of cycles. This is usually accomplished by plotting the allowable stress amplitude for a specific number of cycles as a function of the associated mean stress on a Haigh diagram. Figure 2.2 presents the four most widely used empirical relationships for describing the effect of mean stress on the fatigue strength. The governing equations (Bannantine et al. 1990) are as follows:

$$Soderberg\ (USA) \quad : \quad \frac{\sigma_a}{\sigma_e} + \frac{\sigma_m}{F_y} \quad = 1 \qquad (2.1)$$

$$Goodman\ (England) \quad : \quad \frac{\sigma_a}{\sigma_e} + \frac{\sigma_m}{F_u} \quad = 1 \qquad (2.2)$$

$$Gerber\ (Germany) \quad : \quad \frac{\sigma_a}{\sigma_e} + (\frac{\sigma_m}{F_u})^2 = 1 \qquad (2.3)$$

$$Morrow\ (USA) \quad : \quad \frac{\sigma_a}{\sigma_e} + \frac{\sigma_m}{\sigma_f} \quad = 1 \qquad (2.4)$$

where,

σ_a = the allowable alternating stress amplitude,

σ_e = the endurance stress (the fatigue limit stress),

σ_m = the mean stress $\left(\sigma_m = \frac{\sigma_{max} + \sigma_{min}}{2}\right)$,

F_y = the yield stress,

F_u = the tensile stress, and

σ_f = the failure stress.

A mean stress can be superimposed over the fluctuating stress either by the service loads themselves or by a residual stress produced during manufacturing.

2.5.5 Effect of loading frequency

Increasing the loading frequency in a fatigue test produces two simultaneous changes. First, the speed of stress application will increase. Secondly, the dwelling time of the specimen at low stresses will decrease. Many researchers have experimentally determined the effect of varying the frequency at room temperature on the endurance limit of iron steel, and copper. No effect was realized on the endurance limit when the frequency varied up to 83.3 Hz. Higher frequencies tend to raise the endurance limit. In conclusion, over a wide range, the loading frequency does not influence the fatigue life at room temperature. However before any frequency is established for fatigue testing checks should be made to assure that the frequency is within the insensitive range.

2.5.6 Effect of corrosive environments

The simultaneous action of corrosion and fatigue has a detrimental effect on the fatigue strength. Environmental effects produce cracks in fewer cycles than would be required in more inert environment. Once fatigue cracks have formed, the corro-

sive aspect may also accelerate the rate of crack growth. In addition, cyclic loading causes localized cracking of the oxide film formed on the surface of the metal as a result of the corrosive environment. Corrosion fatigue is considered a time-dependent process which is highly influenced by the loading frequency and the formation of localized pits at the surface of the metal. These pits later act as stress concentration spots causing a severe reduction in the fatigue strength of the metal.

2.5.7 Effect of residual stresses

Residual stresses play an important role in fatigue failures by radically changing the mean stress. Fatigue cracks originate at regions of maximum tensile stress and usually at the surface of the metal. An intentionally produced thin surface layer of residual compressive stress can greatly enhance the fatigue strength. Moreover, of great importance for the fatigue behaviour is the residual stress pattern set up around local surface irregularities such as fillets, holes, and notches. As a result of the formation of stress concentration regions around surface irregularities, yielding occurs much sooner than in the bulk of the metal. At these locations, high values of residual stresses are confined to a very narrow region causing the rapid initiation of cracks.

The negative evidence of the effect of residual stress on fatigue arises from fatigue

tests performed on welded structures. Obviously, the welding process produces high residual tensile stresses which result in an adverse influence on the fatigue strength. The most spectacular improvements in fatigue have been achieved by surface treatments such as shot peening, carburizing, and nitriding, all of which produce major changes in the properties of the material due to the formation of a compressive residual stress layer at the surface.

2.6 Wind-Induced Fatigue Damage

Wind gusts are caused by mechanical disturbance to the flow resulting from the roughness of the ground surface. As such, wind is considered a time-variant loading which may cause a large number of significant stress fluctuations during the typical life time of tower-type structures. Stress fluctuations result mainly from the gust action present in strong winds. The cumulative effect of these fluctuations is of great importance in the design process.

The common practice of basing design wind velocities on the highest instantaneous velocity recorded by some nearby anemometer, usually leads to conservative estimates. An alternative method is to use the statistical theory of extreme values which can predict the average number of years between recurrences of any specified

wind velocity. As such, design wind velocities could be based on the annual maximum value for a number of years instead of relying on one critical measurement. In addition, the recurrence period could be chosen to match the expected lifetime of the structure, and an appropriately smaller design wind velocity could be used for more temporary structures. The chief merits of the statistical approach are that it is realistic and ensures that similar structures are designed to a consistent standard of safety.

In 1962, structural response analysis of loads resulting from wind gusts was pioneered by Davenport using power spectrum techniques. The study proved that the greater part of the fatigue damage resulted from gust components acting at frequencies close to the natural frequency of the structure. In a previous study (Davenport 1961), statistical concepts of the stationary time series were used to determine the response of a simple structure to a turbulent, gusty wind. Davenport then expanded his investigation to include line-like structures such as suspension bridges, tall masts, and overhead power transmission lines. General expressions for the response of such structures to gusty winds were developed (Davenport 1962). The study pointed out two principal differences in the response of "point" and "line" structures to wind gusts. First, a point structure is likely to have only one mode of vibration, whereas a line structure is likely to have many modes. Secondly, a point structure is only affected by the velocity fluctuations of the wind at a point, while for a line structure,

the variations of the wind velocity across the span are also important. Moreover, factors which take proper recognition of the dynamic effect of wind on structures such as tall buildings, towers, and bridges were formulated by Davenport in 1967.

An assessment of the sensitivity of lattice towers to fatigue induced by wind gusts was studied by Wyatt (1984). Moreover, the work presented by Patel and Freathy (1984), considered a method of simplifying the analysis procedure of wind-induced fatigue damage. The proposed method is suitable for a first assessment of fatigue performance, and has the advantage of its ability to be presented in calculation sheets or a computer program. It is particularly instructive to express the main limitations of the method as pointed out by its authors. These are: (1) the assumption of a linear relationship between the stress and the wind fluctuation, (2) the use of linear S-N curves, and (3) the manner in which the effects of resonance are accounted for.

In an attempt to study the dynamic behaviour of transmission towers, Jensen and Folkestad (1984), compared the results of field measurements for a Vega transmission tower on an island on the West Coast of Norway with results obtained from analytical work. The dynamic response of the tower structure was recorded by accelerometers placed at the top of the steel mast, and electrical resistance strain gauges mounted on the concrete reinforcement in the foot of the tower. Strain

gauges were also mounted on the main members at the base of the steel mast. The results were handled and presented in an easily comprehensible manner by showing the number of vibrations on the different vibration range levels and their time of occurrence. By comparing these recordings with the corresponding wind measurements, the relationship between wind and vibrations could be plotted.

An example of field measurements for transmission tower structures was expressed in the work of Mackey et al. 1974. Results were obtained for a series of full-scale tests on a free-standing latticed steel tower under strong winds. The tower was equipped with anemometers at four levels for measuring horizontal wind velocities. In addition, electro-optical tracking systems were used to measure the displacements at various heights. Based on actual response records, the structural characteristics which directly affect the dynamic behaviour of the tower were obtained and compared with theoretical computations. Another example of full-scale observation of latticed steel transmission towers under the action of wind gusts was studied by Hiramatsu et al. in 1988. The study investigated the torsional response characteristics of steel towers through full-scale observation and analytical estimation.

A study carried out by Lambert et al. (1988), described full-scale instrumentation and analysis of tall guyed latticed steel masts. The objective was to correlate

wind speed and direction with structural stresses in welds. The study outlined a method of predicting residual fatigue life from past meteorological records when regular inspection is difficult. It also suggested a global way of treating wind direction effects by assuming that a direction factor could be used to account for the reduced probability of wind blowing in the most adverse direction. Moreover, the investigation demonstrated the feasibility and value of collecting specific field data from actual structures. These field measurements provide more confidence in the analytical predictions especially when fatigue is a major consideration.

A simple relationship between the gust response factor and the fatigue damage was introduced by Dionne and Davenport (1988). The method provided wind-induced fatigue damage estimates from gust factors used in quasi-static design. Statistical concepts were used to quantify the probability of fatigue failure. Probabilities of static and fatigue failures were related using a relationship between mean strength and fatigue endurance limit. The final product of the study was presented by a set of curves relating the frequency to the gust response factor for different material properties.

In wind loading codes for buildings, there are no distinct rules or well defined methods for estimating fatigue damage of structural members due to wind loading. Although the stochastic nature of wind loads can be best modeled by

variable-amplitude fatigue loads, yet there are different methods available for relating variable-amplitude fatigue data to constant-amplitude data.

An extensive laboratory investigation of fatigue effects in welded steel beams subjected to variable-amplitude loadings was conducted by Schilling et al. (1978). The first objective was to acquire fatigue data on welded bridge members under both variable-amplitude loading and random sequence stress spectra. Another objective was to develop an analytical method of predicting variable-amplitude fatigue behaviour from constant-amplitude fatigue data. Results obtained from the statistical analysis of the test data did not show any statistically significant difference between the constant-amplitude test data and the transformed variable-amplitude data.

In general, transmission line structures are sensitive to dynamic wind forces because of their flexibility and slenderness. Wind-induced damage results mainly from hurricanes, tornadoes, and winds associated with thunderstorms. As such, additional knowledge concerning the response and behaviour of large flexible structures to wind effects could be extremely helpful in producing more economical design of electrical transmission line structures. The paper presented by Mehta (1984), contains a commentary on wind-induced damage documentation experiences, and remarks on design implications. Photographs of collapsed transmission towers under the influence of wind forces are shown in Figures 2.3 and 2.4.

2.7 Fatigue at Low Temperatures

Fatigue behaviour at low temperatures has received much less attention than that at room and elevated temperatures. Comprehensive summaries of S-N fatigue behaviour of some metals at low temperatures were introduced by Teed (1950), and Forrest (1963). Their prime objective was to provide a general trend for long-life fatigue strengths at low temperatures (-40°C to -196°C) compared to room temperature. However, stress concentration factors were not correlated in the study. Spretnak et al. (1951) performed low temperature fatigue tests on notched and unnotched specimens. The results showed that at short lives, low temperatures are usually beneficial to constant amplitude unnotched S-N fatigue behaviour, while at longer lives, notched fatigue strength are usually slightly better or similar to room temperature values.

In 1935, Boone and Wishart published what appears to be the first paper on "Low Temperature Fatigue". The materials tested ranged from duralumin to rail steel and cast iron. Results obtained from the rotating bending fatigue tests conducted in this study indicated that the endurance limit of all tested materials increased with a decrease in temperature. Their work also indicated that the notch sensitivity as measured by the effective stress concentration factor (ratio of fatigue limit of unnotched specimen to fatigue limit of notched specimen) tended to decrease as

the test temperature was lowered.

An interesting feature noticed by Kenneford et al. (1960) was that, for mild steel, the notch sensitivity decreased slightly with temperature when tested with a zero minimum stress, but increased when tested with a zero mean stress (fully reversed stress cycle). Strain-life (ϵ-N) low cycle fatigue behaviour studied by Nachtigal (1974), Polák and Klesnil (1976), and Mikukawa et al. (1970), indicated that long-life fatigue resistance increased at low temperatures, while short-life fatigue resistance decreased as a result of low ductility and low fracture toughness.

The problem of notch sensitivity and crack growth rate at low temperature was studied by Read in 1972. Four representative sheet materials were tested (7075 Aluminum, Ti-6A1-4V, Fibre-glass, and Carbon filament reinforced plastics). The study indicated the existence of a transitional stress intensity factor where crack growth rate was accelerated by lowering the temperature until that value was reached. Below this value, the reverse seemed to be true.

The Symposium on Fatigue at Low Temperatures (Stephens 1983), sponsored by the ASTM committees E-9 on Fatigue and E-24 on Fracture testing, provides an important contribution to the overall understanding of the fatigue behaviour at low temperatures. Metal alloys investigated included aluminum, magnesium, titanium,

austenitic stainless steel, manganese stainless steel and other steels and iron. The temperature ranged from 0°C to -269°C.

The predominant subject matter of that Volume was fatigue crack growth tests conducted under constant-amplitude loading conditions. The tests were carried out with different specimen configurations that included compact type, center cracked panel, and bend specimens. The specimen thickness varied from about 1 to 25 mm. Moreover, the load ratio ($R = P_{min} / P_{max}$) was primarily 0.0 or 0.1 except for a few tests at R = 0.35, 0.50, 0.70, and 0.80. Loading frequencies ranged from 0.00056 Hz to 100 Hz. Crack length measurements were obtained either by using optical microscopes, or by a crack opening displacement gauge (COD).

The results of the presented investigations indicated that low temperature fatigue resistance was more sensitive to chemical composition and microstructure than fatigue resistance at room temperature. Factors that directly affect the fatigue performance at low temperatures include, ductile / brittle transitions, fracture toughness, and the crystalline structure or microstructure of the tested materials. As such, depending on the type of steel material, low temperatures could be beneficial or detrimental or had a little influence on the total fatigue life of a structural component.

2.8 Standards and Specifications Regarding Fatigue of Steel Structures

Standards and Specifications for fatigue design of steel structures are all expressed in the form of S-N curves relating the allowable stress range to the total fatigue life of various types of structural details. A brief description is given in the following sections.

- ### CAN/CSA-S16.1-M94 (1995)

The Standard uses the "stress range" concept for determining the fatigue life of a structural detail. This concept reflects the results of a comprehensive research project conducted by Fisher in the area of fatigue strength of steel beams (1972 and 1974), states that the difference between the maximum and minimum applied stresses (the stress range) accounts for nearly all the variations in fatigue life for a given steel member or detail. The Standard provides an extensive list of design conditions and situations which are grouped into nine stress range categories based on the shape of the structural detail and the presence of weld.

- ### LRFD-AISC (1993)

In the design of members and connections subjected to repeated variation of live load, the Load and Resistance Factor Design Specification gives consideration

to the number of stress cycles, the expected range of stress, and the type and location of the member or detail. The Specification classifies the loading conditions according to the number of stress cycles which is equivalent to the number of load applications per day over a specified number of years. It also assigns stress range categories based on the type and location of the member or detail, including two types of mechanically fastened connections. The design strength of properly tightened ASTM A325 and A490 bolts subject to tensile fatigue loading is also given in this specification.

• AASHTO Specifications (1989)

The provisions for the fatigue design of steel bridge details in the AASHTO Specifications are based on a set of S-N curves defining the strength of different classes of details. The curves were developed based on an extensive research investigation sponsored by the National Cooperative Highway Research Program (NCHRP Reports 102 and 147) under the principal supervision of Professor John W. Fisher (Fisher et al. 1970, and Fisher et al. 1974). The testing program involved 530 test beams and girders each with two or more details. The experimental program was statistically designed, and was conducted under controlled conditions so that the analysis of the test data would reveal the parameters that were significant in describing the fatigue behaviour of the test specimens. Three different types of steel were used to study the influence of yield stress on fatigue life. The types of steel

used were ASTM A36, A441, and A514. This provided a range of nominal yield stress that ranged from 248 to 690 MPa.

The design curves were developed from linear regression analyses of the test data using the 95% confidence limits defining the lower bounds of the fatigue resistance. All S-N curves have similar slopes with a value of approximately -3.0 (Keating and Fisher, 1986).

Different stress range categories were used to classify the fatigue strength of the details used in the testing program. Rolled beams were used to define Category A, longitudinal welds and flange splices for Category B, welded stiffeners and short attachments (50 mm) for Category C, 100 mm attachments for Category D, cover plated beams for Category E, and thick cover plates and long attachments for Category E'. The last two Categories (E and E') were developed based on an investigation of the behaviour of full-scale welded bridge attachments by Fisher et al. 1980. The current AASHTO fatigue design curves are shown in Figure 2.5. A detailed documentation of other American fatigue test data could be found in NCHRP Report 286 (Keating and Fisher, 1986).

- **European Convention Constructional Steel Work Recommendations**

(ECCS, 1985)

The proposed ECCS fatigue strength curves shown in Figure 2.6 are based on fatigue test data obtained from different sources. The first source is NCHRP Reports 102 and 147 (Fisher et al. 1970, and Fisher et al. 1974). The second is a series of fatigue tests conducted in West Germany, Poland, England, and Holland. These tests were sponsored by the Office of Research and Experiments (ORE), of the International Union of Railways (ORE Report D 86 (1971), and ORE Report D 130 (1974 - 1979).

The ECCS fatigue strength curves differ slightly from the AASHTO requirements. A set of 15 equally spaced S-N curves on a log-log scale have been used to define the fatigue strength of details ranging from base metal to cover plated beam members. Fatigue test data for a particular structural detail can be compared with these curves, where a specific curve is chosen to define the fatigue strength of that detail. As such, uniformity is maintained, as there is no need to develop a new curve for each new detail.

At a given number of cycles, the equal vertical spacing between the curves corresponds to approximately 10% variation in fatigue strength. For a life range up to

5×10^6 cycles, the slope of all curves is equal to -3.0. However, at 5×10^6 cycles, two options are provided. The first option does not depend on the type of loading (constant or variable-amplitude loading). In that option, the slope of all curves at 5×10^6 cycles changes to -5.0 until 50×10^6 cycles where a cut off is provided to define the fatigue limit. The second option represented by the solid lines in Figure 2.6 are straight line extensions of the -3.0 slope S-N curves. The reference fatigue strength is the stress range value corresponding to the fatigue life at 2×10^6 cycles.

In their comprehensive evaluation of fatigue test data and design criteria on welded details, Keating and Fisher (1986), pointed out several shortcomings for the proposed ECCS fatigue curves. These can be summarized as follows:

1. The accuracy of using 15 different stress range categories to define the fatigue resistance of a structural detail is questionable.

2. Providing a constant cycle fatigue limit at 5×10^6 cycles for all details is not compatible with the actual fatigue test data. Test results indicate that the constant cycle fatigue limit occurs at increasing cycles as the severity of the detail increases.

3. The change in slope of all the S-N curves from -3.0 to -5.0 for fatigue resistance below the constant cycle fatigue limit is not in agreement with random variable fatigue results. Test results conducted under variable-amplitude loading

support the use of the -3.0 slope for all stress cycles.

In general, the most significant difference between the ECCS fatigue design curves as compared to the AASHTO curves, is the constant-amplitude fatigue limits. For stress Categories A through C, the ECCS limits are more conservative, while for Categories D to E', the AASHTO limits are lower.

2.9   Fatigue Tests on Welded Details

Since the adoption of the AASHTO fatigue Specifications in 1974, several major fatigue studies have been carried out on similar beam-type specimens. Moreover, with the development of fatigue codes in different countries, the principal objective of the NCHRP Report 286 (Keating and Fisher, 1986) was to compile and review all available fatigue data of welded steel details. New sources of data were compared with the appropriate existing AASHTO fatigue curves. This allowed the re-evaluation of the AASHTO Specifications so that they more accurately reflect the current state of knowledge.

The database for welded steel bridge details included the original NCHRP Reports 102 and 147 data used to develop the current AASHTO fatigue provisions. Other National Cooperative Highway Research Program projects were also

66

included. The test variables in the study were mainly the type of steel, and the stress range. Some studies dealt with constant-amplitude loading such as, NCHRP Reports 181, 206, 227. Other studies such as NCHRP Reports 188 and 267 dealt with variable-amplitude stress cycles.

Fatigue test data on welded details conducted in several countries other than the United States were also well documented in the NCHRP Report 286 (Keating and Fisher, 1986). These included Japanese data, ORE data, English fatigue data, ICOM fatigue data (conducted by the Swiss Federal Institute of Technology), East and West German data, and Canadian fatigue data.

The Japanese test data particularly emphasized the size effect and its role in the assessment of fatigue strength. The specimens tested tended to simulate members of welded box girders and other welded joints commonly used in bridge structures. Three basic types of specimens were employed. The first two types were longitudinal groove welds in flat plates and longitudinal welded box girders. These correspond to Category B details of the AASHTO code. The third type of specimens included non-load-carrying cruciform and fillet welded joints that were compared to the Category C detail. All tests were conducted under constant-amplitude loading. The results indicated that the AASHTO curves provided a good lower bound estimate of the fatigue resistance.

The Office of Research and Experiments (ORE) of the International Union of Railways carried out a test program (ORE Report D 130, 1974-1979) that involved two types of specimens. The first type included structural members and details commonly used in bridges. These specimens were tested under constant-amplitude loading. The second type consisted mainly of simple specimens that were tested to investigate the effects of eccentricity and variable-amplitude loading on the fatigue strength. In addition, box beams with internal diaphragms and transverse groove welds were tested under axial loading. Moreover, identical specimens were tested under both constant-amplitude and spectrum loading to check the accuracy of Palmgren-Miner cumulative damage hypothesis for fatigue life prediction. Because of the limited number of test data, the regression analysis yielded little useful information. However, the data obtained were suitable for checking the current AASHTO design curves, and for providing data not presented by the original curves.

The English fatigue data compiled in the database of fatigue strength of welded details included two test programs. The first program (Maddox 1982), studied the effect of improving the fatigue lives of welded details by shot peening the fillet welds. Such improvement was more effective on transverse welds than on welds of longitudinal attachments. In that program, two types of small-scale test specimens were used, a longitudinal fillet-welded attachment, and a transverse fillet-welded

attachment. All tests were conducted under constant-amplitude loading. Results obtained from transverse attachments could be compared to Category C of the AASHTO Specifications. Results from longitudinal attachment specimens were between Category E and Category D resistance curves.

The second fatigue test program (TRRL 1979) was concerned with studying intermittent fillet welds. Test specimens used were welded to wide flange beams. Several varying weld gap patterns were studied in the constant moment region. The different weld hit-miss ratios ranged from 1:1 to 1:25. All tests were conducted under constant cycle loading. Although test results were consistent with the fatigue resistance defined by Category C, the current AASHTO fatigue provisions classify this type of detail as Category E. In general, the use of intermittent welds should not be encouraged for details subjected to cyclic loading. This weld pattern introduces defects which mainly occur at the weld termination locations.

Fatigue tests conducted by the Swiss Federal Institute of Technology (ICOM) dealt with the fatigue life of welded beams with attachments (Hirt and Crisinel 1975; Yamada and Hirt 1982; Smith et al. 1984). In these investigations, fatigue crack propagation and fatigue crack improvement techniques were studied. All tests were conducted under constant-amplitude loading. Plain welded beam test results were consistent with the Category B resistance curve. The fillet welded rectangular web

attachment results fell above the Category E curve. Moreover, results obtained from flange tip attachment specimens were also consistent with the Category E design curve. In addition, some flange surface attachments were also tested. Their results fell between Categories C and D curves of the AASHTO Specifications.

A research program of fatigue testing of welded beams (Berger 1982) was conducted in conjunction with the development of the fatigue specifications for steel structures in East Germany. The test specimens used were welded beams with different types of attachments. These included, flange tip attachments, flange surface attachments, and cover plate details. The specimens were tested under constant cycle loading using two different stress ratios, -1.0 and 0.50. The results were found to be consistent with the equivalent stress categories defined by the AASHTO Specifications for the particular types of attachments involved. Based on the results of this investigation, it was also concluded that the stress range concept could be used in the new edition of the East German steel structures specifications.

In West Germany, the objective of a study carried out by Minner and Seeger in 1982, was to investigate the applicability of correlating fatigue test results on small-scale specimens to full-size welded beams. The testing program involved the use of both rolled and welded high strength steel beams with yield stress values of 448 MPa and 690 MPa. All tests were conducted under constant-amplitude loading

with a stress ratio of 0.10. Three different detail types were examined: web stiffeners welded to flanges, staggered welded splices, and flange butt welds. Test results fell significantly below the equivalent fatigue strength curves of the AASHTO Specifications. The main reason for the reduced fatigue strength was attributed to welding deficiencies.

A study on the fatigue behaviour of welded steel elements in Canada was initiated by Comeau and Kulak in 1979. Two types of web attachments were studied: plates intersecting the web plate, and gusset plate details used for lateral bracing of bridge beams. The test data for the long web plate attachments were in good agreement with the Category E resistance curve. Moreover, the web gusset plate results were consistent with the Category D curve of the AASHTO Specifications.

A second testing program (Baker and Kulak 1984) was conducted in order to examine the effect of backing bars on the fatigue strength of transversely loaded groove welds. Only one simple plate specimen configuration was tested. The results obtained fell between the Category B and C curves. Category C provided a lower bound to the test data.

Based on the previous review, Keating and Fisher (1986), proposed a revised set of fatigue design curves that better estimate the fatigue resistance of welded steel

bridge details. The proposed new curves differ slightly from the AASHTO curves in that they all have a constant slope of -3.0. It was concluded that the proposed curves would better reflect the results obtained from the expanded fatigue database. In addition, the proposed set of curves would be consistent with fatigue resistance curves used in other countries.

A study to evaluate distortion-induced fatigue cracking in the webs of steel bridge girders was performed by Fisher et al. in 1990. It provided a detailed review of past field measurements undertaken on a variety of bridges that had experienced fatigue cracking as a result of web gap distortion. The types of structures covered in the review included girder-floor-beam bridges, multigirder bridges, box girder bridges, and tied-arch bridges with box girder tension ties. The investigation indicated that the welded connections were more resistant to web gap distortion than bolted connections. In addition, recommendations were provided for changes to the AASHTO provisions for the design of end connections of stringers and floorbeams.

2.10   Fatigue Data on Cold-Formed Steel Sections

In 1981, Klippstein studied the fatigue behaviour of sheet-steel fabrication details. He presented the test results of 24 beam specimens consisting of cold-formed

72

back-to-back channels and welded I-beams. It was concluded that the conservative fatigue-design curves used for plate-steel fabrication details can also be used for the fatigue design of sheet-steel details. Research carried out by Libertini et al. (1977) has revealed that cold-working of sheet-steel can improve the large cycle fatigue resistance, but may result in the degradation of small cycle fatigue resistance.

Table 2.1

Safety Factors Specified for Fatigue Design.
(Civil Aeronautics Manual, 1959)

Minimum Number of Test Specimens	(Applied Stress Level) / (Critical Stress Level)
4	1.10
3	1.25
2	1.50
1	2.00
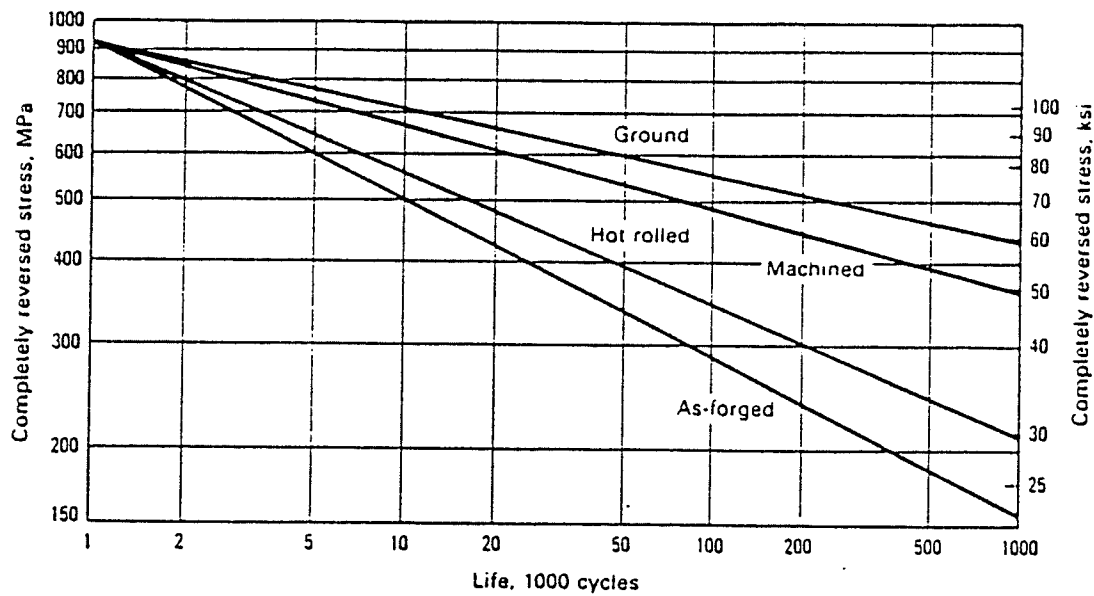
Figure 2.1: Effect of Surface Conditions on the Fatigue Properties of Steel (302-321 HB). (Boyer, 1986)
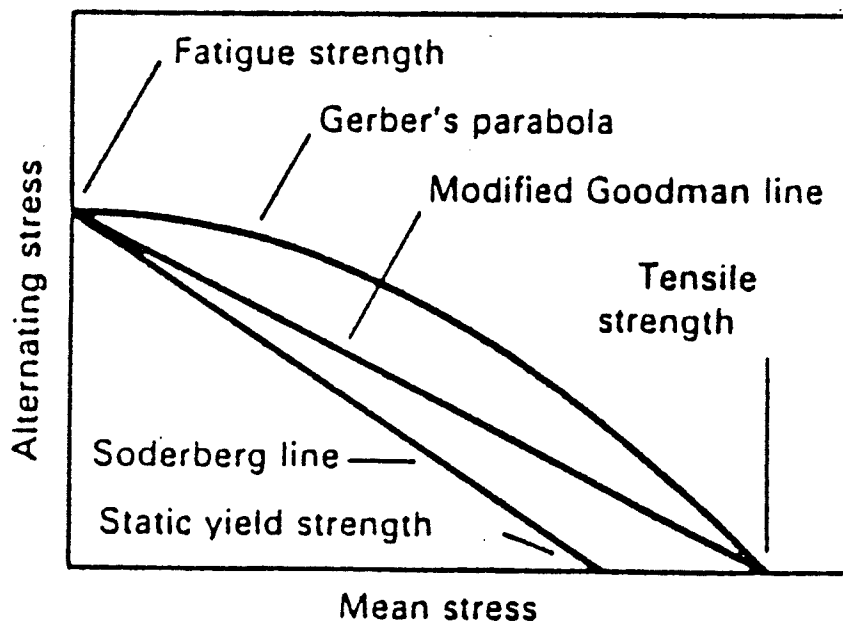
Figure 2.2: Effect of Mean Stress on the Alternating Stress Amplitude. (Boyer, 1986)

75
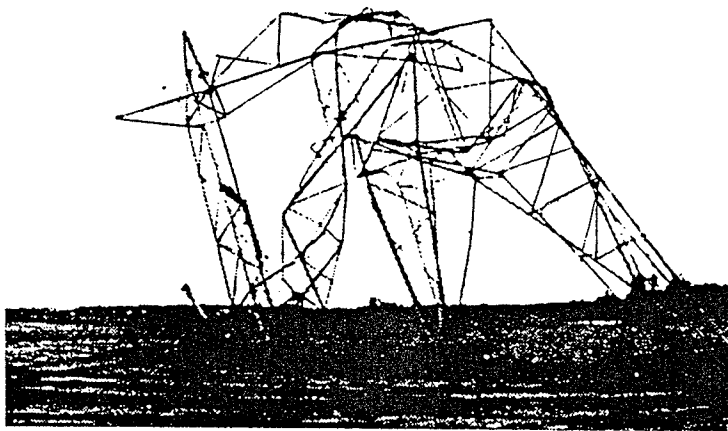
Figure 2.3: Collapse of Transmission Line Tower Due to Wind Forces. (Mehta, 1984)
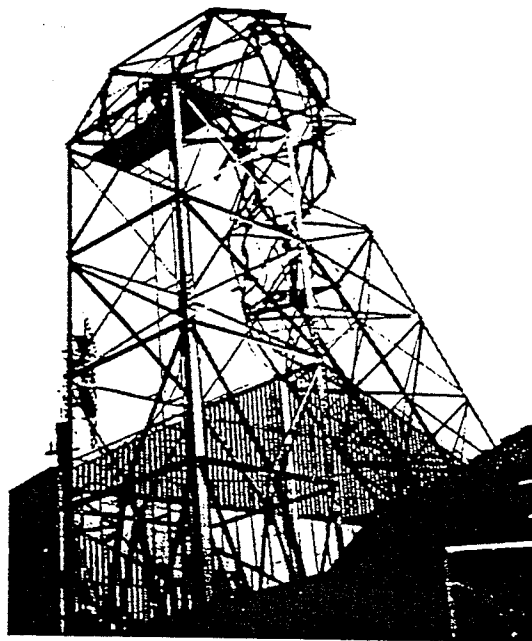
Figure 2.4: Damage of Lattice Lighting-Tower. (Mehta, 1984)
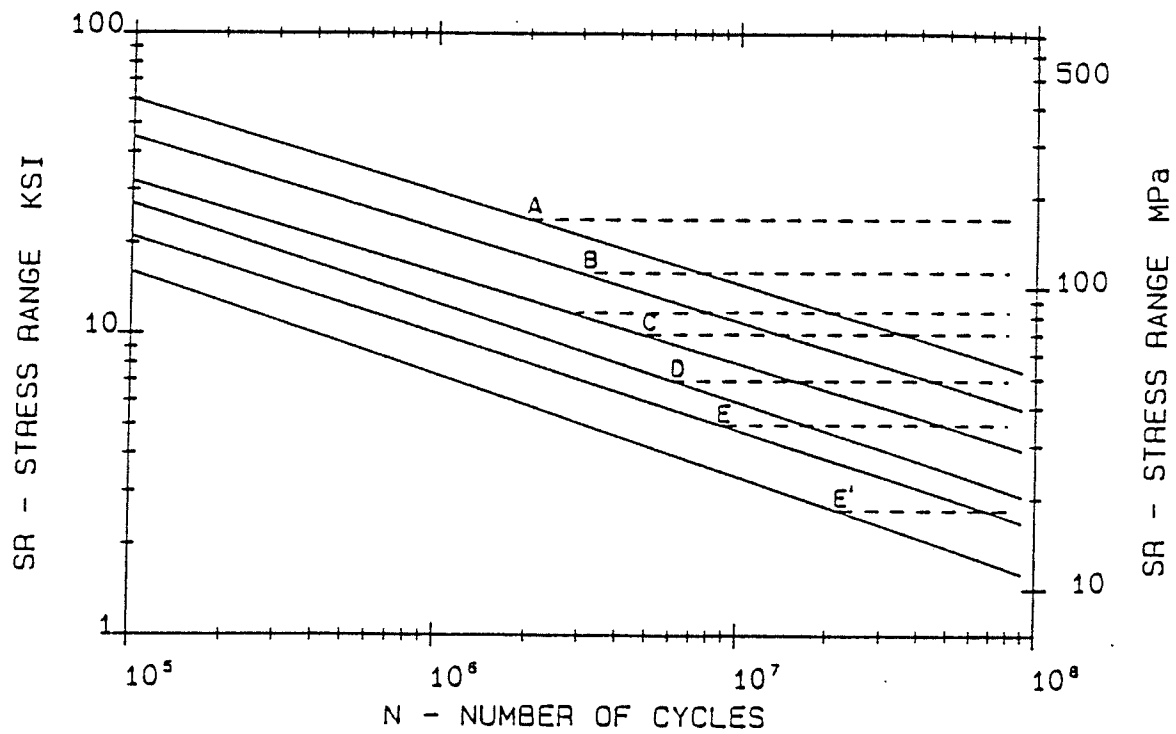
Figure 2.5: AASHTO Fatigue Design Curves. (1989)
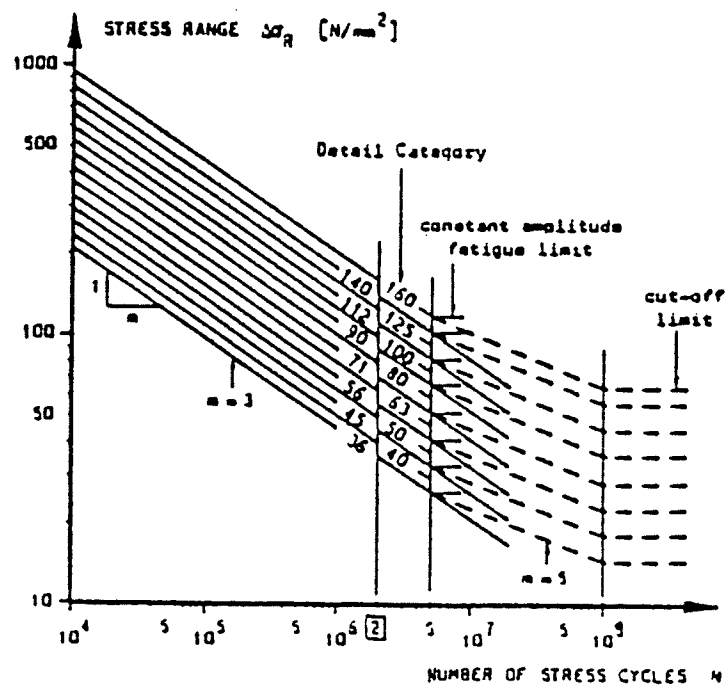
Figure 2.6: Fatigue Design Curves Adopted by the ECCS Recommendations.

(Keating and Fisher, 1986)

CHAPTER 3

Experimental Program

3.1   Scope and Design Variables

The prime objective of the experimental program was to investigate the fatigue behaviour of full-size cold-formed steel members typical of those used for constructing transmission towers. A total of 52 constant-amplitude axial fatigue tests were performed under load-controlled conditions with a load ratio of -1.0 (fully reversed load cycle). The loading frequency ranged from 1 Hz to 2.5 Hz depending on the stroke level of the test specimen. The experimental program involved the use of five cross sectional shapes as shown in Figure 3.1. The average section dimensions for each shape are listed in Table 3.1. The recorded values of the thickness (measured by a micrometer) are for the base metal with the galvanizing thickness deducted.

One set of specimens (42 specimens) were produced by SAE in Italy using ASTM A715 Grade 60 steel with a minimum specified yield stress of 415 MPa. The other set of specimens (10 specimens) were fabricated in Canada using CAN/CSA-G40.21-M 300W steel with specified yield stress of 300 MPa. Table 3.2 lists the

results of tension tests performed at room temperature ($\simeq 25°C$) on galvanized and ungalvanized standard coupons cut from flat portions of the specimens. The results obtained from tests on ungalvanized A715 and G40.21 steel specimens confirmed the minimum specified yield strength values of 415 MPa and 300 MPa respectively.

The specified thickness of the A715 steel for the channel specimens (BN section) was 5.0 mm, and for all other shapes the specified thickness was 4.0 mm. For the G40.21-Grade 300W steel the specified thickness for the channel specimens (HBN section) was 5.0 mm. The section properties for each shape are listed in Table 3.3. These properties are based on the average recorded dimensions for each cross sectional shape with the galvanizing thickness deducted.

The specimens were tested at two different temperature levels, subfreezing temperature of -50°C and room temperature ($\simeq 25°C$). Table 3.4 gives a detailed summary of the number of fatigue tests performed for each cross section, test temperatures, steel material types involved in the investigation, and the nominal slenderness ratios of the specimens. All specimens were supported at the ends through bolted connections and were tested until fatigue cracking occurred. Some tests were discontinued after the specimen exceeded the level of 10^6 cycles.

Prior to fatigue tests, static tension tests were performed on singly symmetric sections connected through one leg (90°-angle, 60°-angle, and lipped angle sections). These tests were conducted to determine the ultimate tensile capacities of the sections at room temperature, and to correlate the results with those obtained from theoretical finite element analysis. Percentages of the obtained ultimate capacities ($\simeq 17\%$ to 60%) were later used in fatigue testing of the specimens.

3.2 Specimen Description and Identification

All fatigue test specimens were galvanized, and their total length was 1500 mm. Holes of 17.5 mm (11/16") diameter were drilled at the ends of the specimens to connect it with the 12.7 mm (1/2") thick gusset plate through the use of properly tightened ASTM A490 structural bolts of 15.9 mm (5/8") diameter. Actual dimensions of each specimen together with out-of-plane and imperfection measurements were recorded in a pre-test observation sheet. Other information regarding the thickness and surface finish of the galvanizing coating, and the presence of initial flaws or defects were also included in the observation sheet.

A three-character designation system was used to identify test specimens and their category. The first character identifies the shape of the specimen as follows:

BA for plain 90°-angles, **BC** for 60°-angles, **BB** for lipped angles, **BG** for T-shaped sections, and **BN** for back-to-back channels section. The second character is the nominal slenderness ratio of the section $\frac{L}{r_{critical}}$. The third character refers to the number of the test specimen within its category. Specimens fabricated using steel type CAN/CSA-G40.21-M 300W were identified by a letter H preceding the identifying number.

3.3 Experimental Test Setups

Two test setups were employed in this study. The first setup was used in association with a Universal MTS testing machine of 5000 kN capacity. However, the second test setup was mounted inside an MTS-1000 kN capacity Universal testing machine, and was used only for testing back-to-back channels sections at room temperature ($\simeq$ 25°C). Pictures of the test setups are shown in Figures 3.2 and 3.3 respectively. Detailed explanation of these setups are given in the following subsections.

3.3.1 Test setup # 1

A schematic representation of test setup # 1 is illustrated in Figure 3.4. It mainly consisted of a cold chamber which could easily achieve and maintain a temperature

81

of -50°C. The chamber was mounted on a mobile table to provide easy access in and out of the MTS-5000 kN testing machine. The cold chamber had circular holes at its top and bottom ends in order to allow steel extension pipes with outside diameter of 168 mm ($6\frac{5}{8}$") and wall thickness of 14 mm ($\frac{9}{16}$") to pass through. The upper extension pipe was welded on one end to a 19 mm ($\frac{3}{4}$") thick plate, and the other end was welded to a steel pipe cap whose details are illustrated in Figure 3.5. A hole of 76 mm (3") diameter was threaded into the pipe cap where a matching threaded high alloy steel rod of the same diameter was used to connect the pipe cap to a load cell of 1000 kN capacity as shown in Figure 3.6. A similar steel rod was used to connect the load cell to the 102 mm (4") thick upper plate of the MTS-5000 kN capacity testing machine. Load cell rings were used to tighten and untighten the upper grip system.

Two lower grip systems were used with test setup # 1. The first system was employed for testing the plain 90°-angle and the 60°-angle sections. The maximum alternating fatigue load applied using this system was ±110 kN. The second system was used for alternating fatigue loads ranging from ±120 kN to ±350 kN. Figure 3.7 shows the first lower grip system which resembles the upper grip system except that the lower plate of the MTS machine was only 38 mm ($1\frac{1}{2}$") thick compared to 102 mm (4") thick upper plate.

The second lower grip system used with test setup # 1 is shown in Figure 3.8. The lower plate of the MTS machine was removed, and the pipe cap was welded to a 89 mm ($3\frac{1}{2}$") thick plate using 25 mm (2") size fillet weld. This plate was then gripped using the hydraulic wedge grip system of the MTS machine. In addition, a new plate was welded to the top of the extension pipe. This plate had a total of eight threaded holes with diameter of 19 mm ($\frac{3}{4}$") as shown in *section A-A* of Figure 3.8. Eight ASTM A325 structural bolts of 19 mm ($\frac{3}{4}$") diameter were used for this connection.

3.3.2 Test setup # 2

This setup was used for testing a total of ten back-to-back channel specimens at room temperature. Five of those were fabricated from ASTM A715 Grade 60 steel, whereas, the other five were fabricated from CAN/CSA-G40.21-M 300W steel. The test setup was mounted inside an MTS-1000 kN capacity Universal testing machine as illustrated in Figure 3.9. The cyclic loading frequencies for this group of tests ranged from 1.56 Hz to 2.60 Hz, and the alternating fatigue loads ranged from ±150 kN to ±375 kN.

Eight high strength bolts were used to connect the 1000 kN capacity load cell to a circular plate of 308 mm ($12\frac{1}{8}$") diameter and 146 mm ($5\frac{3}{4}$") thickness. Another

eight high strength bolts of 25.4 mm (1") diameter and 229 mm (9") length were used to connect the circular plate to a 76 mm (3") thick rectangular plate whose details are shown in Figure 3.10. Such assembly of plates were designed to ensure an even distribution of the load from the actuator of the testing machine to the specimen, and to prevent any localized failure of the connection.

The bottom part of the test setup is composed of a 51 mm (2") thick rectangular plate attached to the rigid floor through the use of six high strength Allan-Head bolts of 25.4 mm (1") diameter. Both the top and bottom plates (76 mm or 3" thick) were connected to stiffened angles placed back-to-back and separated by 12.7 mm ($\frac{1}{2}$") gusset plate. Figure 3.11 gives detailed dimensions of the stiffened top angles used with this test setup.

3.4 End Connections

The end connections were designed to simulate actual conditions experienced in transmission tower construction. ASTM A490 structural bolts of 16 mm ($\frac{5}{8}$") diameter were used to connect the specimen to the 12.7 mm ($\frac{1}{2}$") thick gusset plate. The number of bolts used for each shape was determined by preliminary capacity calculations based on the level of the applied fatigue load.

In order to ensure friction type (slip-critical) connections during cyclic loading, all bolts were properly tightened using the turn-of-nut method according to the ASTM Specifications for Structural Joints Using A325 or A490 Bolts (1988). When properly implemented, turn-of-nut method provides more uniform tension in the bolts than does the torque-controlled tensioning method because it is primarily dependent upon bolt elongation into the inelastic range.

For the purpose of accommodating the variety of cold-formed section shapes used in this investigation, several types of end supports were employed. The experimental program involved the use of six different connection types (A, B, C, D, E, and F) for test setup # 1, and one connection detail (Type G) for test setup # 2. Table 3.5 illustrates the type of connection used with each test series, the number of specimens tested, and the test setup type.

In connecting singly symmetric sections (90°-angle, 60°-angle, and lipped angle sections), a channel extension was connected to the gusset plate as shown in Figure 3.12. This extension was used in order to allow for easy replacement and to minimize the event of damage for the gusset plate. Connection types A and B were used for testing singly symmetric sections connected through one leg as shown in Figures 3.13 and 3.14 respectively. However, for angles connected through both legs,

connection types C and D were utilized. Details of these connections are illustrated in Figures 3.15 and 3.16. The lug angle used for transmitting the load was a plain rolled section ($76 \times 76 \times 9.5$ mm or $3 \times 3 \times \frac{3}{8}$") for the case of the 90°-angle and the lipped angle sections. A built-up angle was used to accommodate the 60°-angle section as shown in Figure 3.16. For this particular section, the bolts were placed in a staggard orientation because of the difficulty of placing any two bolts on one horizontal line.

The gusset plate used to connect the T-shaped (BG) section is shown in Figure 3.17. Three bolts were used to connect the webs of the section to the gusset plate. Moreover, clip angles were used to connect the flanges of the section to the gusset plate using two bolts for each flange. Due to the long flange lips of the section, the web holes could not be drilled in the center of gravity of the section. This resulted in eccentrically applied loads which caused several failures at the bottom weld section of the connection.

Connection type F was used in testing five back-to-back channels sections at a temperature of -50°C. Four vertical angles were welded to both the gusset plate and the base plate as shown in Figure 3.18. These angles were used to stiffen the gusset plate and strengthen the horizontal bottom weld section of the connection.

The top and bottom connections used with test setup # 2 are shown in Figures 3.19 and 3.20 respectively. For these connections, back-to-back stiffened angles were used to connect the gusset plate to the base plate through the use of ASTM A490 structural bolts of 25.4 mm (1") diameter. A picture of the top connection is shown in Figure 3.21. In addition, four vertically oriented angles were used with each connection (top and bottom) to stiffen the gusset plate and prevent it from bending at the end section.

3.5   Instrumentation

The instrumentation mainly consisted of five Linear Variable Differential Transducers (LVDT's). Four of these were horizontally oriented at the mid-height section of the specimen to record the lateral displacements. The fifth LVDT was located at the bottom end of the specimen in a vertical position to measure any relative displacement between the gusset plate and the specimen. In testing some back-to-back channels sections, the fifth LVDT was mounted horizontally at the bottom end of the specimen in order to record the lateral movement of the flange tips during cyclic loading. Figure 3.22 illustrates the locations of the LVDT's for the various cross sections.

Electrical resistance strain gauges with 5mm gauge length, and 350 Ω resistance, were mounted on the test specimen at the top and bottom connections as shown in Figure 3.23. These gauges were used to monitor the cyclic stress strain behaviour at several intervals of the fatigue life. The vertical centerline of the gauges was located 25 mm apart from the center of the end hole. However, the horizontal centerline of the gauges was coinciding with the extremity of the end hole of the specimen where most fatigue failures occurred. Considering the 60°-angle section, several failures were observed at a horizontal plane 60 mm apart from the mid-height section of the specimen. Consequently, strain gauges were placed at that hot spot location.

An amplifier was used in conjunction with the strain gauges to eliminate any noise in the signal. Moreover, the test temperature was continuously monitored through the use of a thermocouple attached directly to the specimen. The data was recorded through the use of an automatic data acquisition system.

3.6 Test Procedures

Fatigue test procedures could be summarized in the following sequence:

1. The average dimensions of each specimen was accurately recorded together with out-of-straightness and initial imperfections. In addition, locations of

irregular surface conditions, and visually apparent defects were also included in the observation sheet of the specimen.

2. Electrical resistance strain gauges were mounted on the test specimen at the top and bottom connections to monitor the cyclic stress strain behaviour. An amplifier was used in conjunction with the gauges to eliminate any noise in the signal.

3. The specimen was vertically aligned in the testing machine as shown in Figure 3.24.

4. Four Linear Variable Displacement Transducers (LVDT's) were placed at the mid-height section to record the translations and rotations during cyclic loading. A fifth transducer was vertically mounted at the specimen's end to record any relative displacement between the gusset plate and the specimen as illustrated in Figure 3.25.

5. A triangular load-control test program with load ratio of -1 was prepared using a Microprofiler built inside the MTS machine. The obtained signal was checked using an electronic osscillioscope before hydraulic was applied to the testing machine.

6. The test data were recorded through the use of an automatic Data Acquisition system. (Validyne UPC 607 A/D)

7. For low temperature tests, the specimen's temperature was continuously monitored by a thermocouple. Assurance was made that the test would never start before a steady temperature of -50°C had been maintained.

Table 3.1

Average Measured Cross Sectional Dimensions

Section[a]	Dimensions (mm)							
	A	B	B'	B_1	C	S	r	t
BA		71.23	63.28				4.00	3.95
HBA		70.70	61.90				4.30	4.50
BC		83.40	65.50				6.50	4.00
HBC		86.40	70.40				4.75	4.50
BB		83.60	64.70		30.80		5.23	4.22
HBB		78.90	62.10		24.70		3.98	4.42
BG	131.70	52.60		52.30	14.50	13.60	6.80	4.20
BN	112.10	74.70	51.00		15.50	12.70	6.85	5.00
HBN	106.10	66.00	46.00		24.40	12.70	5.50	4.50

[a] Cross sectional shapes are shown in Figure 3.1.

Table 3.2

Tensile Strength (MPa)

Section [a]	Specified Strength	Coupon Yield Strength	
		Galvanized	Ungalvanized
BA	415	469	424
BC	415	477	434
BB	415	445	418
BG	415	438	419
BN	300	481	434
HBA	300	409	289
HBC	300	415	315
HBB	300	418	311
HBN	300	401	290

[a] Cross sectional shapes are shown in Figure 3.1.

Table 3.3

Average Section Properties

Section[a]	A	I_x	I_y	J	C_w	r_x	r_y
	mm^2	$10^3 mm^4$	$10^3 mm^4$	mm^4	mm^6	mm	mm
BA	530	434	98	2759	0.00	28.6	13.6
HBA	603	481	112	4073	0.00	28.2	13.6
BC	595	346	201	3173	0.00	24.1	18.4
HBC	700	423	260	4725	0.00	24.6	19.3
BB	787	1132	327	5174	331	37.9	20.4
HBB	822	942	327	5353	190	33.8	20.0
BG	1925	3377	3319	10266	3604	41.9	41.5
BN	2564	5115	4395	21368	4354	44.7	41.5
HBN	2300	3966	3850	15531	5538	41.5	40.9

[a] Cross sectional shapes are shown in Figure 3.1.

Table 3.4

Number of Fatigue Test Specimens

Section		BA $<$ Th.= 4 mm		BC $<$ Th.= 4 mm		BB $<$ Th.= 4 mm		BG Th.= 4 mm		BN [b] Th.= 5 mm	
		No.	Length (mm)	No.	Length (mm)	No.	Length (mm)	No.	Length (mm)	No.	Length (mm)
ASTM A 715 Grade 60	ROOM TEMP.	13[a]	1500	13[a]	1500	8[a]	1500	3	1500	5	1500
	TEMP. -50 C										
	TOTAL = 42										
CAN / CSA G 40.21-M 300W	ROOM TEMP.								HBN	5	1500
	TEMP. -50 C								HBN	5	1500
	TOTAL = 10										
Nominal Slenderness Ratio (L/r)		109		81		70		36		36 - 37	

[a] Three specimens were tested with both legs connected.

[b] No. of specimens for "BN" and "HBN" sections refers to a section composed of 2 channels.

Table 3.5

Type of Connection Used with Each Test Series

Test Series			Steel Type	Number of Specimens	Test Setup	Connection Type
90°- angle section	(BA)	(One leg connected)		10	# 1	A
60°- angle section	(BC)	(One leg connected)		10	# 1	A
Lipped angle section	(BB)	(One leg connected)		5	# 1	B
90°- angle section	(BA)	(Both legs connected)	ASTM A715 Grade 60	3	# 1	C
60°- angle section	(BC)	(Both legs connected)		3	# 1	C
Lipped angle section	(BB)	(Both legs connected)		3	# 1	D
T - Shaped section	(BG)			3	# 1	E
Back-to-Back Channel section	(BN)			5	# 2	G-Top & G-Bottom
Back-to-Back Channel section	(HBN)		CAN / CSA	5	# 2	G-Top & G-Bottom
Back-to-Back Channel section	(HBN) [a]		G40.21-M 300 W	5	# 1	F

[a] This series of tests were conducted at -50°C.
All other tests were conducted at room temperature (25 $^{\circ}$C)

BA and HBA

BC and HBC

BB and HBB

BG

BN and HBN
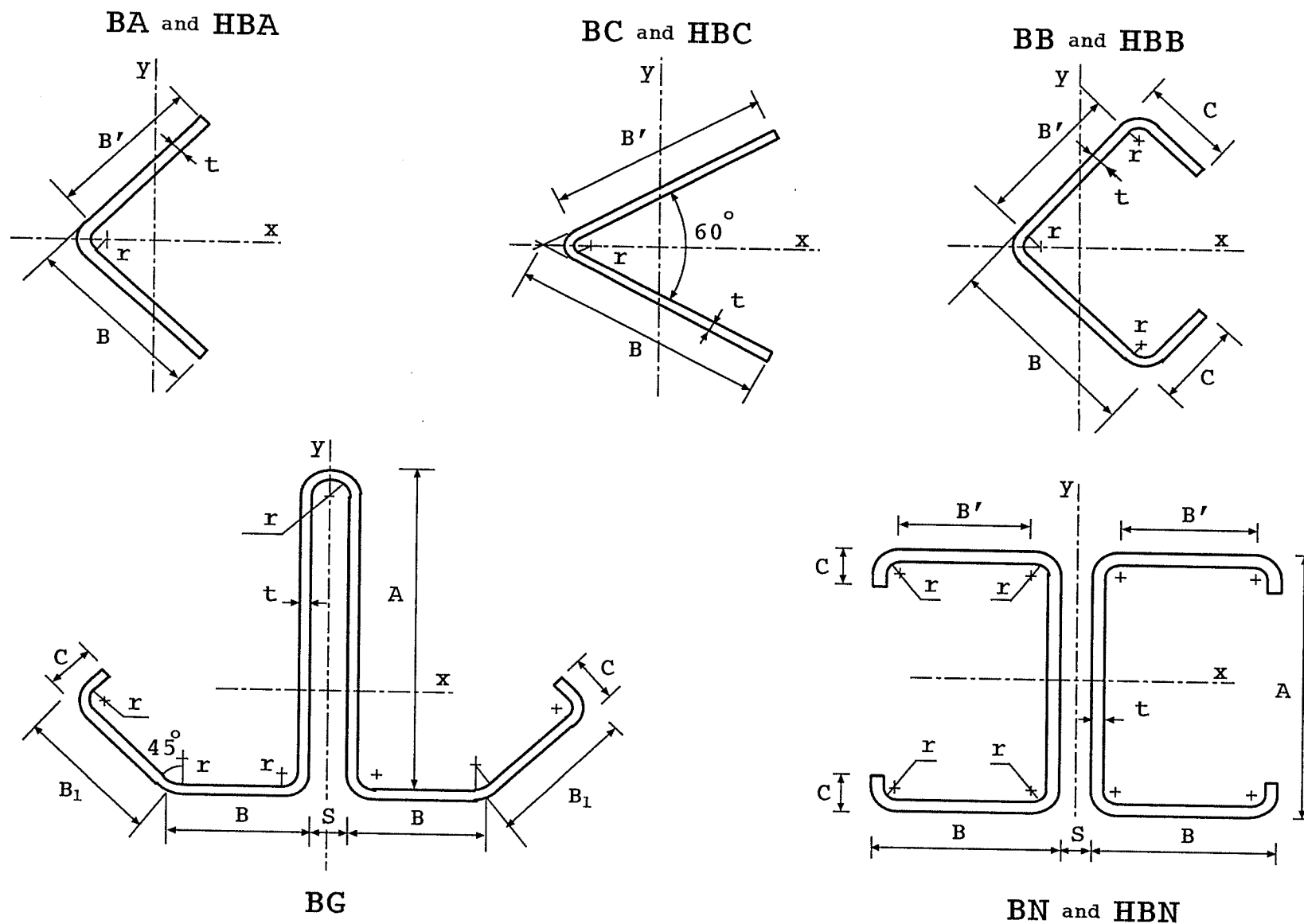
Figure 3.1 : Nominal Cross Sectional Dimensions.
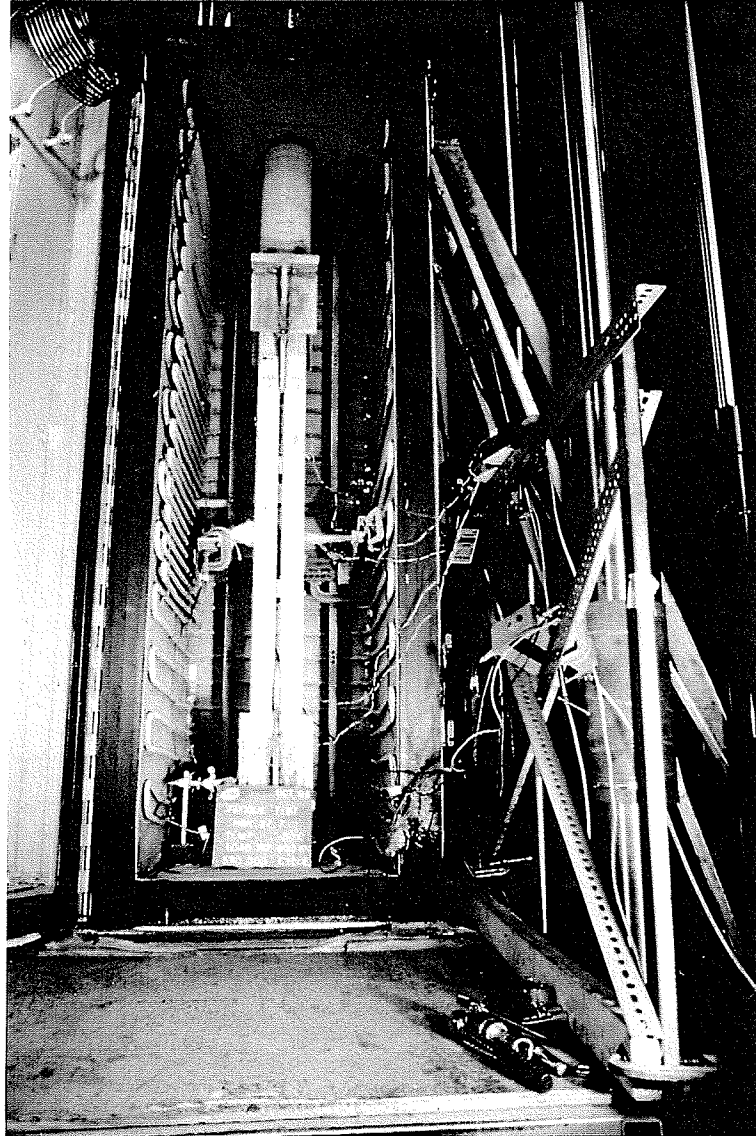
Figure 3.2: Fatigue Test Setup # 1.
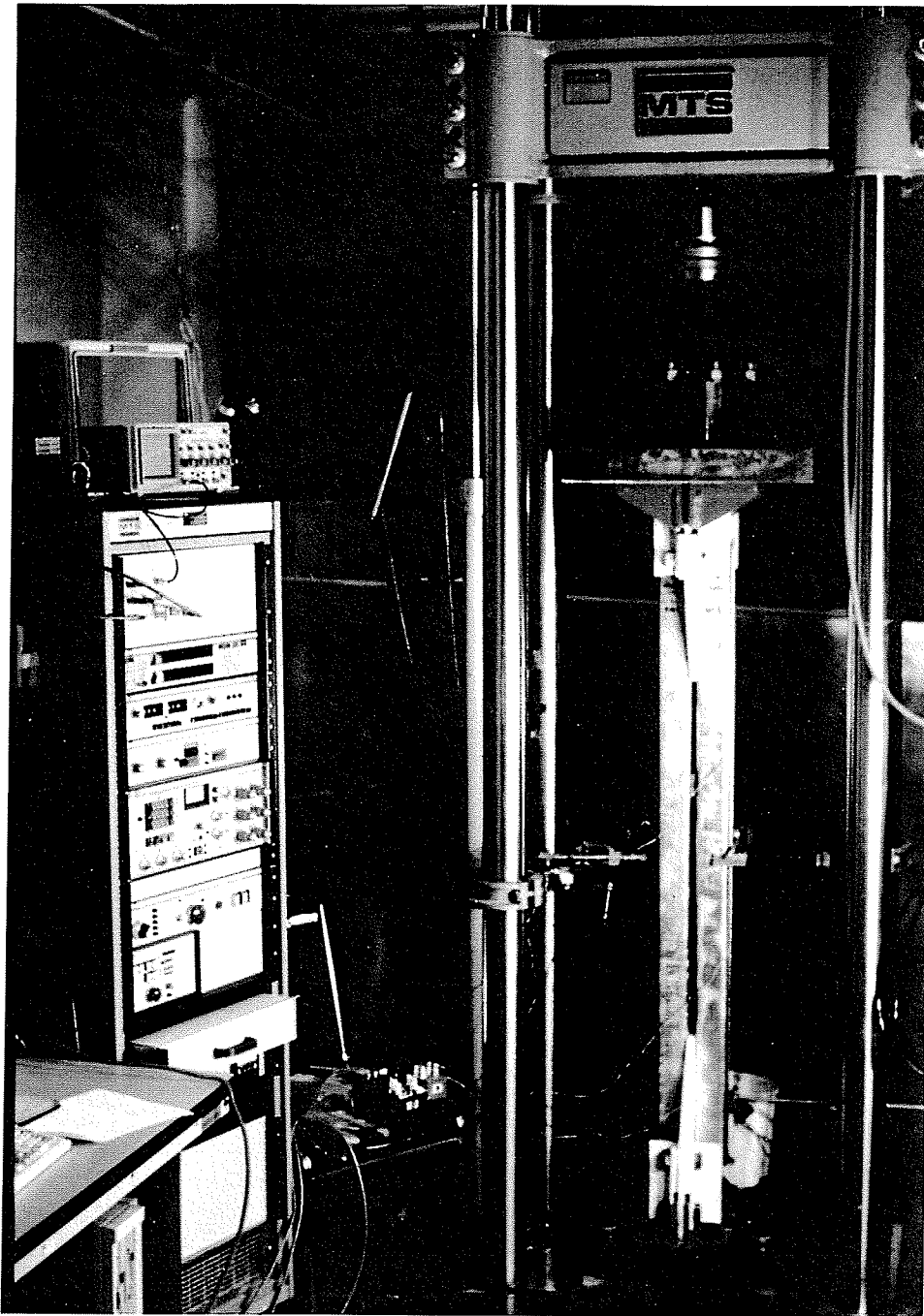
Figure 3.3: Fatigue Test Setup # 2.

Load Cell (Capacity 1000 kN)

Cooling Chamber
(101.6 mm th. insulating material)

(3517.90)

Upper Extension Pipe
(168.3 mm O.D. - 14.3 mm th.)

Test Specimen (1500 mm)

Lower Extension Pipe
(168.3 mm O.D. - 14.3 mm th.)

Plywood 38.1 mm th.

(863.60)

Hydraulic Wedge Grip System

(0.00)

292.1 101.6
1676.4
101.6
2438.4 mm
1500
1079.5 mm
406.4 101.6
355.6

101.6 609.6 101.6

HSS 50.8 x 50.8 x 3.18

1016 mm

Schematic of Fatigue Test Set-up # 1

14.30

76.20

168.30

139.70

14.30

76.20

Threaded Depth = 2.291 mm

Inside Diameter = 73.914 mm

Weld size = 14 mm

Pipe wall

45°

7.15

1.59

Threaded portion 76.20 mm Diam.
12 Track per inch

14.30

14.30

168.30 mm

Figure 3.5 : Pipe Cap Detail for Test Setup # 1.

100

PL. 101.60 mm th.

57.15 mm

27.00 mm

63.50 mm

38.10 mm

Load Cell Rings

Load Cell (1000 kN Capacity)

Threaded High Alloy Steel Rods
76.20 mm Diam. & 228.60 mm length

Cold Chamber
(Insulating Material 101.60 mm th.)

Pipe Cap
(Details shown in Figure 3.5)

Weld Size = 14 mm

PL. 200 x 300 x 19.05 mm th.

Upper Extension Pipe
168.30 mm O. Dia. & 14.30 mm th.

Test Specimen
(Total Length = 1500 mm)
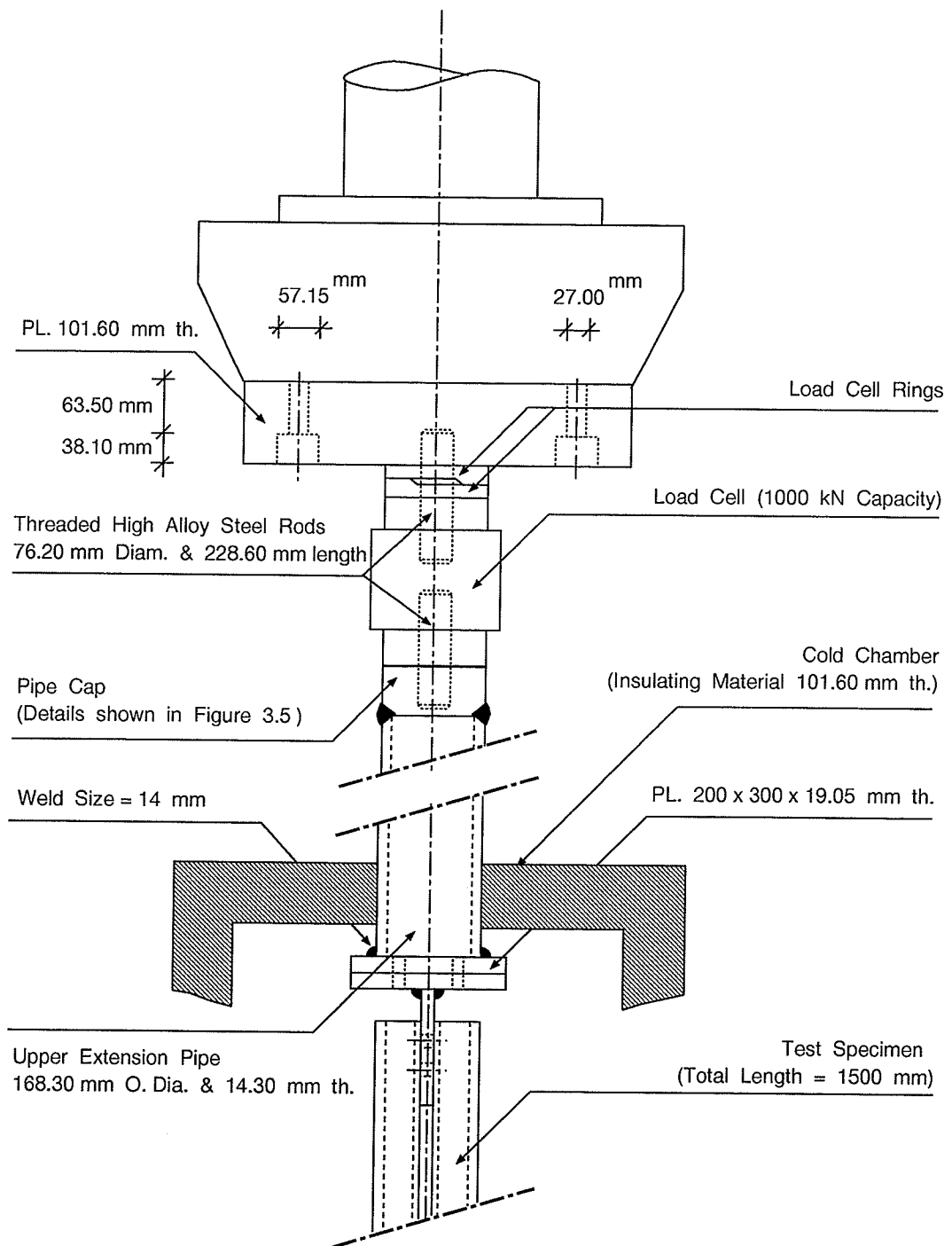
Figure 3.6 : Upper Grip System for Test Setup # 1.

101

Test Specimen

Cooling Chamber
Insulating Material (101.6 mm th.)

Lower Extension Pipe
168.3 mm O. Diam. & 14.30 mm th.

Plywood 38.1 mm th.

38.10

76.20   406.40   76.20

558.80

Pipe cap
(Details shown in Figure 3.5)

280

40 72.5   55   72.5 40

19.05 mm

weld size = 14 mm

58.65

200   82.70

58.65

SEC. A-A

19.05

374.65

weld size = 14 mm

A   A

76.20

38.10

76.20   304.80   76.20

457.20
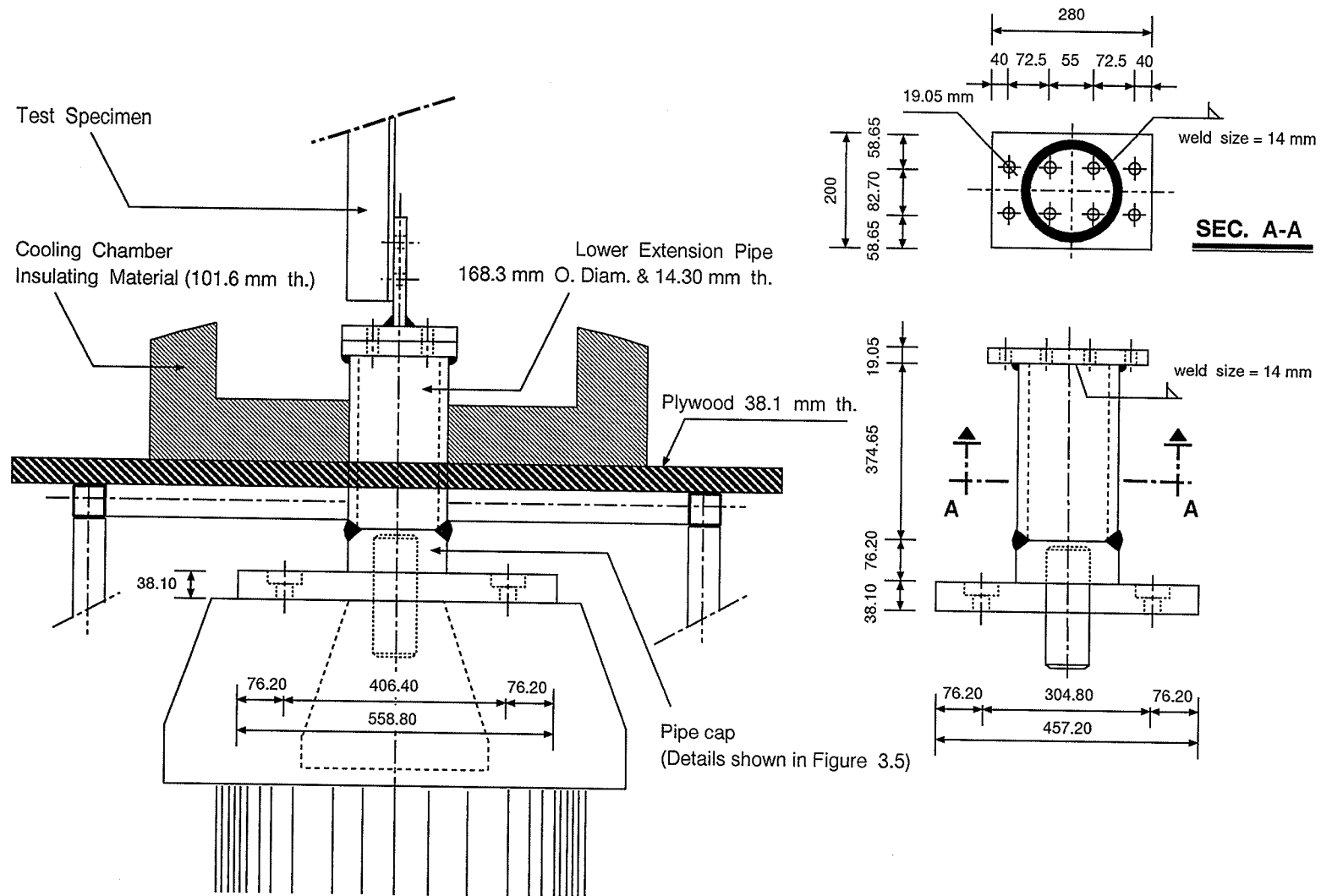
Figure 3.7 :   First Lower Grip System Used with Test Setup # 1.
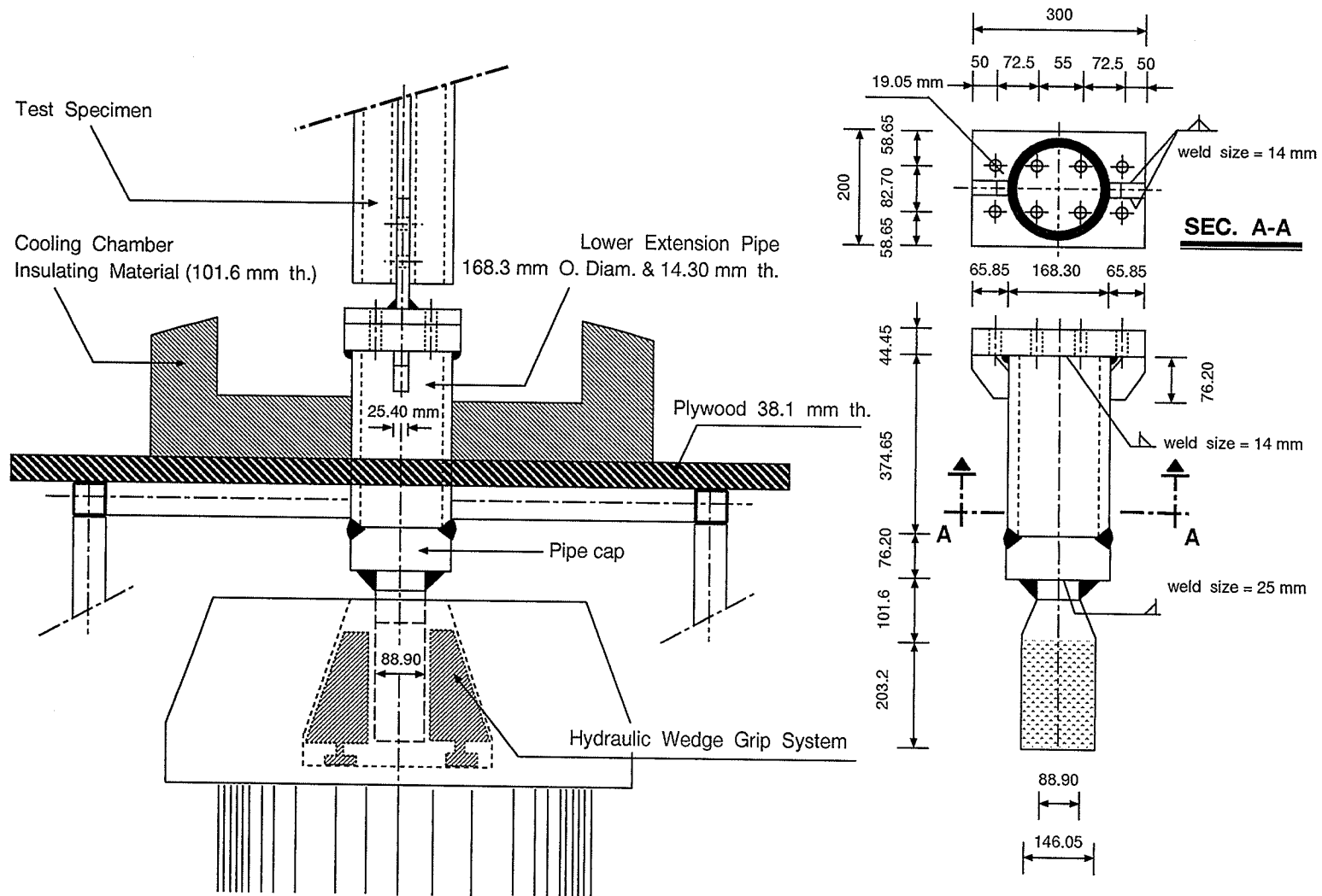
Figure 3.8 : Second Lower Grip System Used with Test Setup # 1.
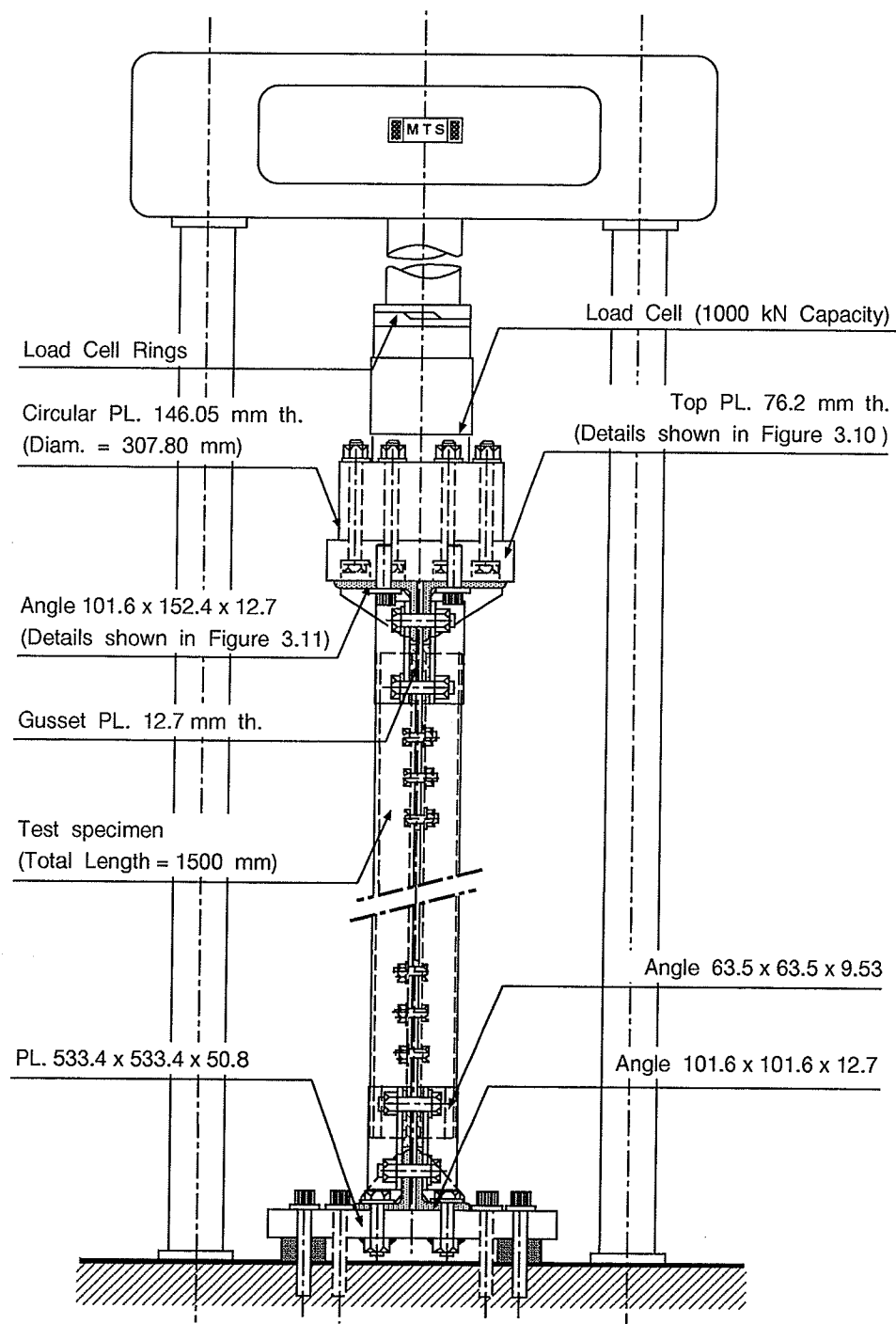
Figure 3.9 : Schematic of Fatigue Test Setup # 2
Used with the 1000 kN- MTS Testing Machine.
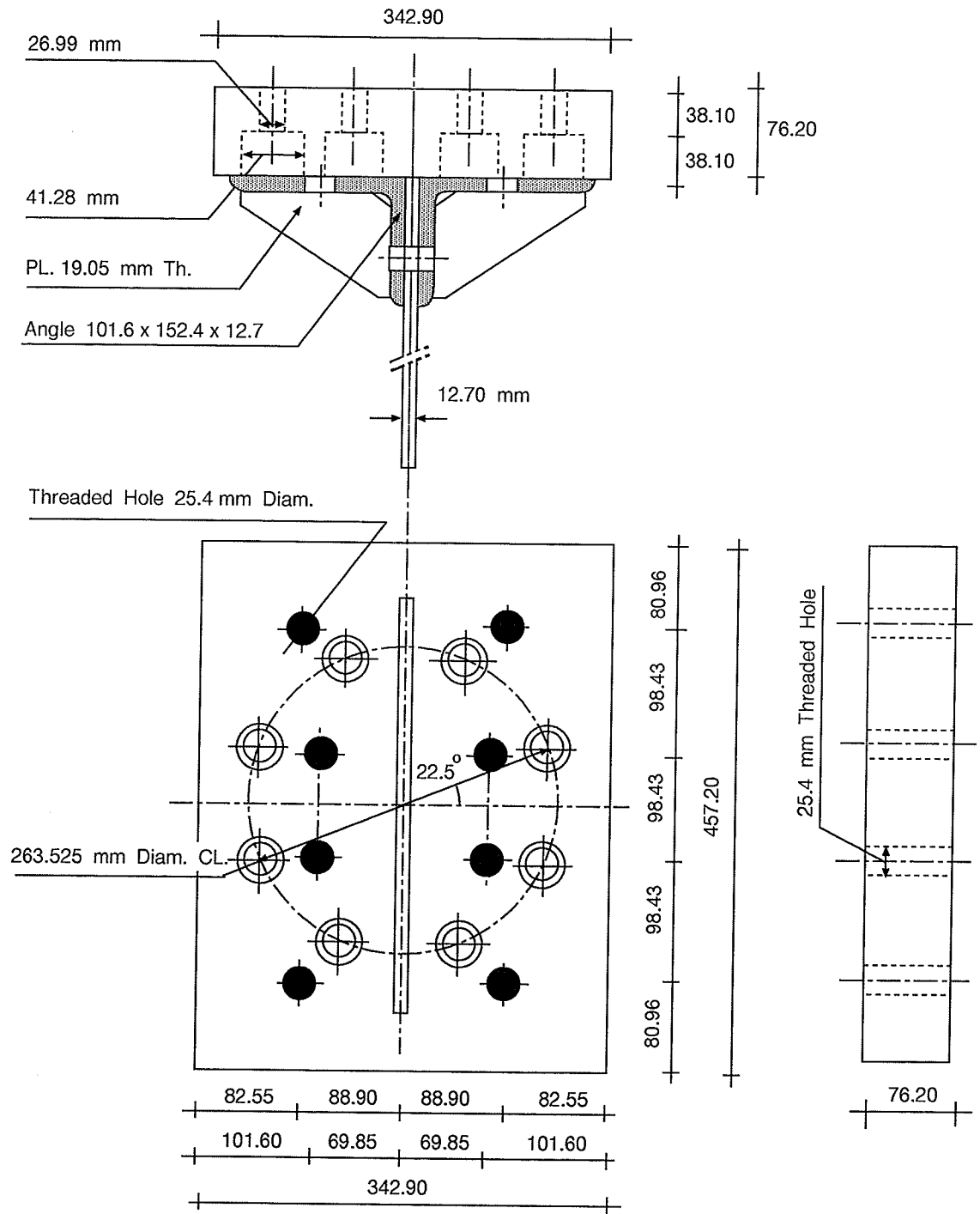
Figure 3.10 : Details of Top Plate Used with Test Setup # 2.

105
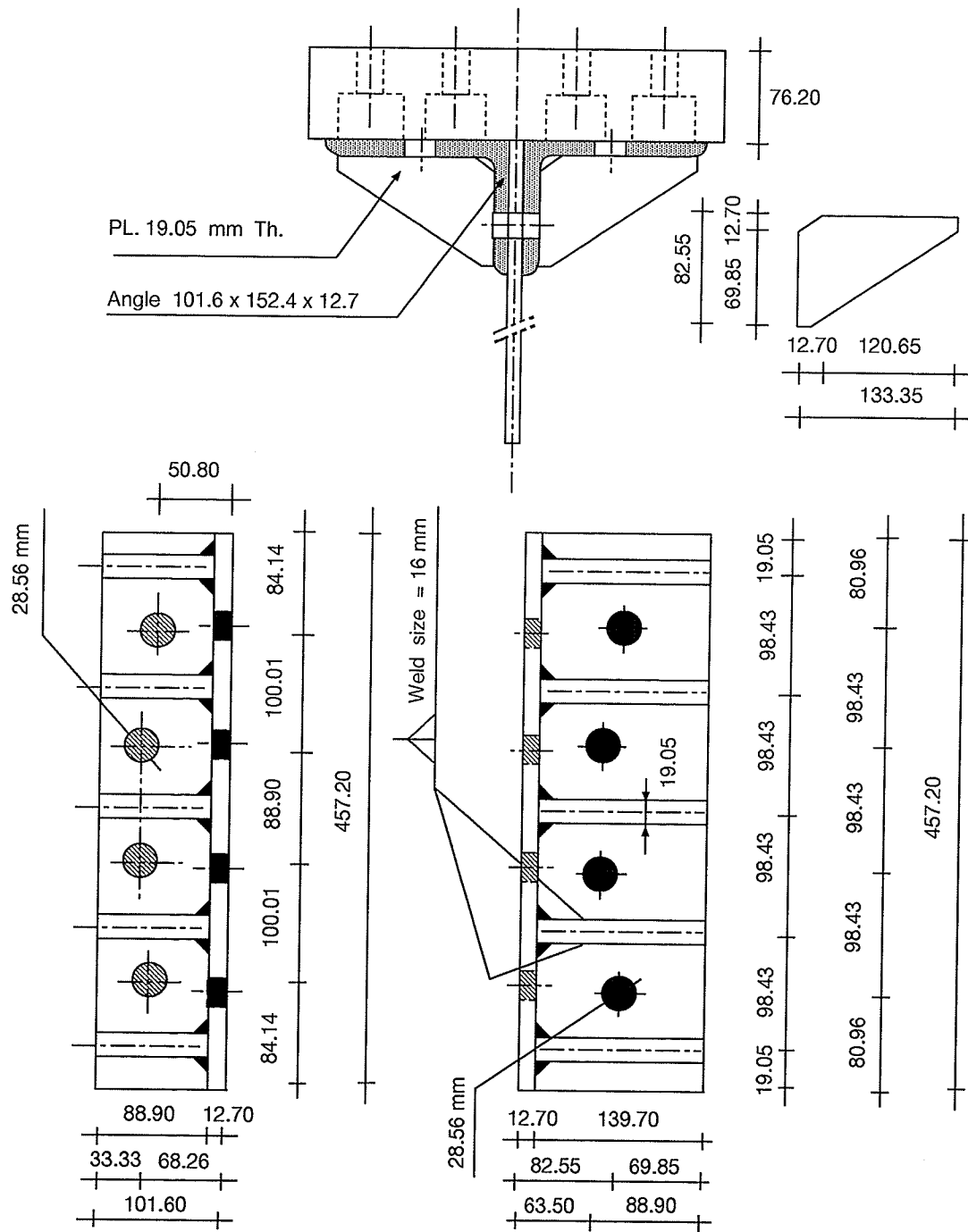
Figure 3.11 : Details of Top Angles Used with Test Setup # 2.

106

Figure 3.12: End Connection Used for Testing Singly Symmetric Sections.

CHANNEL sec.   Web 254 x 9.525
FL. 76.2 x 15.875

Weld size = 10 mm

Hole Diam. = 20 mm

ASTM A490 High-Strength Bolts
15.88 mm Diam. (5/8")

SCALE 1: 50
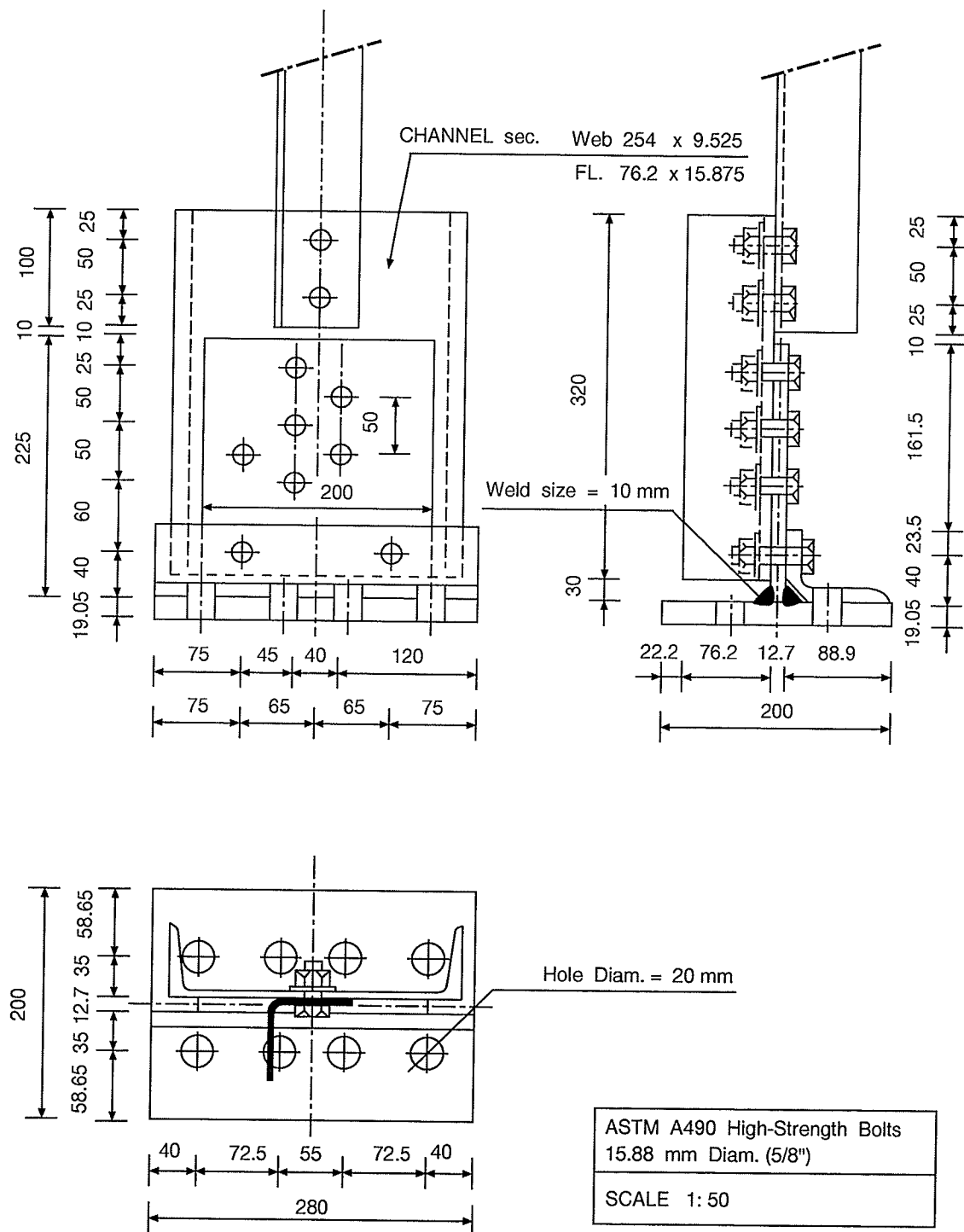
Figure 3.13 : Connection Type " A " Used with Test Setup # 1.

CHANNEL sec.   Web 254 x 9.525
FL. 76.2 x 15.875

Weld size = 10 mm

Hole Diam. = 20 mm

ASTM A490 High-Strength Bolts
15.88 mm Diam. (5/8")

SCALE 1: 50
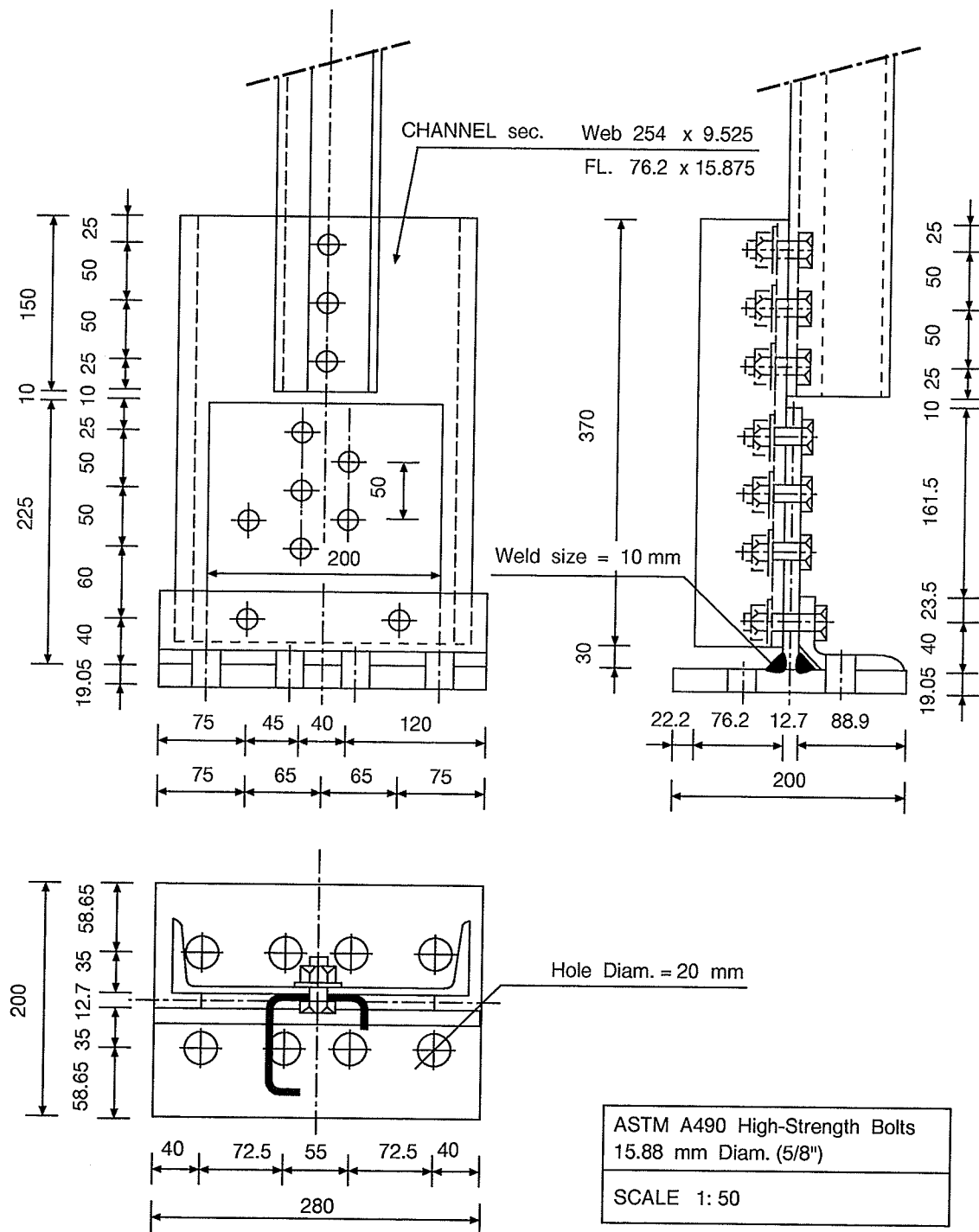
Figure 3.14 : Connection Type " B " Used with Test Setup # 1.

109
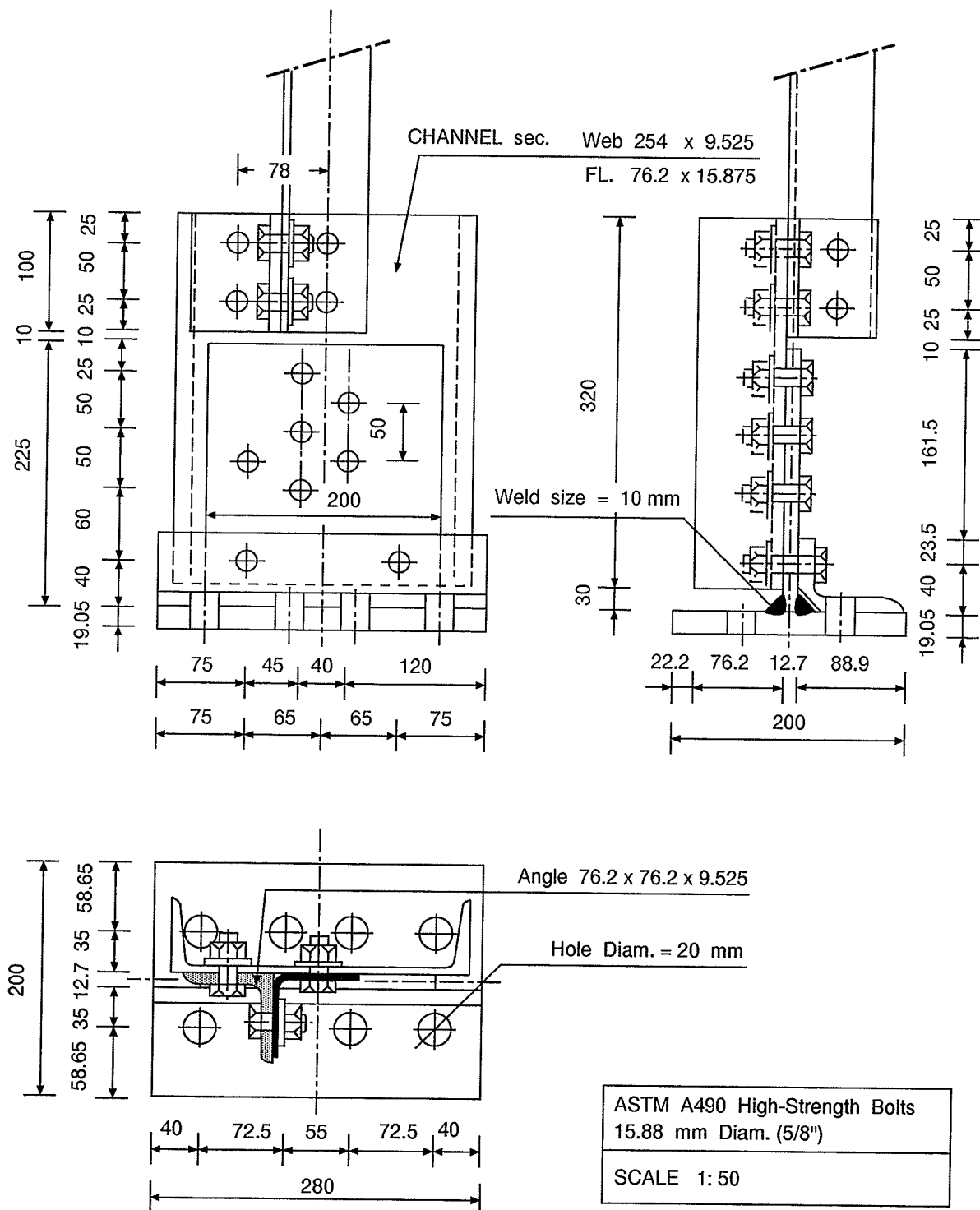
Figure 3.15 : Connection Type " C " Used with Test Setup # 1.

110
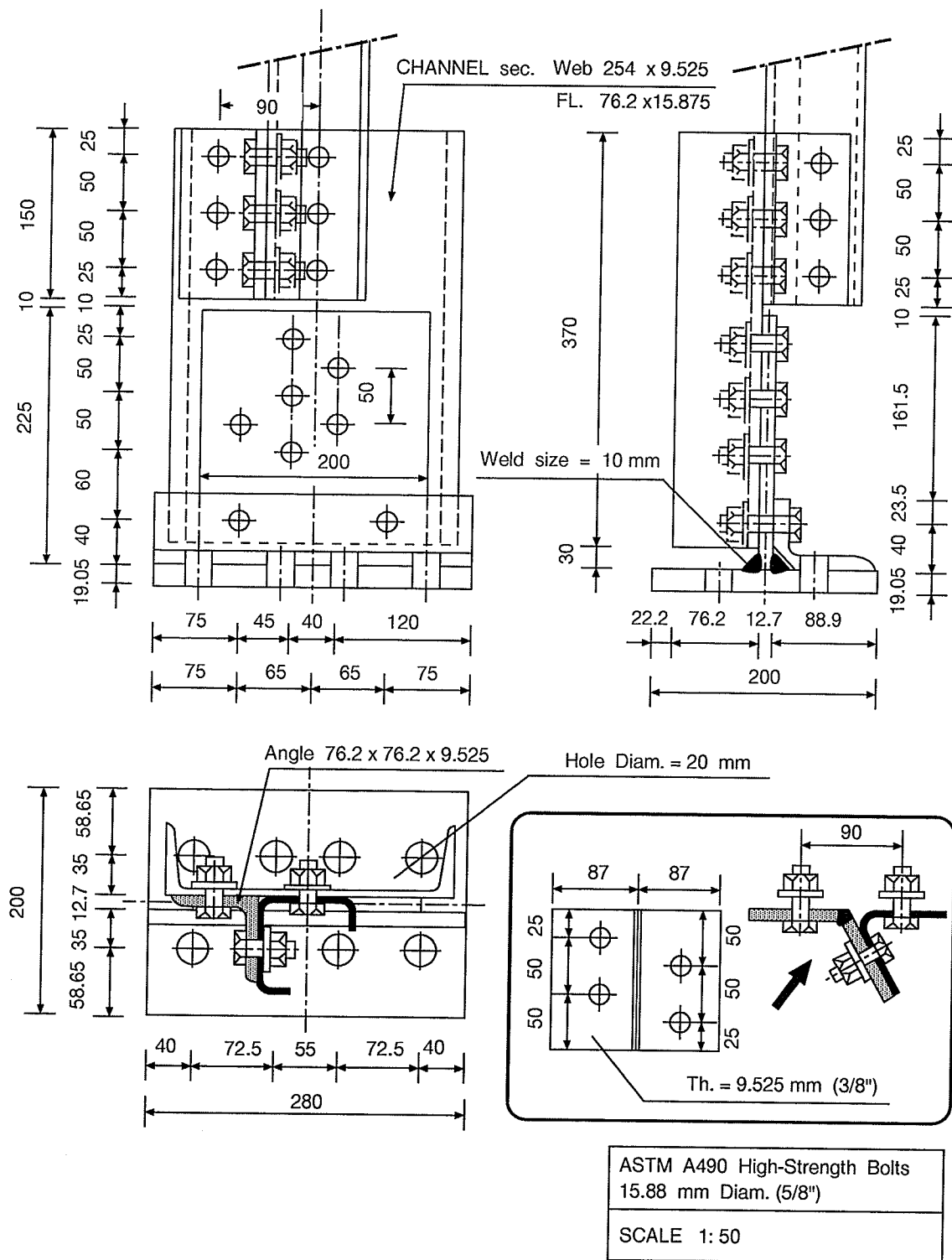
Figure 3.16 : Connection Type " D " Used with Test Setup # 1.

111

Weld size = 10 mm

Angle 76.2 x 76.2 x 9.525

Hole Diam. = 20 mm

ASTM A490 High-Strength Bolts
15.88 mm Diam. (5/8")

SCALE 1: 50
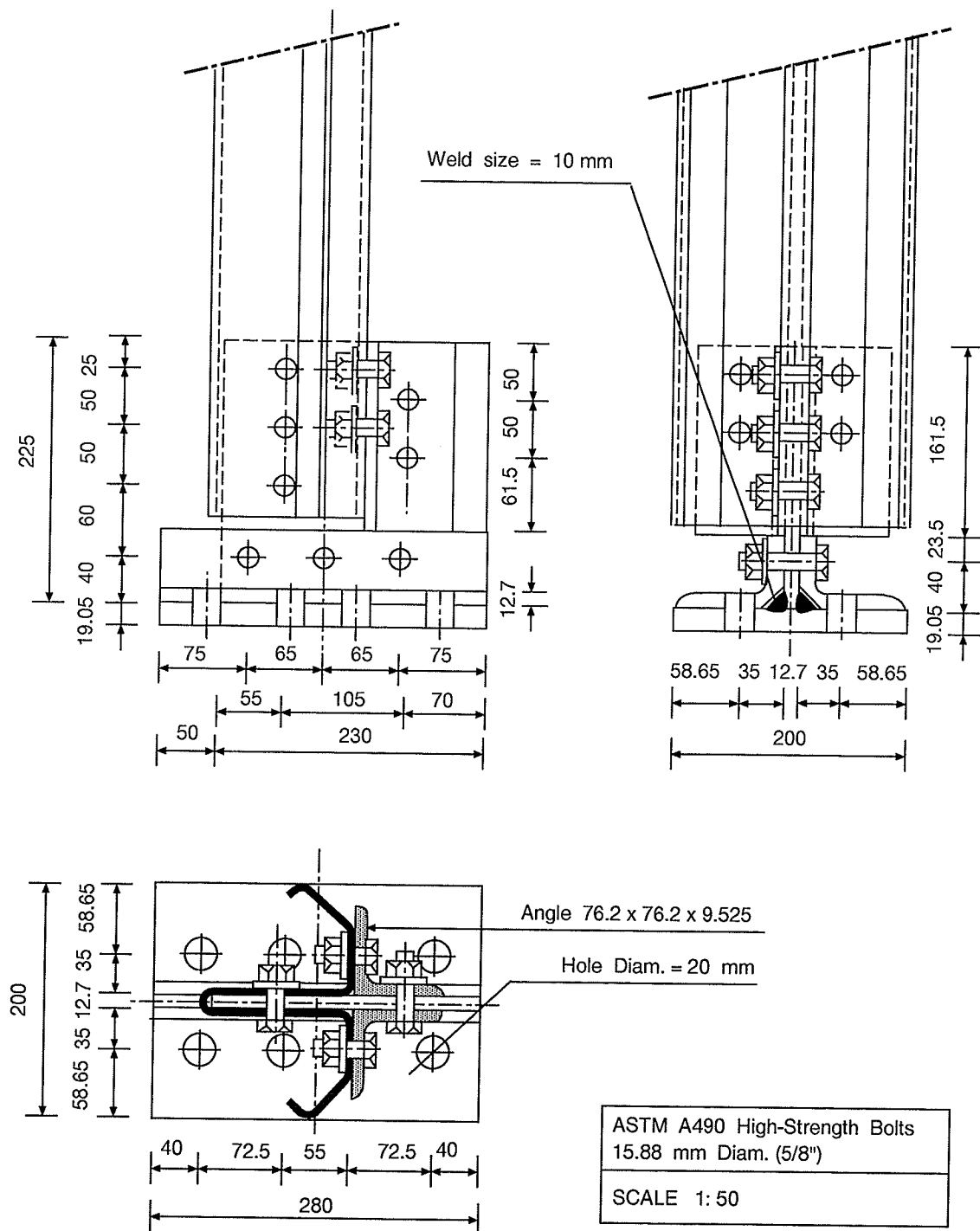
Figure 3.17 : Connection Type "E" Used with Test Setup # 1.

112
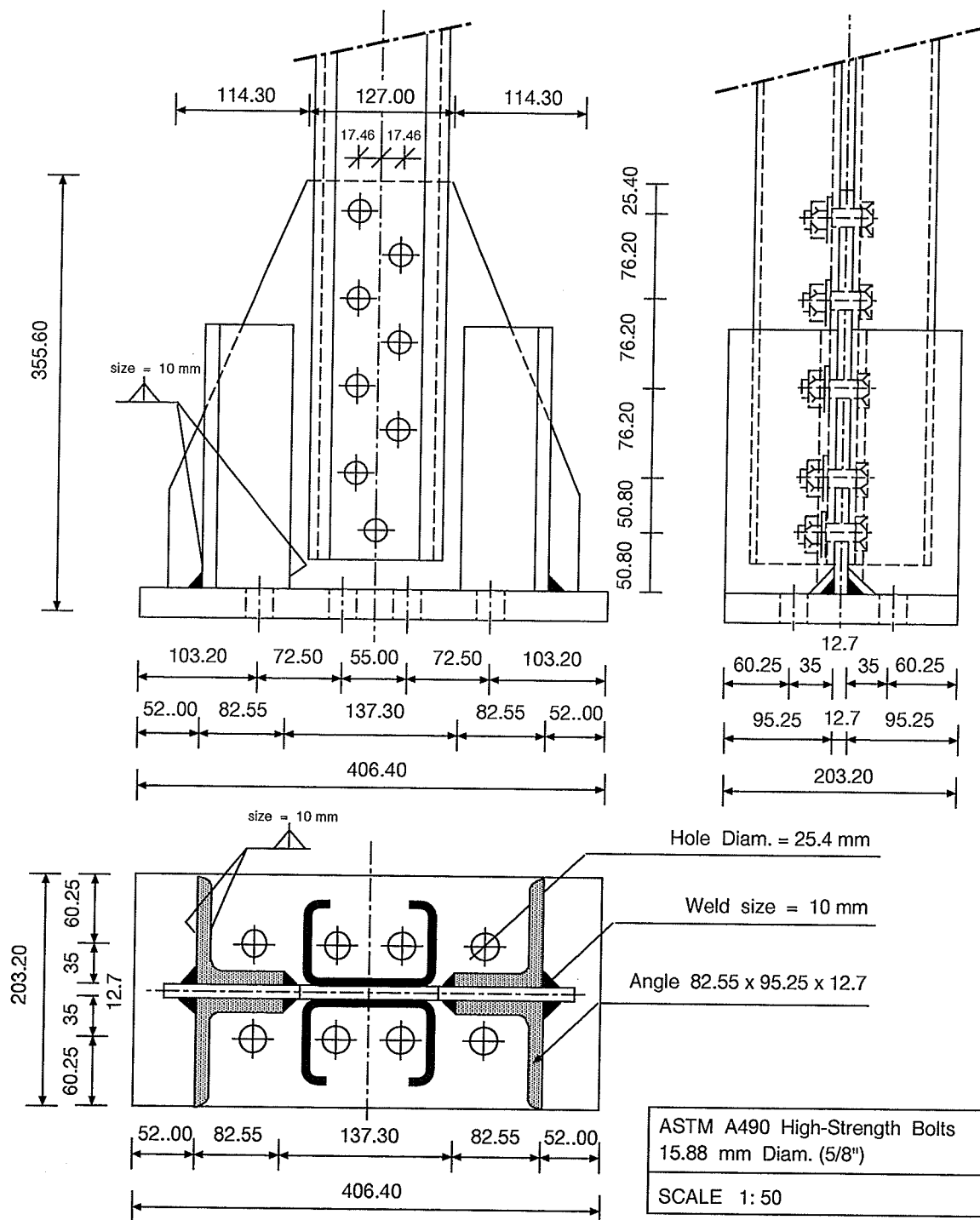
Figure 3.18 : Connection Type "F" Used with Test Setup # 1.
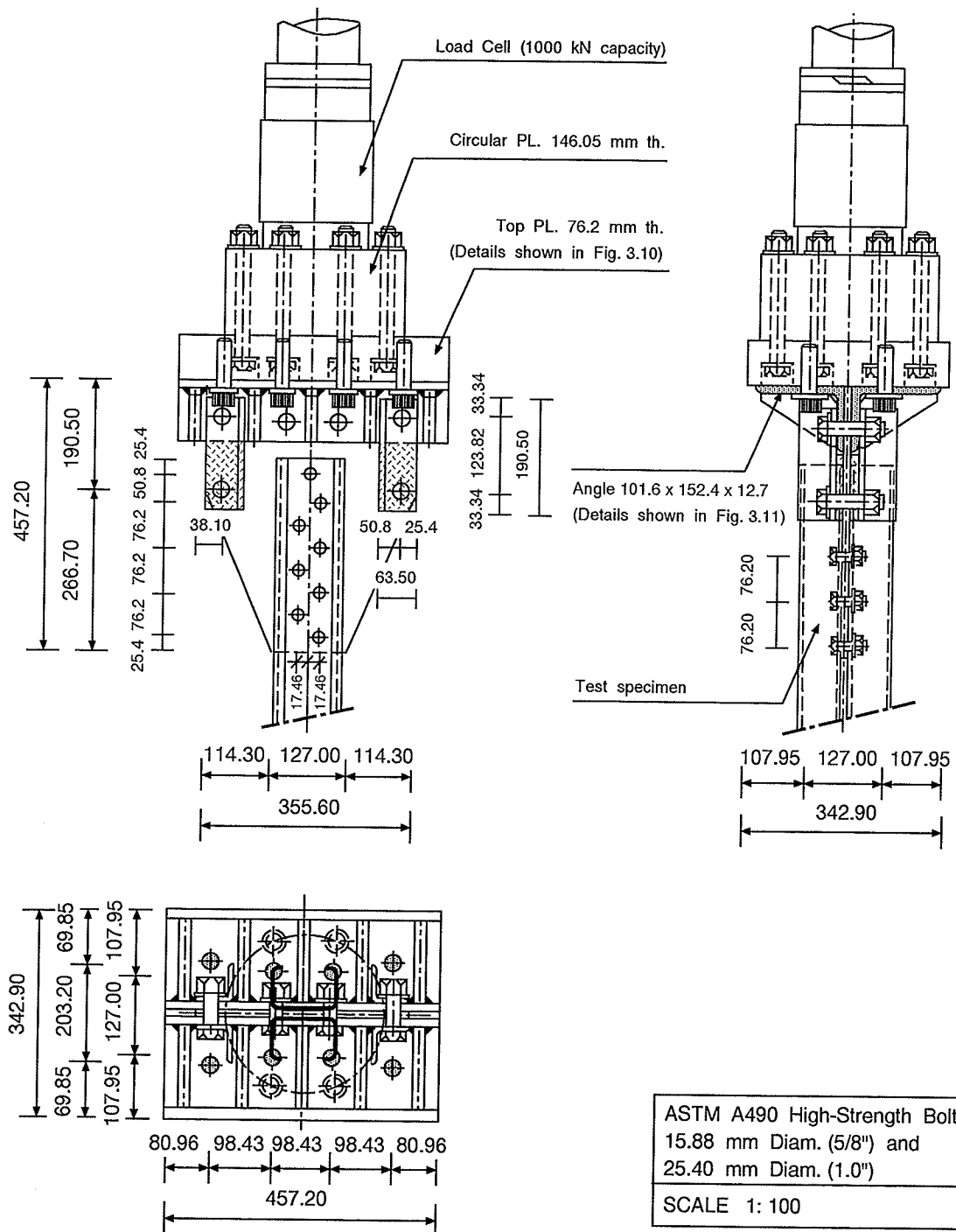
Figure 3.19 : Connection Type " G - Top " Used with Test Setup # 2.

114
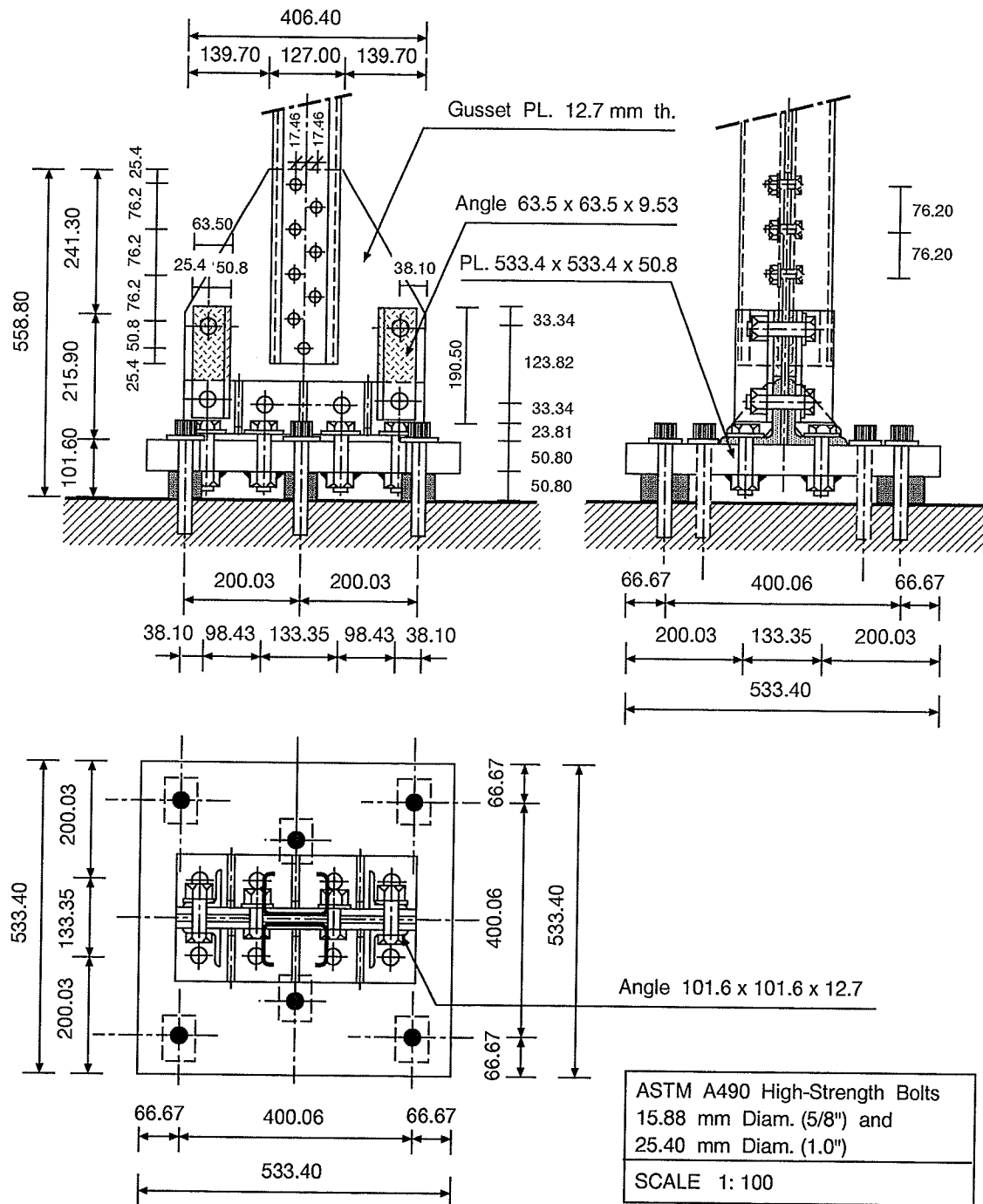
Figure 3.20 : Connection Type " G - Bottom " Used with Test Setup # 2.

115
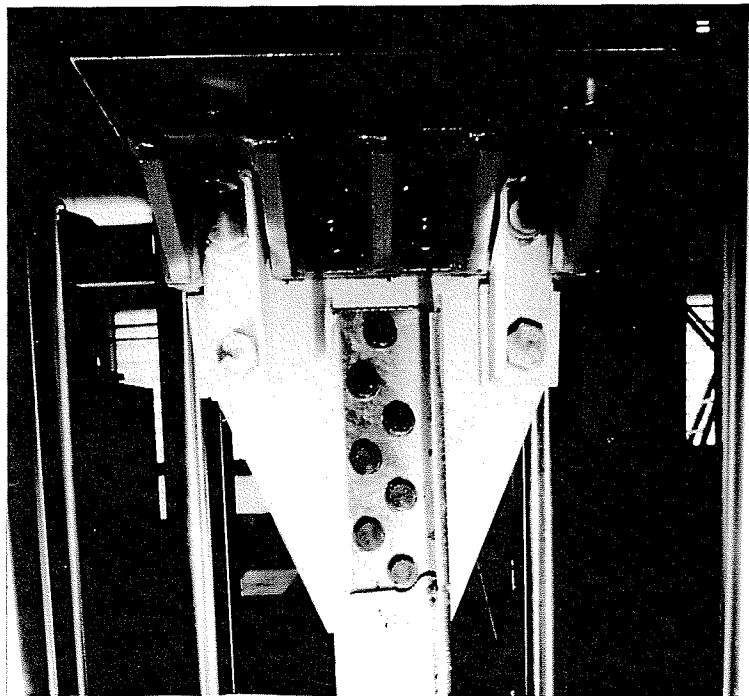
Figure 3.21: End Connection Used for Testing Back-to-Back Channel Sections.

BA   BC   BB   BG   BN

(a) Mid-Height Section.

CASE 1

(b) Bottom End Section.

CASE 2
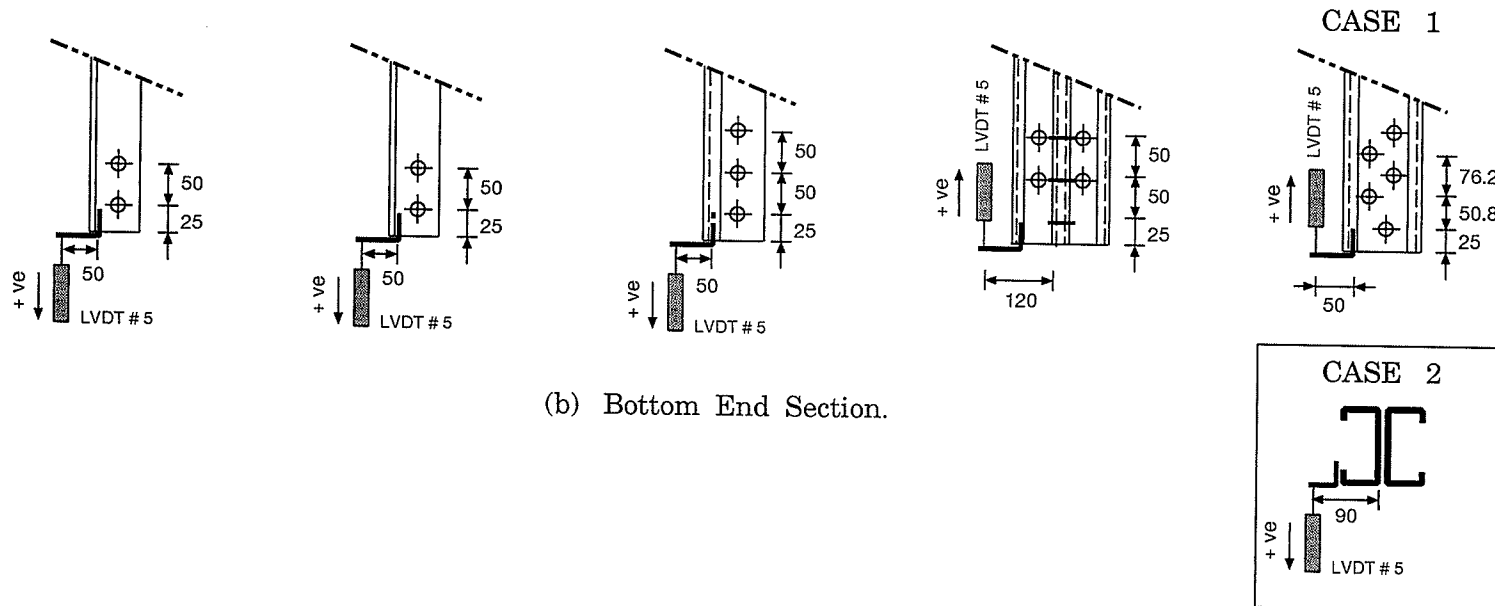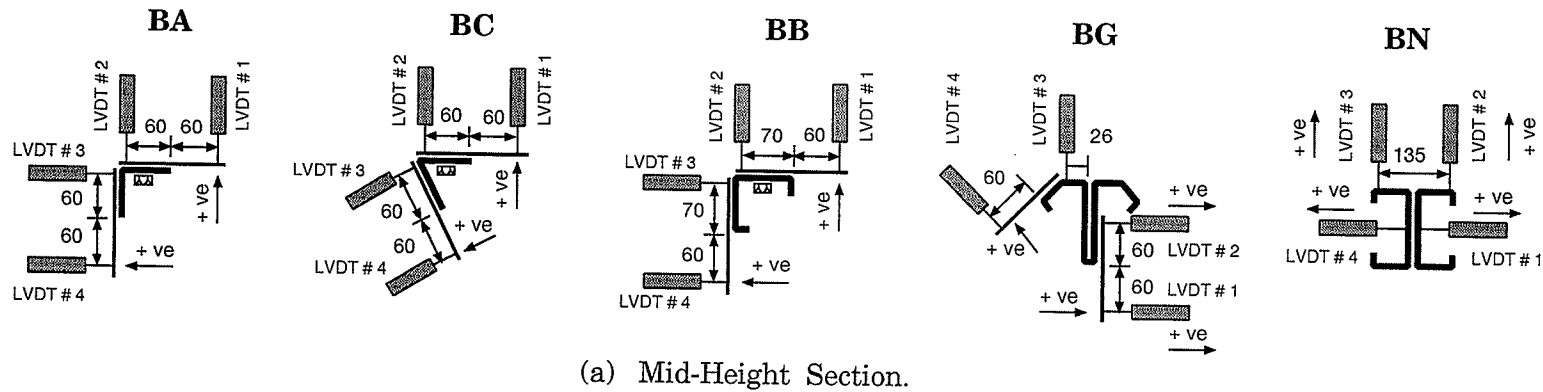
Figure 3.22 : Location of LVDT's for the Various Cross Sections.
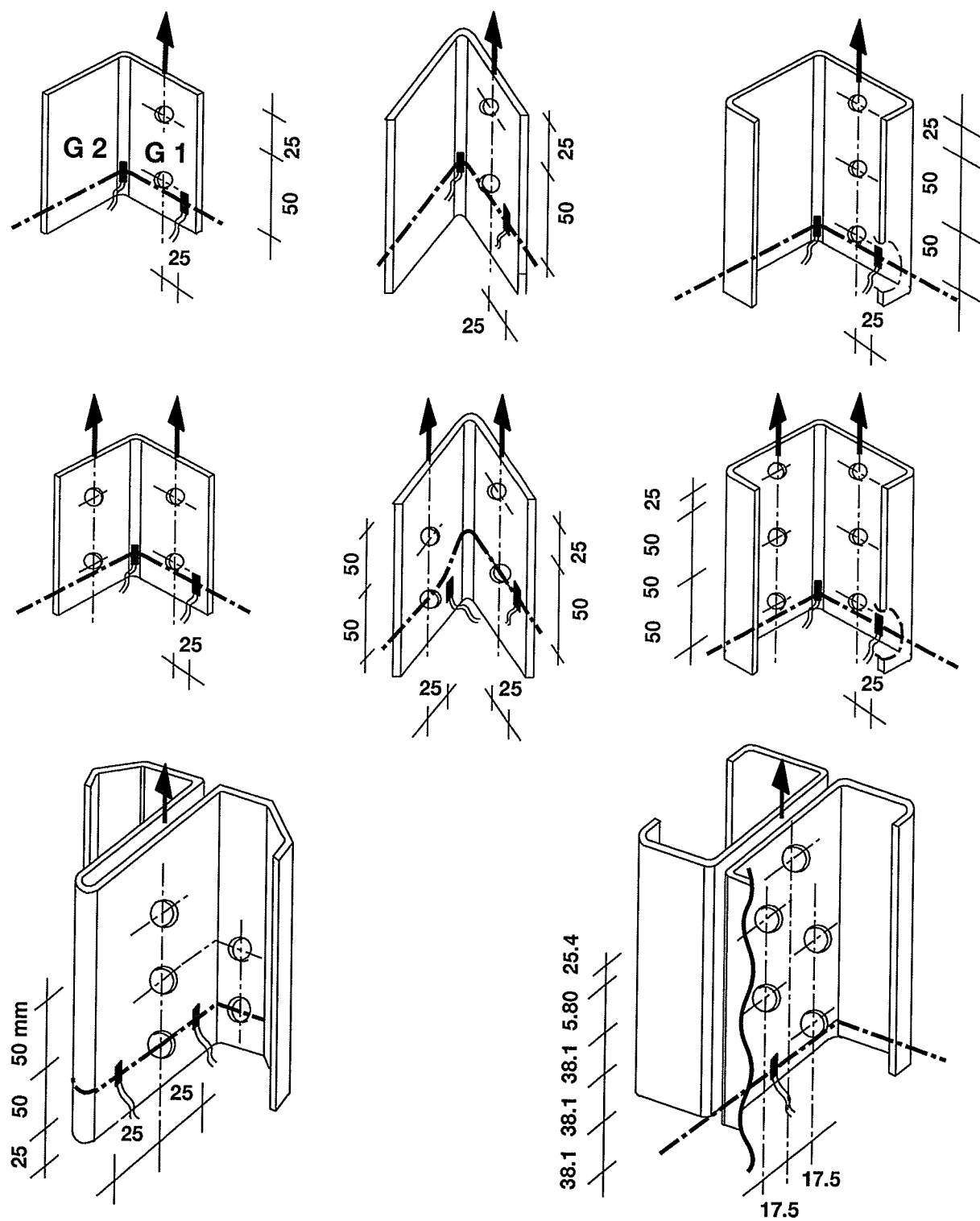
Figure 3.23 : Location of Strain Gauges at the End Connection of Test Specimens.

Figure 3.25 : Displacement Transducers Placed on a Back-to-Back Channel Specimen.

Figure 3.24 : Aligning the Test Specimen.

CHAPTER 4

Experimental Test Results and Evaluation of Fatigue Strength

4.1 Introduction

The overall objective of the this study was the development of mathematical design relationships that could define the fatigue strength of cold-formed steel members. This objective was accomplished through an extensive experimental program that permitted the formulation of mathematical relationships between the fatigue strength and the total fatigue life for the various cross sectional shapes involved in the investigation.

In this chapter, the results of the experimental work are summarized for the different parameters involved in the testing program. Each cross sectional shape was first examined in terms of crack initiation and growth patterns. Following that

stage, the stress strain response and the hysteresis behaviour of the sections were discussed. In addition, an evaluation of fatigue strength relationships was performed for the various cross sections. Finally, comparisons were made with current fatigue design guidelines of North American standards.

4.2 Static Tension Tests

Prior to fatigue testing, a total of 5 tests were performed on singly symmetric sections (plain 90°-angle [BA], 60°-angle [BC], and lipped angle [BB] sections) to determine their ultimate tensile capacities at room temperature ($\simeq 25°C$). Load ratios of the obtained capacities (17% to 60%) were later used in fatigue testing of the specimens.

Figures 4.1 to 4.10 give the results of the static tension tests in the form of two groups of curves. The first group relates the ultimate tensile capacity of the section (kN) to the longitudinal strains. A minimum of three strain gauges were used for each specimen. The first gauge (G1) was mounted 25 mm apart from the vertical centerline of the end hole. The second gauge (G2) was placed on the curved portion of the section on the same horizontal plane of G1. The third strain gauge was mounted on the extension of the vertical bolt line of the connected leg at the mid-

height location of the member. The second group of curves express the relationship between the applied load (kN) and the corresponding vertical deflection (stroke in mm) as recorded by the testing machine.

For all specimens, failure was observed to occur at the net section due to the presence of high stress concentrations. A through crack originated at the end hole location and started to proceed towards the unstiffened portion of the cross section. When the crack reached strain gauge G1, the member cross section had been reduced in area, and the crack growth pattern had become highly progressive causing the net section failure of the member. A summary of the static tension test results is given in Table 4.1.

4.3   Crack Initiation and Growth

In general, initiation and growth of fatigue cracks are most likely to occur in areas subjected to high tensile stress ranges, and where initial flaws or discontinuities exist. These specified locations are characterized by the presence of high stress concentrations which provide a favourable condition for crack growth.

The high tensile stress range is brought about by the combination of two effects. One is the geometrical stress concentration produced by the presence of the discontinuity which magnifies the nominal stress due to loading. The second effect is attributed to the presence of residual tensile stress field at the end hole zone of the test specimen. The combined effect of having residual tensile stresses and the stresses due to applied repeated loads is a tension-tension stress range at the region of the discontinuity, even in cases of nominal stress reversals. Fatigue cracks were observed during tension and compression cycles, but the continued progressive crack growth was observed only in tension cycles. In addition, all cracks were observed to propagate in a direction perpendicular to the principal tensile stress .

- **90°-angle section (BA)**   (Tested at room temperature $\simeq 25°C$)

For specimens connected through one leg, three different modes of crack propagation were observed. The first mode caused net section failure of the section and was observed for specimens BA-109-3, BA-109-5, and BA-109-6. The fatigue crack was observed to originate from a point on the circumference of the end hole. As shown in Figure 4.11, the plane of the crack was forming an angle that ranged from 28° to 32° with respect to the vertical plane of the member. When this crack reached the edge of the stress concentration zone surrounding the end hole, a noticeable change in its direction was observed. Following that stage, a gradual crack

growth took place in a horizontal direction towards the free edge of the section. The significant change in the direction of the crack is attributed to the corresponding change in the direction of the principal tensile stresses between the region of high stress concentrations (end hole zone), and the surrounding region.

In the same manner, a second crack was observed to originate from another point on the circumference of the end hole. The plane of the crack was inclined by an angle that ranged from $58°$ to $62°$ with respect to the vertical plane of the member. In general, it was observed that crack initiation planes were always perpendicular to each other as evident in Figure 4.11.

The second mode of crack growth resulted in block shear failures for specimens BA-109-4, BA-109-9, and BA-109-8. These failures were observed to occur in association with the three highest cyclic load levels used for testing this series of specimens ($\pm$ 75, $\pm$ 80, and $\pm$ 90 kN respectively). Figure 4.12(a) illustrates the first type of block shear failure. A fatigue crack originated from the extremity of the end hole and continued to grow under cyclic loading in a direction that formed $\simeq 30°$ with the vertical (longitudinal) plane of the member. This stage was followed by a sharp change in the plane of the crack to proceed horizontally towards the free edge of the section as was the case for the first mode of crack growth. However, the second crack was observed to propagate in a vertical plane through the net

124

section until complete separation of part of the section was witnessed as shown in Figure 4.12(a).

Another block shear mode of failure is shown in Figure 4.12(b). The horizontal and vertical cracks were observed to follow the outer edge of the stress concentration zone surrounding the holes. Such stress concentration was due to the presence of high tensile forces in the bolts ($\simeq 103$ kN/bolt) to ensure friction type connection during cyclic loading.

The third mode of crack growth was observed for specimens BA-109-2, and BA-109-7. Gross section failures were observed for these specimens as shown in Figure 4.13. Millscale surface irregularities and the presence of initial flaws might have induced the critical condition of crack initiation for these specimens.

For 90°-angle sections connected through both legs, fatigue cracks were found to initiate from two surface points located at the edge of the end hole as shown in Figure 4.14. The first fatigue crack was observed to propagate towards the free edge of the section. During the crack propagation stage of this crack, a second crack started propagating in an opposite direction towards the second connected leg of the specimen. As the first crack approached the edge of the member, the rate of crack growth in the second connected leg became extremely progressive leading to

the net section failure of the member as illustrated in Figure 4.14.

- **60°-angle section (BC)**   (Tested at room temperature $\simeq 25°C$)

For specimens connected through one leg, three modes of crack initiation and growth were observed. The fatigue crack propagation stage for all tested specimens of this series had one major common feature: cracks initiated and grew from the load-carrying leg in a plane perpendicular to the vertical (longitudinal) plane of the member. Four out of ten specimens followed a crack propagation path similar to the first mode of the 90°-angle section connected through one leg. However, the direction of principal stresses were different for both sections. Fatigue cracks originated from two points on the edge of the end hole and grew in separate planes, each one perpendicular to the direction of the principal stress at that point. Net section failures for this test series are shown in Figure 4.15.

The second mode of crack growth was similar to the third mode of the 90°-angle section connected through one leg. For specimens BC-81-3 and BC-81-7, fatigue cracks followed the path of the outer edge of the stress concentration zone surrounding the region of the discontinuity as illustrated in Figure 4.16. Crack initiation points are usually characterized by the presence of initial micro-flaws or any other type of surface irregularities.

The third type of crack initiation was primarily due to the presence of an engraved letter at the back side of the load-carrying leg of the member. Consequently, the existence of such notch at 60 mm from the mid-height plane of the specimen provided a favourable condition for fatigue crack initiation at that particular location. Identical modes of gross section failures were observed for three specimens in this test series. Figure 4.17 shows the engraved letter at the back side of a typical 60°-angle section.

In connecting the specimens through both legs, bolts were oriented in a staggard position as shown in Figure 4.18. Gross section failures were observed to occur at a horizontal plane 60 mm apart from the mid-height section of the member. Cracks originally initiated from an engraved letter at the back side of one leg in a pattern similar to the case of specimens connected through one leg. Furthermore, net section failure was observed for one specimen (BC-81-12). A fatigue crack first originated from the stress concentration zone of one leg and started propagating towards the free edge of the member. In addition, a second fatigue crack started propagating in the opposite direction towards the other connected leg. This crack followed the staggard bolt pattern as illustrated in Figure 4.18.

- **Lipped angle section (BB)** (Tested at room temperature $\simeq 25°$C)

For specimens connected through one leg, a total of five specimens were tested . As evident in Figure 4.19, two crack initiation and growth patterns were observed. For both patterns, the first fatigue crack initiated at the end hole region of the load-carrying leg of the member. However, unlike the 90°-angle section, after the crack had grown out of the stress concentration zone it suddenly changed its direction to proceed horizontally towards the second leg of the section. After 80% to 90% of the total fatigue life of the specimen was consumed in propagating this crack, a second crack initiated from the stress concentration zone in an opposite direction towards the lip of the load-carrying leg of the member. Figure 4.20 shows specimen BB-70-3 (connected through one leg) during failure.

For lipped angle specimens connected through both legs, typical net section failures were observed for all specimens. Crack initiation and growth patterns were similar to the case of corresponding sections connected through one leg. However, the crack followed the net section path of the member. The plane of failure was always through the middle of the end holes of the specimen either at the top or bottom connections. The failed portions of two lipped angle section connected through both legs are illustrated in Figure 4.21.

- **T-shaped section (BG)** (Tested at room temperature $\simeq 25°C$)

The crack initiation process for these sections consumed approximately 50% to 60% of the total fatigue life. Such early crack initiation was attributed to the presence of high eccentricity in loading. Consequently, this resulted in high values of stress reversals on the cross section.

The crack propagation pattern followed four stages as indicated in Figure 4.22. The first crack originated from the end hole on one side of the web towards the flange on the same side. Following that stage, a second crack originated from the same end hole and grew horizontally in the opposite direction -with respect to the first crack- towards the apex of the web. This crack propagation stage ended at 90% to 95% of the total fatigue life as shown in Figure 4.22.

During the third stage, a fatigue crack initiated at the end hole of the flange and proceeded towards the lip of the section until complete separation of one side took place after 98% to 99% of the total fatigue life was consumed. The final stage of crack propagation was a sudden fracture of the reduced cross section after small number of stress reversals ($\simeq 1\%$ of the total fatigue life). Figure 4.23 shows a T-shaped section at failure.

In considering the fractured portion of the member shown in Figure 4.24, it was observed that the first three stages of crack propagation produced a smooth fractured surface. On the contrary, the final stage was characterized by a rough irregular fractured surface which resulted from the sudden failure of the section at that location.

- **Back-to-Back Channel sections (BN and HBN sections)**

These section were built up using two back-to-back channels separated by a plate thickness of 12.7 mm (1/2"). Bolts connecting the section to the gusset plate were oriented in a staggered position as shown in Figure 4.25. Two tie plates (76 × 46 × 8 mm or 3" × $1\frac{13}{16}$" × $\frac{5}{16}$") were used to connect the channels to form an I-section. As the section was concentrically loaded, the maximum permissible longitudinal spacing of the connectors (S_{max}) joining the two channels, was calculated based on the AISI specifications (1991) for compression members as follows:

$$S_{max} = \frac{l \, r_{cy}}{2 \, r_1} \qquad (4.1)$$

l = unbraced length of the compression member.

r_1 = radius of gyration of the I-section about the axis

  perpendicular to the direction in which buckling would

  occur for the given conditions of end support and

130

intermediate bracing.

r_{cy}= radius of gyration of one channel about its centroidal

axis parallel to the web.

(i)   BN and HBN section tested at room room temperature $\simeq$ 25°C

In this series of tests, a total of ten specimens were tested (five specimens for each steel type). The crack initiation pattern was similar for all specimens tested. The first fatigue crack always originated from the stress concentration zone surrounding the end hole of one channel, it then started propagating through the web in a horizontal plane towards the flange on the far side with respect to the point of crack initiation. When approximately 70% to 80% of the web area had fractured, a second crack originated from the same point of initiation of the first crack but grew in an opposite direction towards the near flange. The test was terminated after a crack had propagated to at least 50% of the total width of one flange.

Compound fatigue failures were observed for specimens BN-36-2,   BN-36-3, and HBN-37-3.   Such failures were characterized by the origination of fatigue cracks from two different locations simultaneously as shown in Figure 4.26. A crack first originated at the top side of the left channel. It was then followed by another crack at the bottom side of the right channel in a cross sequential manner. Crack

initiation and growth patterns were similar to those described for the case of simple fatigue failures.

(ii) HBN sections tested at a temperature of -50°C

A total of five specimens were tested in this series. Although the locations of crack initiation were similar to specimens tested at room temperature ($\simeq 25°$C), yet, this series of tests were characterized by the appearance of very short crack sizes. This was mainly attributed to large reductions in fracture toughness and formability associated with low temperatures. The crack initiation process consumed approximately 80% to 85% of the total fatigue life of the specimen. However, crack propagation rates were so fast and occurred at short periods of time leading to the sudden brittle fracture of the specimen as shown in Figure 4.27.

Test results and failure locations for the 90°-angle (BA-section) and the 60°-angle (BC-section) are summarized in Tables 4.2 and 4.3. In addition, Tables 4.4 and 4.5 present the results for the lipped angle section (BB-section) and the T-shaped section (BG-section). Test results for angles connected through both legs are given in Table 4.6. Finally, results for back-to-back channel sections are given in Tables 4.7 and 4.8 respectively.

4.4 Stress-Strain Response and Hysteresis Behaviour

True stress control can easily be achieved only at small deformations but becomes unmanageable when cracks form in the material. Consequently, in the present study load was chosen as the control function and a triangular wave form (Figure 4.28) was adopted. Alternating fatigue loads were applied in a fully reversed load cycle (Load Ratio = -1).

4.4.1 Scope

In this section, the experimental test results of the 52 full scale cold-formed steel members tested under constant amplitude fatigue loads are discussed in detail. Singly symmetric sections connected through one leg (BA, BC, and BB sections) are treated first in subsection 4.4.2. Similar sections connected through both legs are discussed in subsection 4.4.3. Finally, the T-shaped section (BG), and the back-to-back channel sections (BN and HBN) are treated in subsections 4.4.4, and 4.4.5 respectively. The general format used to present the results of each test series includes the following:

1. An overview of the stress-strain response together with the hysteresis behaviour of the specimen during fatigue loading. The latter is expressed in terms of a relationship between the applied load and the vertical stroke

recorded by the testing machine.

2. A description of lateral displacements of the specimen as recorded by four displacement transducers placed in a horizontal plane at the mid-height section.

3. A relationship between the applied fatigue load and the resulting displacements at the bottom end section of the test specimen.

4.4.2 Singly symmetric sections connected through one leg (BA, BC, and BB sections)

A total of 25 fatigue tests were performed in this test series. All specimens were fabricated using ASTM A715 Grade 60 steel and were tested at room temperature ($\simeq 25°C$).

- **Stress-strain and load-stroke responses**

Typical behaviour of this test series is illustrated in Figures 4.29, 4.30, and 4.31 for specimens BA-109-6, BC-81-4, and BB-70-4 respectively. Cycle dependent softening was observed for all tested specimens, this was evidenced by the exponential increase of strains as the number of cycles increased. The runaway nature of the

process is clearly demonstrated by the stress-strain response given in Figures 4.29(a), 4.30(a), and 4.31(a).

The overall response of the specimens can be explained by the load versus displacement relationship recorded at approximately 1% and 98% of the total fatigue life. As evident in Figure 4.29(b), specimen BA-109-6 exhibited an average stroke increase of 11% at 99% of the total fatigue life. Such increase was observed only in tension cycles where the crack opening process takes place. Furthermore, no remarkable change occurred in the stroke values recorded for the compression cycles throughout the test. In general, the average recorded increase in stroke for this test series ranged from 1.0% to 34.6% for the 90°-angle section (BA), from 1.0% to 24.4% for the 60°-angle section (BC), and from 1.5% to 26.3% for the lipped angle section (BB).

- **Lateral displacements at the mid-height section**

Four Linear Variable Differential Transducers (LVDT's) were placed at the mid-height section of each specimen at the positions illustrated in Figures 4.32, 4.33, and 4.34. Displacement values for the edges were obtained by direct interpolation between the two bounding points of measurement.

For the three cross sectional shapes (BA, BC, and BB), the measured displace-

ment magnitudes differed considerably depending on the value of the applied load. However, there were some common features that governed the out-of-plane translations at the mid-height plane of the different cross sections.

As evident from Figures 4.32, 4.33, and 4.34 displacement magnitudes recorded at both the edge and the heal of the connected leg (LVDT #1, and LVDT #2) were two to four times larger than corresponding values recorded for the unconnected leg (LVDT #3 and LVDT #4). It was also noted that during compression cycles, the largest displacement magnitude was that recorded for the edge of the connected leg (LVDT #1). However, in tension cycles, the transducer placed near the corner of the connected leg (LVDT #2) recorded the highest lateral displacement value. During the crack propagation stage in tension cycles, a relative increase in the magnitude of the displacement was observed compared to initial values recorded at the beginning of the test. Such increase was more pronounced for values measured at the edges of the sections.

- **Longitudinal displacements at the bottom end section**

Typical curves showing the relationship between the applied fatigue load and the corresponding longitudinal displacement at the bottom end section of the specimen are illustrated in Figures 4.35, 4.36, and 4.37 for specimens BA-109-6, BC-81-4, and

BB-70-4 respectively. The bottom end was chosen as it was stationary from the view point of load application. The main purpose of recording the longitudinal displacement was to ensure proper slip resistant action of the connection. Furthermore, since the recorded displacement values were relatively small compared to lateral displacements of the mid-height section, these values served as a sensitive indicator of crack opening. The process of crack propagation was reflected in the form of an increase in the displacement values in both tension and compression cycles.

4.4.3 Singly symmetric sections connected through both legs (BA, BC, and BB sections)

Three tests were performed for each cross sectional shape. All specimens were fabricated using ASTM A715 Grade 60 steel and were tested at room temperature.

- **<u>Stress-strain and load-stroke responses</u>**

Typical stress-strain response and load-stroke relationship of this test series are demonstrated in Figures 4.38, 4.39, and 4.40 for specimens BA-109-13, BC-81-12, and BB-70-8 respectively.

A particularly interesting feature of the general performance was the ability of

the sections to exhibit large plastic strains per cycle as evident in Figure 4.38(a). This plastic strain can be related to fatigue damage much better than can any other factor in the fatigue problem. The width of the loop is a measure of the amount of plastic strain per cycle. Furthermore, the enclosed area of the loop accounts for the energy dissipated per cycle. Again, cycle dependent softening was observed, that was apparent by the gradual increase in strains as the number of cycles increased. The runaway nature of the process was clearly demonstrated by the exponential increase in strains as the number of cycles increased.

In an attempt to understand the hysteresis behaviour of the sections (load-stroke relationship), the curves obtained were compared to those for corresponding sections connected through a single leg. Figures 4.41 to 4.46 reflect the relative increase in stiffness of the sections as both legs were connected. The average increase in stiffness was 29% for the 90°-angle section (BA), 26% for the 60°-angle section (BC), and 13% for the lipped angle section (BB).

- **<u>Lateral displacements at the mid-height section</u>**

Connecting the sections through both legs was found to have a significant effect on the recorded lateral displacement values at the mid-height plane of the test specimens. In comparing Figures 4.47 and 4.48 for specimens BA-109-8 and BA-109-12 under an alternating fatigue load of $\pm$ 90 kN, it appeared that in compression

138

cycles, the effect of connecting both legs of the section substantially decreased the lateral displacement values recorded at the mid-height section. Such decrease ranged from 40% to 60% for the edge of the connected leg, and from 30% to 40% at the corner region of the angle. However, in tension cycles, connecting the section through both legs had a less pronounced effect on the recorded lateral displacement values at the mid-height section.

Similar behaviour was observed for both the 60°-angle section (BC), and the lipped angle section (BB) as illustrated by comparing Figures 4.49 and 4.50 for specimens BC-81-3 and BC-81-13 respectively. Moreover, mid-height translations for the lipped angle specimens BB-70-3 and BB-70-8 (Figures 4.51 and 4.52) were also compared.

Results indicated that in compression cycles, a considerable decrease of approximately 40% to 60% for the edges and 30% to 40% for the corners was observed. In tension cycles a decrease in the lateral displacement values in the range of 15% to 25% was observed compared to values obtained for similar specimens connected through one leg.

- **Longitudinal displacements at the bottom end section**

  Figures 4.53, 4.54, and 4.55 reflect the effect of connecting both legs on the

139

longitudinal displacement values recorded at the bottom end section of the member. The recorded displacement values for the 90°-angle section (BA), were 20% to 25% less than corresponding values obtained for the case of members connected through single leg as shown in Figure 4.53. Furthermore the average reduction in the displacement values recorded at the end section for both the 60°-angle section (BC), and the lipped angle section (BB) were in the range of 25% to 30%.

On the whole, it was observed that connecting singly symmetric sections through both legs enhanced the stiffness of the sections by approximately 25%. It also reduced the lateral displacement values recorded at the mid-height section. For compression cycles this reduction was in the range of 40% to 60% for the edges of the section and 30% to 40% at the corners. However, for tension cycles, the reduction was in the range of 15% to 25%, and was more pronounced at the corners of the sections.

4.4.4 T-shaped section

(BG-section)

The pattern of holes used in connecting these members with the gusset plate (Figure 4.22), produced high eccentric loads on the cross section. Several repetitive

connection failures were witnessed. Consequently, only three tests were performed for this cross sectional shape. All specimens were fabricated using steel type ASTM A715 Grade 60, and were tested at room temperature ($\simeq$ 25°C).

- **Stress-strain and load-stroke responses**

As evident in Figure 4.56(a), a severe distortion (bend back) in the shape of the hysteresis loops was observed. Specimen BG-36-1 exhibited two different stress-strain responses in tension and compression. Obviously, as cracks open in tension, a substantial reduction in stiffness was realized in tension cycles. The reduction was more pronounced after approximately 95% of the total fatigue life was consumed. In contrast, no significant change of stiffness was observed in compression cycles. The behaviour was characterized by the formation of large irrecoverable plastic strains. These strains were the predominant factor leading to the fatigue failure of the specimen.

No valuable strain gauge data were obtained for specimens BG-36-2 and BG-36-3 (Figures 4.57(a) and 4.58(a)). Only a gradual shift of the entire hysteresis loop towards increasing tensile strains was observed. This could be attributed to the presence of tensile mean strains which were developed as a result of the formation of large plastic strains.

Cycle dependent softening was observed for all three specimens. That was evident by the gradual decrease in the material's resistance to deformation. Moreover, stiffness reduction was more pronounced at final stages of the fatigue life as illustrated in Figures 4.57(b) and 4.58(b). These Figures reflect stiffness deterioration in tension cycles for specimens BG-36-2 and BG-36-3 respectively. For the first specimen (BG-36-2), a loss in stiffness in the range of 20% to 25% took place after 97% of the total fatigue life was consumed. However, the second specimen (BG-36-3) showed a reduction in stiffness in the range of 30% to 35% upon reaching 98% of the total fatigue life of the member.

Unlike the previous two specimens, fatigue testing for specimen BG-36-1 was stopped at 253,000 cycles after only the first stage of crack propagation had been achieved (Figure 4.22). This situation explains the recorded hysteresis behaviour shown in Figure 4.56(b), where almost no significant stiffness reduction was observed.

- **Lateral displacements at the mid-height section**

The out-of-plane lateral displacements recorded for the mid-height section of the specimens are shown in Figures 4.59, 4.60, and 4.61. As evident from these figures, a noticeable decrease in the recorded displacement values was observed upon cracking of the section. Such decrease was less pronounced for values recorded at

142

the edges of the inclined flanges (LVDT #4). This could be explained by referring to Figure 4.22, where the final stage of crack propagation was a sudden fracture for that region of the cross section. In other words, displacement values recorded by LVDT #4 showed negligible change during the first three stages of crack propagation. However, the most significant change in the recorded displacement values was obtained for the location of LVDT #1 which was placed 60 mm apart from the apex of the web.

- **Longitudinal displacements at the bottom end section**

Relationships showing the longitudinal displacement values recorded for the bottom end section of the specimen versus the applied fatigue load are given in Figures 4.62, 4.63, and 4.64. Based on these Figures, it is obvious that as cracking of the section took place (either at the top or bottom connection), the recorded bottom end displacement values decreased considerably. Although for specimen BG-36-1 the test was stopped after only the first crack propagation stage was achieved, yet, the decrease in displacement values recorded at the end section was in the range of 50% to 60% compared to initial readings recorded at the beginning of the test. However, at final stages of fatigue lives, specimens that witnessed at least the first two stages of crack growth showed 80% to 90% decrease in the recorded end displacement values as apparent in Figure 4.64.

143

4.4.5 Back-to-back channel sections

(BN and HBN sections)

A total of 15 tests were performed for this test series. The first group of tests included five specimens fabricated from steel type ASTM A715 Grade 60 ($F_y \simeq 415\,MPa$), and another five specimens fabricated from steel type CAN/CSA-G40.21-M 300W ($F_y \simeq 300\,MPa$). This group was tested at room temperature ($\simeq 25°C$). A second group consisted of five specimens fabricated from steel type CAN/CSA-G40.21-M 300W was tested under temperature controlled conditions, where a steady temperature of -50°C was maintained during the entire test duration.

- **Stress-strain and load-stroke responses**

Typical stress-strain response and the load-stroke loops for the first group are given in Figures 4.65 and 4.66. In that regard, comparisons were made between specimens BN-36-5, and HBN-37-5 fabricated from different steel materials. Both specimens were tested under an alternating fatigue load of $\pm$ 350 kN. However, the response of each specimen varied significantly. Specimen HBN-37-5 fabricated from steel type CAN/CSA-G40.21-M 300W, exhibited large irrecoverable plastic strains as indicated by the large width of the loops shown in Figure 4.66(a). On the other hand, specimen BN-36-5 showed relatively stretched loops with smaller enclosed

144

areas compared to specimen HBN-37-5. As mentioned earlier, the enclosed area of the loop is a measure of the amount of energy dissipated per cycle.

In comparing load-stroke loops for the two specimens, specimen BN-36-5 of steel type ASTM A715 Grade 60 showed a very slight increase in stiffness (approximately 5%). The obtained stiffness values were 208,500 N/mm and 200,000 N/mm for the two types of steel respectively. Moreover, Stiffness deterioration was observed upon cracking of the specimen. Such deterioration was most pronounced at final stages of the fatigue life ($\simeq$ 99%). At that stage, the obtained stiffness reduction ranged from 25% to 30% compared to initial values recorded at the beginning of the test.

Typical cyclic behaviour of back-to-back channel specimens tested at -50°C is demonstrated in Figure 4.67. For all specimens tested, a noticeable decrease in the stroke took place from the beginning of the test until almost half of the fatigue life was reached. The reduction ranged from 0.8% to 2% of the initial stroke of the specimen recorded at the first few cycles. The stroke then increased by increasing the number of cycles until failure occurred. For specimens HBN-37-8, HBN-37-9, and HBN-37-10, very short crack sizes were observed at fracture, this could be attributed to large reductions in fracture toughness and formability that take place at low temperatures.

The significant effect of low temperature on the stress-strain response could be clearly illustrated by comparing specimens fabricated of the same steel type (HBN-37-5 and HBN-37-9). The low temperature reduced the formation of plastic strains as apparent from the width of the loops in Figures 4.66 and 4.67. The phenomenon is related to the considerable decrease in the total strain energy (toughness) associated with low temperatures. In general, the low temperature enhanced the overall cyclic performance of the tested specimens.

- **Lateral displacements at the mid-height section**

As these sections were concentrically loaded, the recorded lateral displacement values were relatively small compared to other cross sectional shapes. It was evident that at early stages of the specimen's fatigue life, approximately equal displacement magnitudes were observed for the two displacement transducers used to measure the out-of-plane translations in both the X-axis direction (LVDT #1 and LVDT #4), and the Y-axis direction of the member (LVDT #2 and LVDT #3). Figures 4.68 and 4.69 show mid-height translations for specimens BN-36-3 and HBN-37-9 at room temperature and -50°C respectively.

After cracking of one or both channels forming the I-section, a noticeable increase in the recorded displacement values was observed. However, it should be emphasized that the quantitative value of such increase depends mainly on the

146

extent of damage present in the section at the time when the readings were recorded.

- **Longitudinal displacements at the bottom end section**

Displacements at the end section were recorded in the longitudinal direction of the member as illustrated by the position of LVDT #5 in Figures 4.70 and 4.71 for specimens BN-36-1, and HBN-37-3 respectively. The total magnitude of such displacements (tension and compression) was approximately 0.1 mm. This value accounts for nearly 5% of the total longitudinal stroke recorded by the testing machine.

After precise observation of end section translations, it was noticed that the flanges at that section were continuously opening and closing in compression and tension cycles respectively. On that basis, another interesting position was chosen for placing the displacement transducer (LVDT #5) as shown in Figures 4.72.

In comparing the bottom end displacements for specimens BN-36-3 and HBN-37-5 (Figures 4.72 and 4.73), it was observed that the recorded values were 30% to 40% higher for the specimen fabricated of steel type CAN/CSA-G40.21-M 300W compared to the other specimen of steel type ASTM A715 Grade 60. Furthermore, it was also apparent that at final stages of the fatigue life, the recorded displacement

values for specimen BN-36-3 (Figure 4.72) decreased with respect to initial values recorded at the beginning of the test. In contrast, specimen HBN-37-5 exhibited larger displacement values upon cracking. The phenomenon could be explained by identifying the cracked channel of the built-up I-section. In that regard, two cases are to be considered. First, if the cracked channel was that where LVDT #5 was attached, this would obviously lead to a reduction in the recorded displacements at the end section. Secondly, if the cracked channel was on the other side of LVDT #5, a noticeable increase in the displacement values would be observed as most of the load will be transferred to the gusset plate connection through the uncracked channel.

4.5 Fatigue Strength Relationships

The plot between the stress range σ_r versus the total fatigue life is commonly referred to as S-N curves. Life steadily increases with decreasing stress until the fatigue limit is reached. It may suffice to say that in this study the concept of fatigue strength was used. The fatigue limit was considered the stress range corresponding to a minimum of 10^6 cycles. The number was based on an expected life of 50 years for a transmission tower and a maximum of 50 alternating wind applications per day which would give a total of $\simeq$ 920,000 cycles (LRFD, 1993).

148

4.5.1 Statistical analysis of test results

For the purpose of evaluating the variability of test data, the ASTM Committee E-9 on Fatigue recommends at least four replicates at each stress range level. However, as the present study was concerned with investigating the fatigue behaviour of full-scale cold-formed steel members for five different cross sectional shapes, and due to time and financial constraints, only one specimen was tested at every stress range level. The exceptions were some tests that were duplicated for both the 90°-angle section (BA), and the 60°-angle section (BC) connected through a single leg.

The prime objective of performing a least squares regression analysis of the test data was to provide quantitative information on the effect of both the stress range (σ_r), and the alternating fatigue load (P), on the total fatigue life (N) for the various cross sections involved in the study.

The predicted model for the effect of stress range on the fatigue life was in the form of a log-log relationship. The model provided the best fit for the test data, and can be expressed as

$$log\,N \;=\; a \;+\; b \; log\,\sigma_r \qquad\qquad (4.2)$$

or

$$N = \frac{10^a}{\sigma_r{}^b} \qquad (4.3)$$

where, σ_r is the stress range in MPa, a and b are constants to provide a best fit line to the fatigue data. b is the slope of the log-log S-N curve which ranges between 3 and 4.5 for most structural details. A similar relationship was obtained for the alternating fatigue load versus the number of cycles to failure. Table 4.9 presents the values of a and b for both S-N and Load-N curves of the different cross sections.

It should be emphasized that this model applies only for fatigue lives ranging from 10^4 to 10^6 cycles. For the predicted model given by Equation (4.2), the logarithm of the fatigue life was assumed to be the dependent variable (y), whereas, the logarithm of the stress range was treated as the independent variable (x). On that basis, Equation (4.2) can be given in the following form

$$\bar{y} = a + b\bar{x} \qquad (4.4)$$

where, $\bar{y}$ and $\bar{x}$ are the mean values of the dependent and independent variable respectively. Using the method of least squares, the slope b of the best fit line is obtained from Little and Jebe, 1975 as:

$$b = \frac{n \sum\limits_{i=1}^{n} x_i\, y_i \; - \; \sum\limits_{i=1}^{n} x_i \; \sum\limits_{i=1}^{n} y_i}{n \sum\limits_{i=1}^{n} x_i{}^2 \; - \; (\sum\limits_{i=1}^{n} x_i)^2} \qquad (4.5)$$

where, n is the number of data points, x_i is the ith value of the independent variable, and y_i is the ith value of the dependent variable.

Substituting in Equation (4.4), the value of a can now be determined as:

$$a = \bar{y} - b\bar{x} \qquad (4.6)$$

Tabulated values of a and b based on least squares regression analysis of the test data are given in Appendix A (Tables A.1 to A.20).

An error term could be incorporated to Equation (4.2). As such, the model can be expressed as:

$$log\, N = a + b\; log\, \sigma_r + \epsilon_i \qquad (4.7)$$

where, ϵ_i is the error term defined as:

$$\epsilon_i = y_i - \hat{y} \qquad (4.8)$$

y_i is the resulting value of log N, and $\hat{y}$ is the corresponding value of log N predicted using the regression line defined by Equation (4.2).

151

The standard error of estimate which is equivalent to the standard deviation for a set of data is given by Kennedy and Neville, (1976) as:

$$S_e = \sqrt{\frac{1}{n-2} \sum_{i=1}^{n} (y_i - \hat{y})^2}$$

(4.9)

where, n is the number of data points, and $y_i - \hat{y}$ is the error term defined by Equation (4.8).

The dispersion limits are usually defined by specified multiples of the standard error of estimate (S_e) from the mean regression line of the data. In the present study, the upper and lower bounds of the confidence interval were calculated on the basis of $2 S_e$. As such, the dispersion limits for the S-N curves could be defined as

$$log N = a + b \, log \, \sigma_r \pm 2 S_e$$

(4.10)

and for alternating fatigue fatigue load, the confidence limits are given as

$$log N = a + b \, log \, P \pm 2 S_e$$

(4.11)

In order to determine whether $log N$ is dependent on $log \, \sigma_r$ and $log \, P$, a significance **t-test** was applied to the slope of the mean regression line. The value of **t** is given by:

$$t = \frac{|b|}{S_b}$$

(4.12)

where, $|b|$ is the absolute value of the slope of the regression line, and S_b is the standard deviation of the slope given as:

$$S_b = \sqrt{\frac{1}{n-2} \; \frac{\sum\limits_{i=1}^{n} (y_i - \hat{y})^2}{\sum\limits_{i=1}^{n} (x_i - \bar{x})^2}} \qquad (4.13)$$

The term $n-2$ is the number of degrees of freedom which refers to the two constraints used in obtaining the regression equation, i.e., in determining a and b.

The calculated value of t from Equation (4.12) was compared to the tabulated values presented by Little and Jebe (1975) for the chosen level of significance $\alpha = 0.05$ (confidence level of 95%), and for a number of degrees of freedom of $n-2$.

Results of the regression analysis using the least square method, and the calculated values of t and the standard error of estimate (S_e) are given in Appendix A (Tables A.1 to A.20). The calculated values of t were significantly greater than the tabulated values. Therefore, it can be concluded that for the 95% confidence level, both the stress range σ_r and the alternating fatigue load P have a significant effect on the fatigue life of the specimens.

153

For singly symmetric sections connected through one leg: 90°-angle section (BA), 60°-angle section (BC), and lipped angle section (BB), and for back-to-back channel sections (BN and HBN), S-N and Load-N plots were based on Equations (4.10) and (4.11) respectively. The resulting plots are given in Appendix B Figures B.1 to B.20. These plots illustrate the mean regression line of the experimental test data, together with both the upper and lower 95% confidence levels. Moreover, the governing log-log relationship for the mean regression line of each test series is also given.

For singly symmetric sections connected through both legs, and for the T-shaped section (BG), only three tests were performed for each cross sectional shape. Consequently, the dispersion limits for these sections were almost coinciding with the mean regression line as evident in Figures B.8 to B.14.

4.5.2 Discussion of test results for S-N and Load-N plots

S-N curves for singly symmetric sections connected through one leg (BA, BC, and BB sections) at temperature of 25°C are shown in Figure 4.74. These specimens were tested under a stress range that varied between 206 MPa and 813 MPa. The negative slopes of the curves obtained from the regression analysis were -4.14, -4.43, and -3.97 for BA, BC, and BB sections respectively. The 12% difference in slope

154

values can be attributed to statistical scatter of the test data.

For a given number of cycles, the fatigue strength of the 90°-angle section (BA) was 4.5% higher than that of the 60°-angle section (BC), and 30% higher than that of the lipped angle section (BB). However, in terms of alternating fatigue loads, and for a predetermined number of cycles, the lipped angle section (BB) was found to withstand 36% higher load than the 60°-angle section (BC), and 60% higher than the 90°-angle section (BA) as shown in Figure 4.75. The fully reversed cyclic loads for this series ($\pm$ 40 kN to $\pm$ 140 kN) were applied at a frequency that ranged from 1 Hz to 1.975 Hz depending on the corresponding stroke level of the specimen.

Figures 4.76 to 4.81 reflect comparisons between the cases of singly symmetric sections connected through one leg, and two legs. For the latter, three tests were performed for each cross sectional shape. Two points are to be addressed herein, the first is the noticeable change of slope of the S-N curves for both the BA and the BB sections. It was found that a significant increase in the fatigue strength for these sections occurs only at long lives while slight improvement takes place at higher stress levels. Such deterioration of the cross section at high stress range levels was attributed to the presence of uneven stress distribution at the region of discontinuity. The concentration of stresses at this region significantly contributed to the fatigue damage of the section. The second point was regarding the the performance

155

of the 60°-angle sections (BC) connected through both legs shown in Figure 4.78. These specimens showed an increase in the fatigue strength of about 12% compared to corresponding specimens connected through a single leg. Two specimens BC-81-11, ($\pm$ 72.5 kN) and BC-81-13, ($\pm$ 90 kN) failed at a gross section 60 mm apart from the mid-height plane of the specimen due to the presence of an engraved letter at the back of one leg. Such surface irregularity formed a favourable condition for fatigue crack initiation. Moreover, the resulting gross section failures significantly affected the slope of the S-N curve to show only 3.6% difference compared to the slope of corresponding specimens connected through one leg. Similar comparisons for both the 90°-angle sections (BA) and the lipped angle sections are given in Figures 4.76 and 4.78. As evident from these Figures, better fatigue performance was observed for angles connected through both legs. The average increase in the stress range for these two sections compared to the case of one leg connected was 25% for the 90°-angle section (BA), and 15% for the lipped angle section (BB). Pictures of fatigue failures for angle specimens are shown in Figures 4.82 to 4.85.

Fatigue performance of the T-shaped section (BG) is given in Figures 4.86 and 4.87. In the range of 10^4 to 10^6 cycles, the fatigue strength of the section was 5% lower than that of the 90°-angle section (BA) connected through one leg. Furthermore, slopes of the S-N and Load-N curves for both the BG and the BA sections were almost equal ($\simeq$ 1% difference).

156

Figure 4.88 presents S-N plots for three groups of specimens: (1) back-to-back channel sections of steel type ASTM A715 Grade 60 (BN) tested at room temperature of $\simeq 25^\circ$C, (2) back-to-back channel sections of steel type CAN/CSA-G40.21-M 300W (HBN) tested at temperature of -50°C, and (3) back-to-back channel sections of steel type CAN/CSA-G40.21-M 300W (HBN) at room temperature of 25°C.

A total of five tests were performed for each group. As a consequent result of the difference in steel types between BN and HBN sections, an obvious change in the slope of the curves could be observed. Moreover, for a given number of cycles, fatigue tests performed at -50°C showed a pronounced increase of stress range of approximately 12% compared to room temperature tests. Stress range values for the three groups varied between 137 MPa and 324 MPa. Furthermore, alternating fatigue loads ranged from a minimum of $\pm$ 150 kN to a maximum of $\pm$ 375 kN. Curves representing the relationship between the applied loads and the fatigue life are given in Figure 4.89. Pictures of typical fatigue failures for the T-shaped section, and the back-to-back channel section are shown in Figures 4.90 and 4.91 respectively.

4.5.3 Comparisons with North American Fatigue Standards

Fatigue design curves for the allowable stress range categories of the Canadian Standard CAN/CSA-S16.1-M94 (1995) are equivalent to those specified in the AASHTO (1989) Specifications. The curves have similar slopes of approximately -3.0 (Keating and Fisher, 1986). The constant amplitude fatigue limit for the different Categories is shown in Figure 4.92. For stress range cycles below this limit, no fatigue crack propagation would be expected.

The test data for singly symmetric sections connected through one leg are plotted in Figure 4.93. Their fatigue lives were consistent with the Category B lower bound resistance curve. The minimum stress range value at which fatigue failure occurred was 206 MPa. Furthermore, the stress range values at which no fatigue cracking was detected at 10^6 cycles were 335 MPa for the 90°-angle section (BA), and 291 MPa for the 60°-angle section (BC).

Fatigue test results for back-to-back channel specimens are plotted in Figure 4.94. The test data were consistent with the Category C lower bound resistance curve. For room temperature tests, the stress range values at which no fatigue cracking was observed were 137 MPa for specimens of steel type CAN/CSA-G40.21-M 300W (HBN-sections tested at 25°C), and 184 MPa for specimens of steel type

158

ASTM A715 Grade 60 (BN-sections tested at 25°C). However, for fatigue tests conducted at -50°C, the fatigue limit for back-to-back channel specimens of steel type CAN/CSA-G40.21-M 300W was 151 MPa at 1.3×10^6 cycles.

Table 4.1

Summary of Static Tension Test Results [a, b]

(Test Temerature = 25°C)

Shape	Specimen	Total Length (mm)	Ultimate Load (kN)
∠	BA - 17	1500	153
∠	BC - 19 A	750	160
	BC - 19 B	750	170
∠	BB - 18	750	259
	BB - 19 A	750	262

[a] All Specimens were Connected Through One Leg.

[b] Steel Type : ASTM A715 Grade 60.

Table 4.2

Fatigue Test Results for 90°-angle Specimens Connected Through One Leg

(Test Temerature = 25°C)

Specimen	Load (kN) ±	Stroke (mm) ±	Freq. (Hz)	No. of Cycles	Stress Range (MPa)	Stress Ratio	Mode of Failure
BA-109-1	40	1.275	1.000	650,000	335	-0.887	Test stopped
BA-109-2	80	2.590	1.000	30,000	674	-0.887	Gross sec.-Mid.
BA-109-3	70	2.385	1.000	60,000	611	-0.889	Net sec.- Top
BA-109-4	75	2.565	1.000	32,000	653	-0.890	Block Shear-Top
BA-109-5	65	2.345	1.150	62,700	589	-0.888	Net sec.- Top
BA-109-6	55	1.840	1.133	105,960	515	-0.890	Net sec.- Top
BA-109-7	60	1.985	1.082	90,200	497	-0.886	Gross sec.- Top
BA-109-8	90	2.915	1.046	15,550	813	-0.889	Block Shear-Top
BA-109-9	80	2.590	1.083	30,580	707	-0.888	Block Shear-Top
BA-109-10	70	2.385	1.139	124,259	666	-0.889	VL. Crack- Top (Test stopped)

Table 4.3

Fatigue Test Results for 60°-angle Specimens Connected Through One Leg

(Test Temerature = 25°C)

Specimen	Load (kN) ±	Stroke (mm) ±	Freq. (Hz)	No. of Cycles	Stress Range (MPa)	Stress Ratio	Mode of Failure
BC-81-1	70	2.050	1.128	78,000	515	-0.897	Gross sec.
BC-81-2	80	2.450	1.091	27,000	566	-0.898	Net sec.-Top
BC-81-3	90	2.815	1.111	31,500	642	-0.898	Net sec.-Bottom
BC-81-4	60	1.765	1.128	218,590	434	-0.897	Net sec. -Top
BC-81-5	75	2.265	1.073	72,000	546	-0.897	Gross sec.
BC-81-6	85	2.700	1.130	43,760	603	-0.897	Gross sec.
BC-81-7	65	1.920	1.359	102,073	455	-0.896	Net sec. -Top
BC-81-8	50	1.460	1.634	339,600	351	-0.896	Net sec. -Top
BC-81-9	45	1.300	1.208	500,000	336	-0.897	Net sec. -Bottom
BC-81-10	40	1.100	1.129	1,200,000	291	-0.899	Test stopped

Table 4.4

Fatigue Test Results for Lipped -angle Specimens Connected Through One Leg

(Test Temerature = 25°C)

Specimen	Load (kN) ±	Stroke (mm) ±	Freq. (Hz)	No. of Cycles	Stress Range (MPa)	Stress Ratio	Mode of Failure
BB-70-1	60	1.220	1.760	600,150	256	-0.923	Net sec. - Bottom
BB-70-2	50	1.030	1.975	1,050,000	206	-0.923	Net sec. - Bottom
BB-70-3	75	1.580	1.575	270,000	305	-0.923	Net sec. - Bottom
BB-70-4	90	1.915	1.396	136,900	381	-0.923	Net sec. - Top
BB-70-5	140	3.140	1.000	16,000	597	-0.935	Net sec. - Bottom

Table 4.5

Fatigue Test Results for T-Shaped Specimens

(Test Temerature = 25°C)

Specimen	Load (kN) ±	Stroke (mm) ±	Freq. (Hz)	No. of Cycles	Stress Range (MPa)	Stress Ratio	Mode of Failure
BG-36-1	180	1.400	1.033	253,000	380	-0.884	Net sec.- Bottom
BG-36-2	210	1.536	1.251	160,000	443	-0.885	Net sec. -Top
BG-36-3	150	1.080	1.741	600,000	317	-0.883	Net sec. - Top

Table 4.6

Fatigue Test Results for Singly Symmetric Sections Connected Through Both Legs

(Test Temerature = 25 °C)

Specimen	Load (kN) ±	Stroke (mm) ±	Freq. (Hz)	No. of Cycles	Stress Range (MPa)	Stress Ratio	Mode of Failure
BA-109-11	66.5	1.630	1.595	355,188	489	-0.766	Net sec.-Top
BA-109-12	90.0	2.220	1.292	75,000	642	-0.767	Net sec. -Top
BA-109-13	110.0	2.989	1.025	22,000	771	-0.765	Net sec. -Top
BC- 81 -11	72.5	1.873	1.529	145,000	510	-0.847	Gross sec.
BC- 81 -12	50.0	1.218	2.040	624,000	352	-0.848	Net sec. -Top
BC- 81 -13	90.0	2.283	1.317	56,600	633	-0.847	Gross sec.
BB - 70 - 6	144.0	2.360	1.100	26,500	566	-0.839	Net sec. -Top
BB - 70 - 7	120.0	1.925	1.302	70,000	470	-0.838	Net sec. -Top
BB - 70 - 8	75.0	1.625	1.662	633,000	294	-0.839	Net sec. -Top

Table 4.7

Fatigue Test Results for Back-to-Back Channel Specimens

(Test Temerature = 25°C)

Specimen	Load (kN) ±	Stroke (mm) ±	Freq. (Hz)	No. of Cycles	Stress Range (MPa)	Stress Ratio	Mode of Failure
BN-36-1	270	1.230	1.99	660,000	219	-0.933	Net-sec. Bottom Right
BN-36-2	325	1.472	1.61	336,000	257	-0.934	Net-sec. Top left & Bottom Right (web only)
BN-36-3	375	1.678	1.61	134,352	304	-0.932	Net-sec. Top Right & Left at spacer plate
BN-36-4	225	1.035	2.16	1,528,000	184	-0.932	Test stopped
BN-36-5	350	1.562	1.61	160,100	286	-0.932	Net-sec. Bottom Left
HBN-37-1	200	1.032	1.61	450,000	182	-0.932	Net-sec. Top Right
HBN-37-2	250	1.212	1.66	258,000	230	-0.932	Net-sec. Bottom Right
HBN-37-3	300	1.414	1.56	120,000	271	-0.932	Net-sec. Bottom Right & Bottom Left
HBN-37-4	150	0.767	2.60	1,290,000	137	-0.932	Test stopped
HBN-37-5	350	1.680	1.61	52,185	324	-0.933	Net-sec. Top , Left

Table 4.8

Fatigue Test Results for Back-to-Back Channel Specimens

(Test Temerature = -50°C)

Specimen	Load (kN) ±	Stroke (mm) ±	Freq. (Hz)	No. of Cycles	Stress Range (MPa)	Stress Ratio	Mode of Failure
HBN-37-6	170	0.995	1.49	1,306,275	151	-0.932	Test stopped
HBN-37-7	200	1.062	1.21	590,000	180	-0.931	Net-sec. Top Left
HBN-37-8	235	1.209	1.29	452,000	208	-0.932	Net-sec. Bottom Left
HBN-37-9	280	1.432	0.92	223,000	249	-0.932	Net-sec. Top & Bottom Left member
HBN-37-10	310	1.567	0.79	133,000	278	-0.932	Net-sec. Top Right

Table 4.9

Log - Log Relationships

σ_r = Ultimate stress range in MPa. P = Alternating fatigue load in kN.		S-N Relationship $\log N = a - b \log \sigma_r$		Load-N Relatioship $\log N = a - b \log P$	
		a	b	a	b
90°- angle section (BA)		16.23	4.14	12.69	4.34
60°- angle section (BC)	(One leg connected)	16.65	4.33	12.80	4.25
Lipped angle section (BB)		15.29	3.97	13.01	4.07
90°- angle section (BA)		21.92	6.08	15.58	5.50
60°- angle section (BC)	(Both legs connected)	16.18	4.08	12.71	4.07
Lipped angle section (BB)		17.72	4.83	14.86	4.83
T - Shaped section (BG)		15.64	3.95	14.36	3.95
Back-to-Back Channel section (BN)		16.19	4.43	17.52	4.81
Back-to-Back Channel section (HBN)		13.85	3.61	14.06	3.64
Back-to-Back Channel section (HBN) [a]		13.96	3.61	14.09	3.58

[a] This series of tests were conducted at - 50°C.
All other tests were conducted at room temperature (25°C)
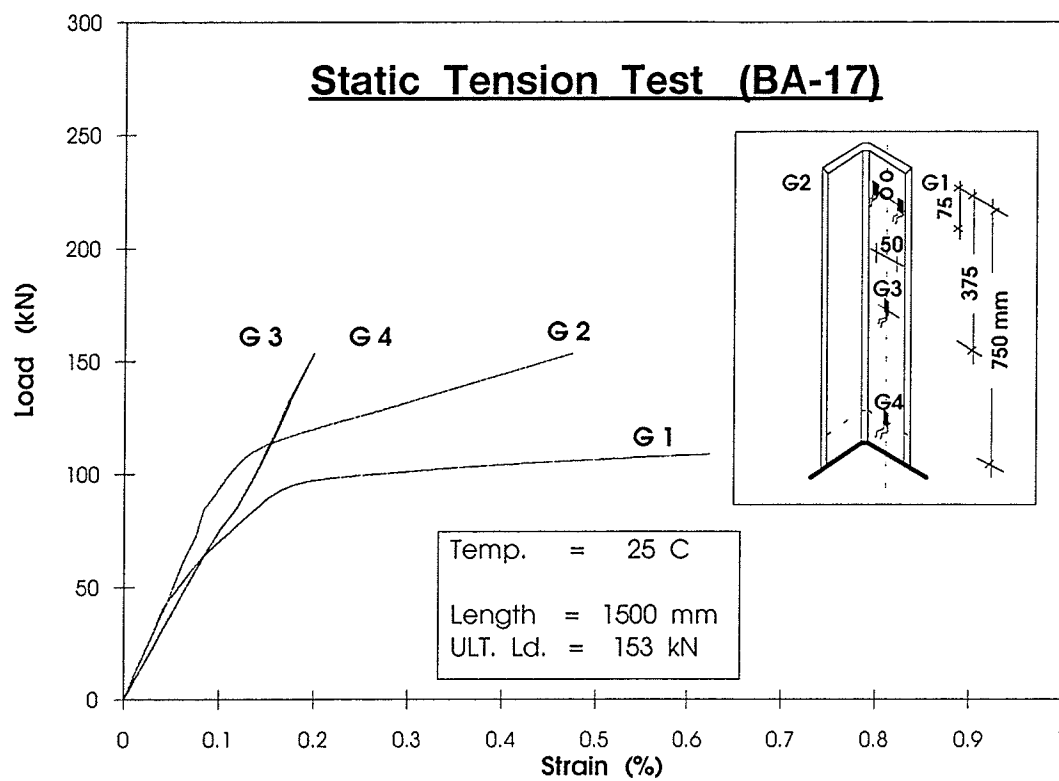
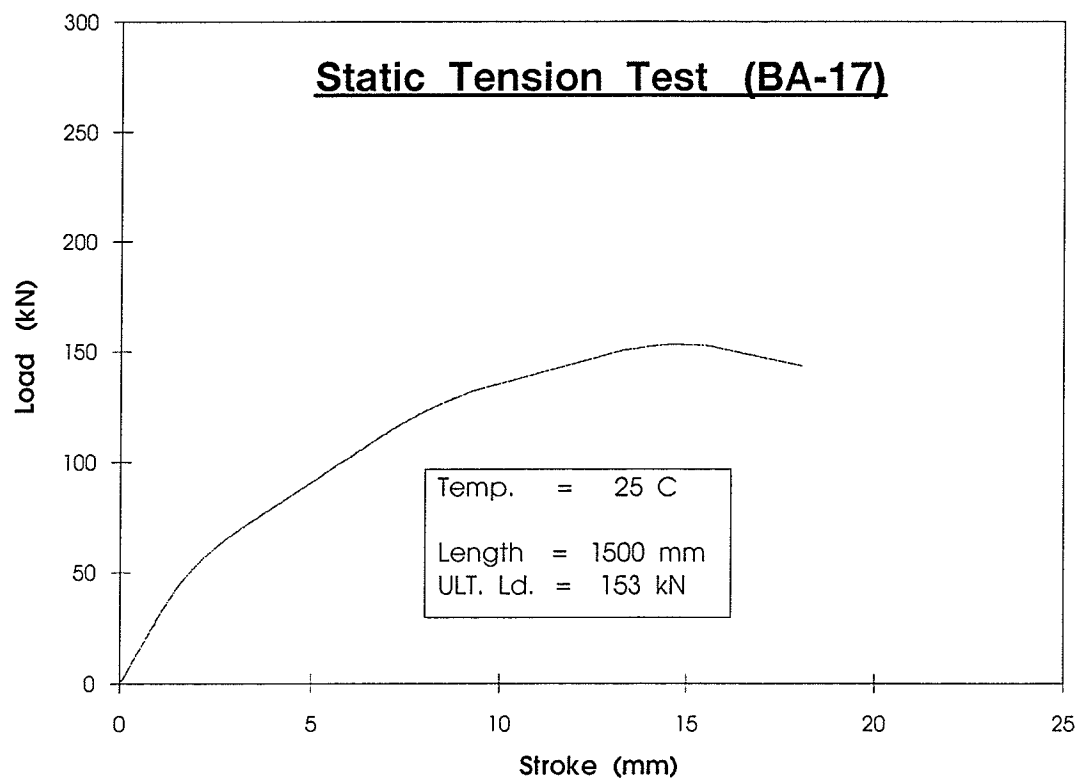Figure 4. 1 : Load-Strain Relationship for the 90°-angle section

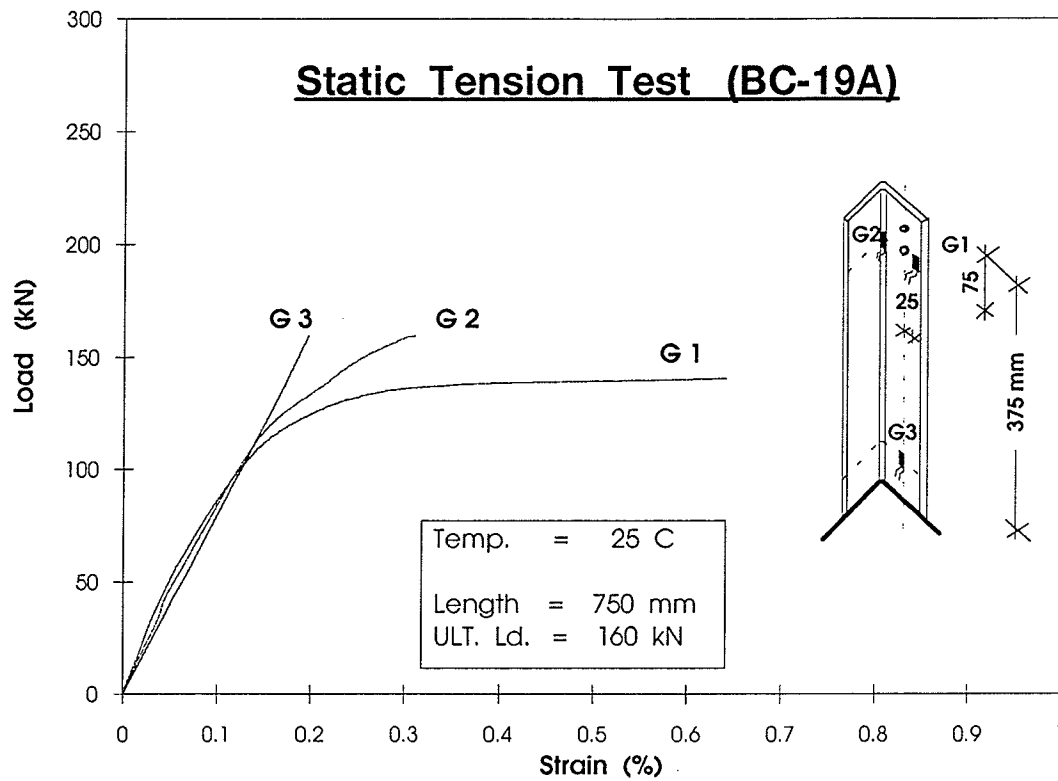Figure 4. 2 : Load-Stroke Relationship for the 90°-angle section

168

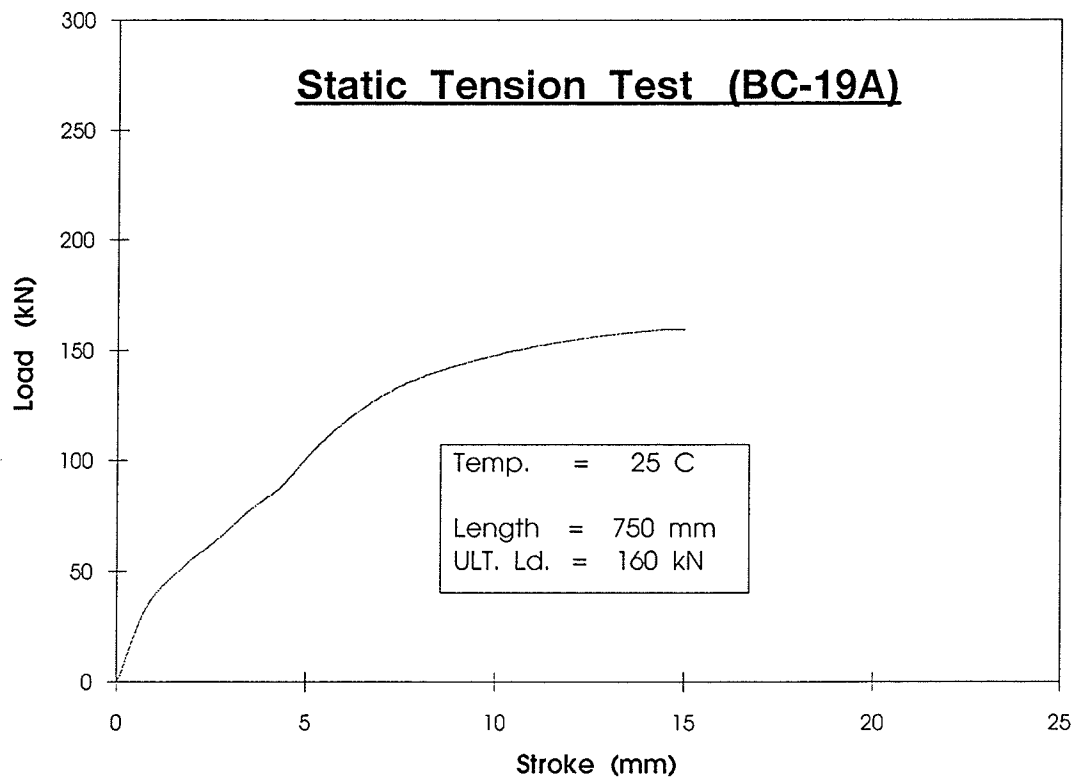Figure 4.3: Load-Strain Relationship for the 60°-angle section

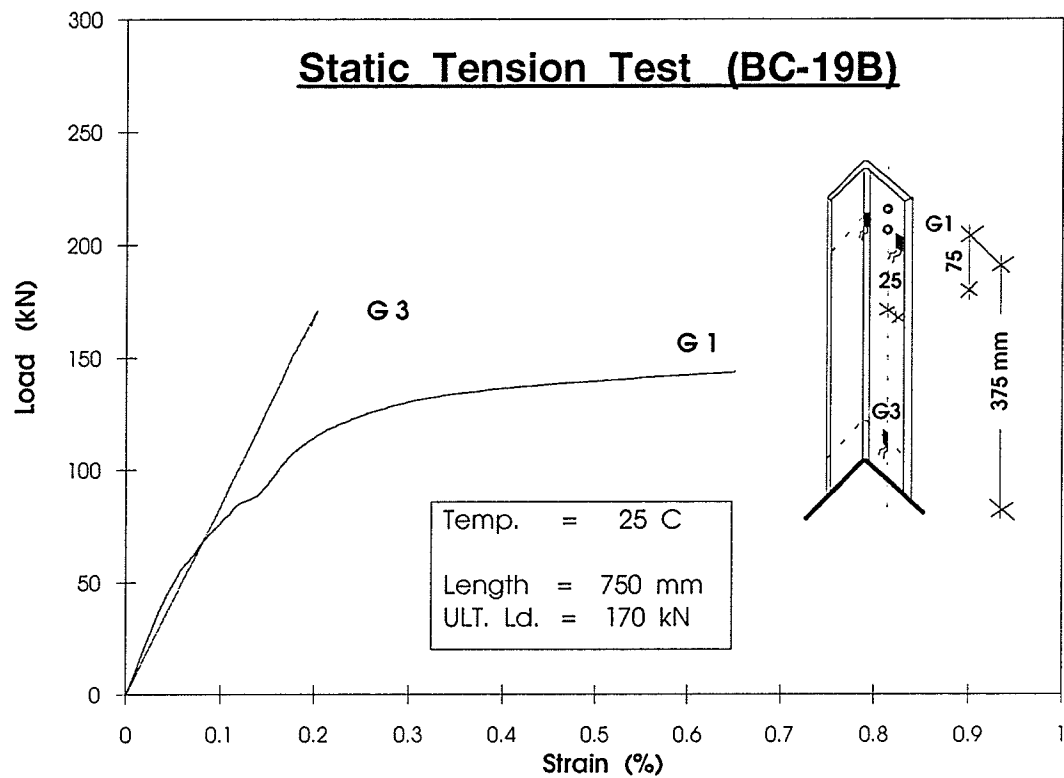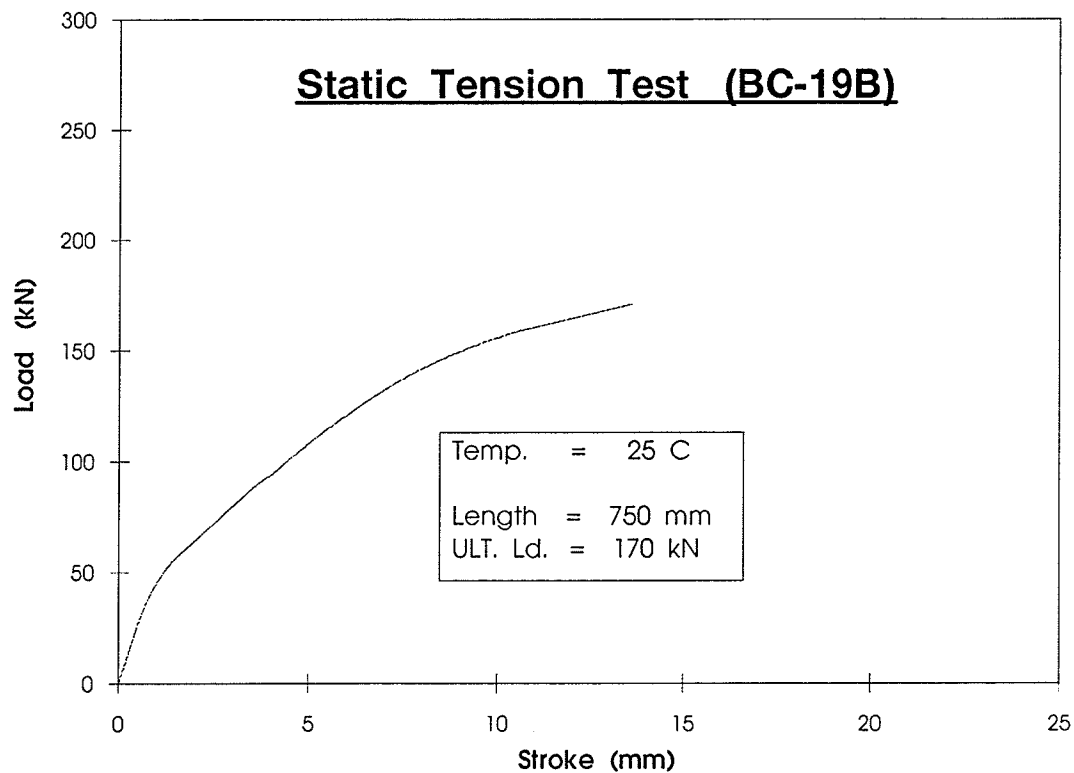Figure 4.4: Load-Stroke Relationship for the 90°-angle section

169

Figure 4. 5 : Load-Strain Relationship for the 60°-angle section

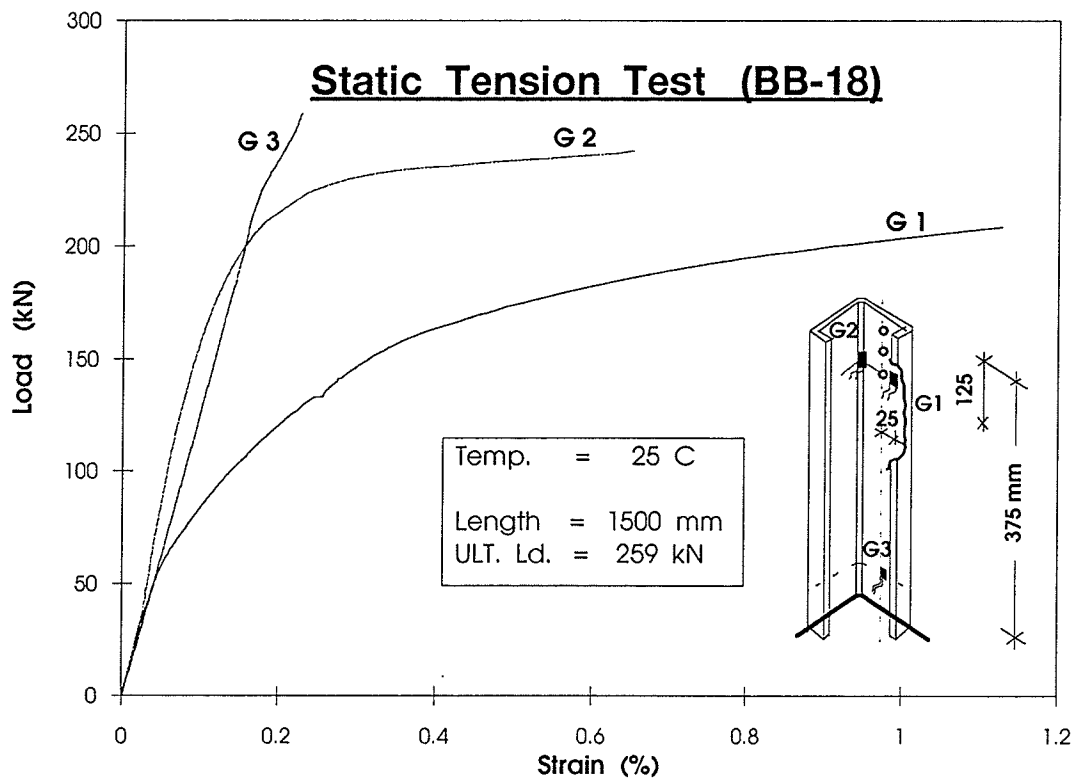Figure 4. 6 : Load-Stroke Relationship for the 60°-angle section

170

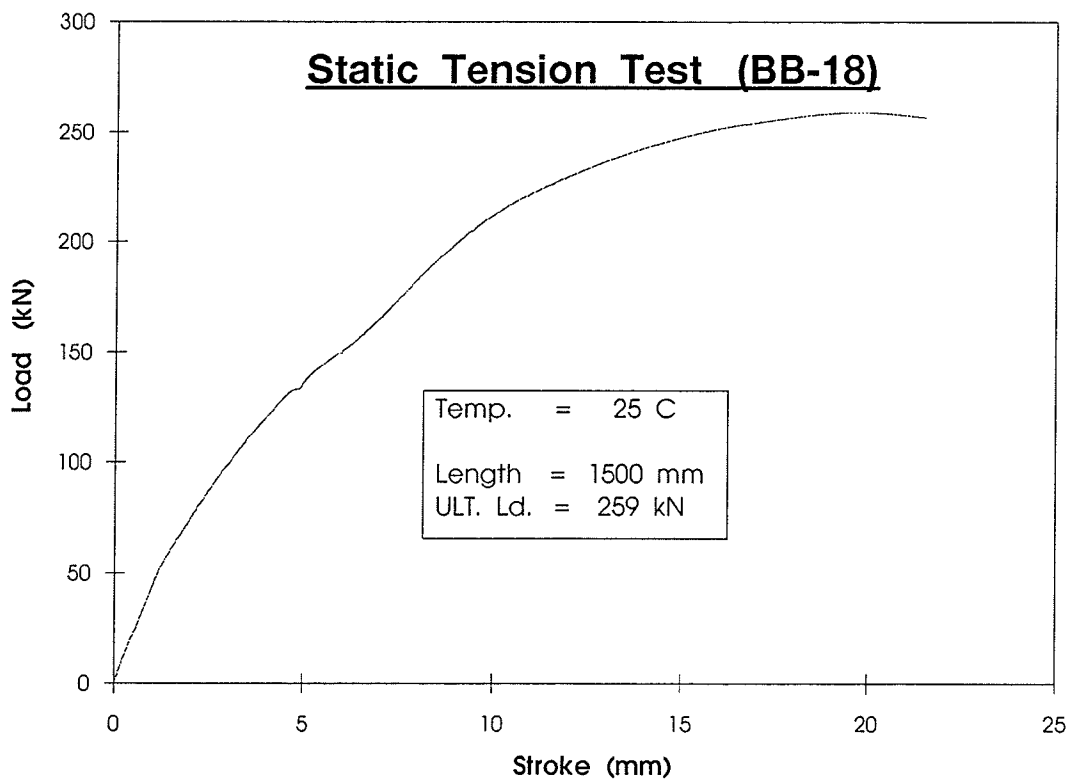Figure 4. 7 : Load-Strain Relationship for the Lipped angle section

Figure 4. 8 : Load-Stroke Relationship for the Lipped angle section
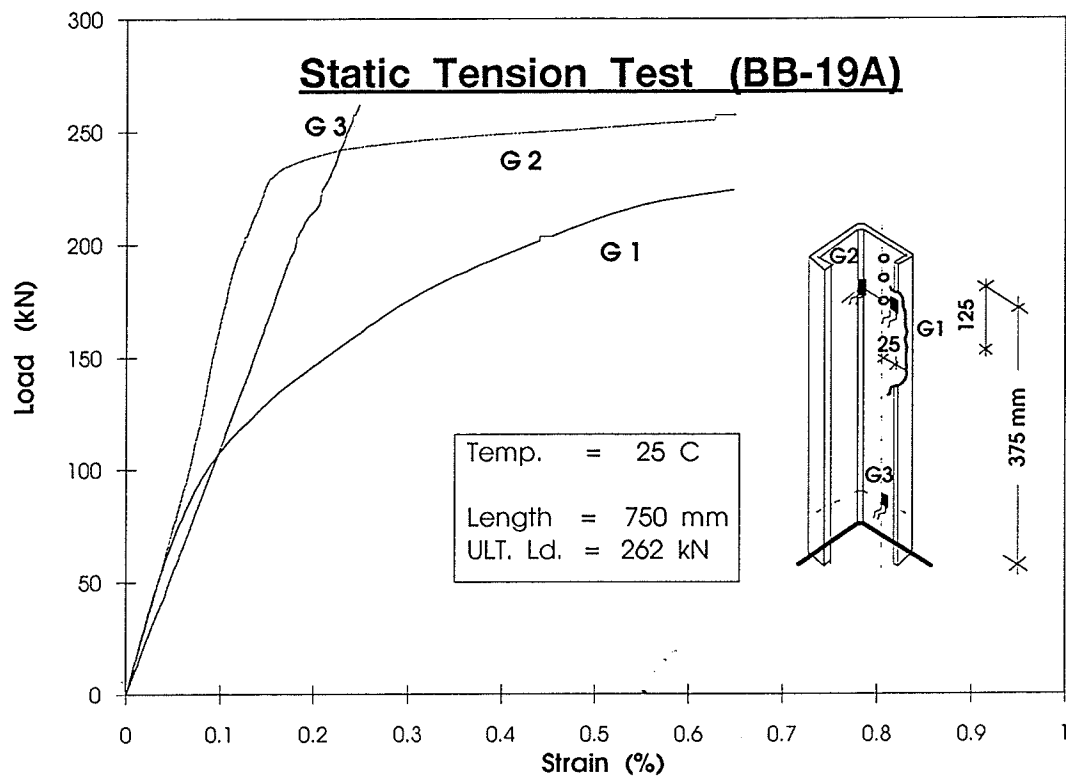
171

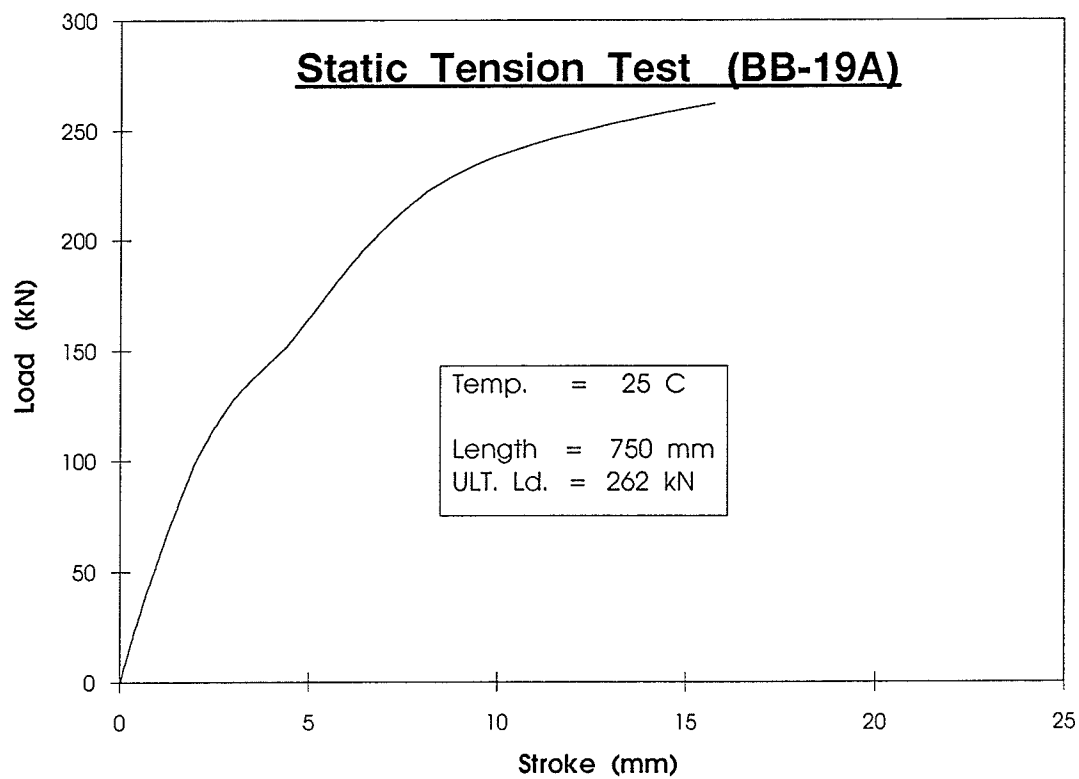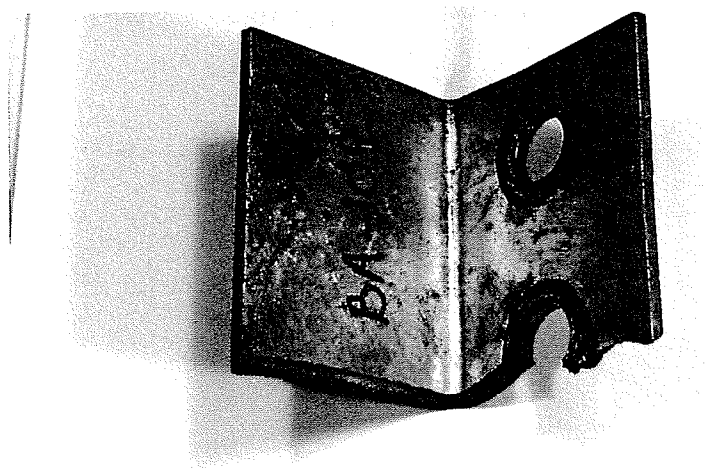Figure 4. 9 : Load-Strain Relationship for the Lipped angle section
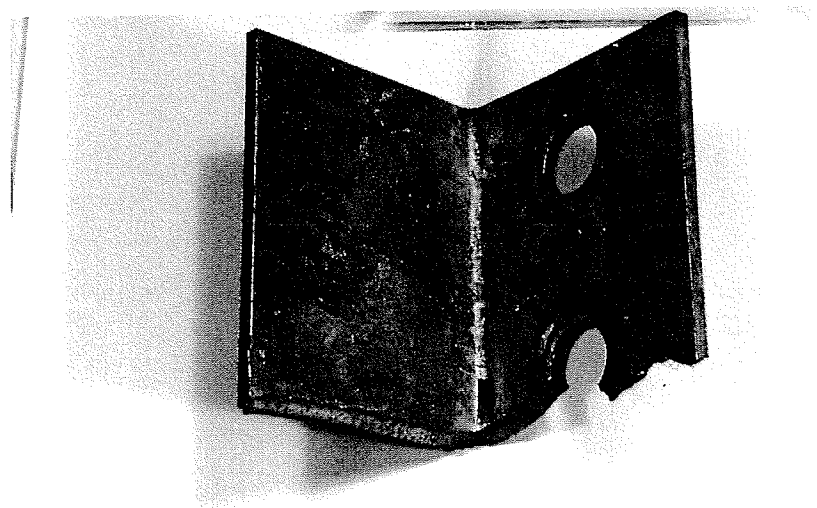

Figure 4. 10 : Load-Stroke Relationship for the Lipped angle section

172

BA-109- 3

(a) Specimen BA-109-3

BA-109- 5

(b) Specimen BA-109-5

Figure 4.11: First Mode of Failure for 90°-angle Specimens Connected Through
One Leg. (Net Section Failure)

BA-109- 4

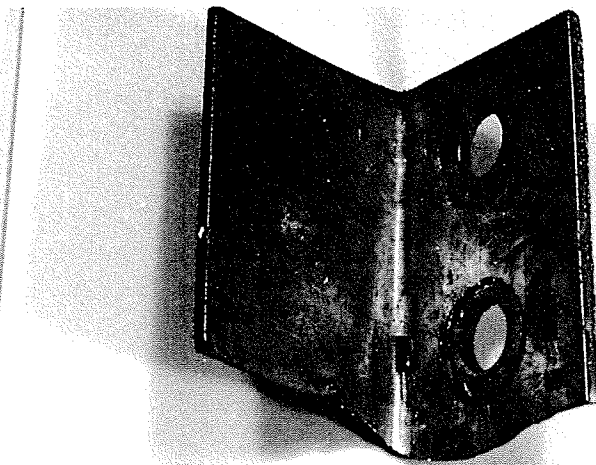(a) Specimen BA-109-4

BA-109- 9

(b) Specimen BA-109-9

Figure 4.12:   Second Mode of Failure for 90°-angle Specimens Connected Through
One Leg.   (Block Shear Failure)

BA-109-7

Figure 4.13: Third Mode of Failure for 90°-angle Specimens Connected Through One Leg. (Cross Section Failure)

BA-109-12

Figure 4.14: Mode of Failure for 90°-angle Specimens Connected Through Both Legs.

BC- 81- 4

(a) Specimen BC-81-4
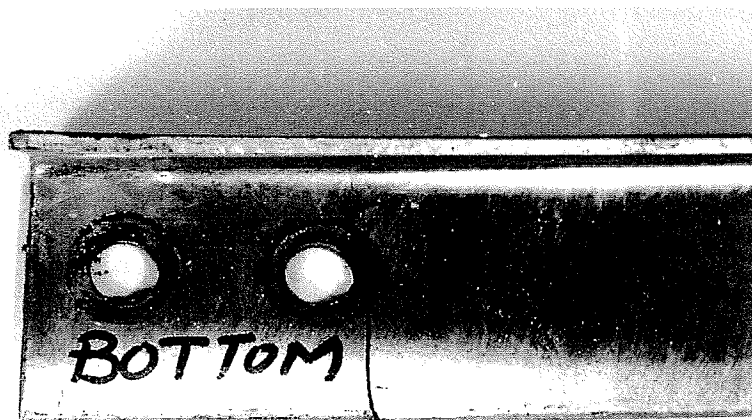
BC- 81- 9

(b) Specimen BC-81-9

Figure 4.15: First Mode of Failure for 60°-angle Specimens Connected Through One Leg. (Net Section Failure)
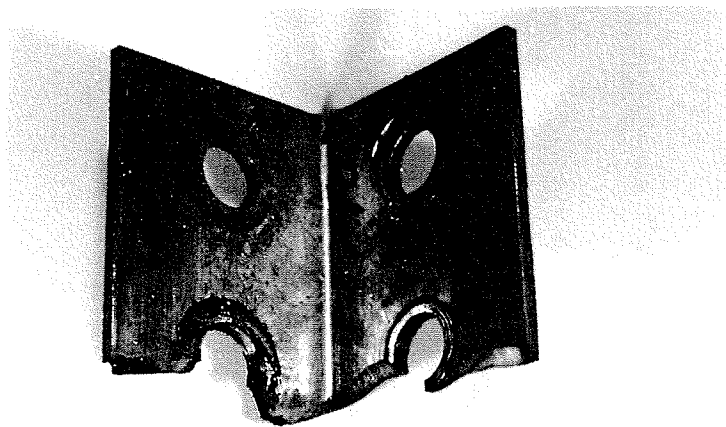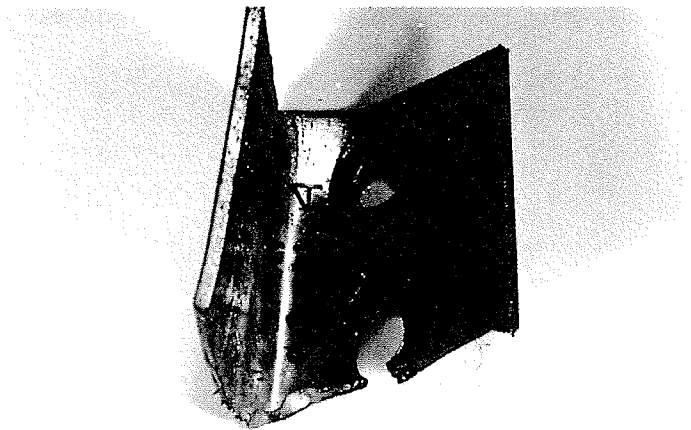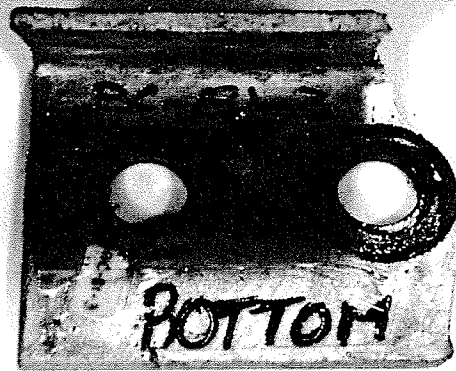
BC- 81- 3

(a) Specimen BC-81-3

BC- 81- 7

(b) Specimen BC-81-7

Figure 4.16: Second Mode of Failure for 60°-angle Specimens Connected Through One Leg. (Gross Section Failure)

Figure 4.17: Engraved Letter at the Back Side of the 60°-angle Specimens.

BC- 81-12

Figure 4.18:   Net Section Failure for a 60°-angle Specimen Connected Through Both Legs.

BB- 70- 1

(a) Specimen BB-70-1
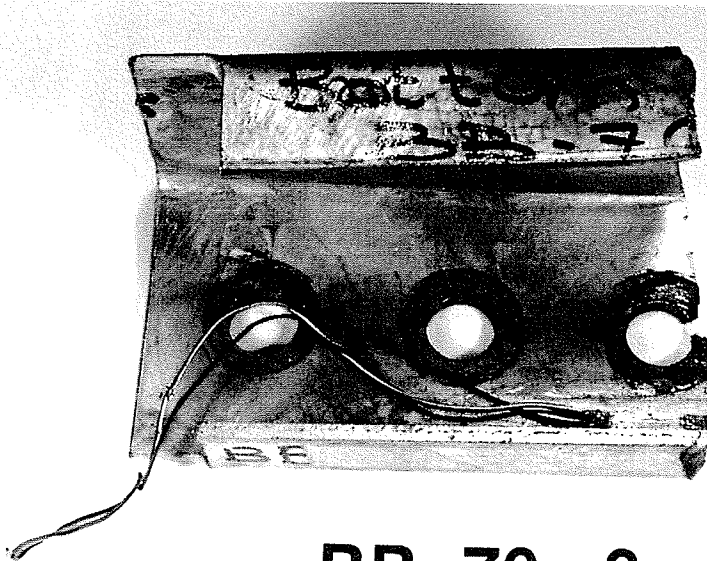
BB- 70 - 3

(b) Specimen BB-70-3

Figure 4.19: Fatigue Failure of Lipped angle Specimens Connected Through One Leg.

Figure 4.20: Lipped angle Specimen BB-70-3 at Failure.
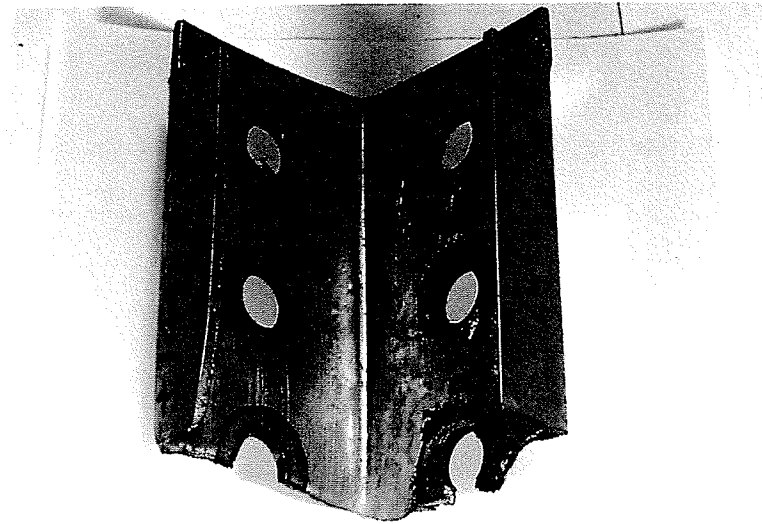
BB- 70- 6

(a) Specimen BB-70-6
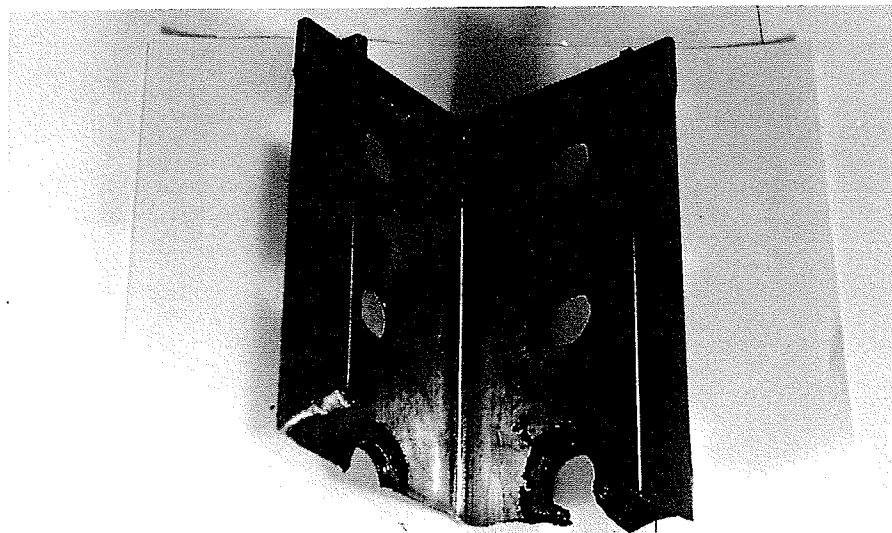
BB- 70- 7

(b) Specimen BB-70-7

Figure 4.21: Net Section Failures of Lipped angle Specimens Connected Through Both Legs.
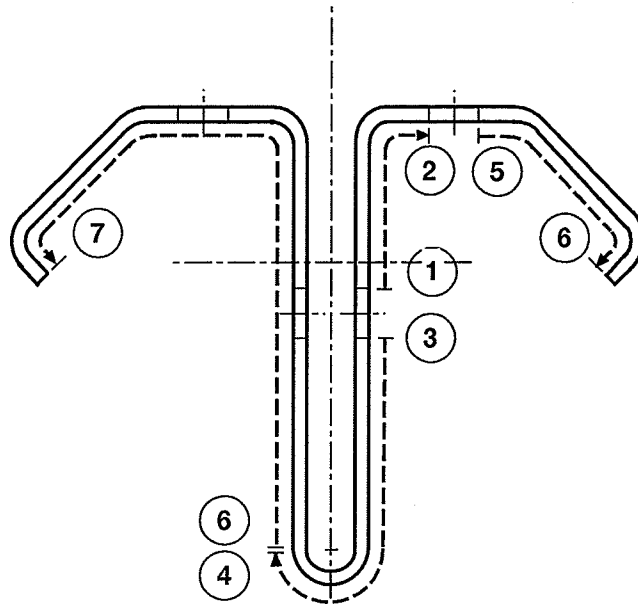
BG - Section.

Stages	% of Total Fatigue Life Consumed	
	From	To
(1) ⟶ (2)	50 - 60	75 - 85
(3) ⟶ (4)	75 - 85	90 - 95
(5) ⟶ (6)	90 - 95	98 - 99
(6) ⟶ (7)	99	100

Figure 4.22 : Crack Propagation Stages for the T - Shaped Section (BG).
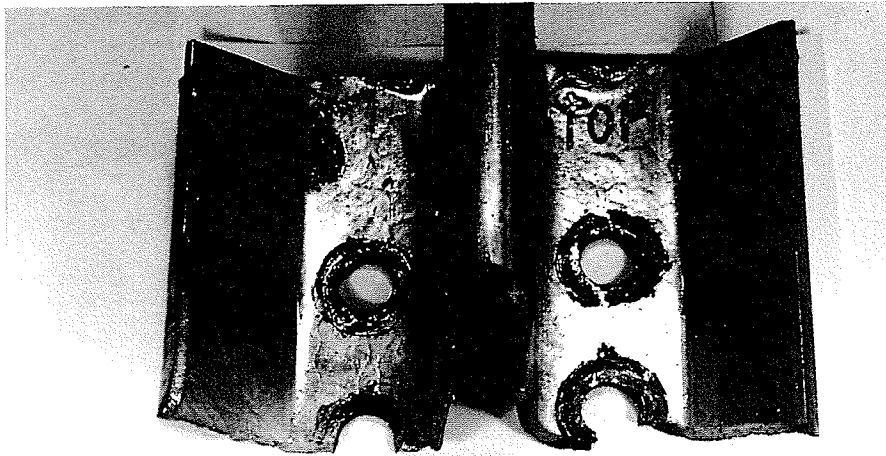
BG - 36 - 2

Figure 4.23: Net Section Failure of T-shaped Specimen BG-36-2.
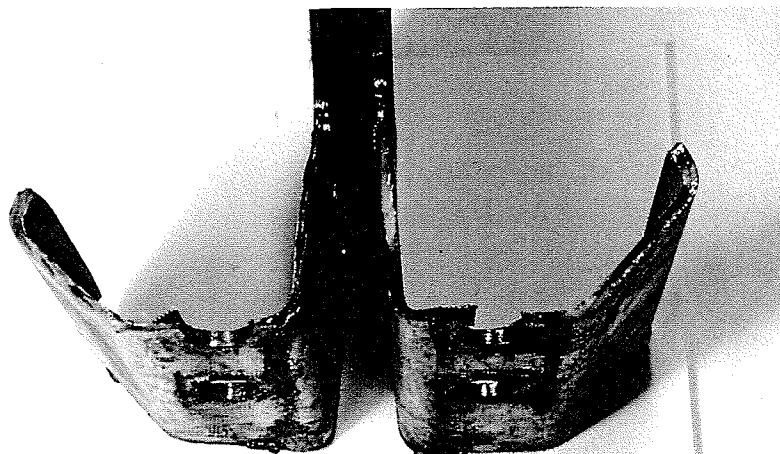
BG - 36 - 2

Figure 4.24: Fractured Surface of T-shaped Specimen BG-36-2.
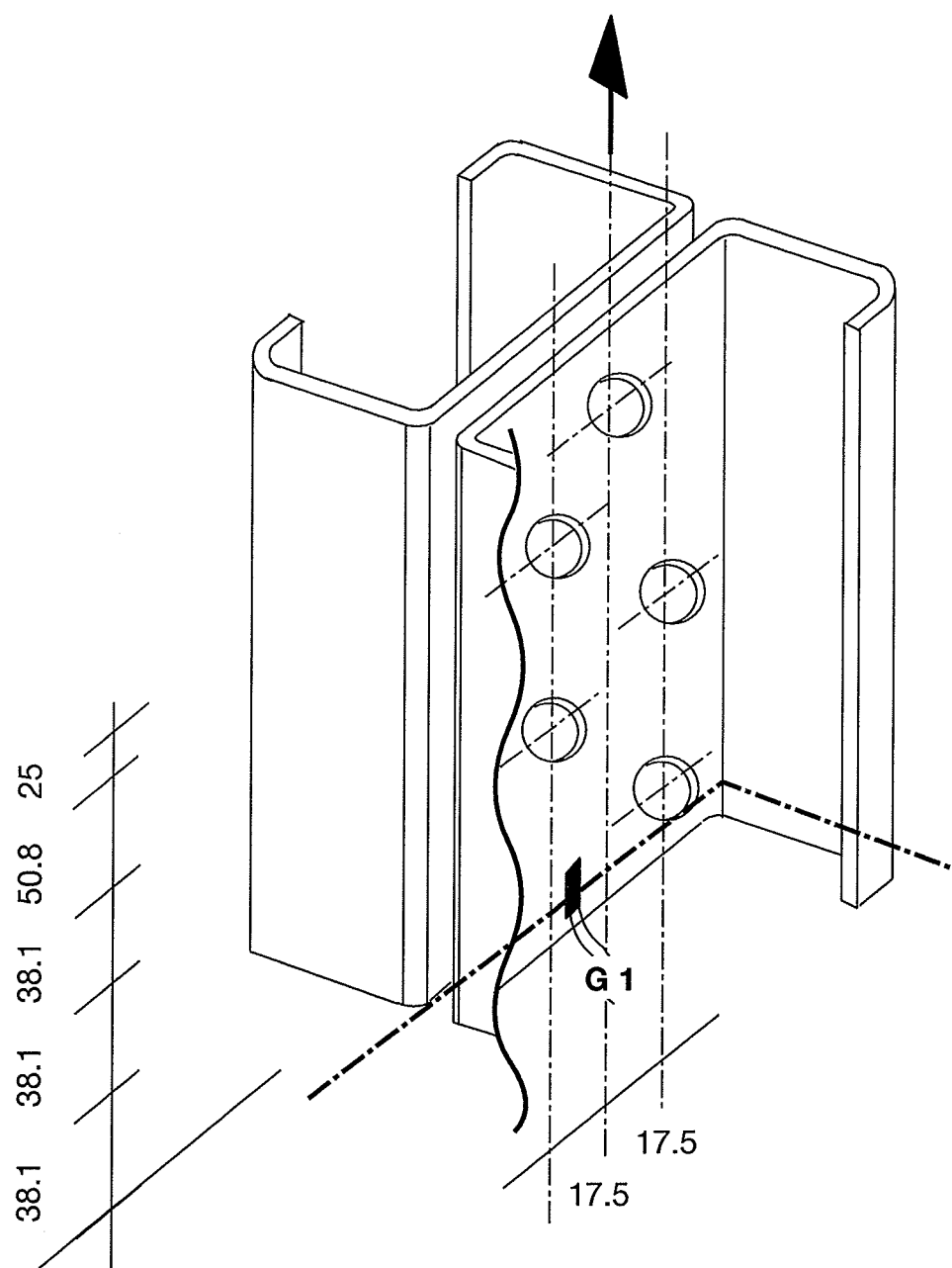
Figure 4.25 : Staggered Bolt Pattern for Back-to-Back Channel Specimens.
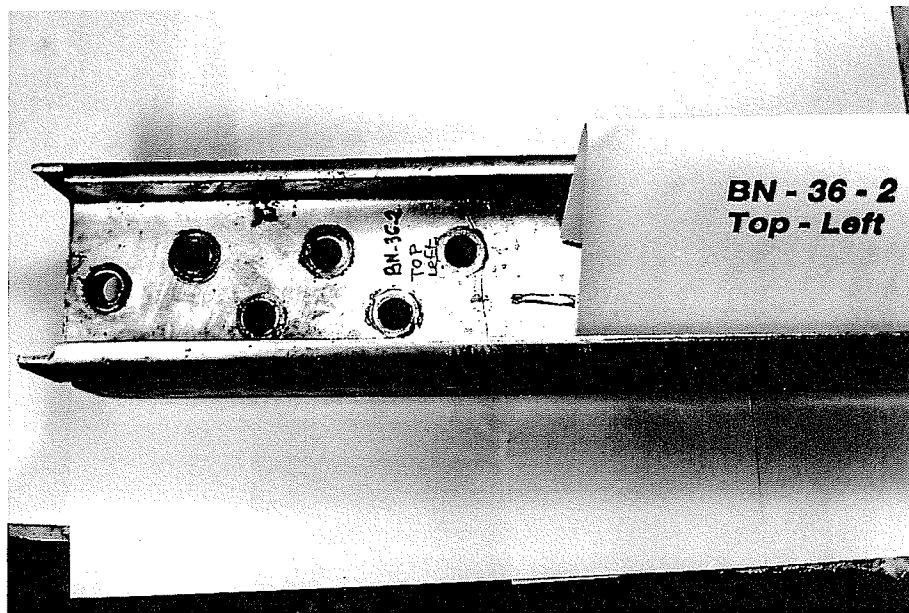
(a)   Top End Portion of Left Channel
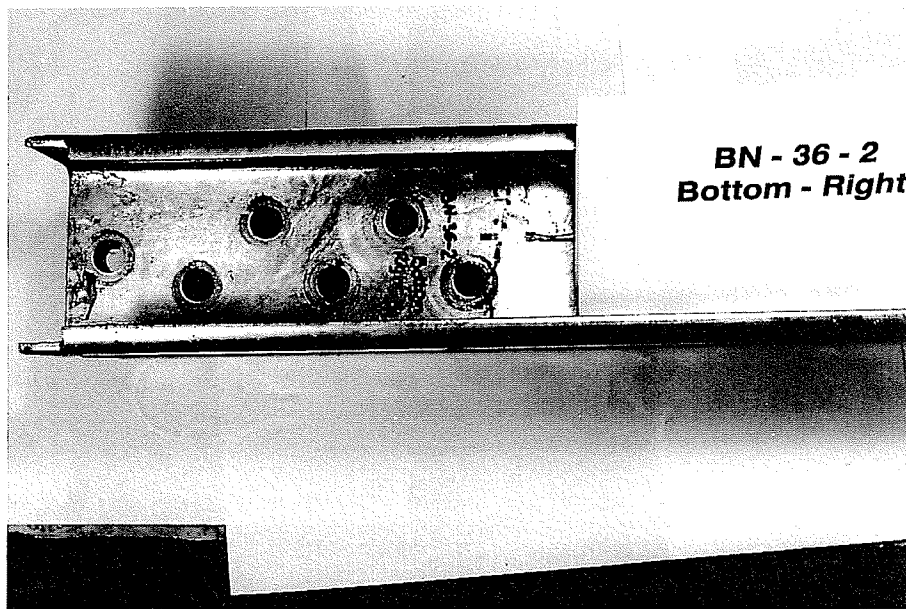
(b)   Bottom End Portion of Right Channel

Figure 4.26:   Compound Fatigue Failure of Back-to-Back
Channel Specimen   BN-36-2.
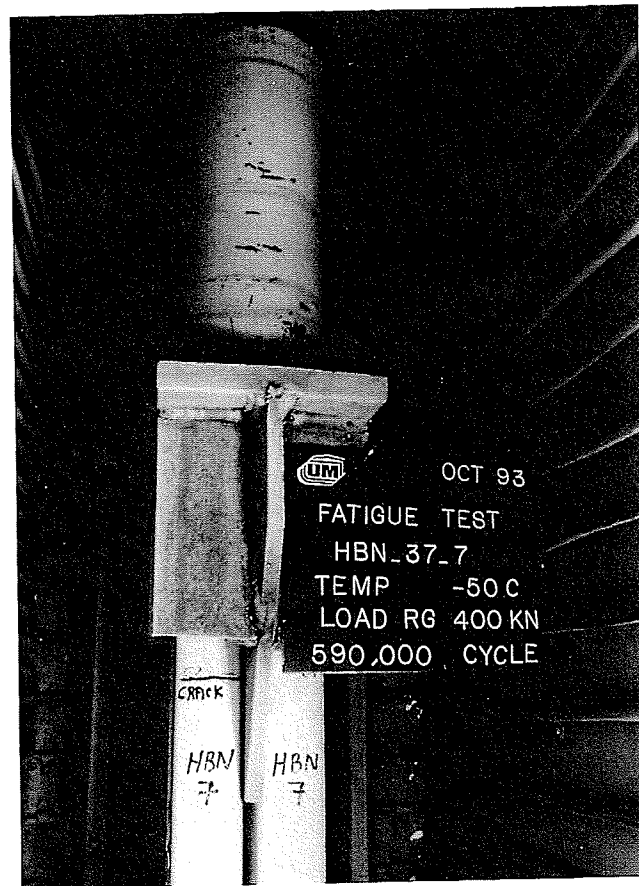
Figure 4.27:   Back-to-Back Channel Specimen   HBN-37-7
Tested at -50°C
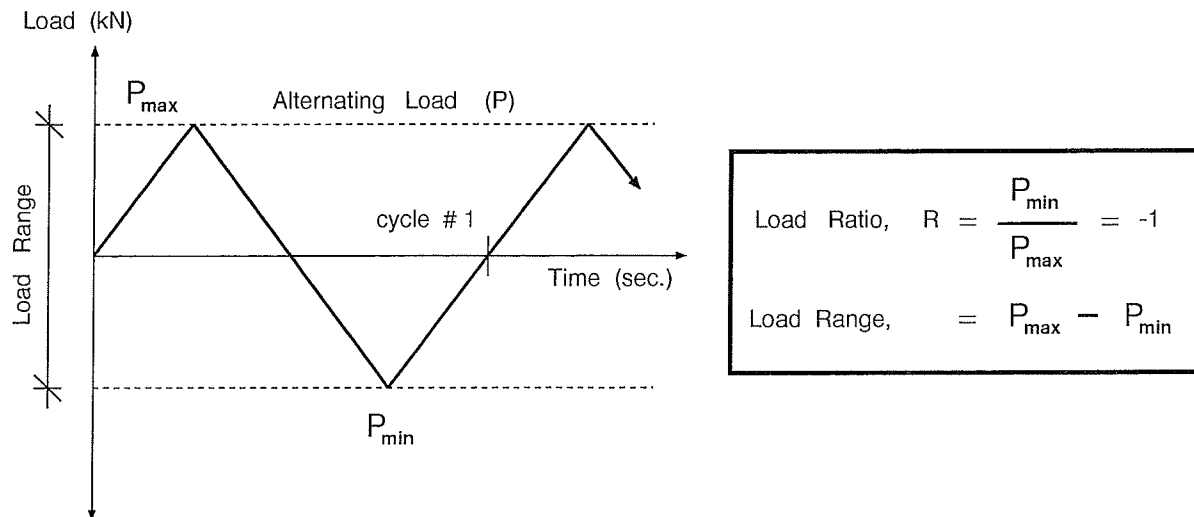
Figure 4.28: Triangular Wave Form Adopted in Fatigue Tests

(a) Stress-Strain Loops.
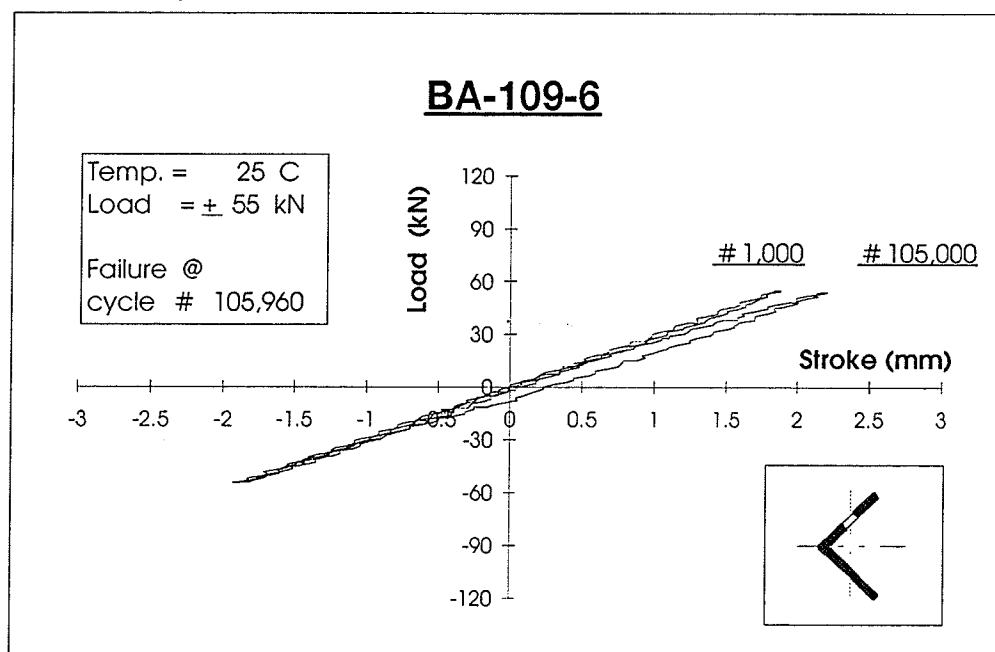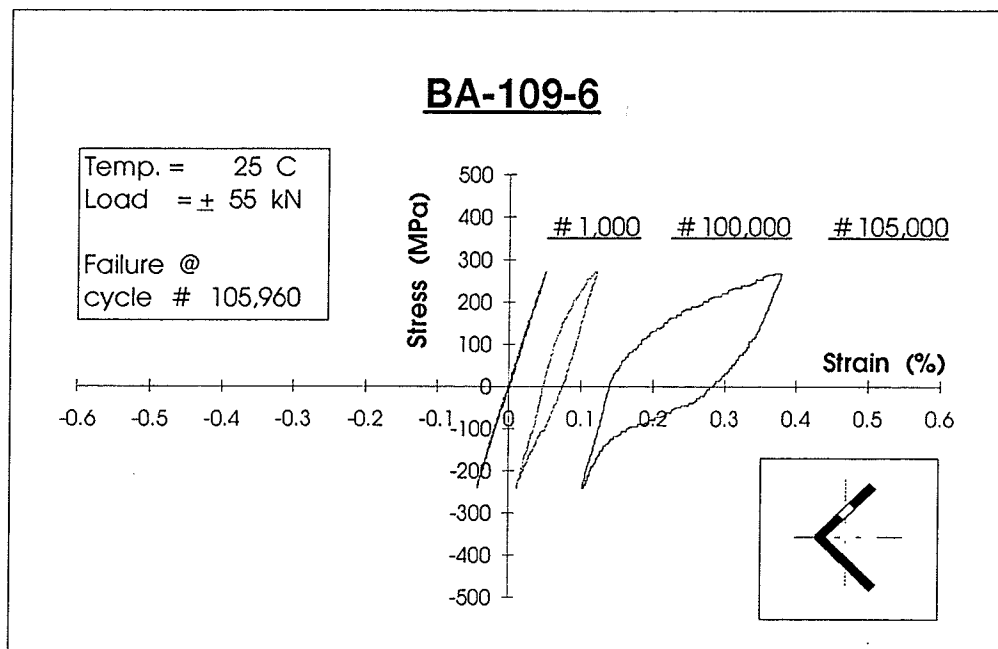
(b) Load-Stroke Loops.

Figure 4. 29 : Stress-Strain and Load-Stroke Loops for Specimen BA-109-6
(One Leg Connected)

187

(a) Stress -Strain Loops.
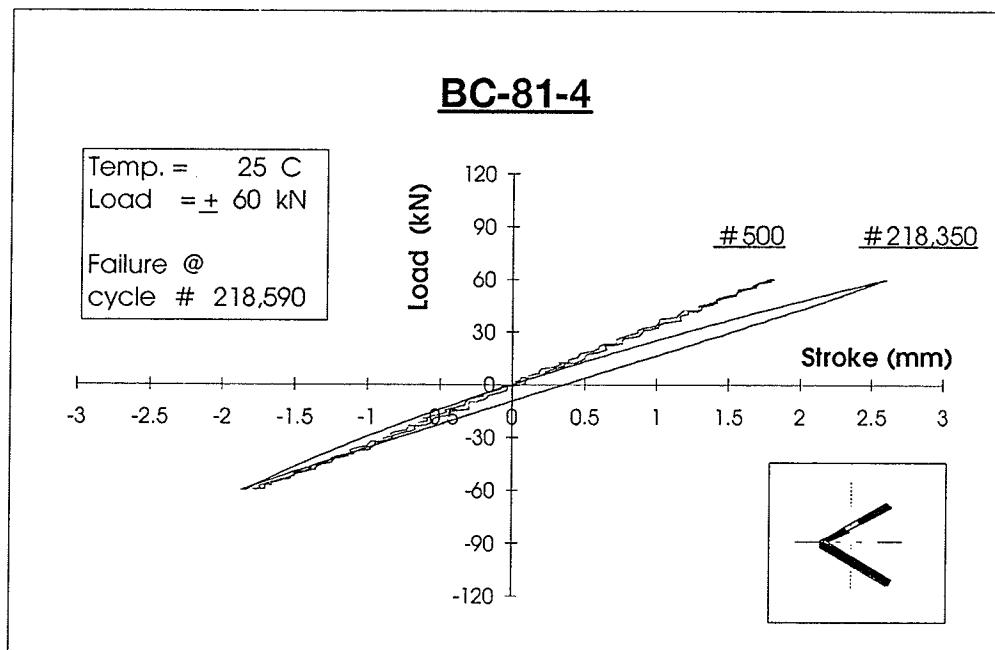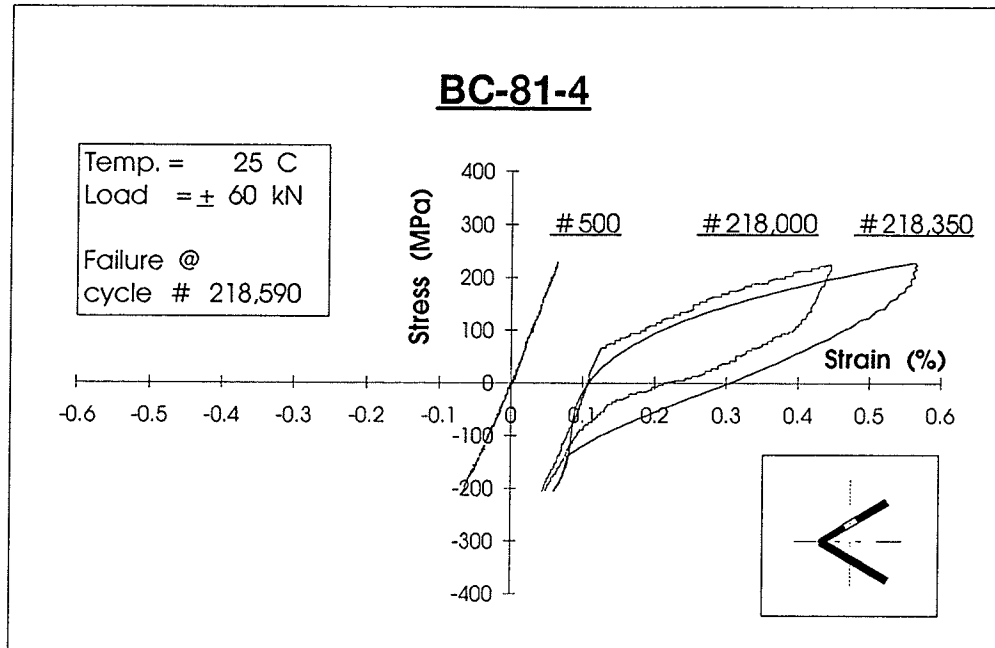
(b) Load-Stroke Loops.

Figure 4.30 : Stress-Strain and Load-Stroke Loops for Specimen BC-81-4
(One Leg Connected)

188

(a) Stress -Strain Loops.
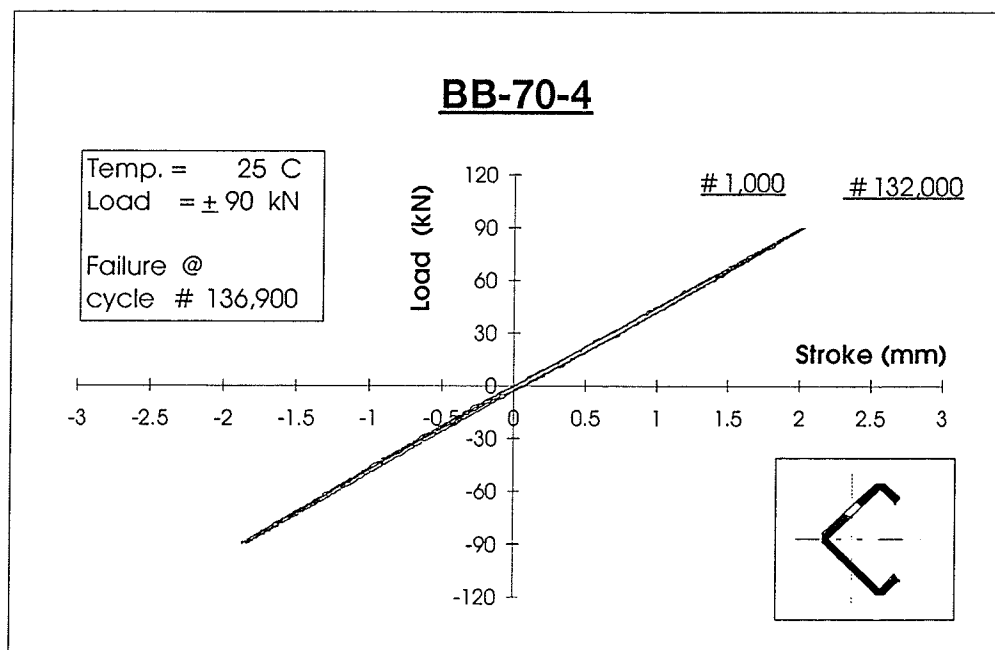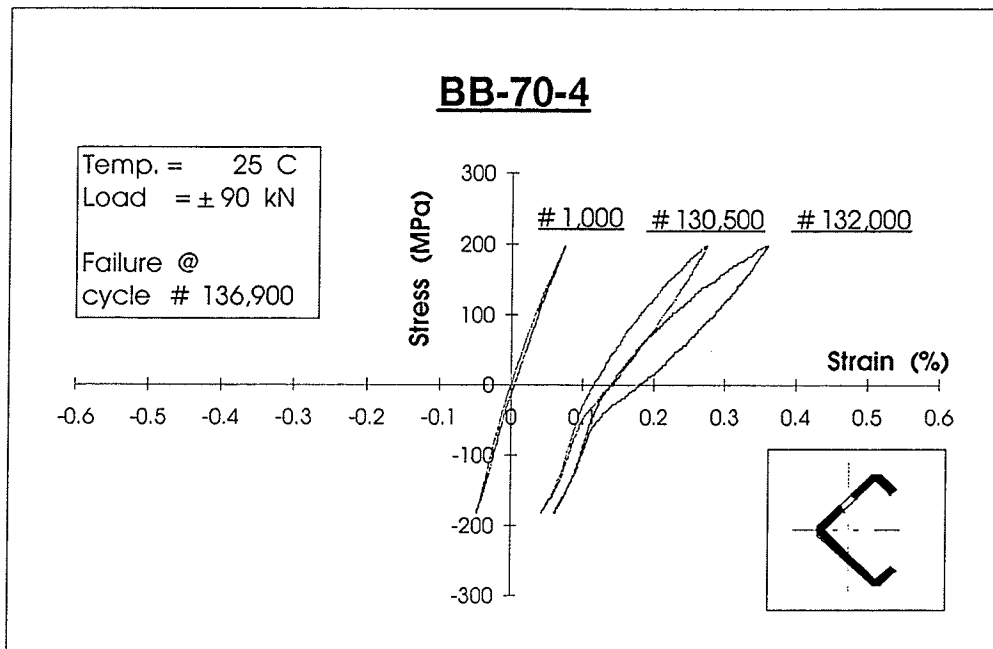
(b) Load-Stroke Loops.

Figure 4. 31 : Stress-Strain and Load-Stroke Loops for Specimen BB-70-4 (One Leg Connected)

189

Figure 4.32 : Lateral Displacements at the Mid-Height Section of Specimen BA-109-6
(One Leg Connected)

Figure 4.33: Lateral Displacements at the Mid-Height Section of Specimen BC-81-4
(One Leg Connected)
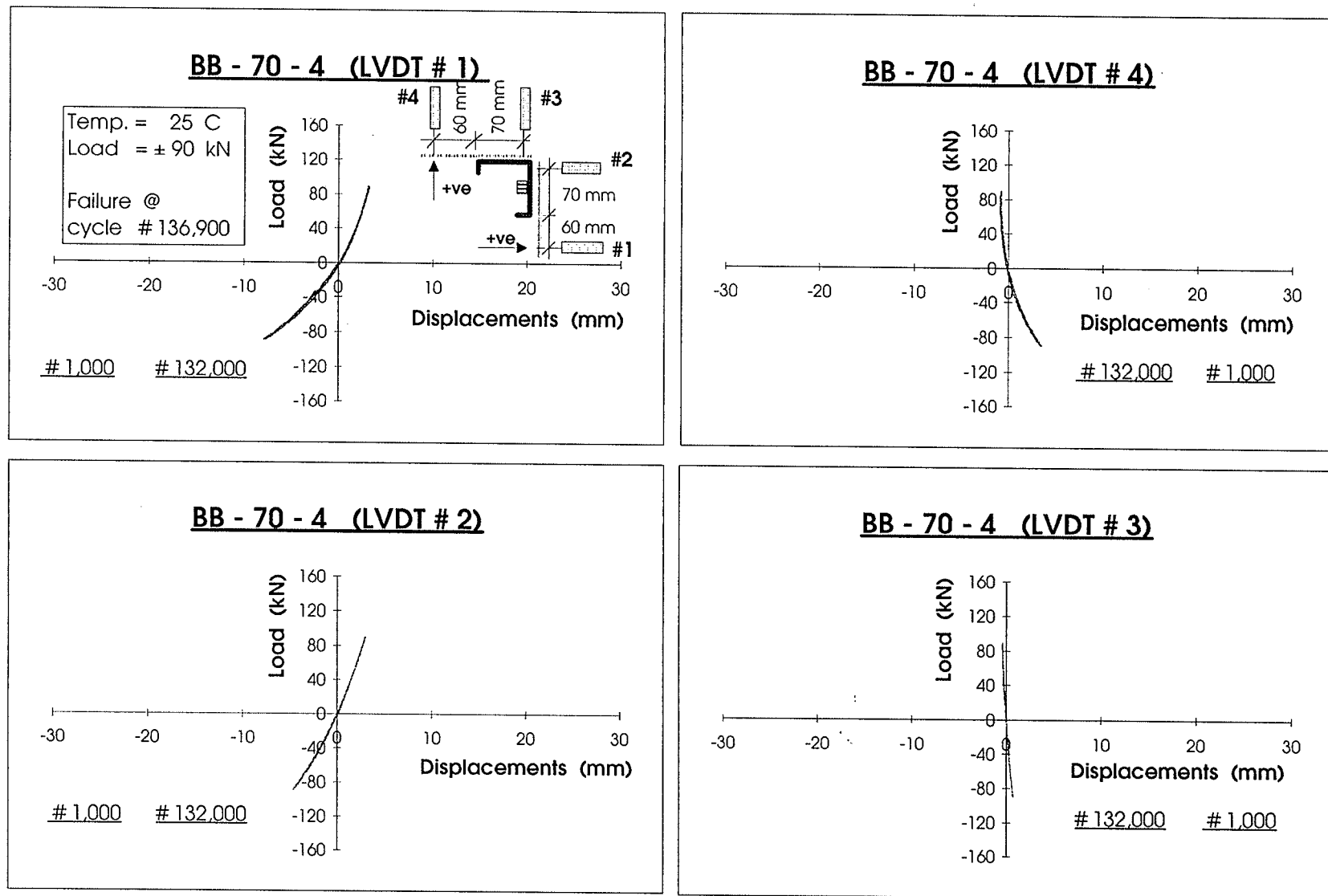
Figure 4. 34 : Lateral Displacements at the Mid-Height Section of Specimen BB-70-4 (One Leg Connected)
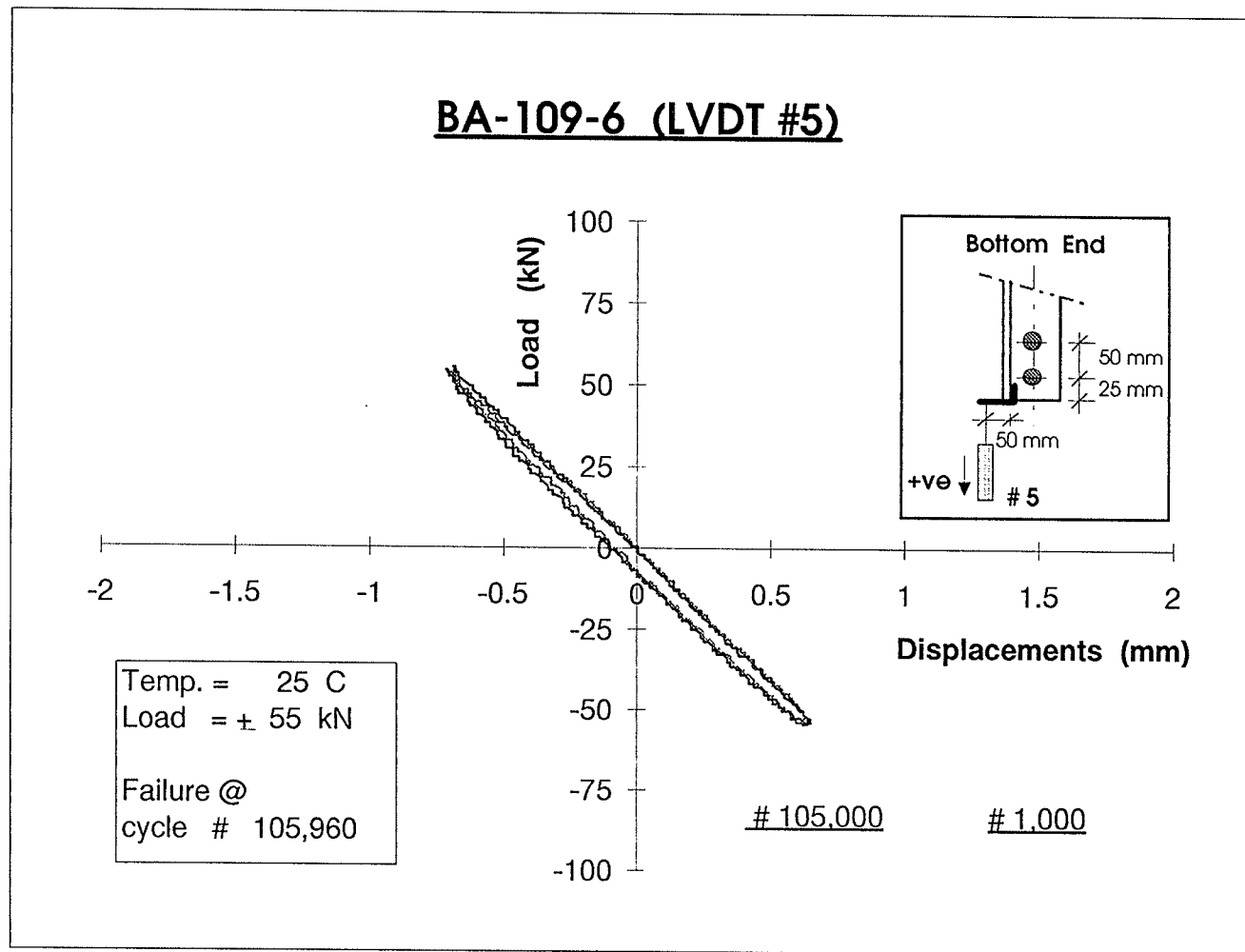
Figure 4.35 : Load-Displacement Relationship at the Bottom End Section of Specimen BA-109-6 (One Leg Connected)
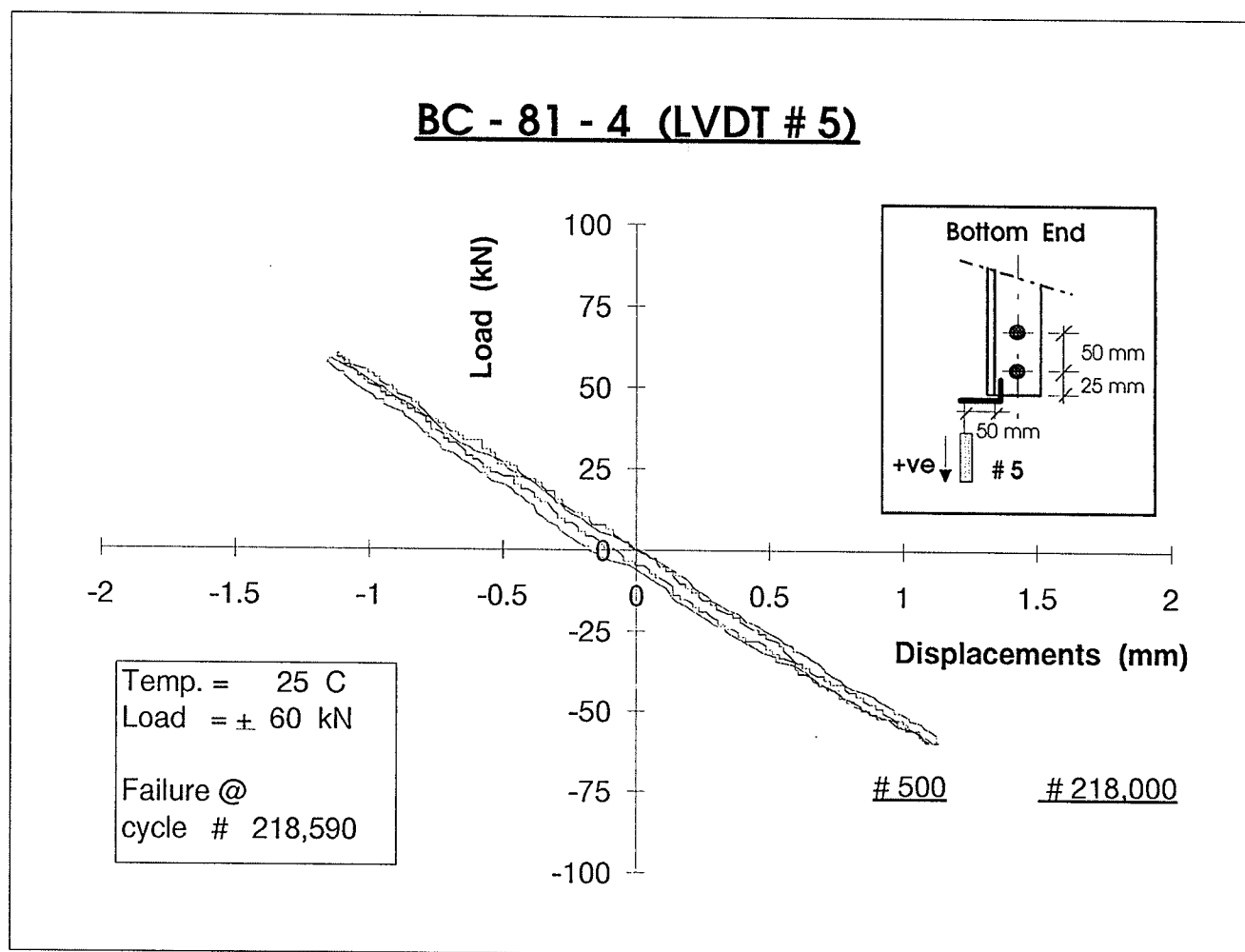
Figure 4. 36 : Load-Displacement Relationship at the Bottom End Section of Specimen BC-81-4
        (One Leg Connected)
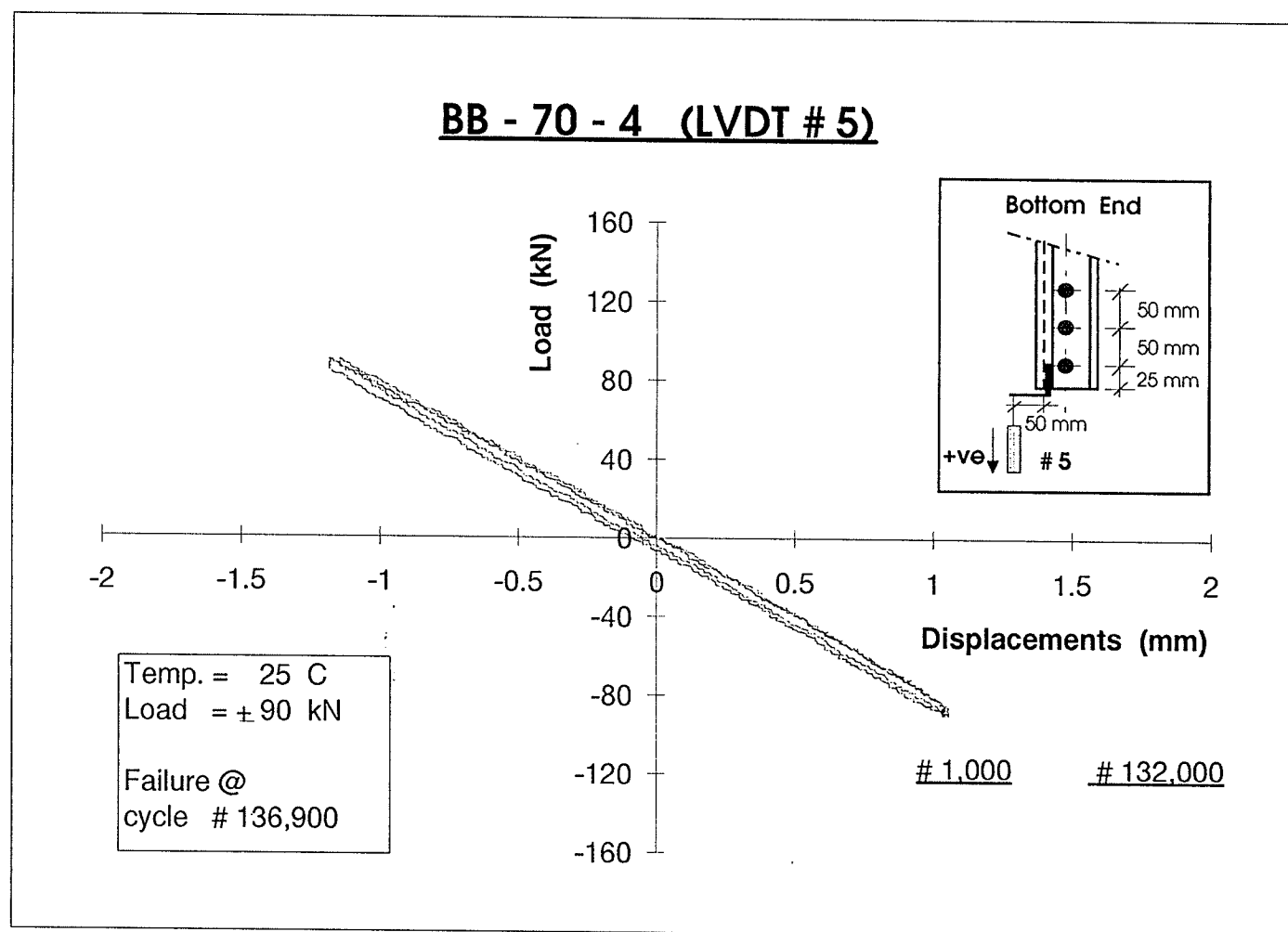
Figure 4.37 : Load-Displacement Relationship at the Bottom End Section of Specimen BB-70-4 (One Leg Connected)

BA-109-13

Temp. =   25 C
Load = ± 110 kN

Failure @
cycle # 22,000

Stress (MPa)

500
400
300
200
100
0
-100
-200
-300
-400
-500

#1,000   #10,000   #20,000   #21,000

Strain (%)

-0.7 -0.6 -0.5 -0.4 -0.3 -0.2 -0.1   0.1 0.2 0.3 0.4 0.5 0.6 0.7

(a) Stress -Strain Loops.

BA-109-13

Temp. =   25 C
Load = ± 110 kN

Failure @
cycle # 22,000

Load (kN)

120
90
60
30
0
-30
-60
-90
-120

#1,000   #21,000

Stroke (mm)

-3 -2.5 -2 -1.5 -1 -0.5   0   0.5   1   1.5   2   2.5   3
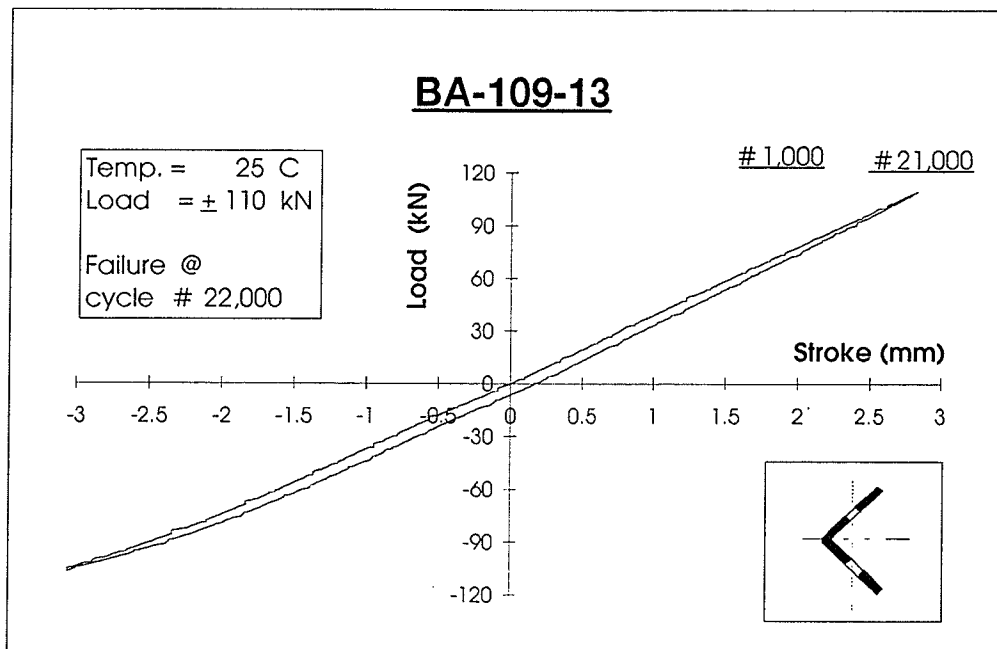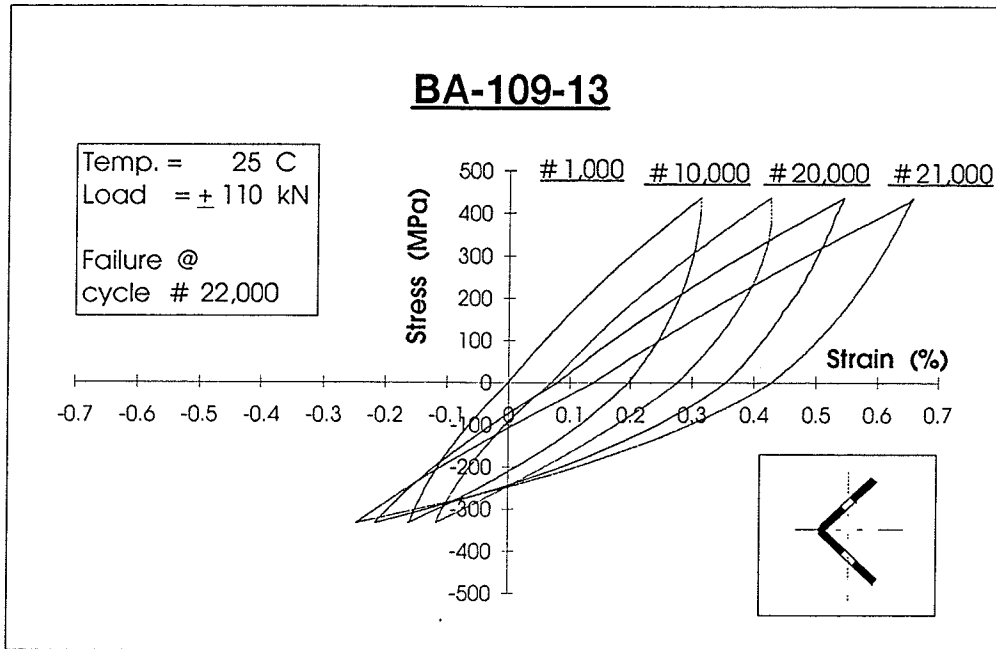
(b) Load-Stroke Loops.

Figure 4. 38 : Stress-Strain and Load-Stroke Loops for Specimen BA-109-13
(Both Leg Connected)

196
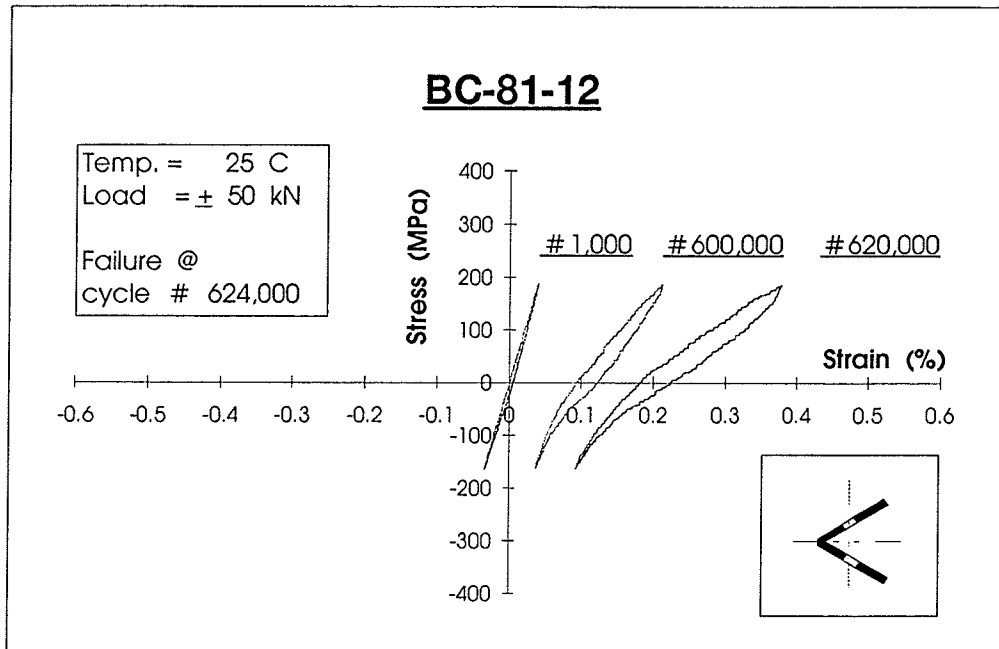
BC-81-12

(a) Stress -Strain Loops.
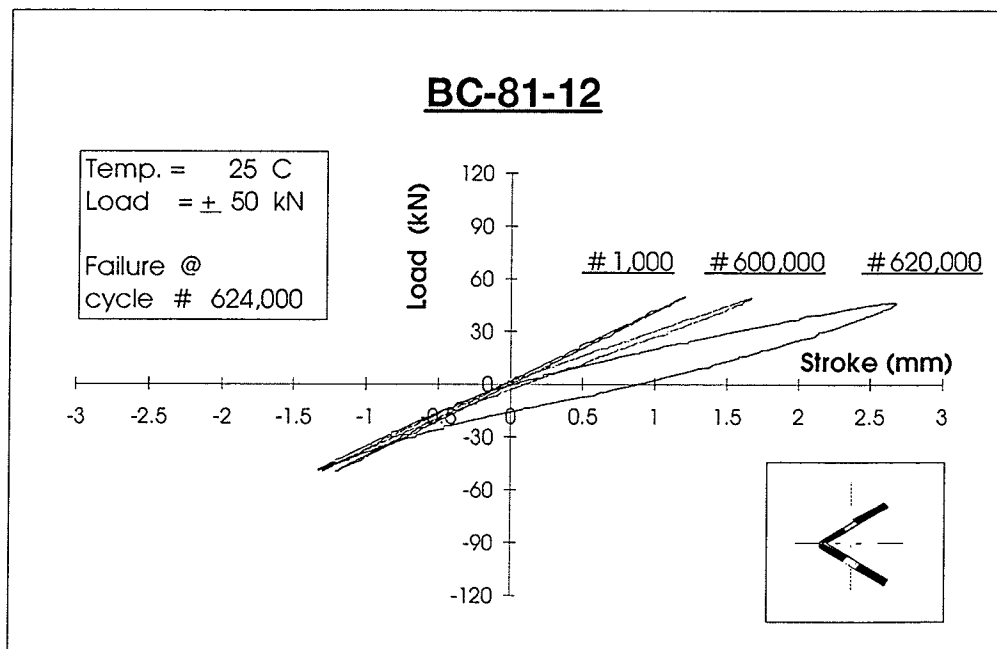
BC-81-12

(b) Load-Stroke Loops.

Figure 4. 39 : Stress-Strain and Load-Stroke Loops for Specimen BC-81-12
(Both Leg Connected)

197
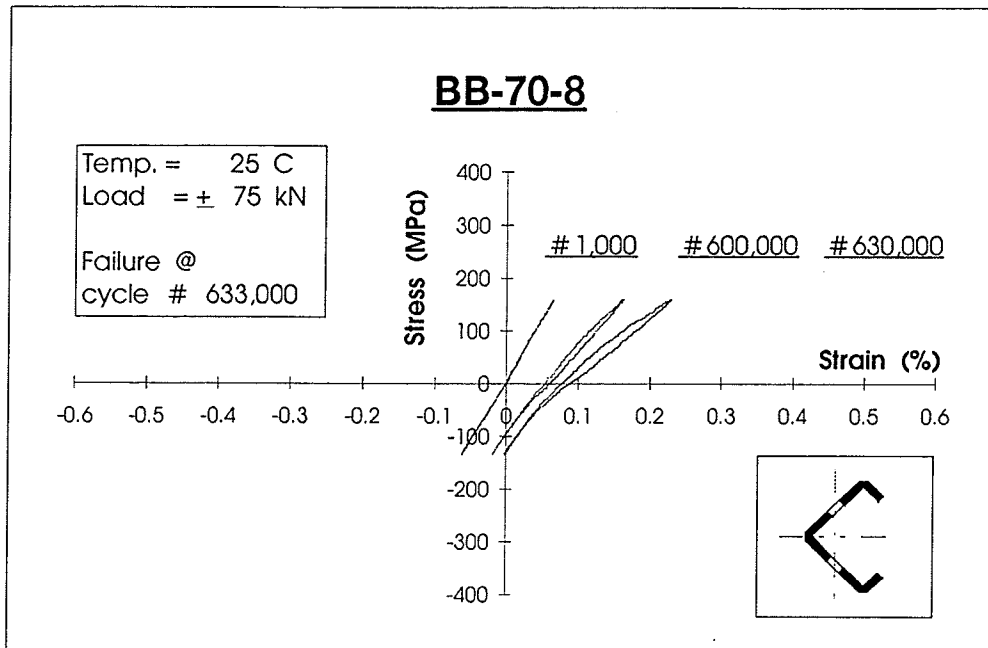
(a) Stress -Strain Loops.
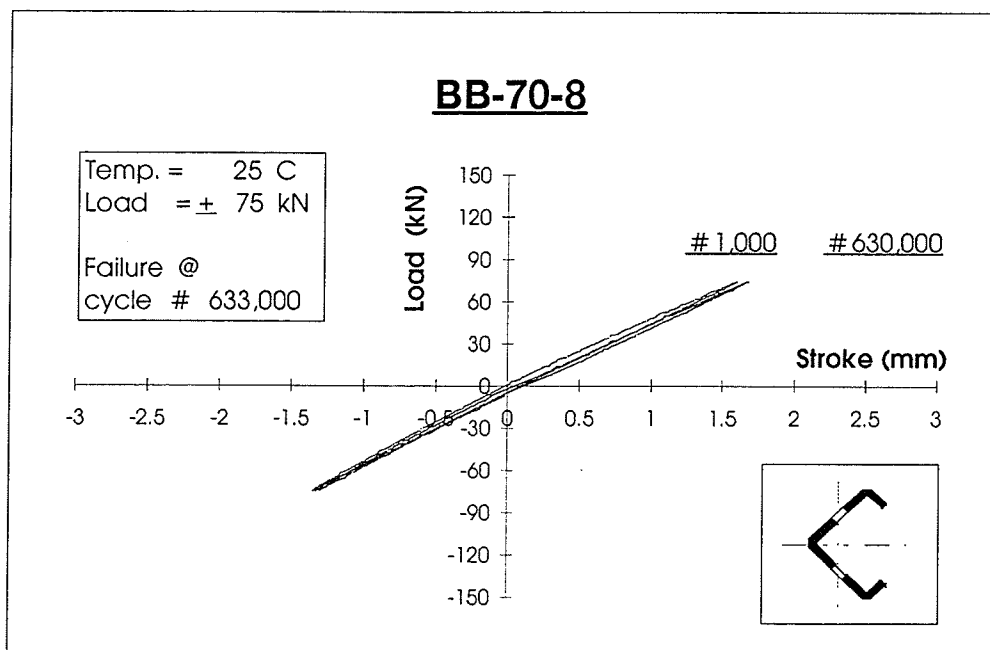
(b) Load-Stroke Loops.

Figure 4. 40 : Stress-Strain and Load-Stroke Loops for Specimen BB-70-8
(Both Leg Connected)

198
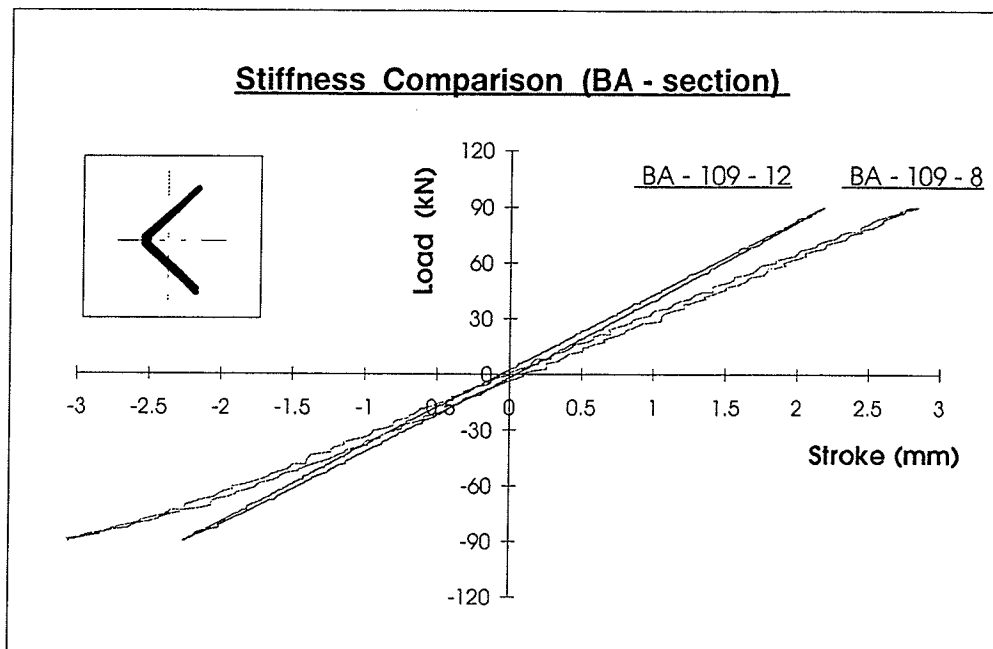
Figure 4. 41 : Load-Stroke Loops for the 90°-angle section
(BA-109-12 : Both Legs Connected)
(BA-109-8 : One Leg Connected)
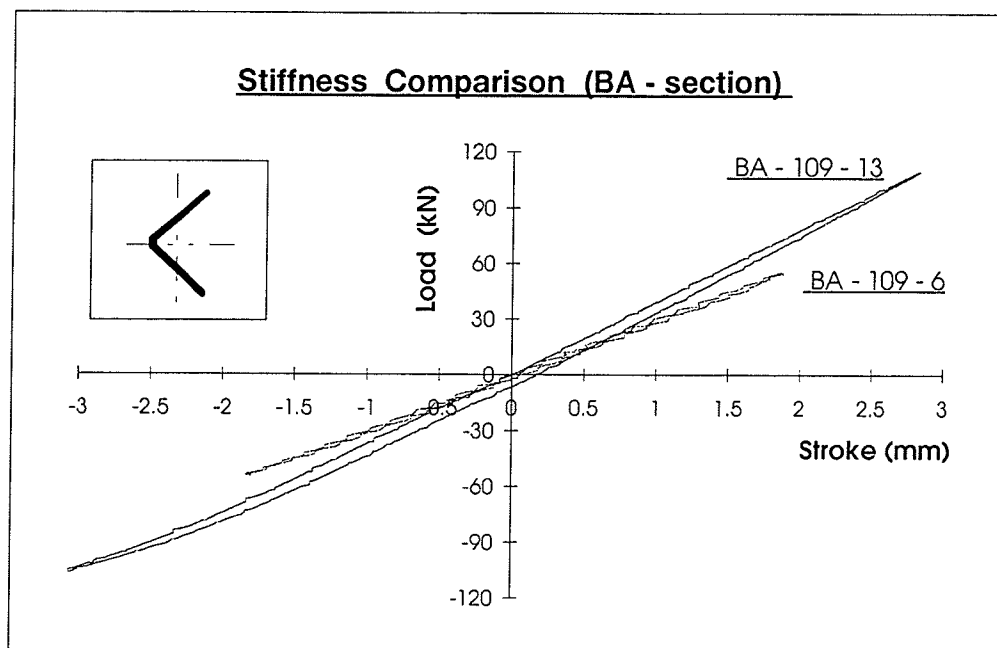
Figure 4. 42 : Load-Stroke Loops for the 90°-angle section
(BA-109-13 : Both Legs Connected)
(BA-109-6 : One Leg Connected)

199

Stiffness Comparison (BC - section)
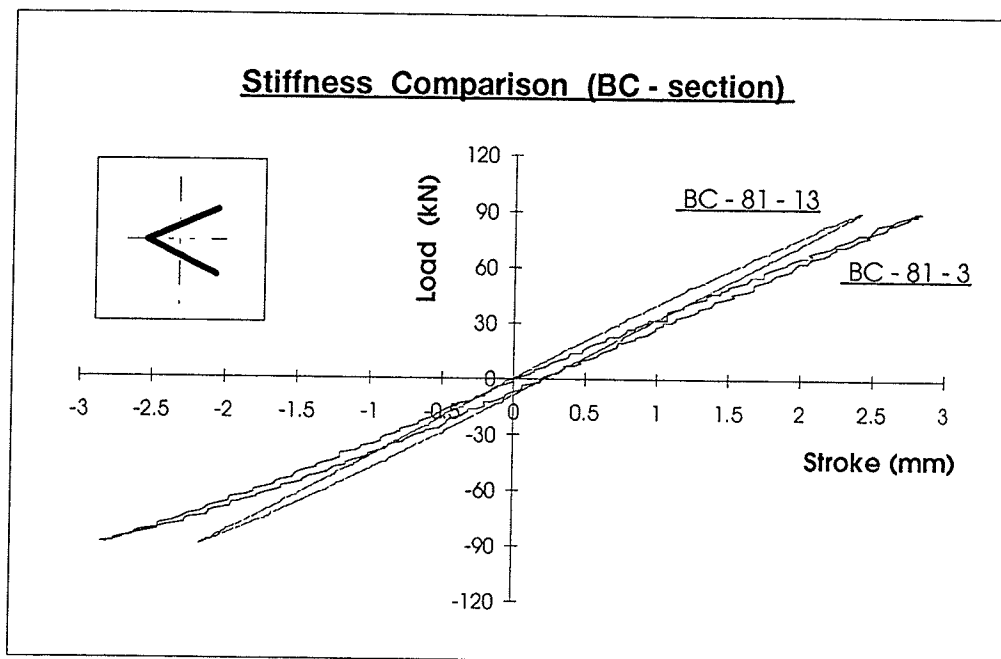
Figure 4. 43 : Load-Stroke Loops for the 60°-angle section
(BC-81-13 : Both Legs Connected)
(BC-81-3 : One Leg Connected)

Stiffness Comparison (BC - section)
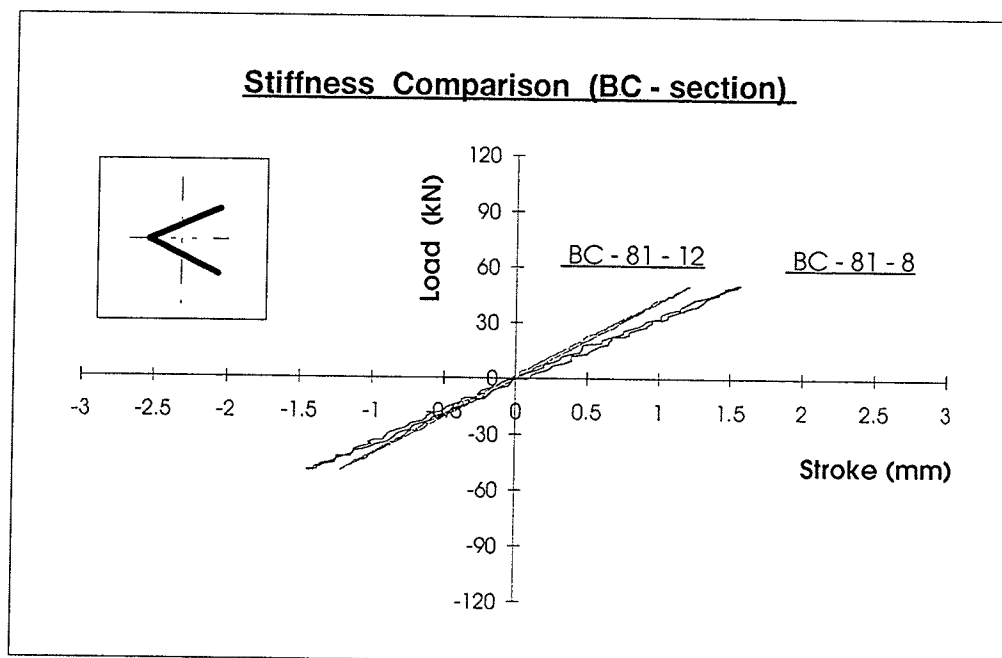
Figure 4. 44 : Load-Stroke Loops for the 60°-angle section
(BC-81-12 : Both Legs Connected)
(BC-81-8 : One Leg Connected)

200
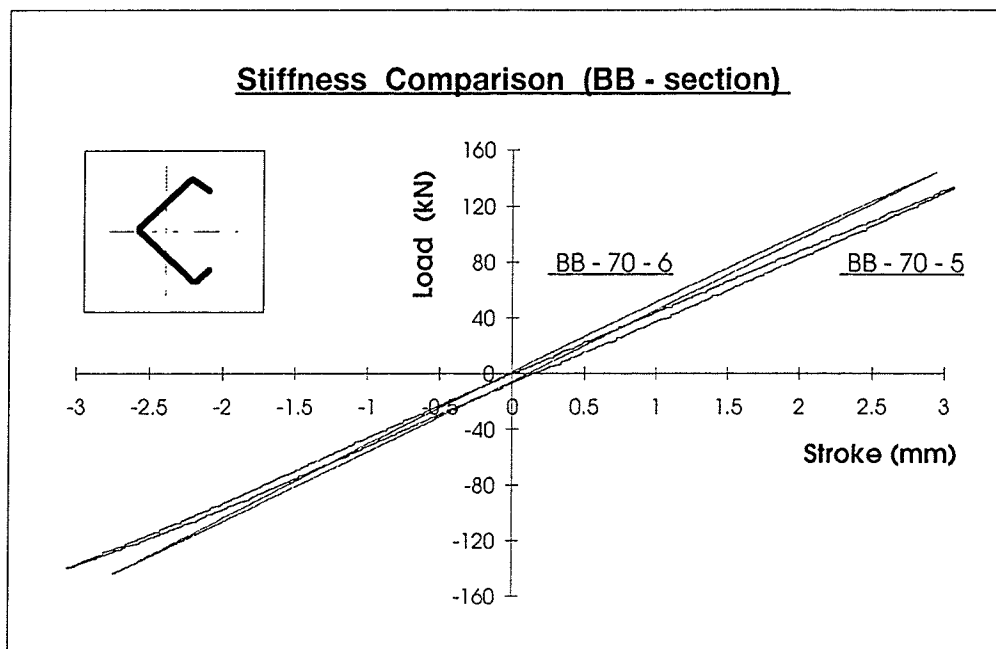
Figure 4. 45 : Load-Stroke Loops for the Lipped-angle section
(BB-70-6 : Both Legs Connected)
(BB-70-5 : One Leg Connected)
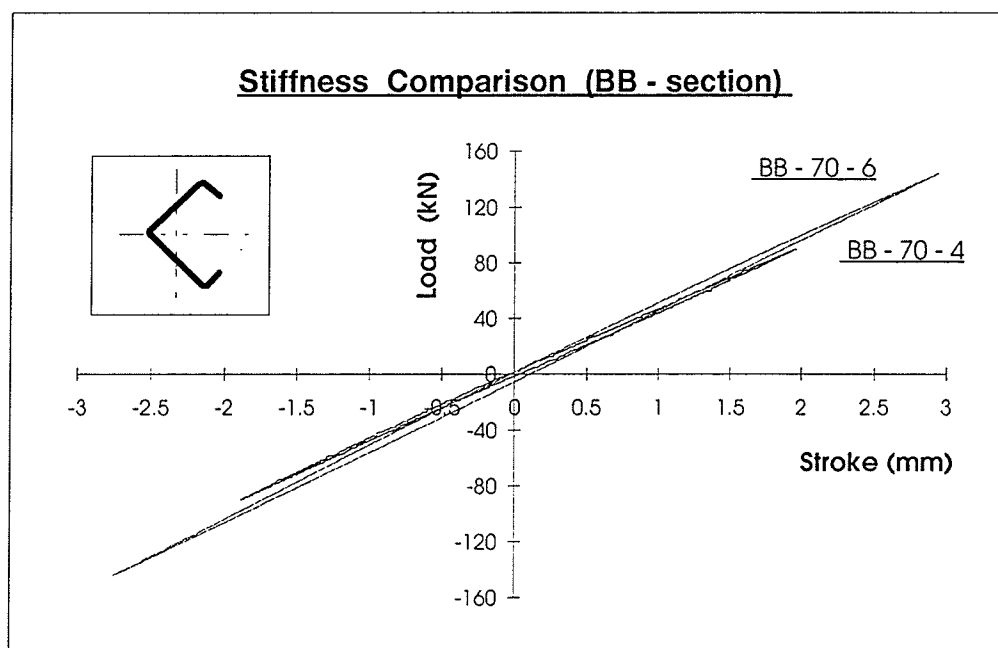
Figure 4. 46 : Load-Stroke Loops for the Lipped -angle section
(BB-70-6 : Both Legs Connected)
(BB-70-4 : One Leg Connected)

201
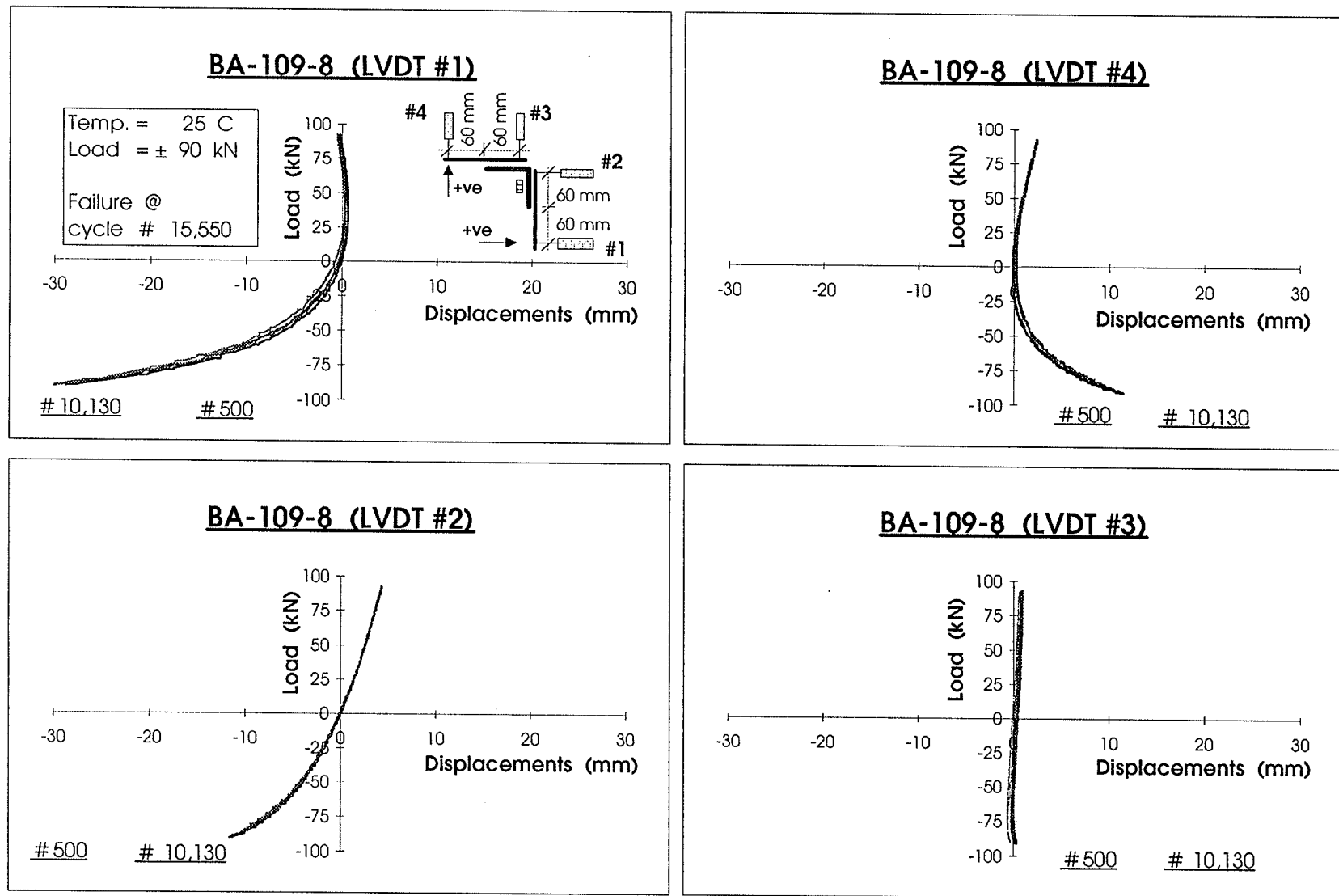
Figure 4.47 : Lateral Displacements at the Mid-Height Section of Specimen BA-109-8
(One Leg Connected)

BA-109-12 (LVDT #1)

Temp. = 25 C
Load = ± 90 kN

Failure @
cycle # 75,000

#4   #3
60 mm 60 mm

#2
60 mm
+ve
60 mm
+ve   #1

Load (kN)
120
90
60
30
0
-60
-90
-120

-30   -20   -10   10   20   30
Displacements (mm)

#2,000   #72,500

BA-109-12 (LVDT #4)

Load (kN)
120
90
60
30
0
-30
-60
-90
-120

-30   -20   -10   10   20   30
Displacements (mm)

#2,000   #72,500

BA-109-12 (LVDT #2)

Load (kN)
120
90
60
30
0
-60
-90
-120

-30   -20   -10   10   20   30
Displacements (mm)

#2,000   #72,500

BA-109-12 (LVDT #3)

Load (kN)
120
90
60
30
0
-30
-60
-90
-120

-30   -20   -10   10   20   30
Displacements (mm)

#2,000   #72,500

Figure 4.48 : Lateral Displacements at the Mid-Height Section of Specimen BA-109-12
(Both Legs Connected)
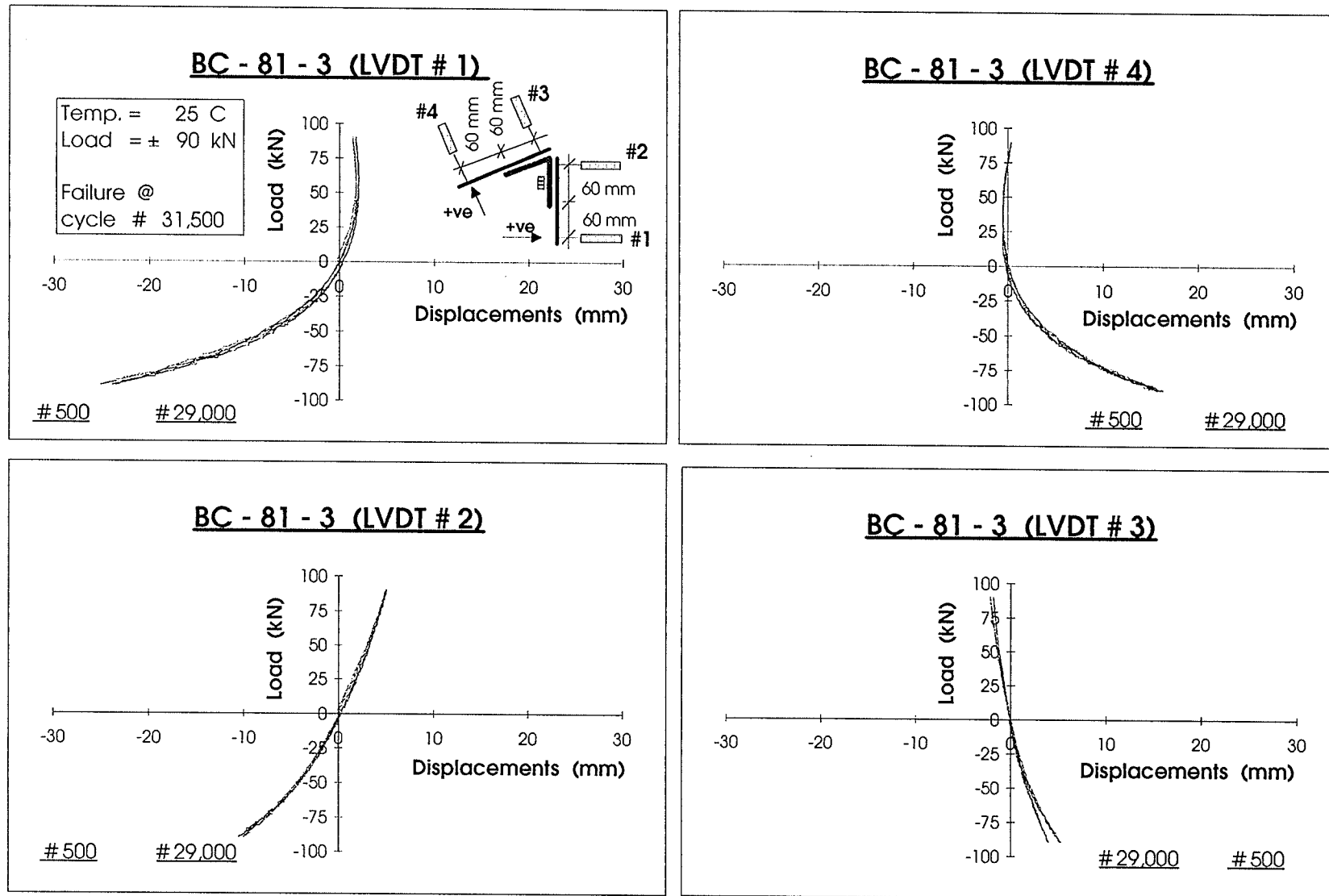
Figure 4.49: Lateral Displacements at the Mid-Height Section of Specimen BC-81-3
(One Leg Connected)
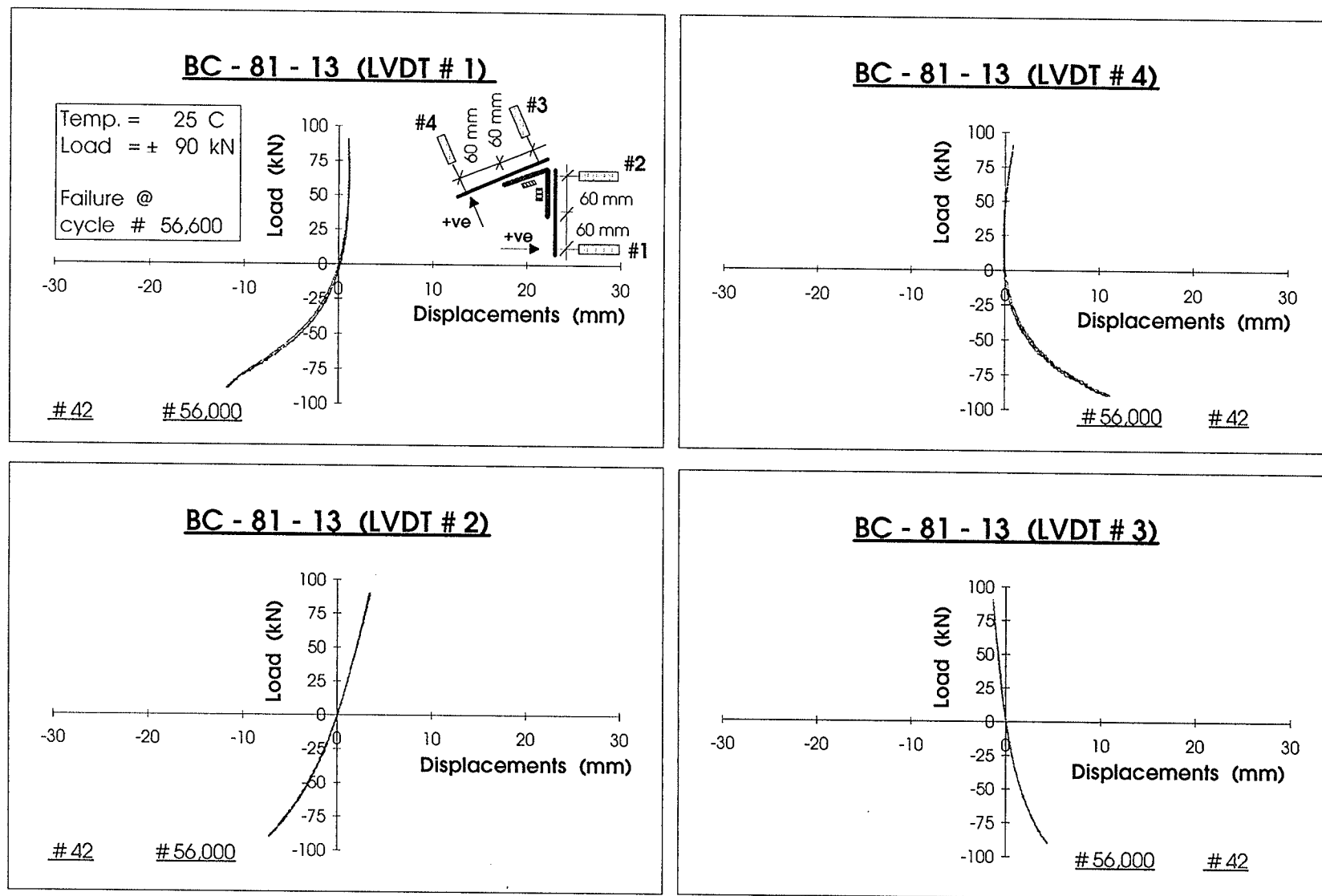
Figure 4.50 : Lateral Displacements at the Mid-Height Section of Specimen BC-81-13 (Both Legs Connected)
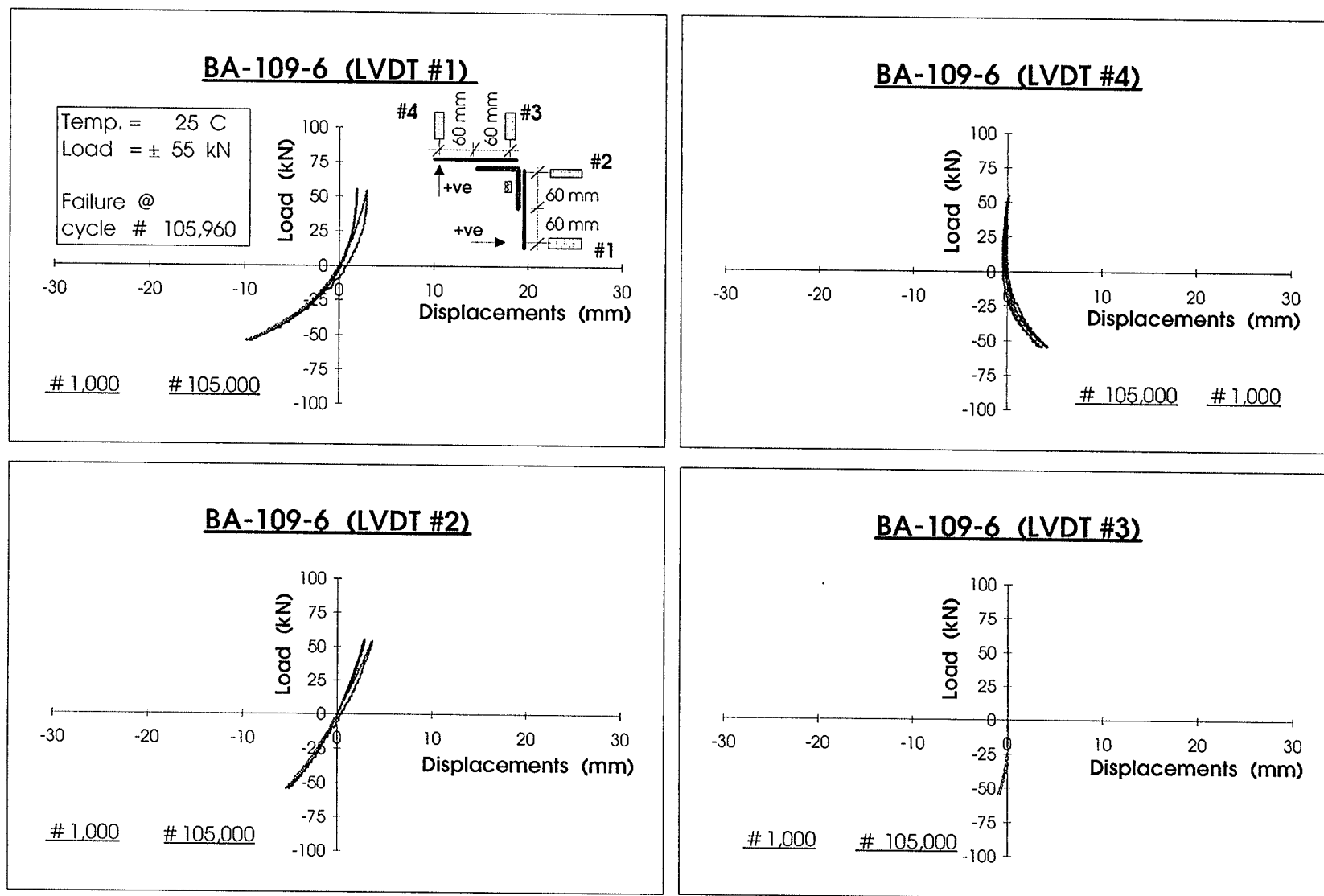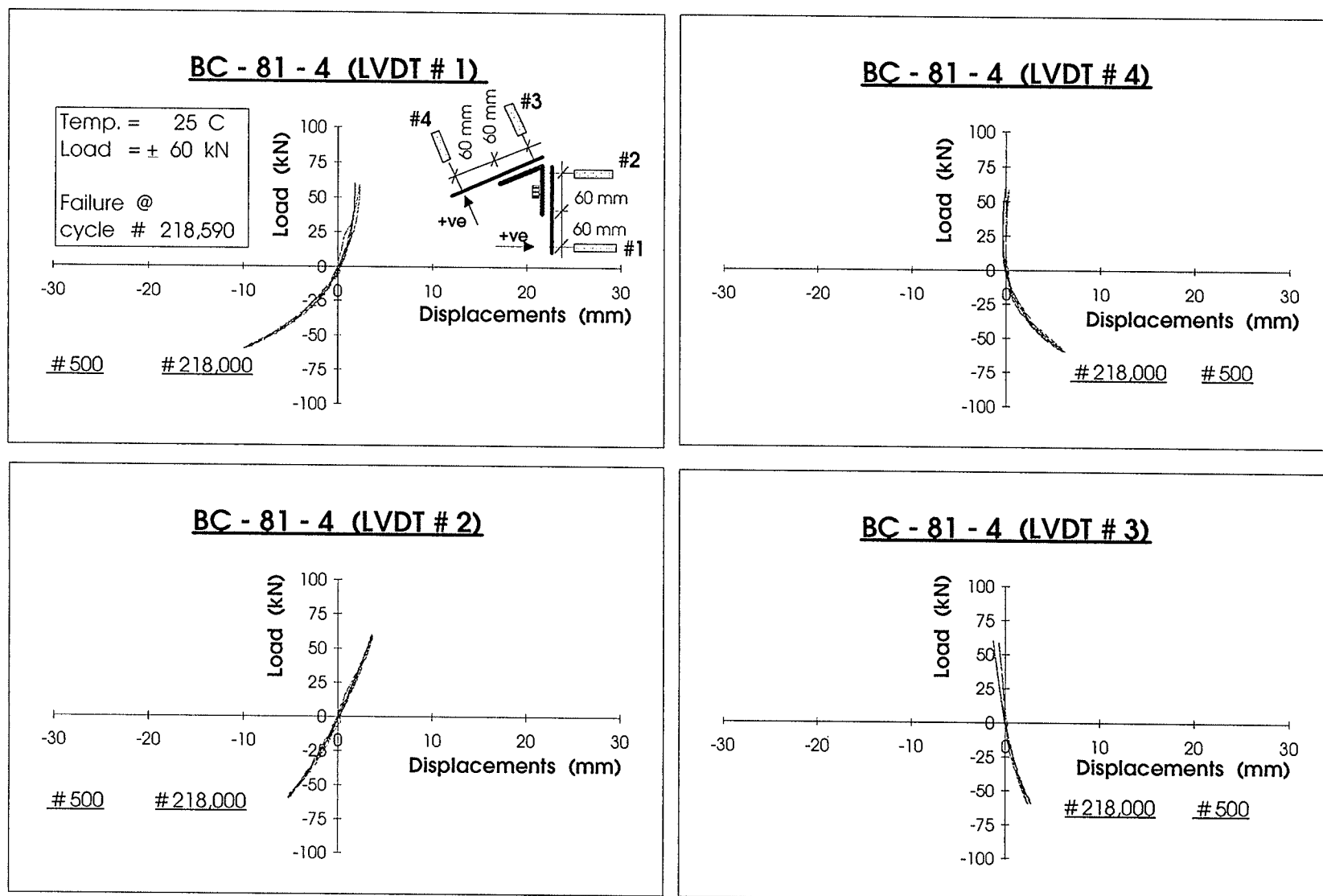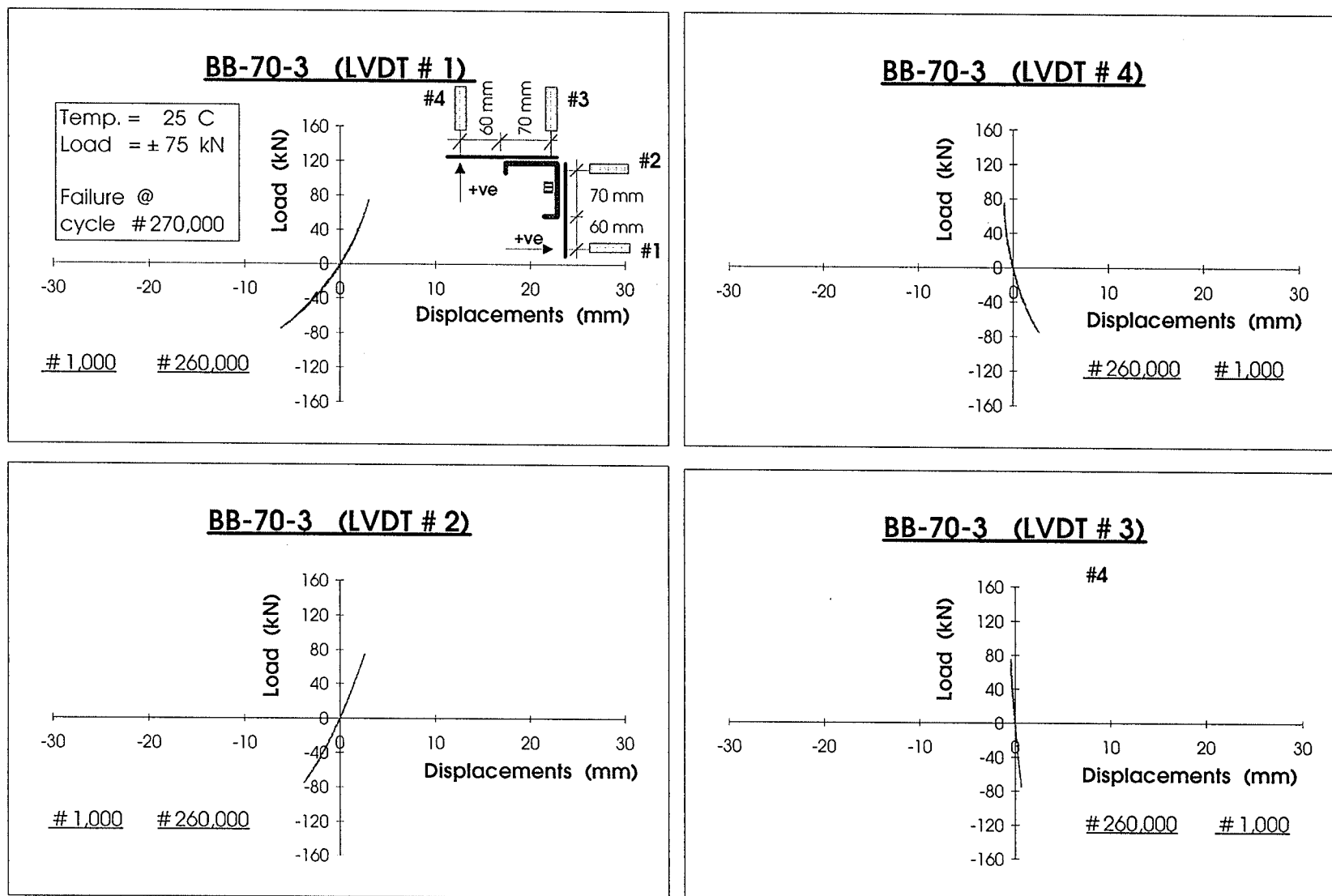
Figure 4. 51 : Lateral Displacements at the Mid-Height Section of Specimen BB-70-3
(One Leg Connected)
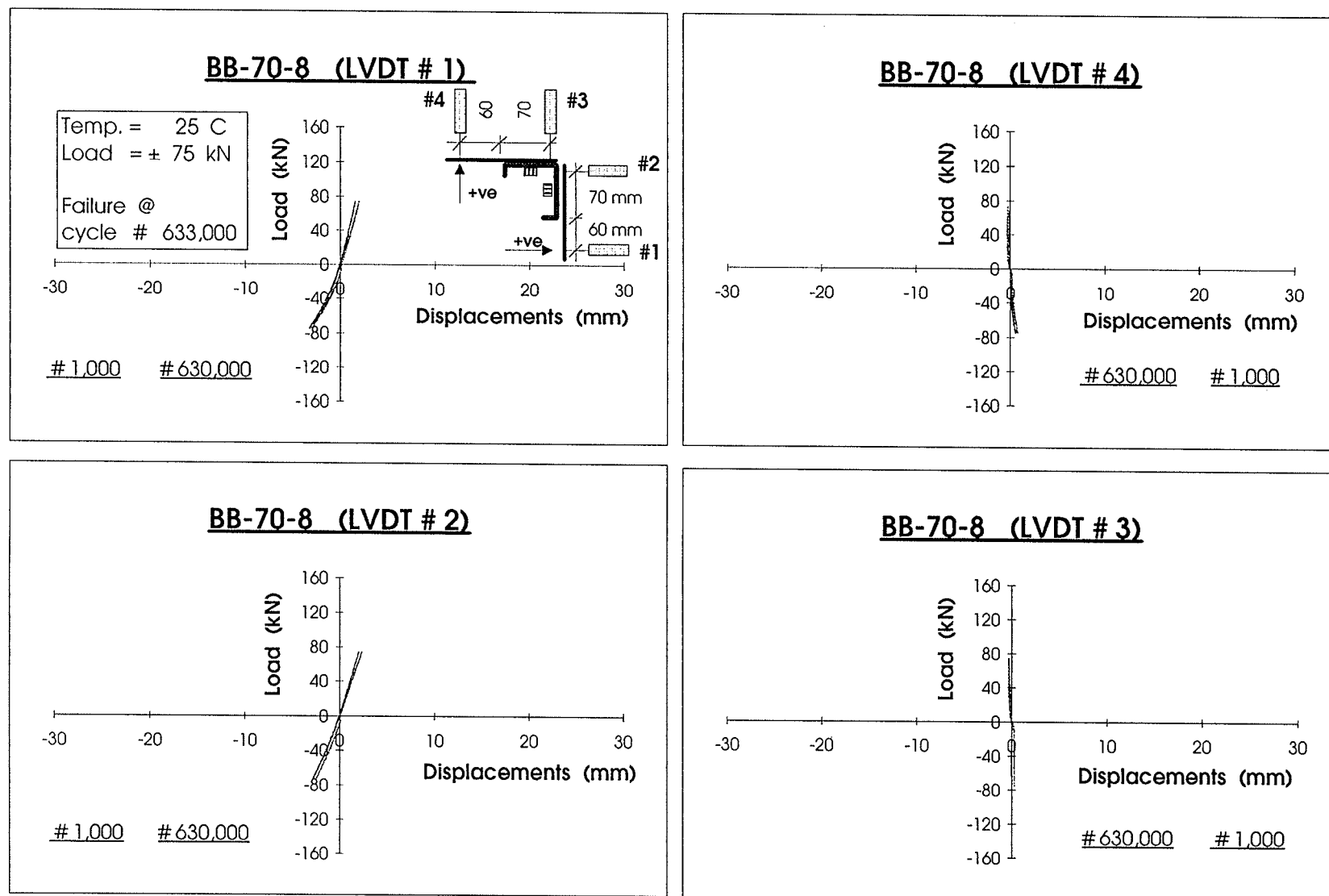
Figure 4. 52 : Lateral Displacements at the Mid-Height Section of Specimen BB-70-8
(Both Legs Connected)
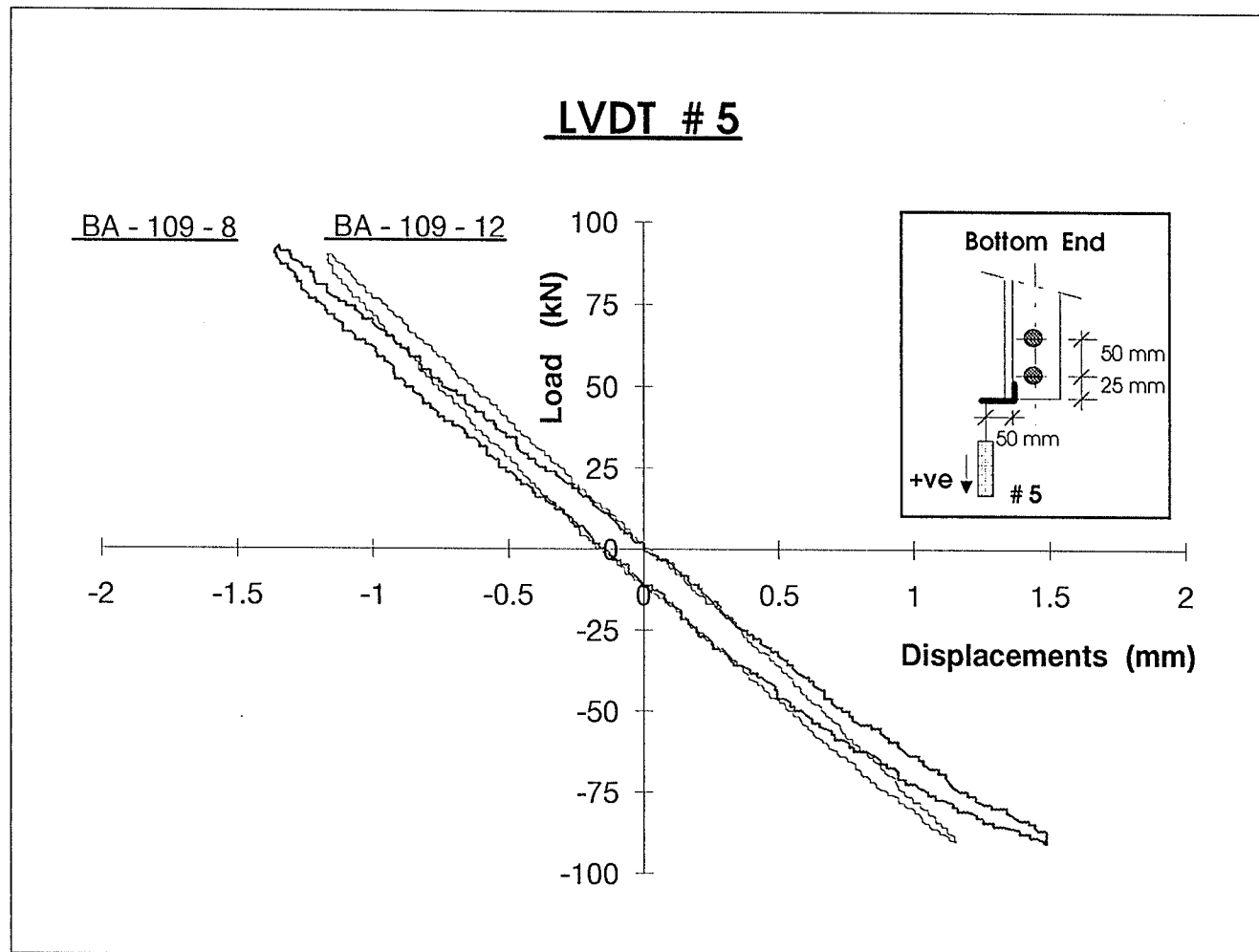
Figure 4. 53 : Bottom End Displacement for the 90°-angle section
(BA-109-12 : Both Legs Connected)
(BA-109-8 : One Leg Connected)
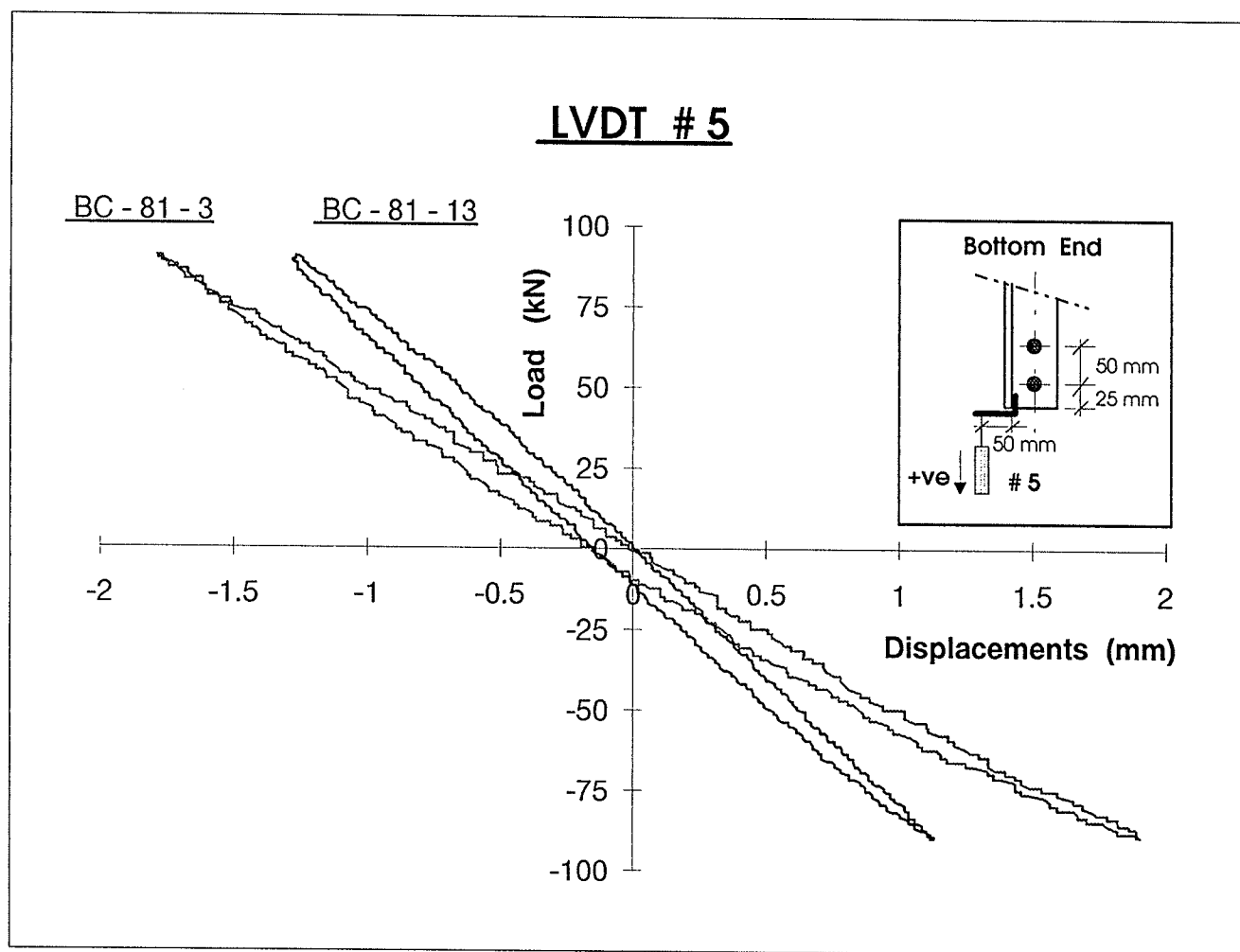
Figure 4.54 : Bottom End Displacement for the 60°-angle section
(BC-81-13 : Both Legs Connected)
(BC-81-3 : One Leg Connected)
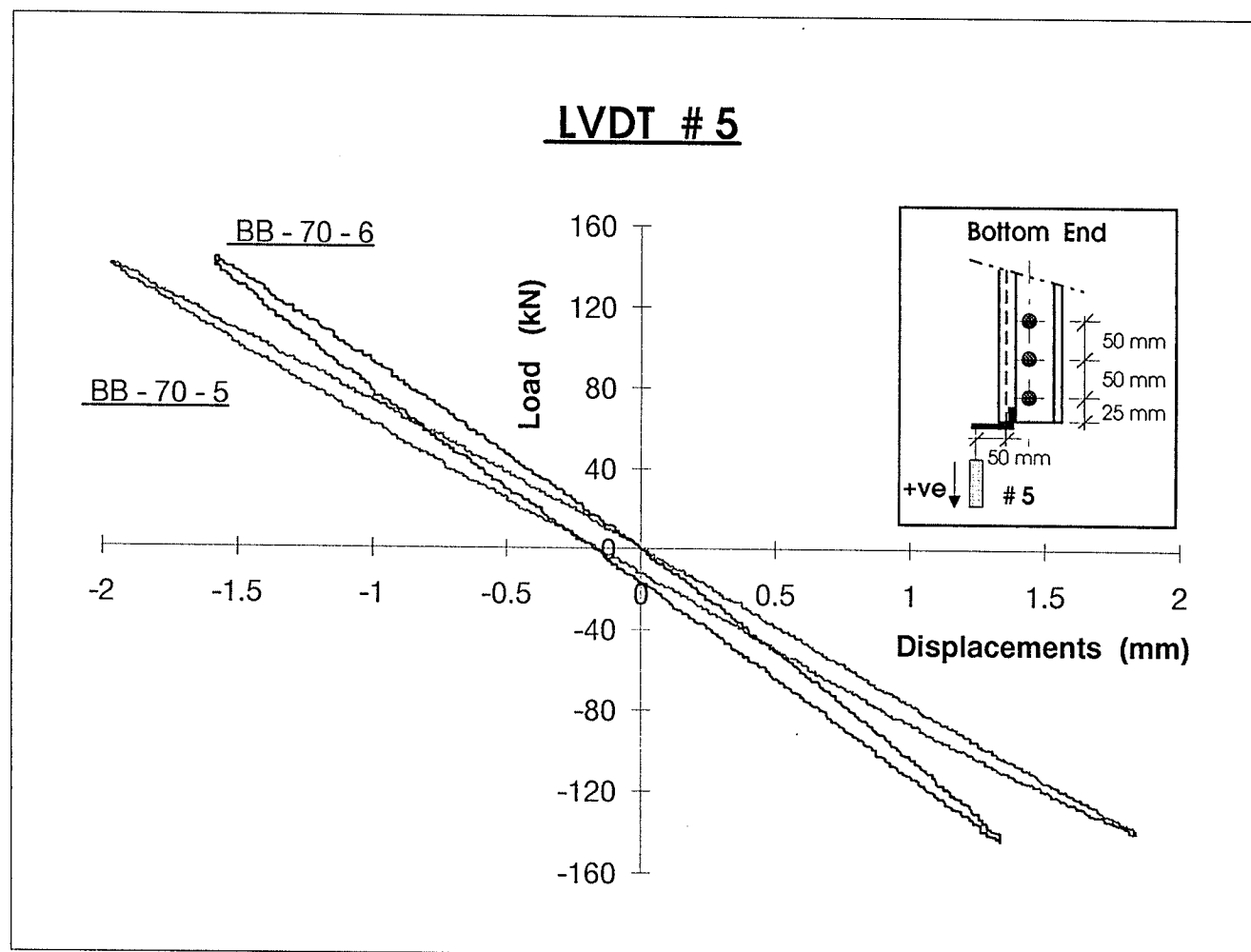
Figure 4. 55 : Bottom End Displacement for the Lipped angle section
(BB-70-6 : Both Legs Connected)
(BB-70-5 : One Leg Connected)

(a) Stress -Strain Loops.
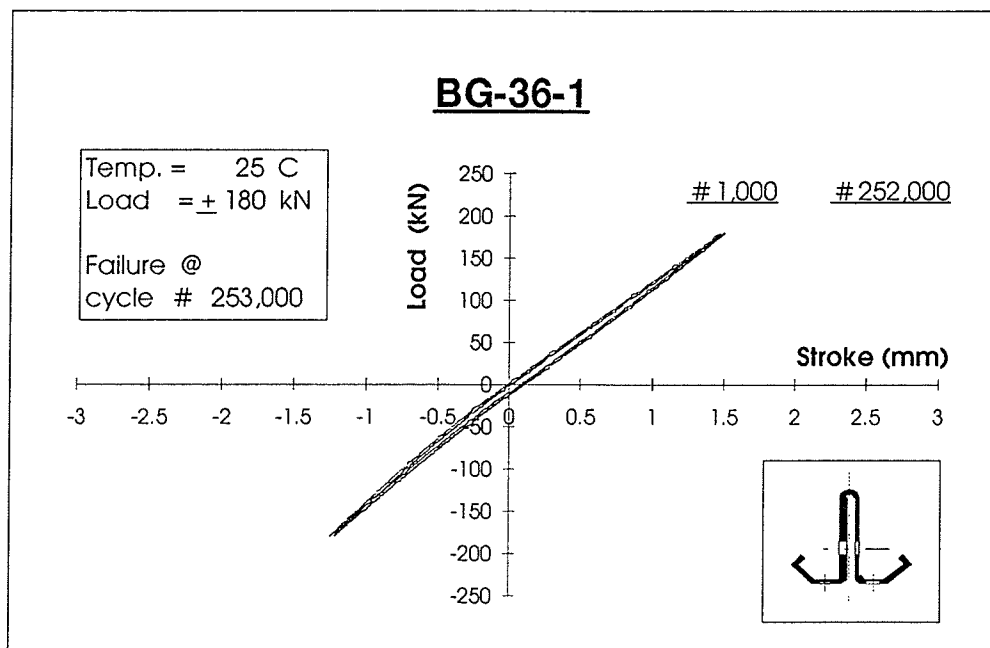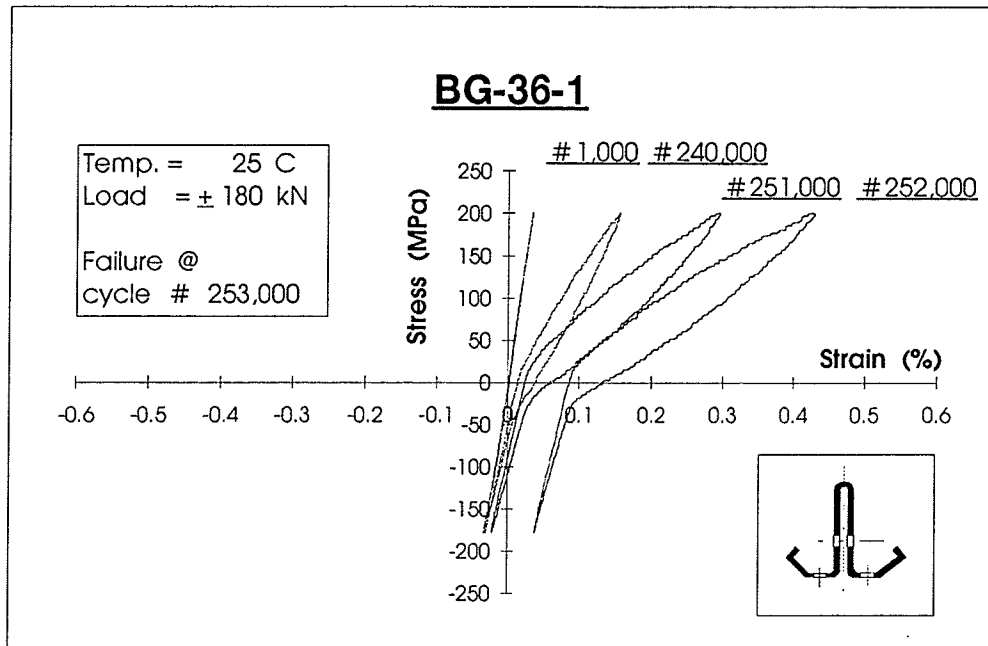
(b) Load-Stroke Loops.

Figure 4. 56 : Stress-Strain and Load-Stroke Loops for Specimen BG-36-1

BG-36-2

Temp. =   25 C
Load = ± 210 kN

Failure @
cycle # 160,000

#2,000   #110,000   #155,000

Stress (MPa)

Strain (%)

250
200
150
100
50
0
-50
-100
-150
-200
-250

-0.6 -0.5 -0.4 -0.3 -0.2 -0.1   0.1 0.2 0.3 0.4 0.5 0.6

(a) Stress -Strain Loops.

BG-36-2

Temp. =   25 C
Load = ± 210 kN

Failure @
cycle # 160,000

#2,000   #155,000

Load (kN)

Stroke (mm)

250
200
150
100
50
0
-50
-100
-150
-200
-250

-3 -2.5 -2 -1.5 -1 -0.5   0.5   1   1.5   2   2.5   3
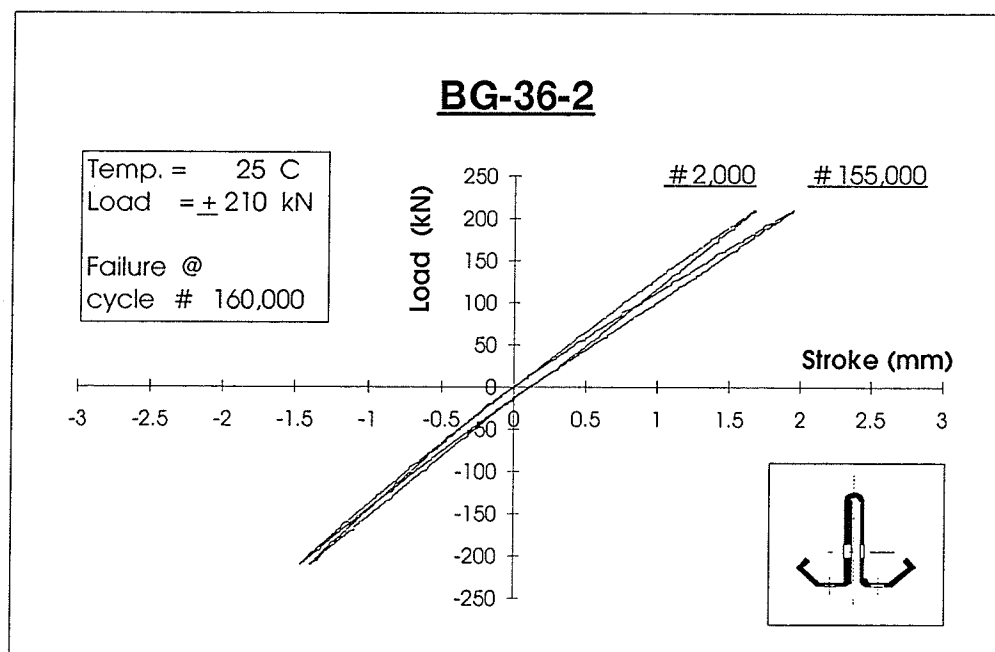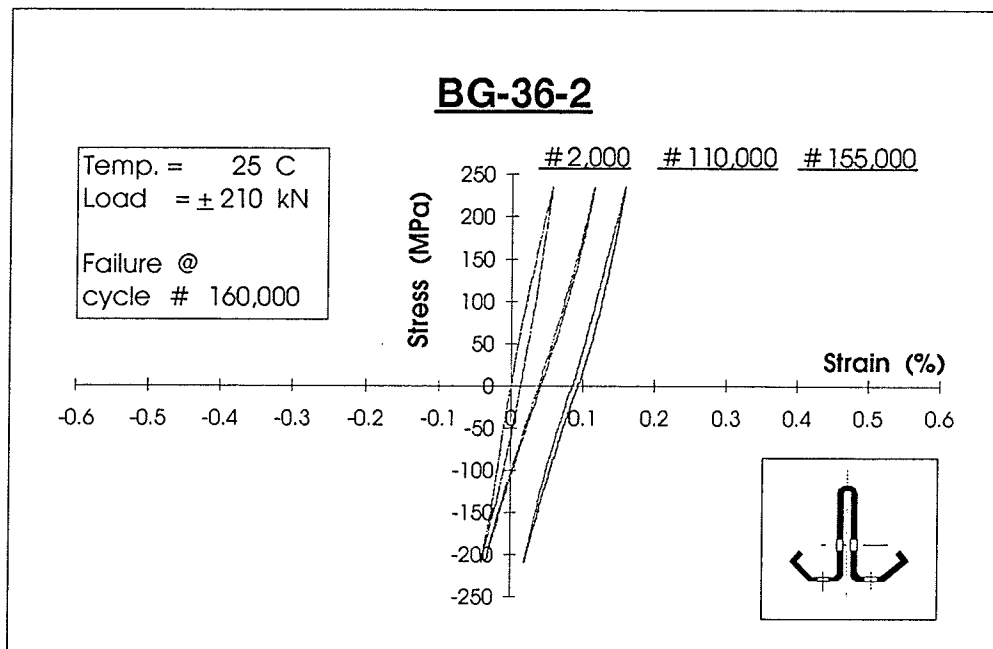
(b) Load-Stroke Loops.

Figure 4. 57 : Stress-Strain and Load-Stroke Loops for Specimen BG-36-2

212

(a) Stress -Strain Loops.
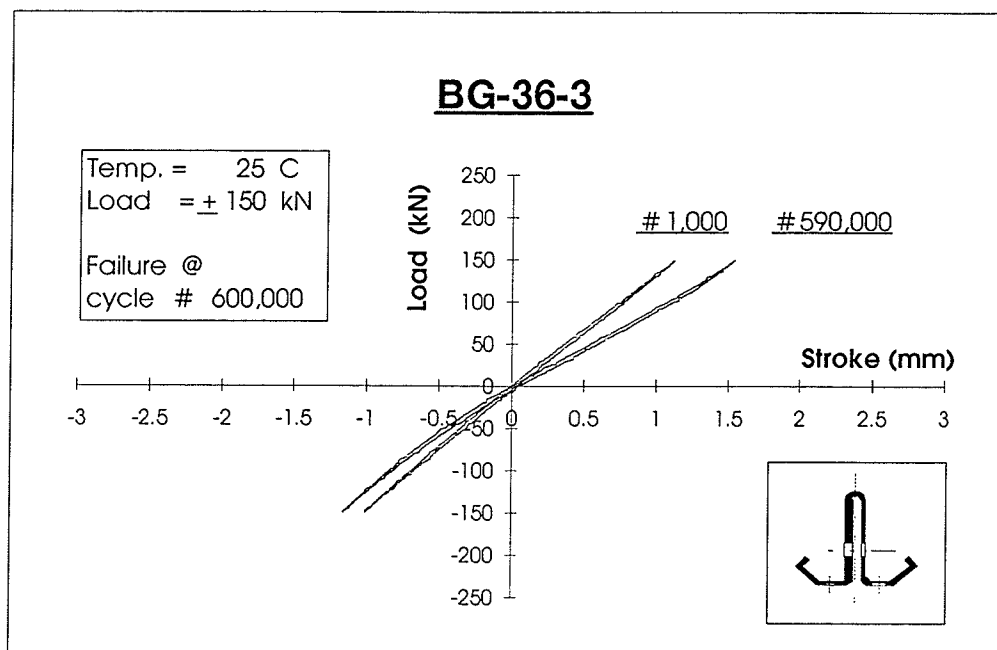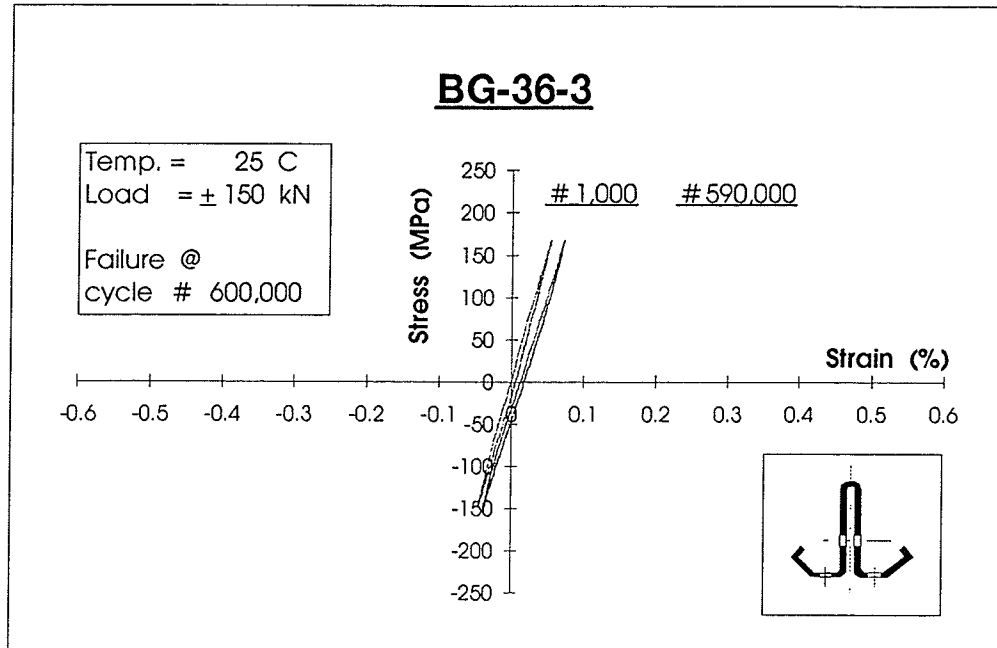
(b) Load-Stroke Loops.

Figure 4. 58 : Stress-Strain and Load-Stroke Loops for Specimen BG-36-3

213
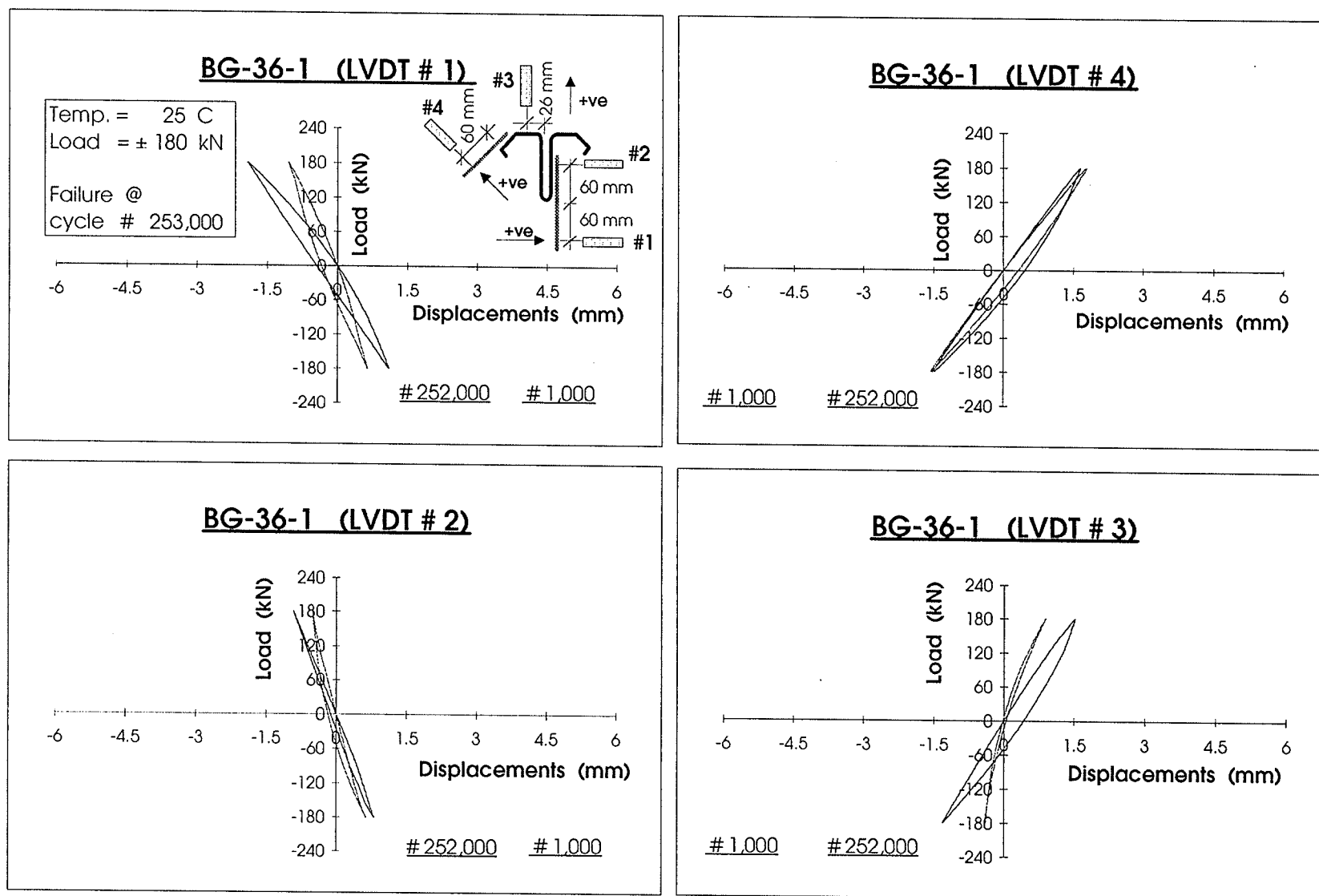
Figure 4.59: Lateral Displacements at the Mid-Height Section of Specimen BG-36-1
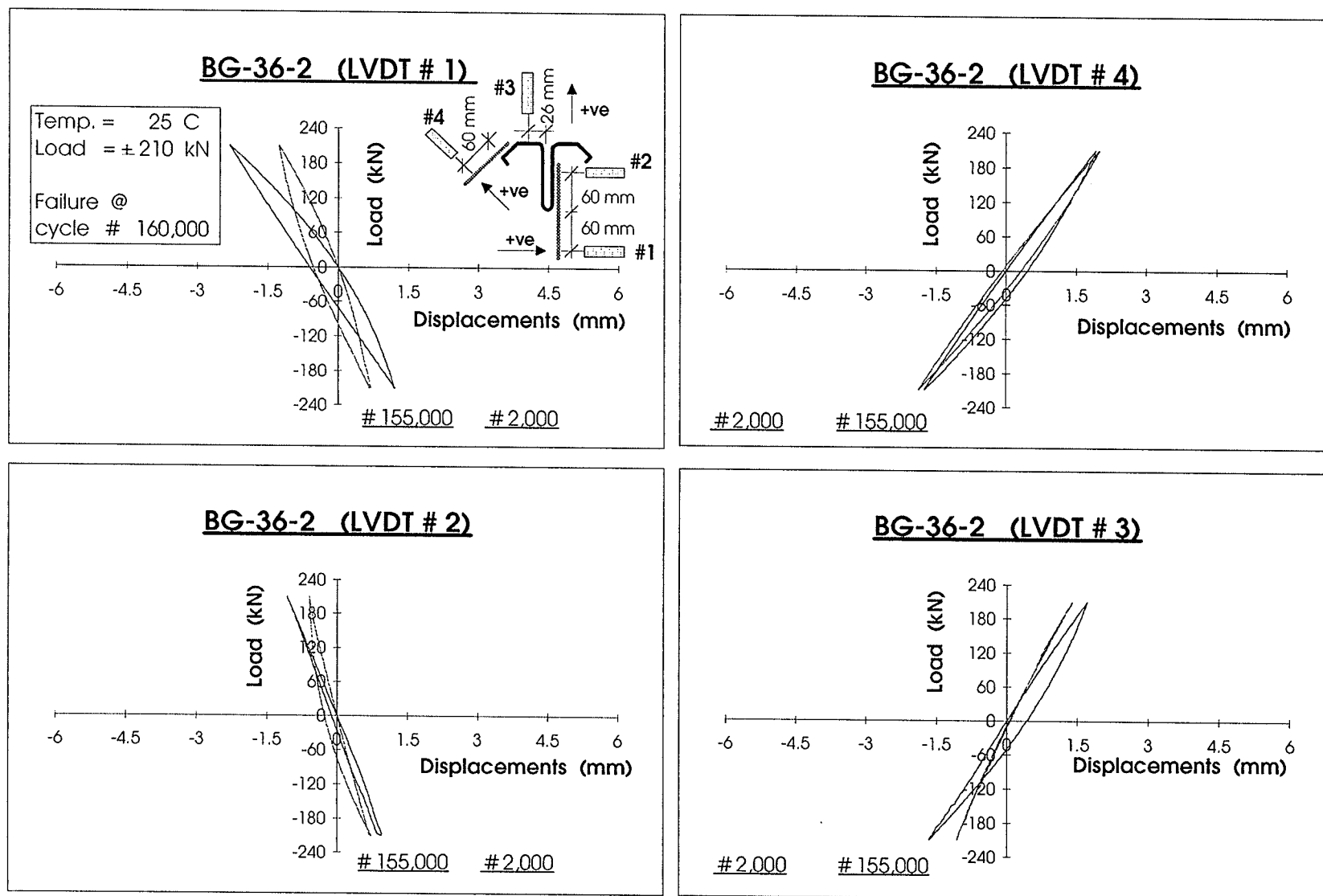
Figure 4.60 : Lateral Displacements at the Mid-Height Section of Specimen BG-36-2

215

BG-36-3   (LVDT # 1)

Temp. =   25 C
Load = ± 150 kN

Failure @
cycle # 600,000

Load (kN)

240

180

120

60

0

-60

-120

-180

-240

-6   -4.5   -3   -1.5   1.5   3   4.5   6

Displacements (mm)

#3   26 mm   +ve

#4   60 mm

+ve

#2

60 mm

60 mm

+ve   #1

600,000   # 1,000

BG-36-3   (LVDT # 4)

Load (kN)

240

180

120

60

0

-60

-120

-180

-240

-6   -4.5   -3   -1.5   1.5   3   4.5   6

Displacements (mm)

1,000   # 600,000

BG-36-3   (LVDT # 2)

Load (kN)

240

180

120

60

0

-60

-120

-180

-240

-6   -4.5   -3   -1.5   1.5   3   4.5   6

Displacements (mm)

600,000   # 1,000

BG-36-3   (LVDT # 3)

Load (kN)

240

180

120

60

0

-60

-120

-180

-240

-6   -4.5   -3   -1.5   1.5   3   4.5   6

Displacements (mm)

1,000   # 600,000

Figure 4. 61 : Lateral Displacements at the Mid-Height Section of Specimen BG-36-3
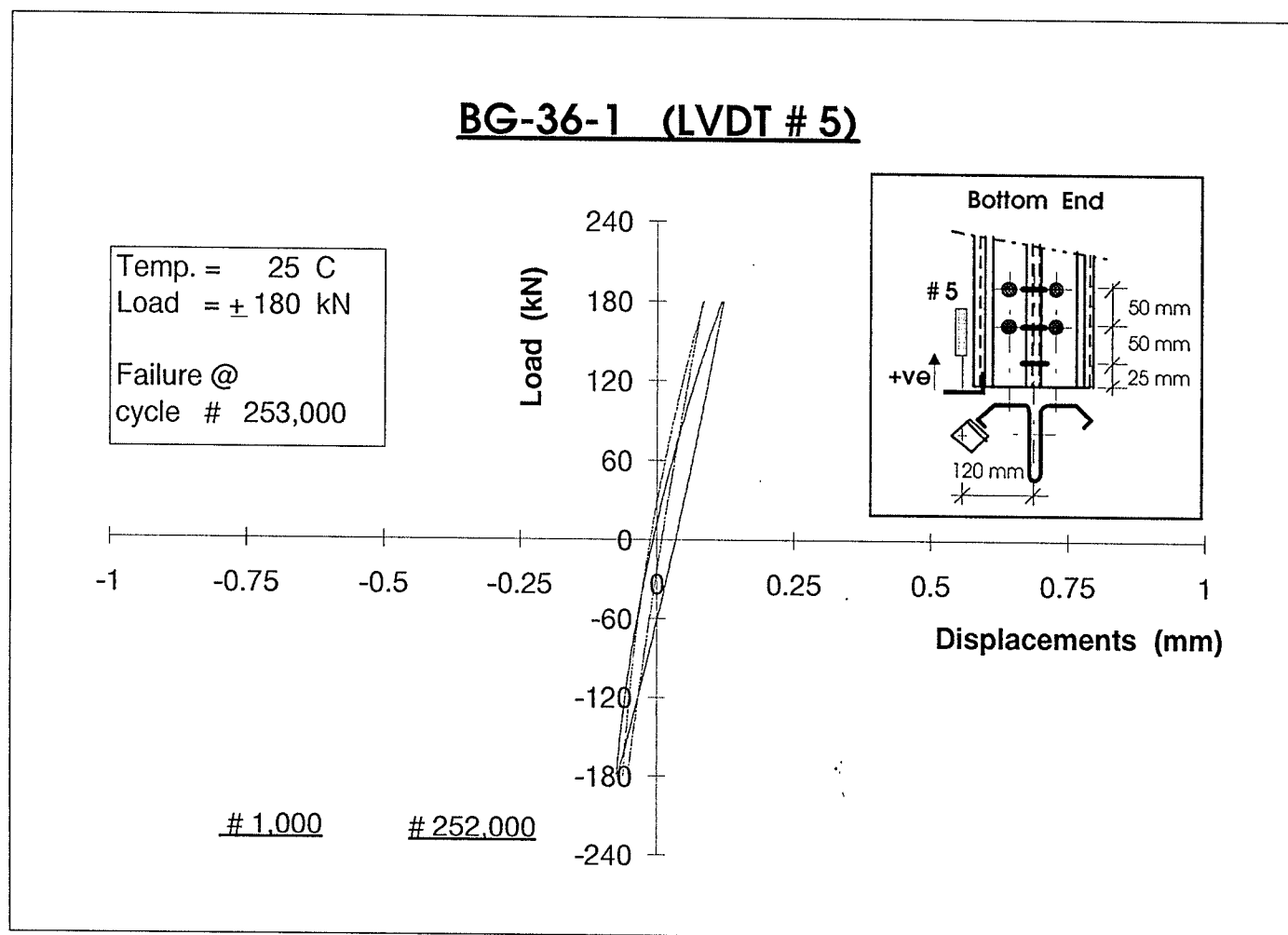
Figure 4. 62 : Load-Displacement Relationship at the Bottom End Section of Specimen BG-36-1
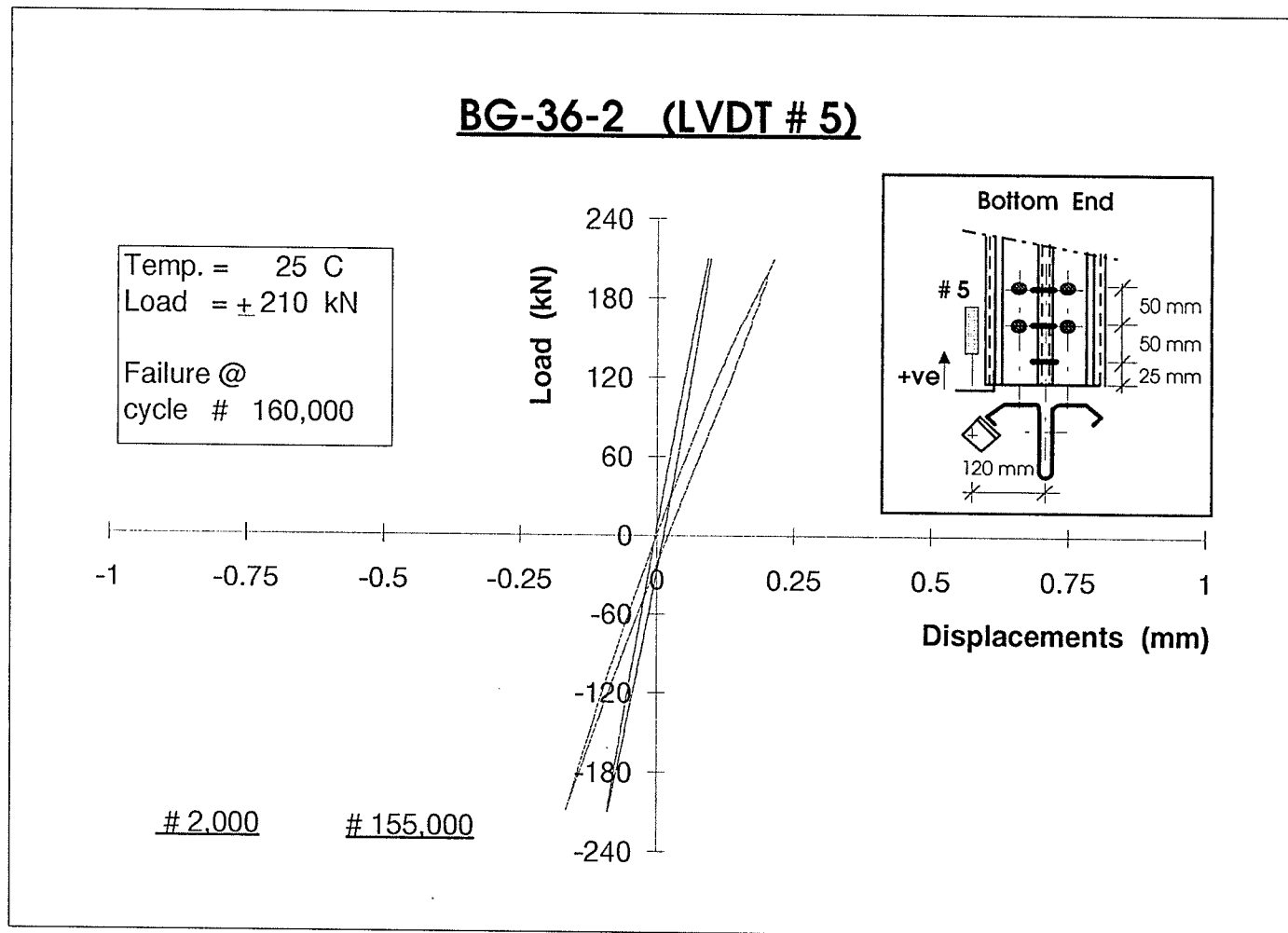
Figure 4. 63 : Load-Displacement Relationship at the Bottom End Section of Specimen BG-36-2

BG-36-3   (LVDT # 5)

Temp. =   25 C
Load = ± 150 kN

Failure @
cycle # 600,000

Bottom End

5

50 mm
50 mm
25 mm

+ve

120 mm

1,000   # 600,000
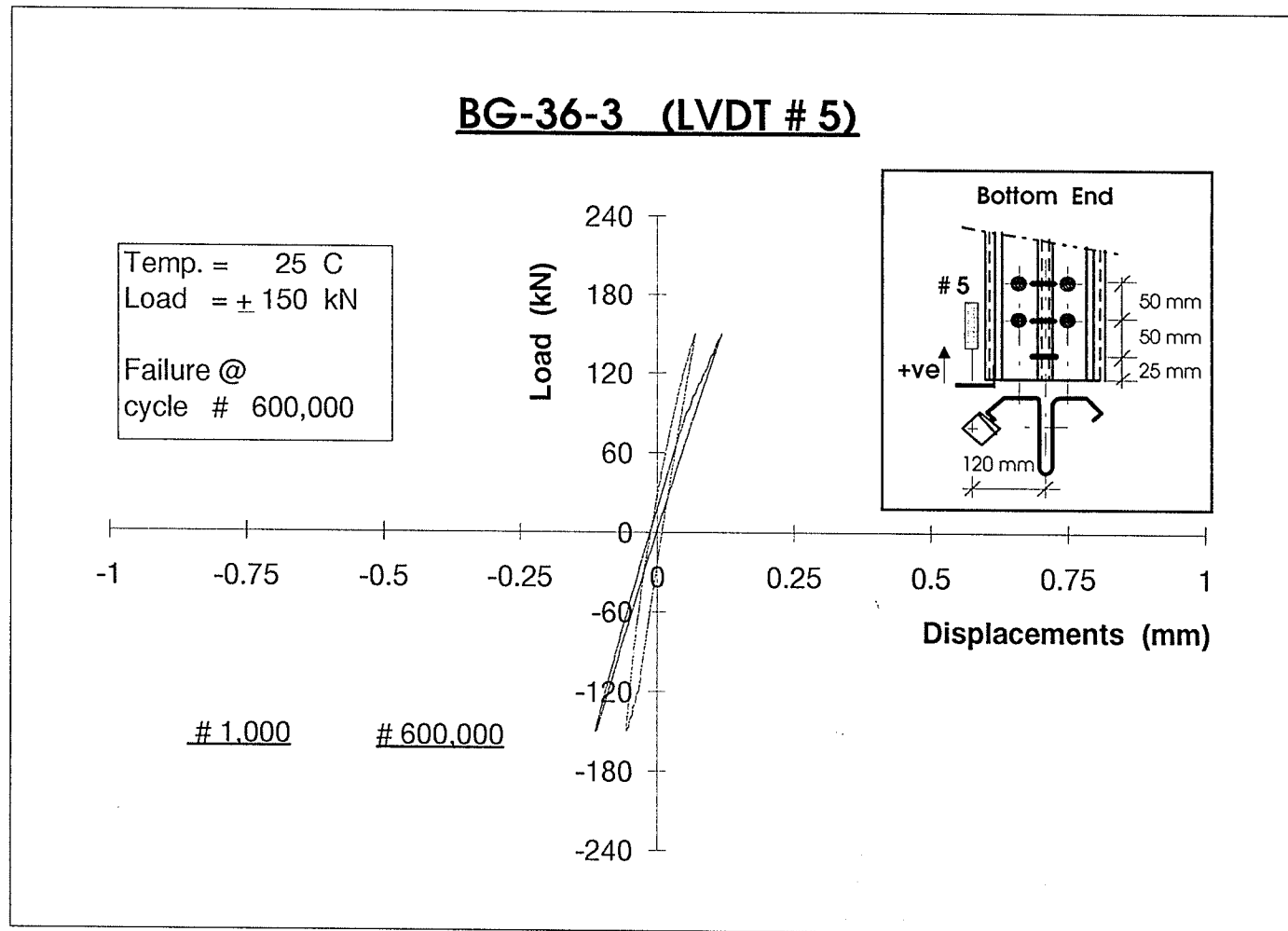
Figure 4. 64 : Load-Displacement Relationship at the Bottom End Section of Specimen   BG-36-3

(a) Stress -Strain Loops.
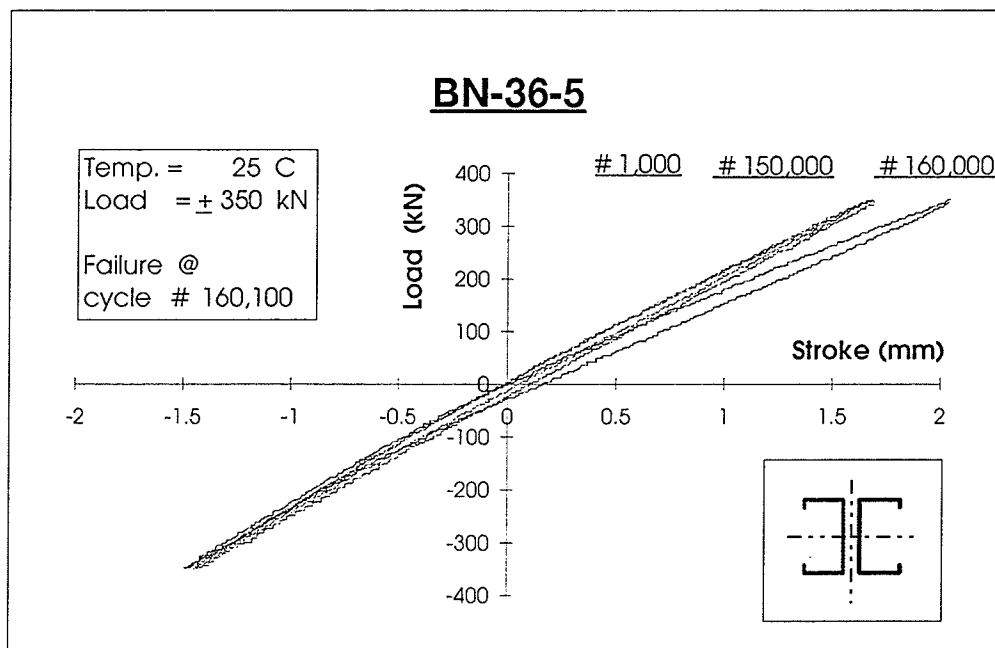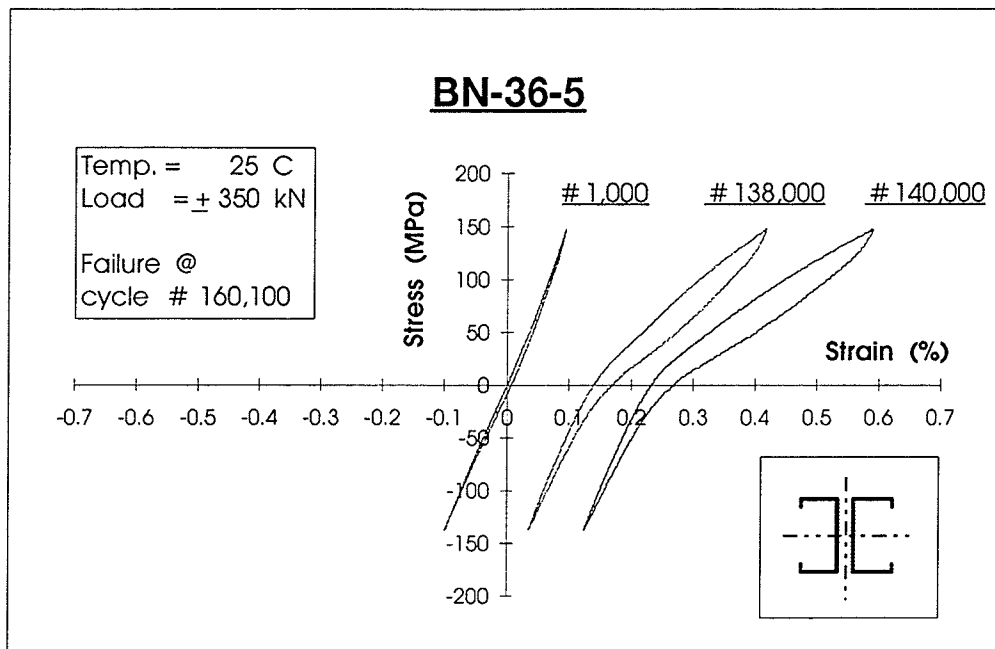
(b) Load-Stroke Loops.

Figure 4. 65 : Stress-Strain and Load-Stroke Loops for Specimen BN-36-5

220

(a) Stress -Strain Loops.
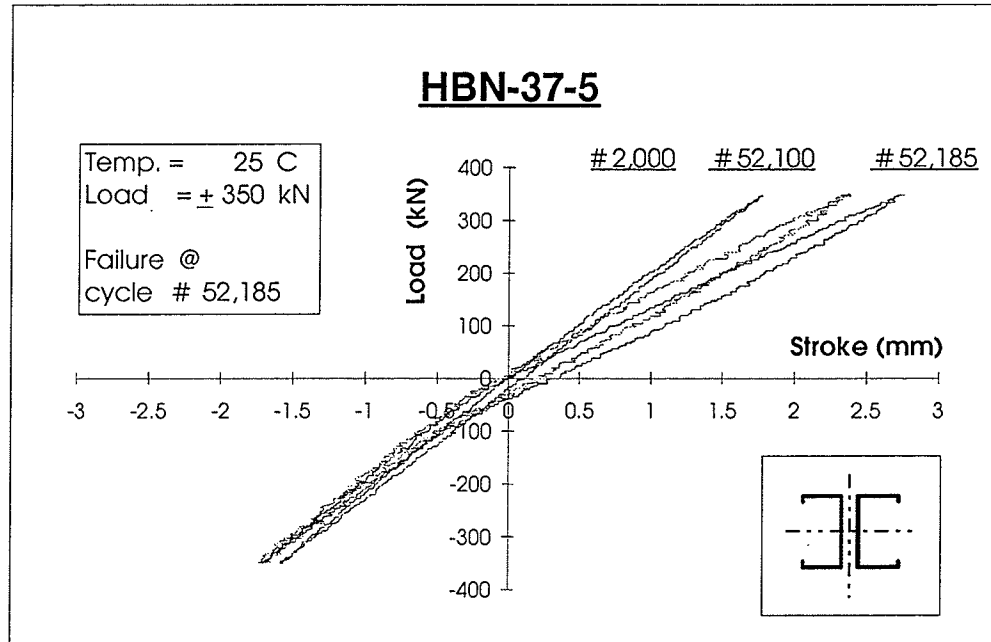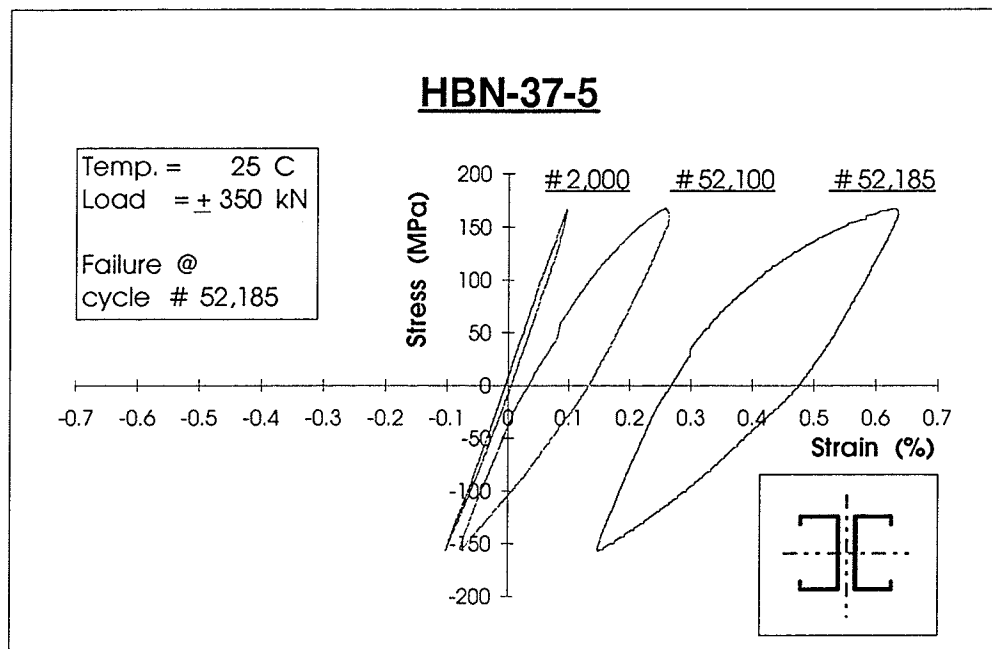
(b) Load-Stroke Loops.

Figure 4. 66 : Stress-Strain and Load-Stroke Loops for Specimen HBN-37-5

221
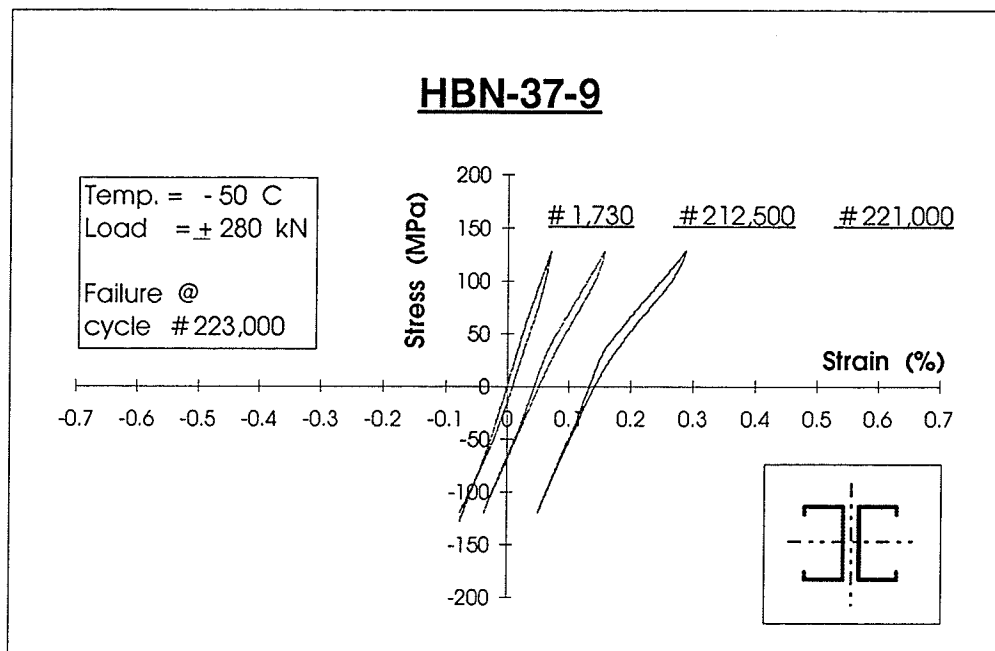
(a) Stress -Strain Loops.
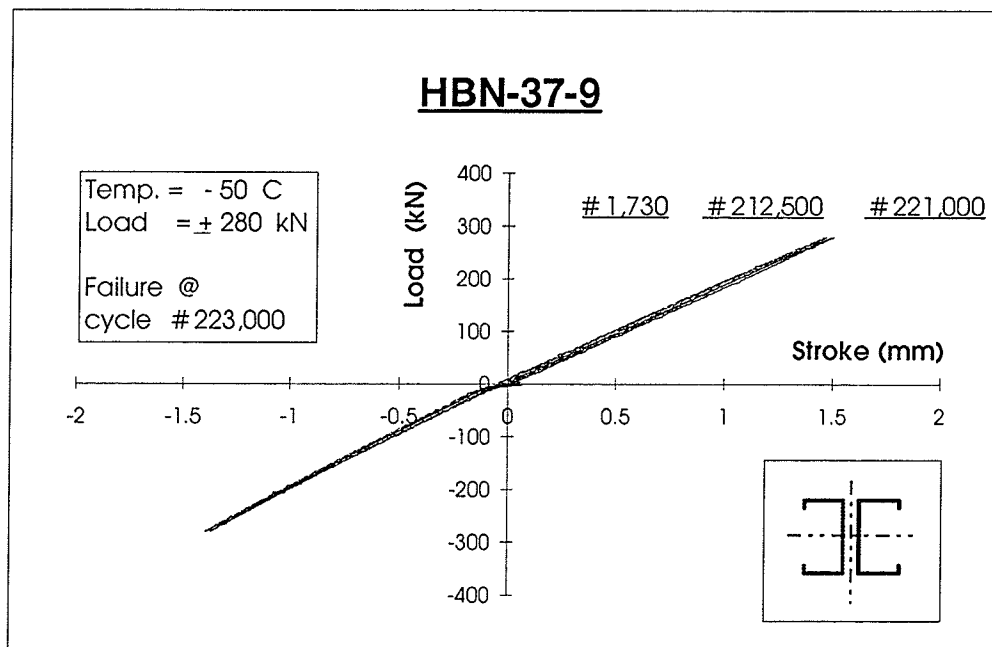
(b) Load-Stroke Loops.

Figure 4. 67 : Stress-Strain and Load-Stroke Loops for Specimen HBN-37-9.
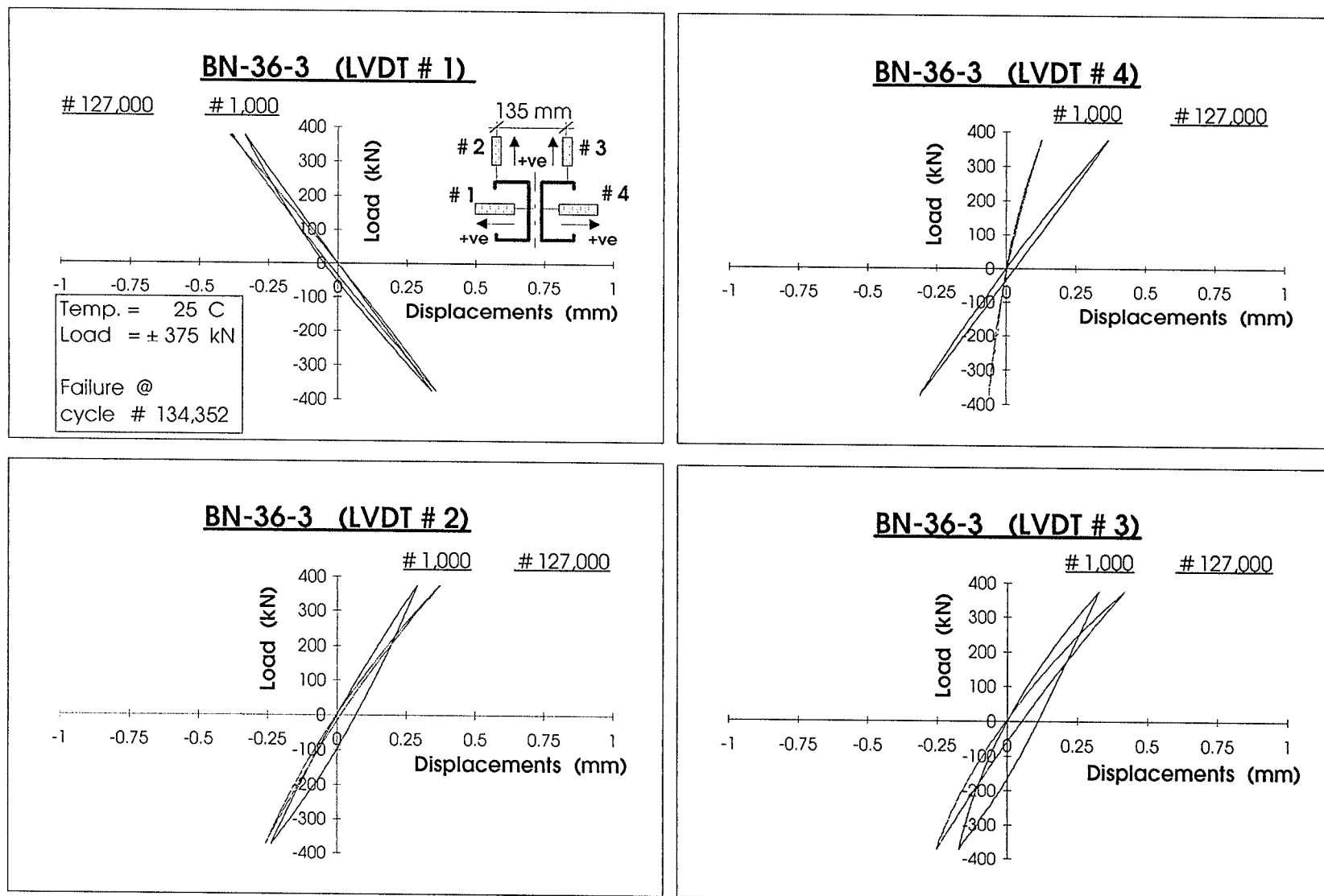
Figure 4. 68 : Lateral Displacements at the Mid-Height Section of Specimen BN-36-3
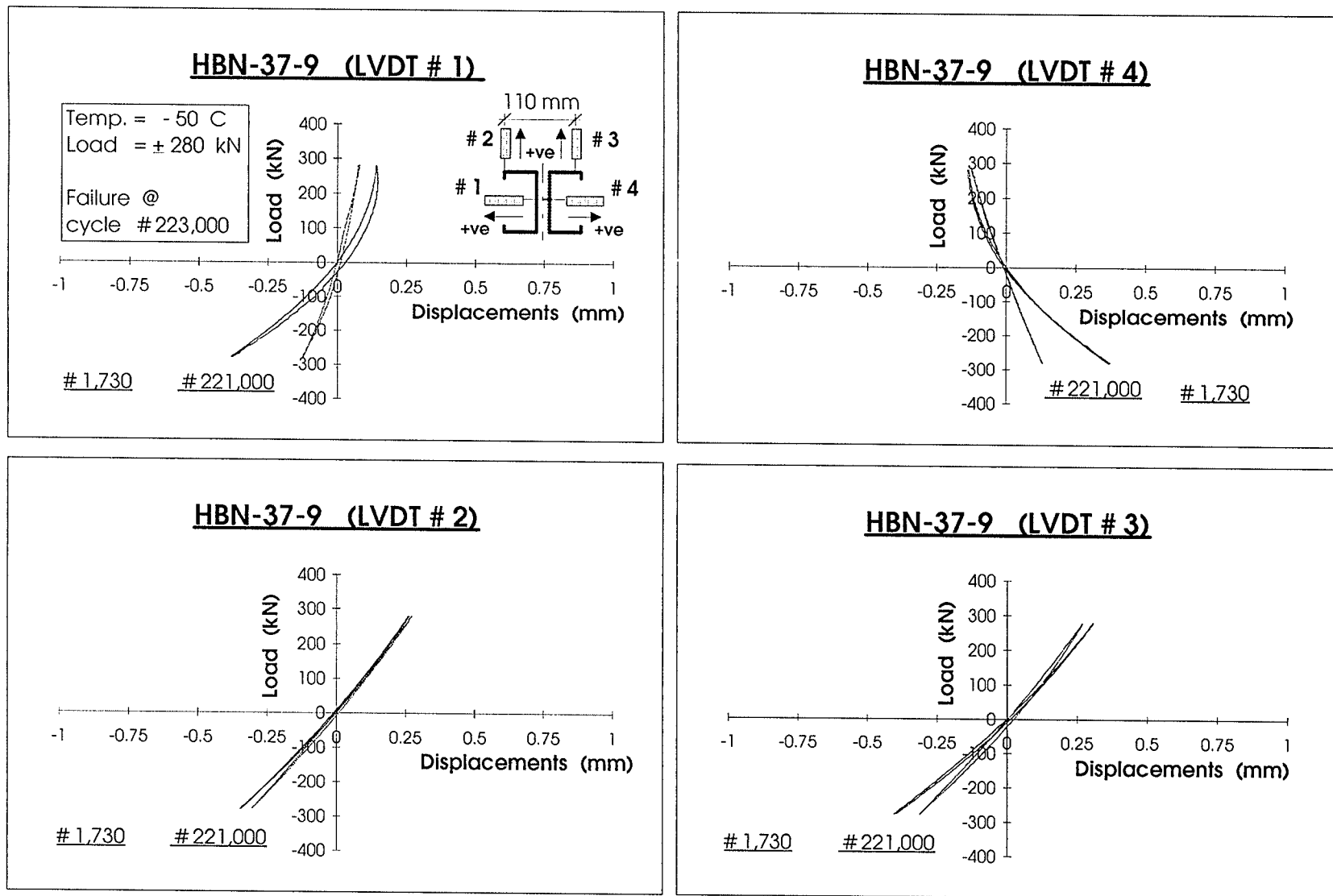
Figure 4. 69 : Lateral Displacements at the Mid-Height Section of Specimen HBN-37-9

BN-36-1   (LVDT # 5)

Temp. =   25 C
Load = ± 270 kN

Failure @
cycle # 660,000

660,000   # 1,000

Load (kN)

Displacements (mm)

Bottom End

5

+ve
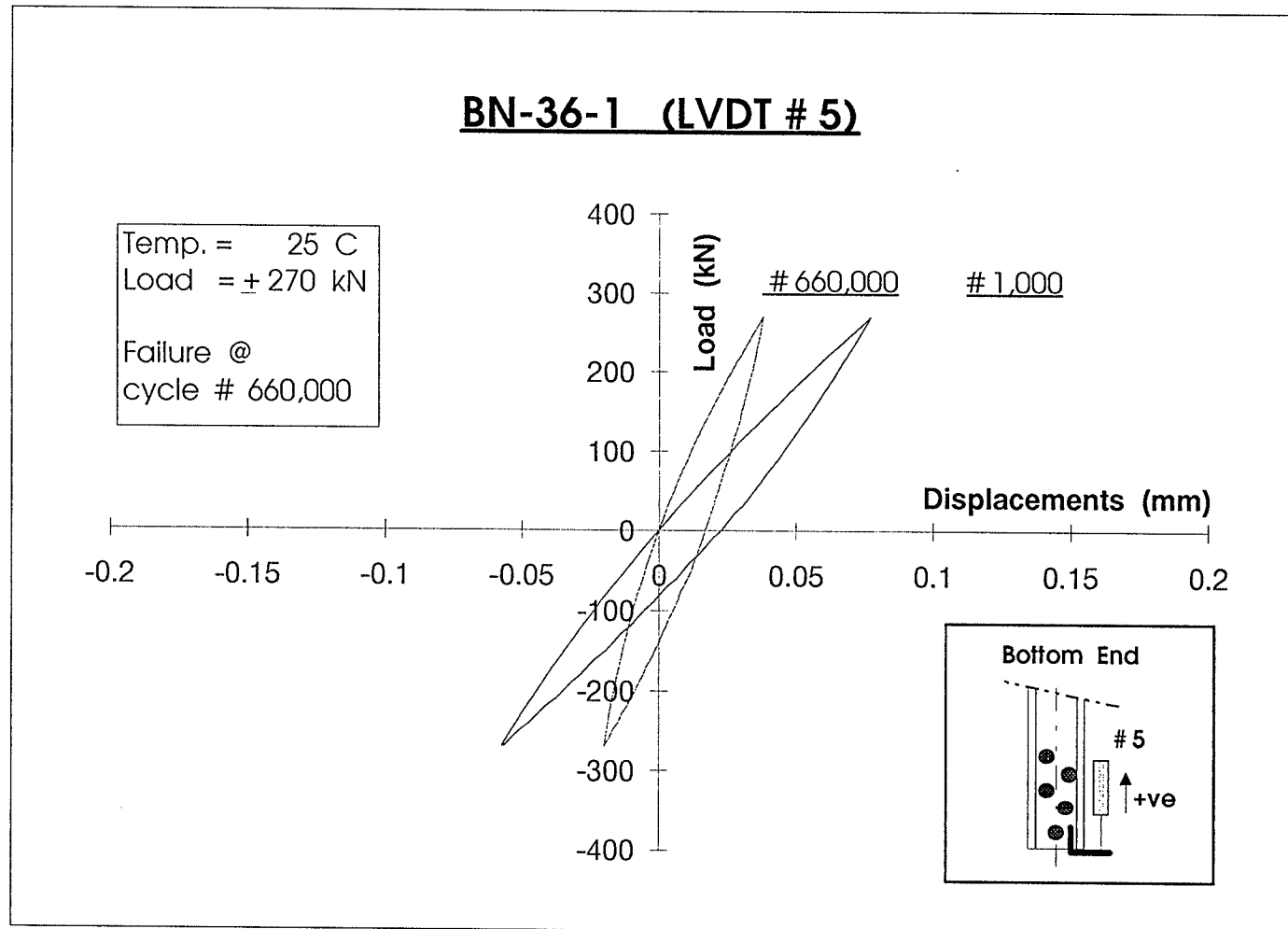
Figure 4.70 : Load-Displacement Relationship at the Bottom End Section of Specimen BN-36-1

HBN-37-3 (LVDT # 5)

Temp. = 25 C
Load = ± 300 kN

Failure @
cycle # 120,000

Load (kN)

400

300

200

100

0

-100

-200

-300

-400

1,000   # 118,000

Displacements (mm)

-0.2   -0.15   -0.1   -0.05   0   0.05   0.1   0.15   0.2

Bottom End

5

+ve
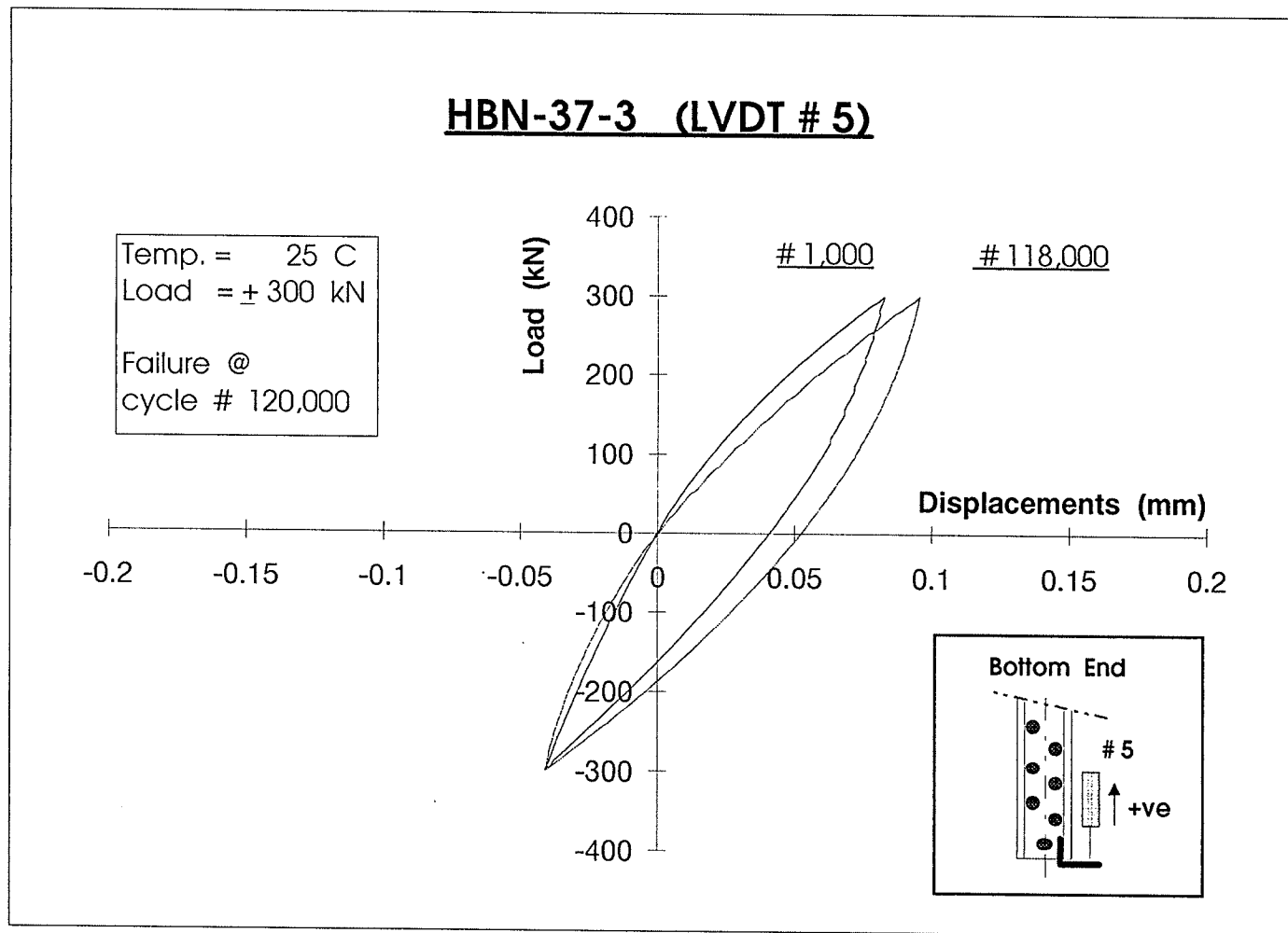
Figure 4. 71 : Load-Displacement Relationship at the Bottom End Section of Specimen HBN-37-3
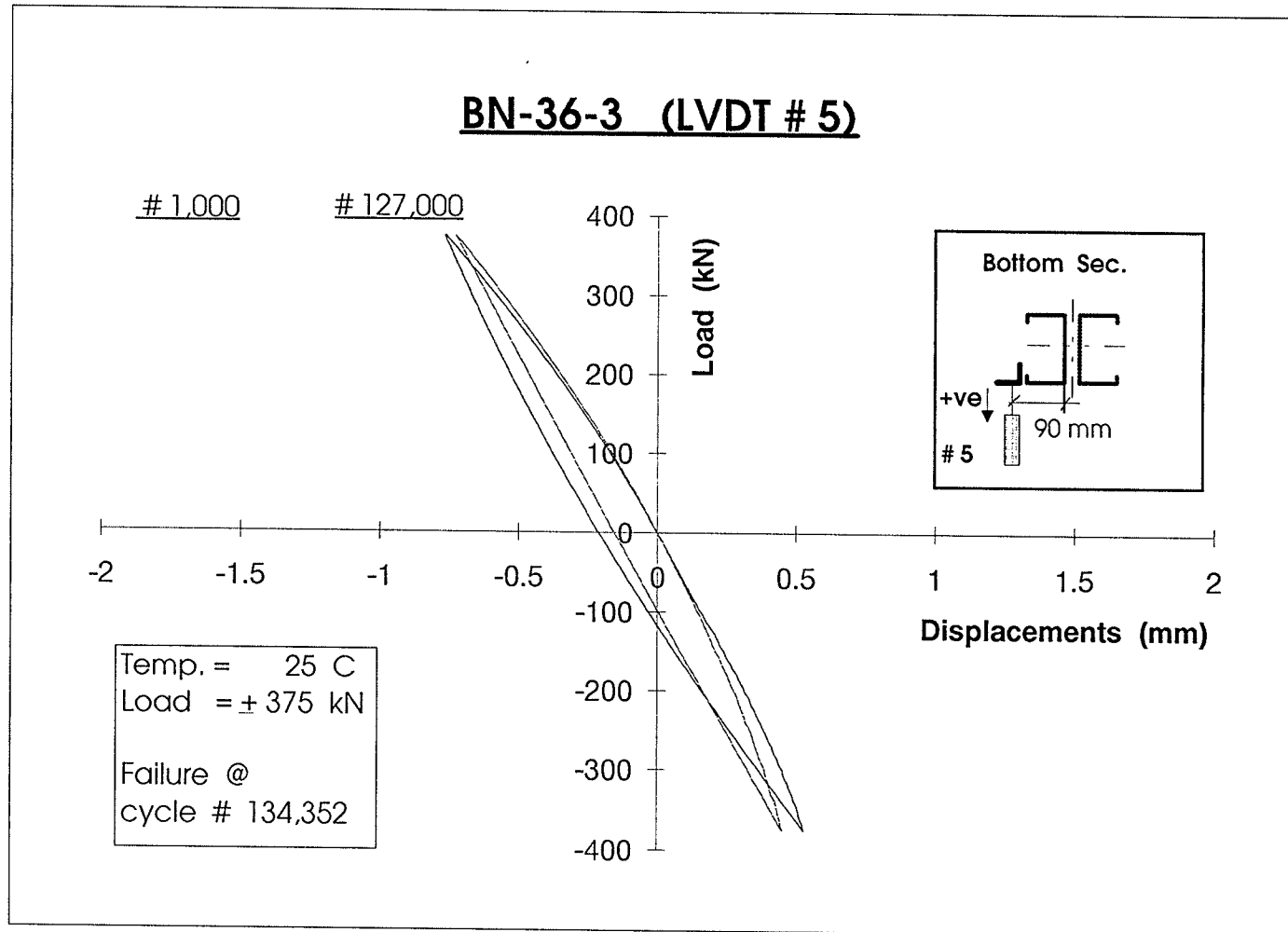
Figure 4. 72 : Load-Displacement Relationship at the Bottom End Section of Specimen BN-36-3

HBN-37-5 (LVDT # 5)

52,000   # 2,000

Load (kN)

400
300
200
100
0
-100
-200
-300
-400

Displacements (mm)

-2   -1.5   -1   -0.5   0   0.5   1   1.5   2

Bottom Sec.

+ve
5
90 mm

Temp. =   25 C
Load = ± 350 kN

Failure @
cycle # 52,185
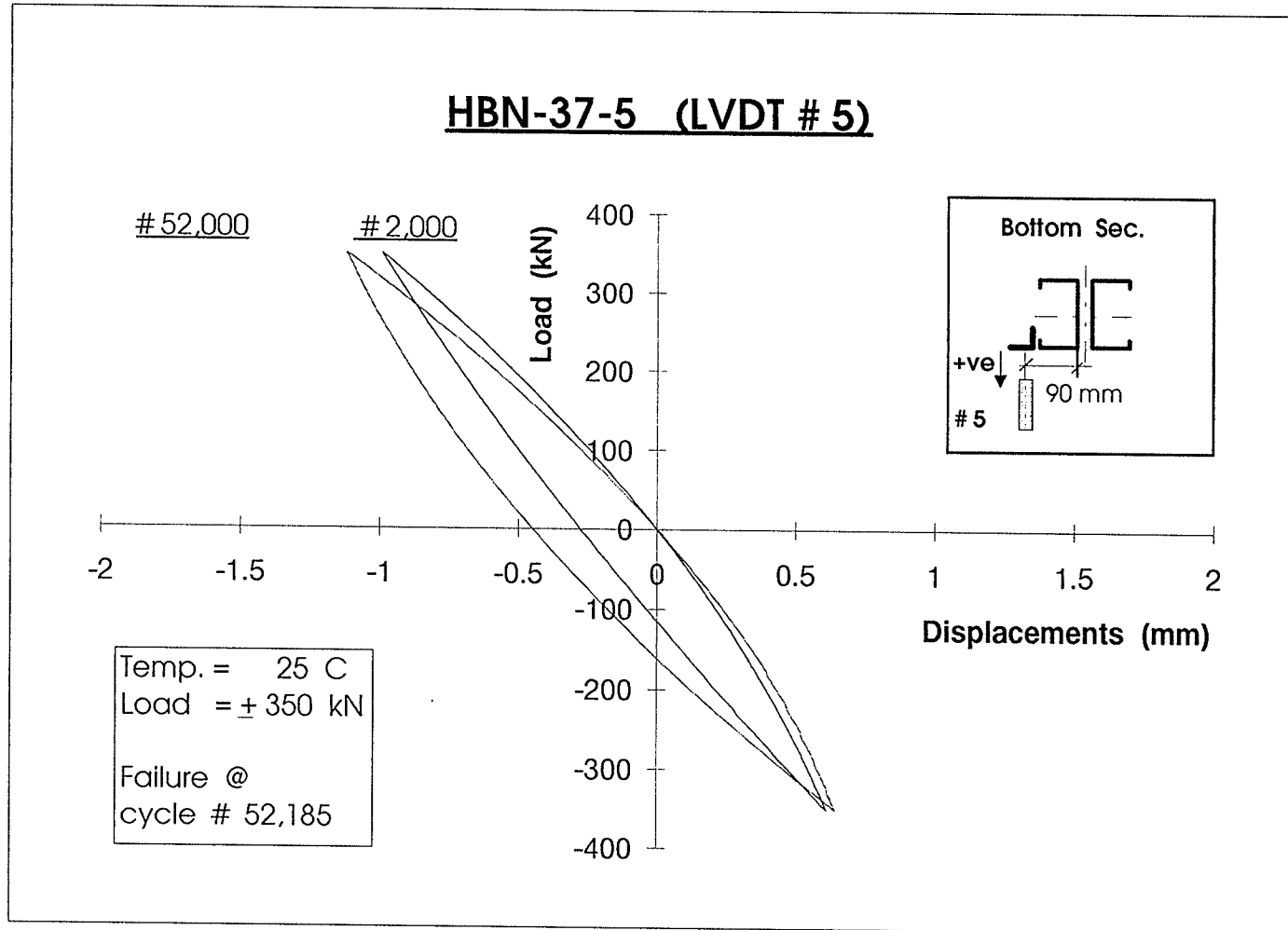
Figure 4. 73 : Load-Displacement Relationship at the Bottom End Section of Specimen HBN-37-5
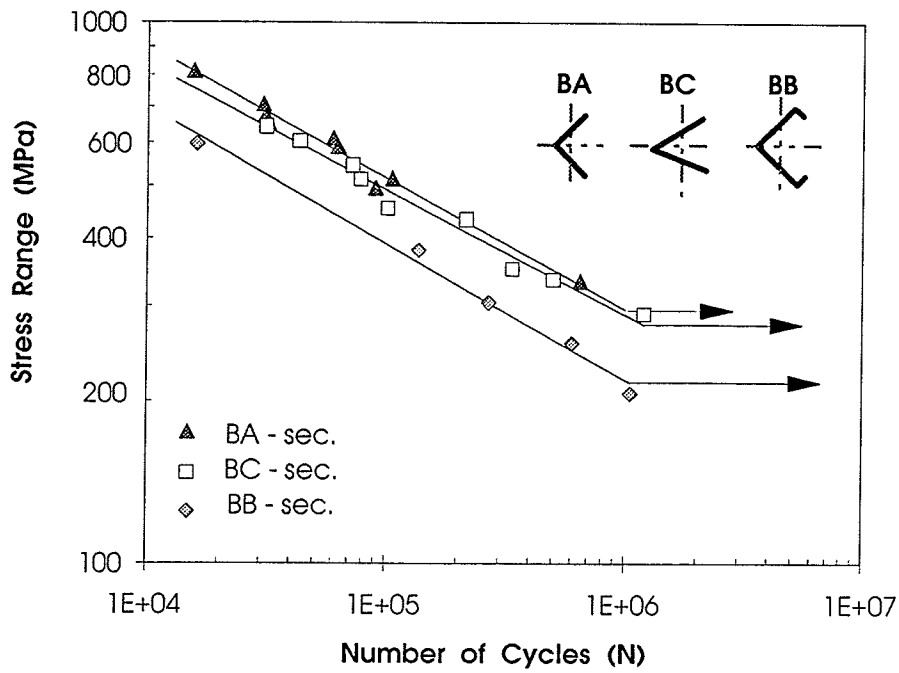
Figure 4.74: S-N Plot for Singly Symmetric sections Connected Through One Leg. ASTM A715 Grade 60 Steel. (Temperature = 25 C)
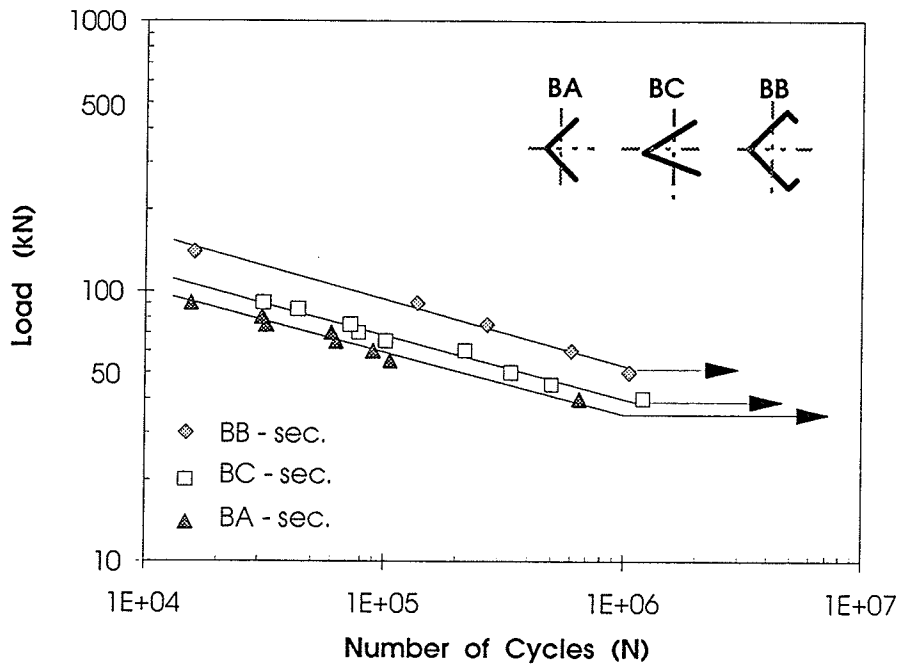
Figure 4.75: Load-N Plot for Singly Symmetric sections Connected Through One Leg. ASTM A715 Grade 60 Steel. (Temperature = 25 C)
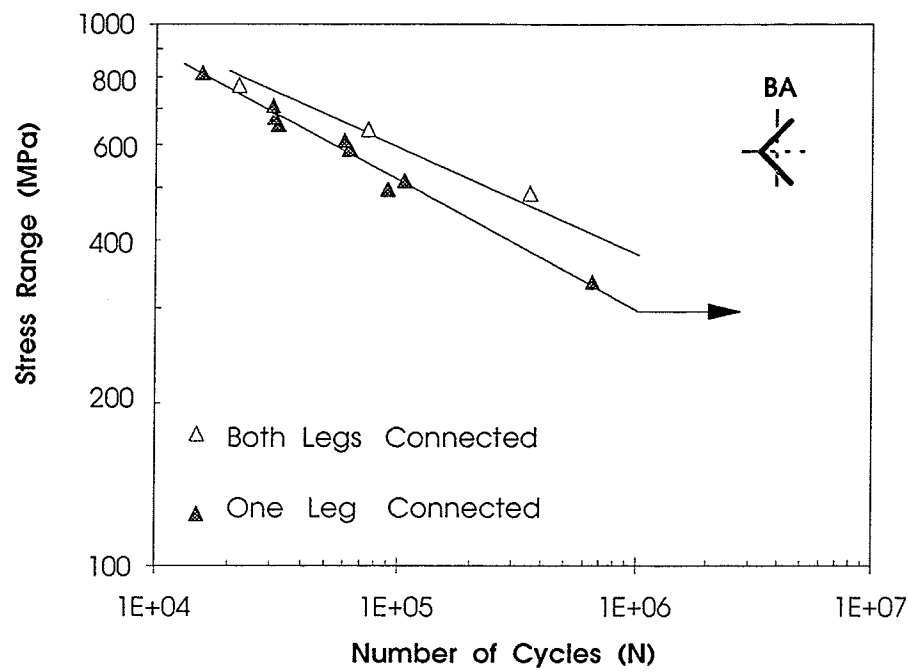
Figure 4.76: S-N Plot for the 90^0-angle section. (Temperature = 25 C)
ASTM A715 Grade 60 Steel.
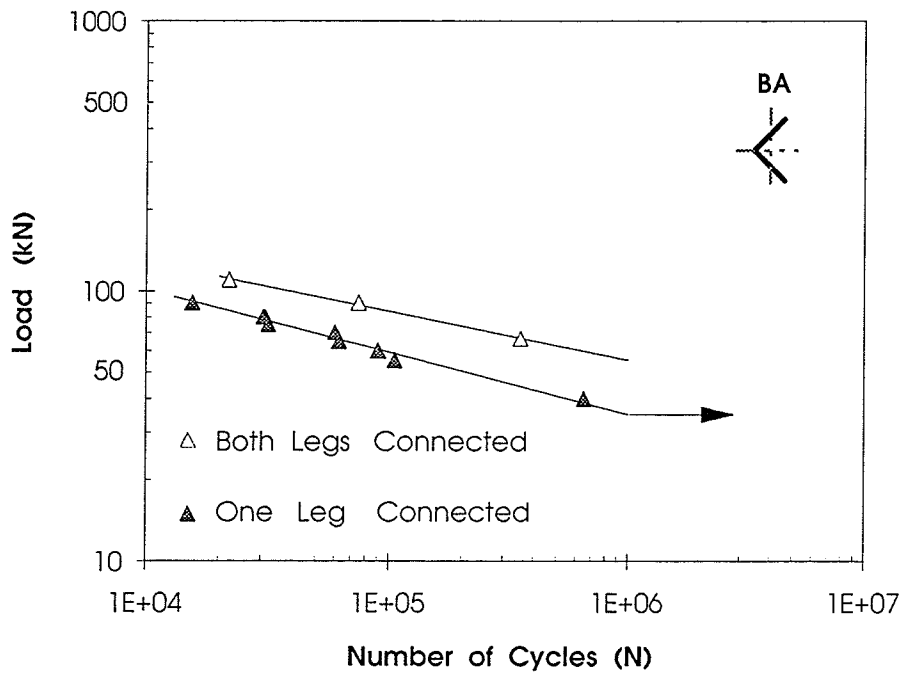
Figure 4.77: Load-N Plot for 90^0-angle section (Temperature = 25 C)
ASTM A715 Grade 60 Steel.

230
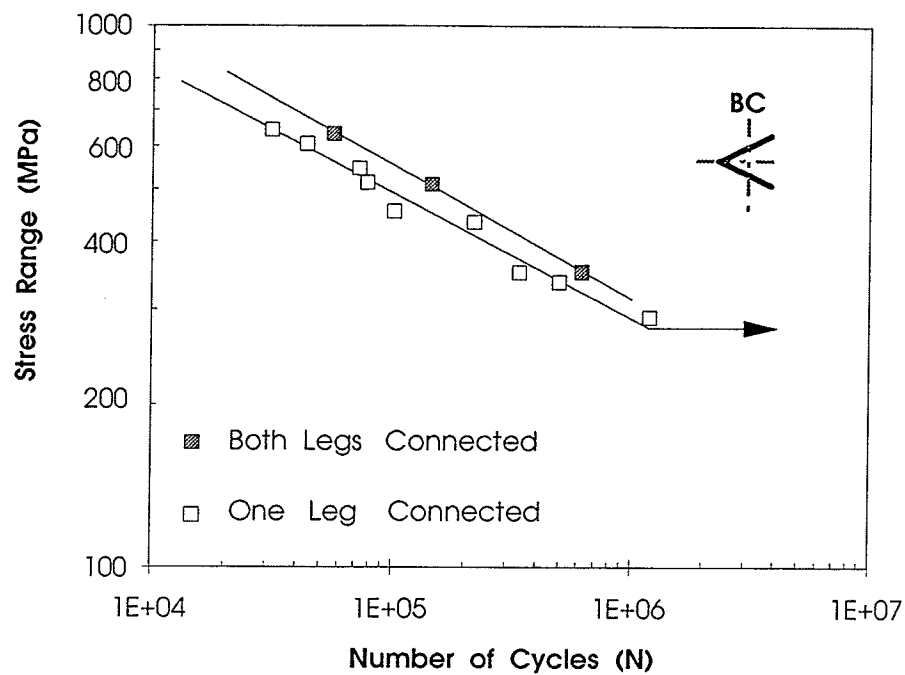
Figure 4.78: S-N Plot for the 60°-angle section. (Temperature = 25 C) ASTM A715 Grade 60 Steel.
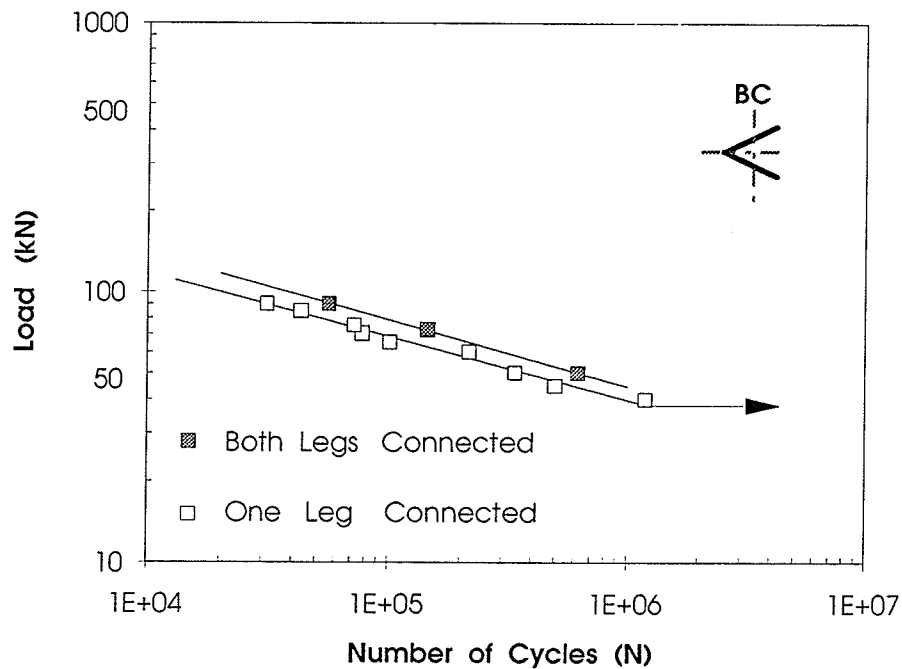
Figure 4.79: Load-N Plot for 60°-angle section Connected Through One Leg. ASTM A715 Grade 60 Steel (Temperature = 25 C)
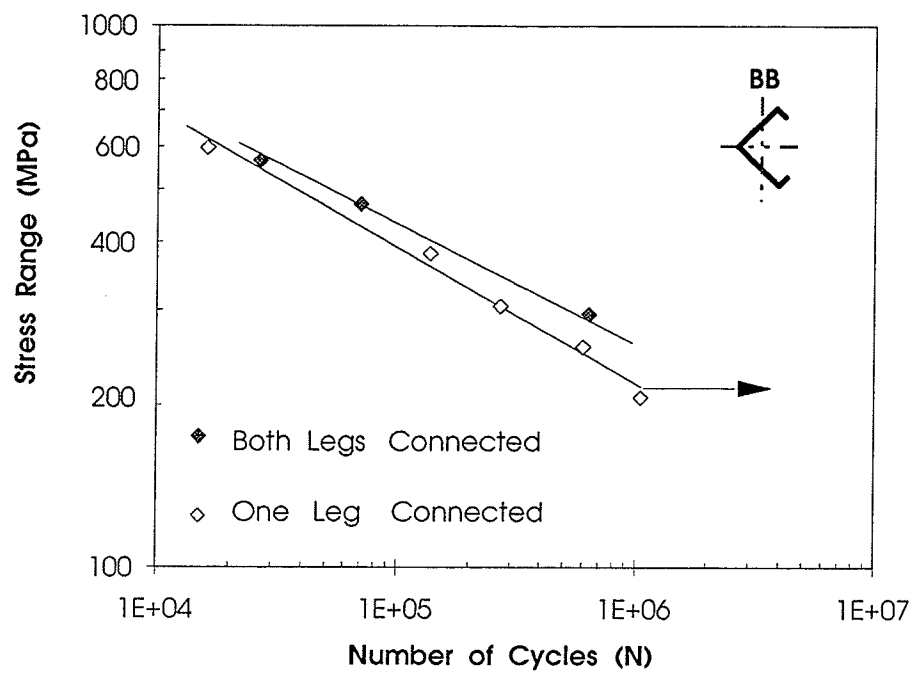
Figure 4.80: S-N Plot for Lipped-angle section. (Temperature = 25 C)
ASTM A715 Grade 60 Steel
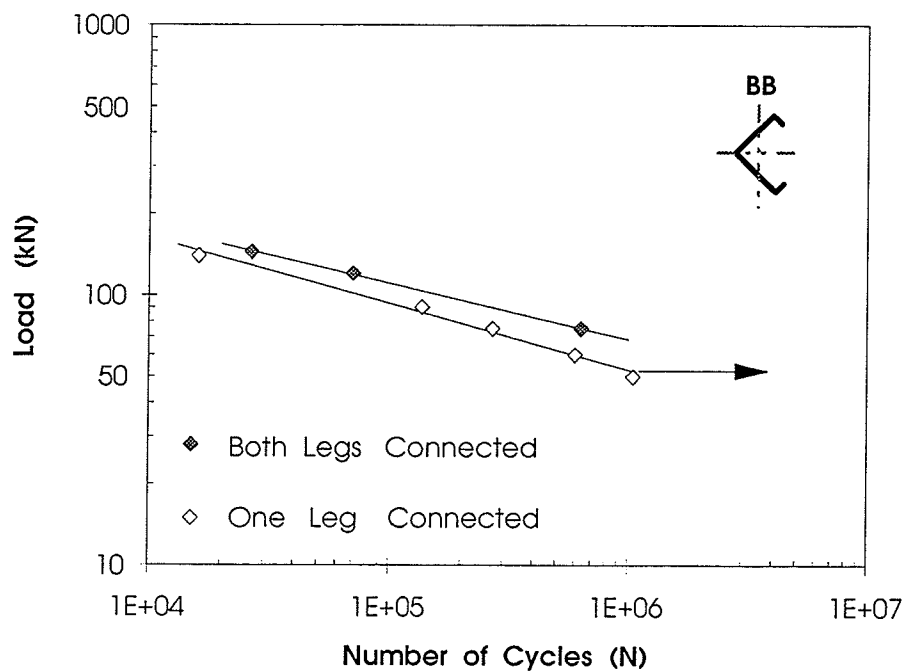
Figure 4.81: Load-N Plot for Lipped-angle section. (Temperature = 25 C)
ASTM A715 Grade 60 Steel

Figure 4.83 : Failure of 60°-angle Specimen Connected Through One Leg.
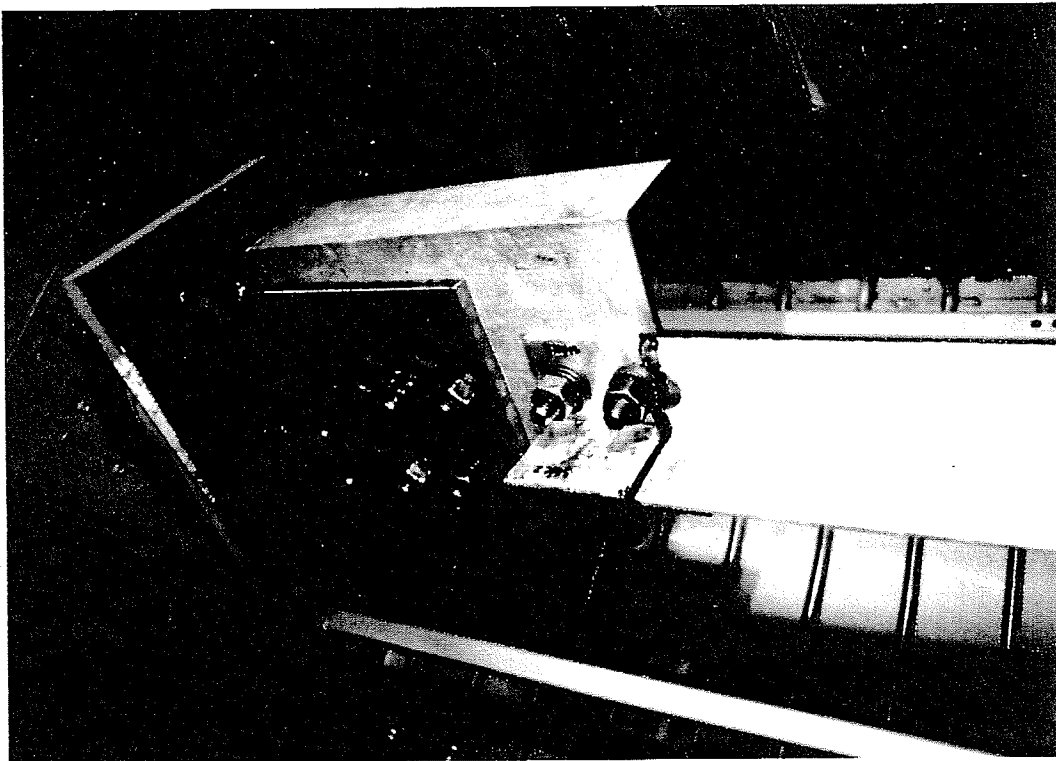
Figure 4.82 : Failure of 90°-angle Specimen Connected Through One Leg.

233

Figure 4.84: Failure of Lipped angle Specimen Connected Through One Leg.
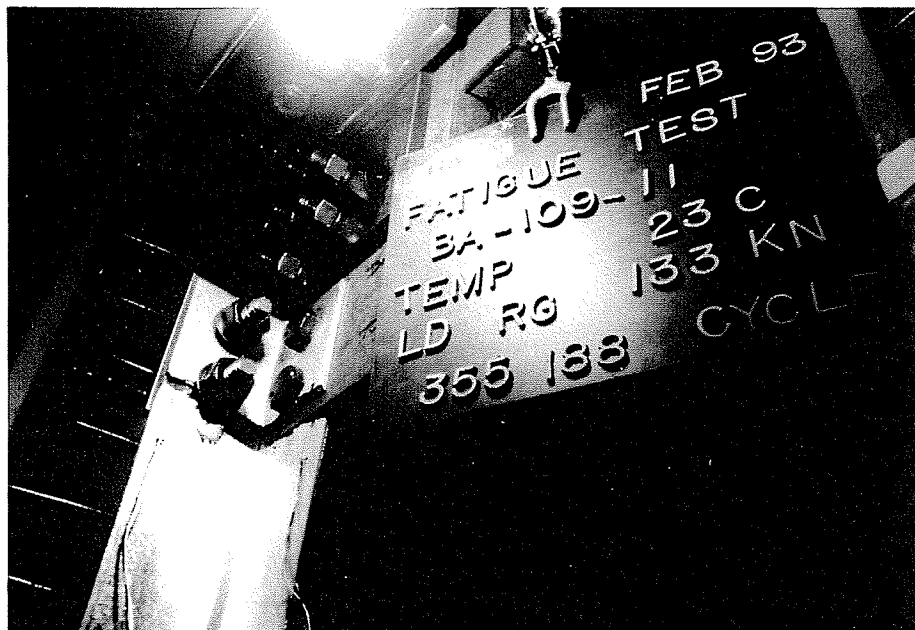
Figure 4.85: Failure of 90°-angle Specimen Connected Through Both Legs.
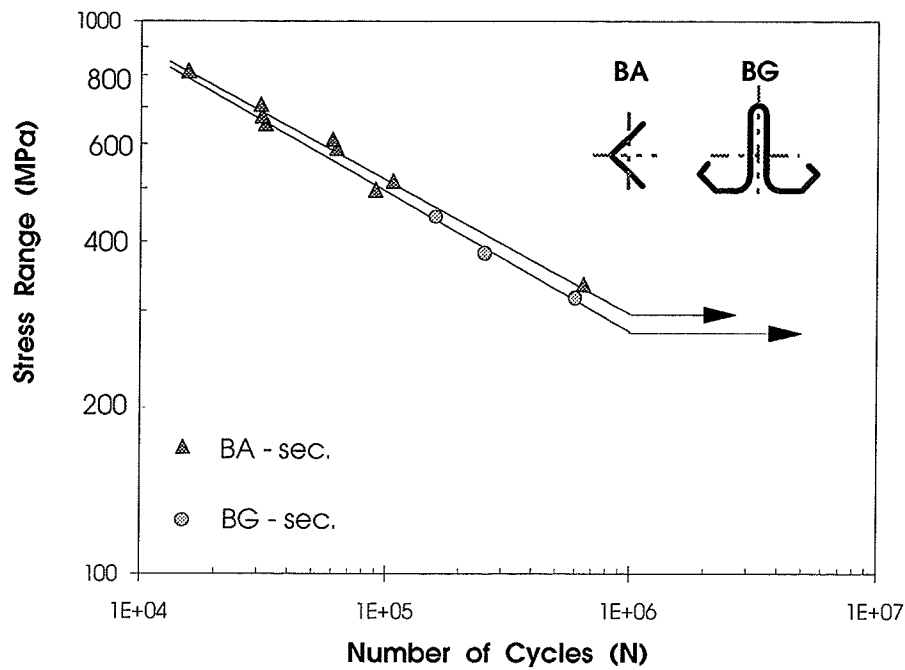
Figure 4.86: S-N Plot for T-shaped section (Temperature = 25 C).
ASTM A715 Grade 60 Steel
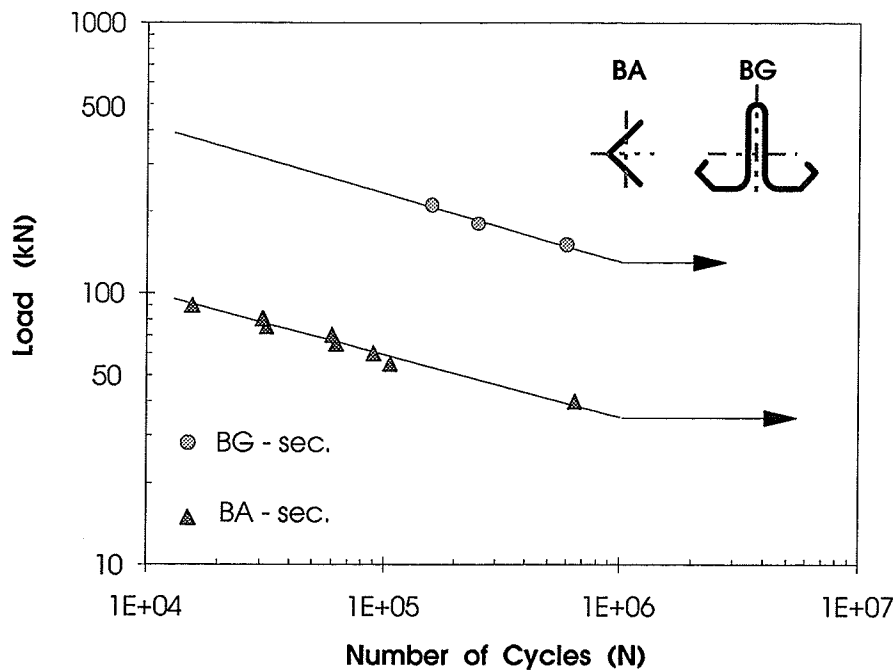
Figure 4.87: Load-N Plot for T-shaped section. (Temperature = 25 C)
ASTM A715 Grade 60 Steel
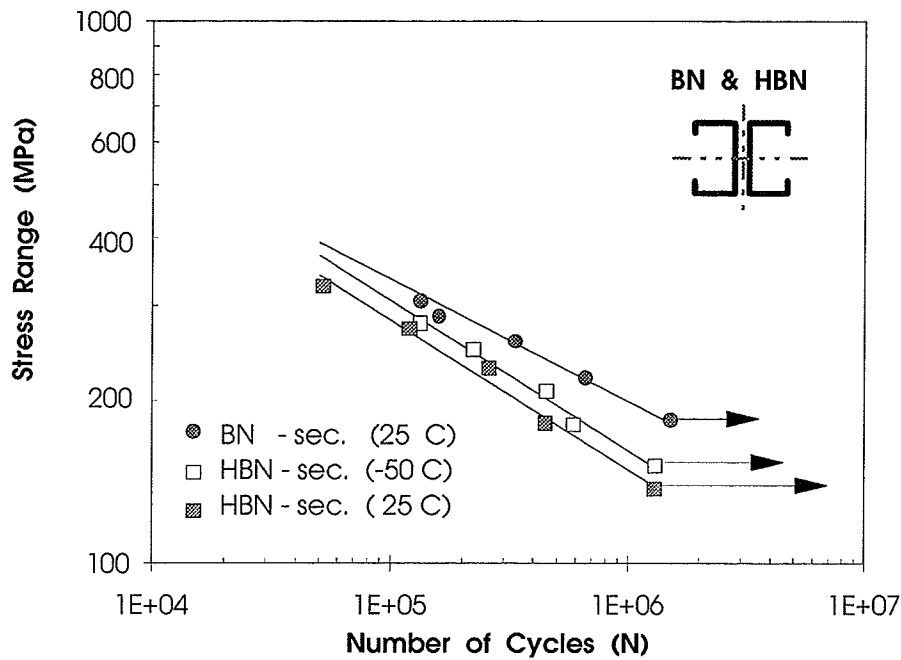
Figure 4.88: S-N Plot for Back-to-Back Channel sections. (BN and HBN)
ASTM A715 Grade 60 and CAN/CSA G40.21-M 300W Steel
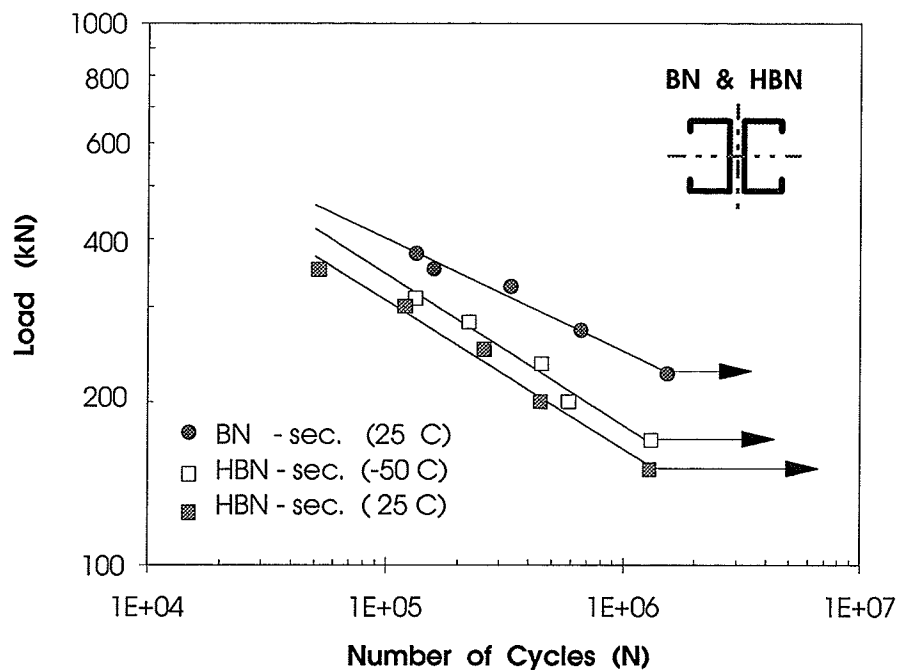
Figure 4.89: Load-N Plot for Back-to-Back Channel sections. (BN and HBN)
ASTM A715 Grade 60 and CAN/CSA G40.21-M 300W Steel

Figure 4.90 : Failure of T-shaped Section (BG).
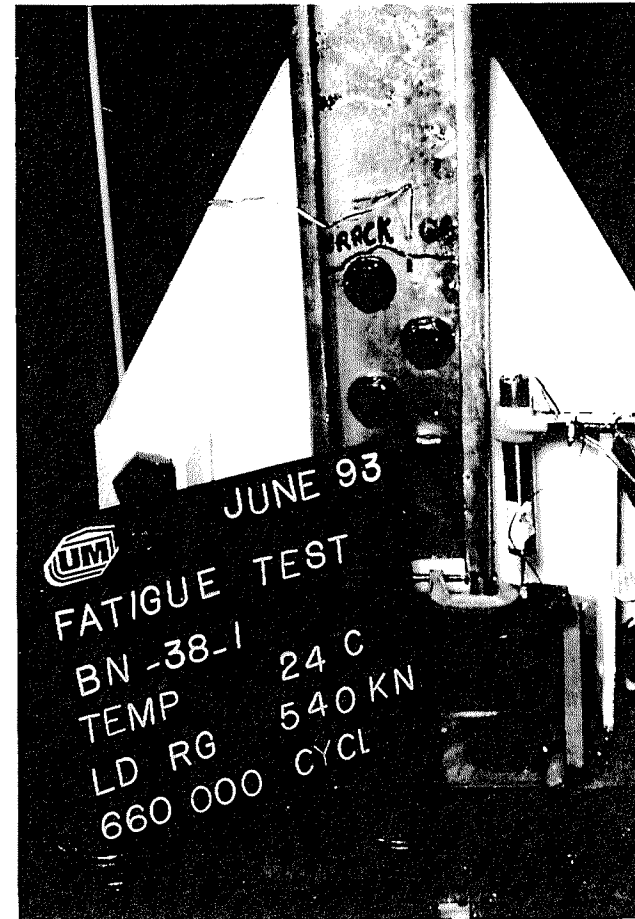
Figure 4.91 : Failure of Back-to-Back
Channel Specimen (BN).
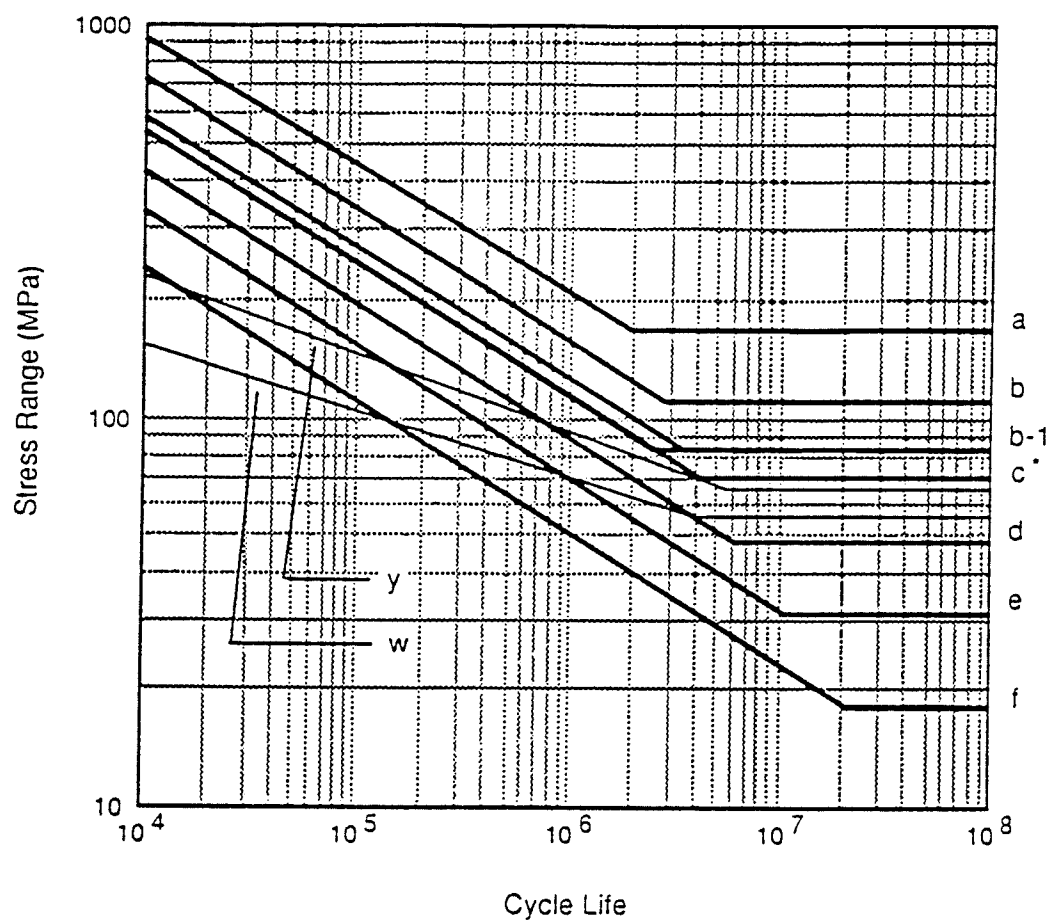
Figure 4.92: CAN/CSA-S16.1-M94 1995   Fatigue Design Curves
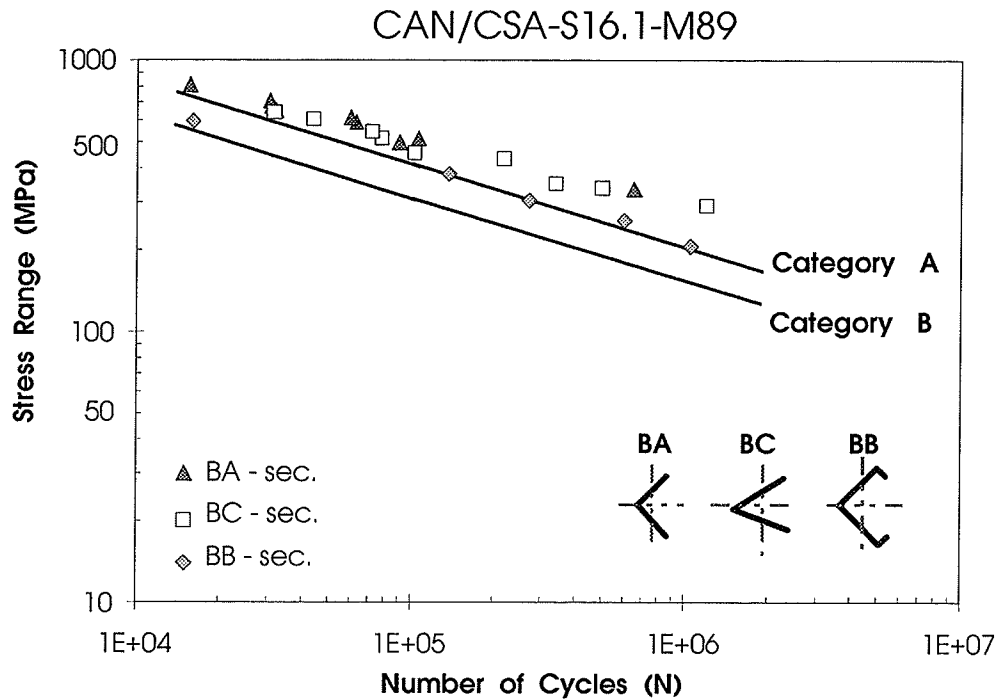
Figure 4.93: S-N Plot for Singly Symmetric Sections. (One Leg Connected).
ASTM A715 Grade 60 Steel. (Temperature = 25 C)
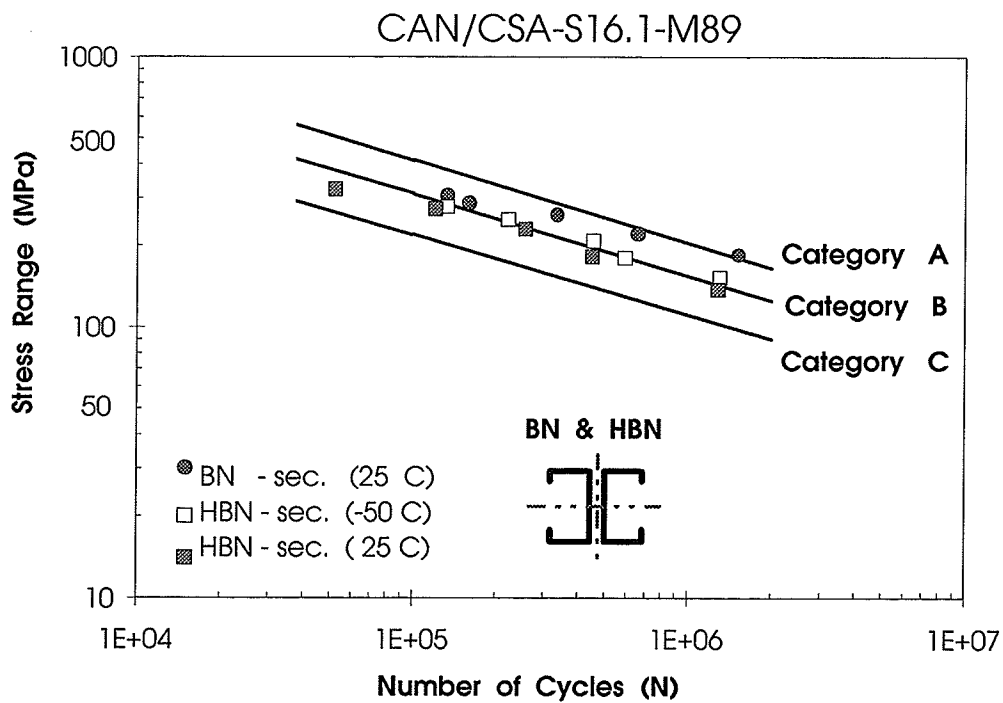
Figure 4.94: S-N Plot for Back-to-Back Channel sections. (BN and HBN)
ASTM A715 Grade 60 and CAN/CSA G40.21-M 300W Steel

239

CHAPTER 5

Finite Element Analysis

5.1 Introduction

The cold-formed plain 90°-angle section is extensively used in latticed electrical transmission towers. These angles are usually connected through one leg and can be subjected to either eccentric tension or compression loading. In the present study, a finite element model was designed to simulate the behaviour of 90°-angle sections connected through a single leg. Both geometric and material nonlinearities were incorporated in the analytical problem. The test specimen was modeled using both quadrilateral and triangular shell elements, particularly well suited to model curved portions. Each element had six degrees of freedom at each node. A newtonian approach was adopted for the nonlinear analysis using the ANSYS finite element program (Swanson Analysis Systems, Inc., 1992).

240

In the work described herein, the finite element analysis was initiated to fulfill two objectives. The first was to ascertain the validity of the model to simulate actual behaviour of the section. As such, special emphasis was given for correlating the experimental results with those obtained from the finite element analysis. The computed strains and translations were found to be in good agreement with those recorded in the experimental program.

The second objective was to obtain fatigue life estimates based on stresses predicted by the finite element method. In that regard, the computed stresses incorporated the effect of localized stress concentrations at the region of the discontinuity (end hole zone). Furthermore, in order to account for irregular load cycles (variable amplitude loading), fatigue life predictions were based on Palmgren-Miner's rule for cumulative damage.

5.2 Single Angles Used as Columns

Nonlinear finite element analysis of single angles has been investigated by several researchers. For the elastic range, Haaijer et al. (1981) simulated an eccentric load test of hot-rolled 90°-angles utilizing the MSC/NASTRAN finite element program. In addition, for the elasto-plastic buckling analysis of single angle

columns, Chuenmei (1984), used a combination of flexural-torsional buckling and local plate buckling analysis. The angle was discretized using non-compatible rectangular plate elements with five degrees of freedom at each node (three translational and two rotational).

To account for the elasto-plastic behaviour, the material was assumed to be isotropic with an elastic-perfectly plastic stress-strain relationship. Von Mises yield criterion and the concept of effective stress were adopted in the finite element formulation. The study concluded that computed ultimate loads were in good agreement with test results.

In 1991, Adluri et al. designed a finite element model for estimating the ultimate strength of 60° equal leg angle under axial compressive loading. The section studied was produced through schifflerizing the hot-rolled 90°-angle members by bending each leg inwards by 15°. This process introduced additional residual stresses into the section. As such, the numerical simulation of residual stresses was considered in the analysis. The recommendations made by the ECCS (1985) were adopted in defining the residual stress pattern for 90°-angles. The member was modeled using eight-noded shell elements with six degrees of freedom at each node. The analytical problem was solved under both geometric and material nonlinearities using the ABAQUS finite element program. Concentric loads were applied through a fictitious

thick end plate attached to the entire cross section at each end. Furthermore, in order to account for eccentricity of loading in actual tower members, the initial geometry of the angle was assumed to be in the form of a half sine-wave with central out-of-straightness equal to 1/2000 to 1/500 of the member length.

On correlating computed and experimental results, the study indicated that the adopted model could reasonably predict failure loads of schifflerized angles under concentric axial compressive loading.

5.3   Quadrilateral and Triangular Shell Elements

In the present study, the cold-formed 90°-angle member was modeled using both quadrilateral and triangular shell elements with six degrees of freedom at each node: translations in the nodal X, Y, and Z directions, and rotations about the nodal X, Y, and Z axes. The chosen element is capable of accounting for plasticity, stress stiffening, large deflections, and large strains.

The geometry, node locations, nodal displacements (u, v, and w), and the element's coordinate system are shown in Figure 5.1. The quadrilateral element is defined by eight nodes, four thicknesses at corner nodes, and the orthotropic

243

material properties. If the element has variable thickness, the thickness at the mid-side nodes is taken as the average of those at the corresponding corner nodes.

For nonlinear materials, five through-the-thickness integration points could be used for the shell elements adopted in the study (quadrilateral and triangular). For linear materials the ANSYS finite element program uses only two through-the-thickness integration points. Moreover, for in-plane analysis, 2×2 integration points are used for quadrilateral shell elements, and only 3 integration points are used for triangular shell elements.

5.4   Sources of Nonlinearity

In any structural system, many sources of nonlinearity significantly influence its structural response. These sources are highly dependent on the structural system, the loading, and the boundary conditions.

For latticed transmission towers, one can identify three major sources of nonlinearity. These include, material nonlinearity, geometric nonlinearity, and joint flexibility and slippage. However, as the present study was concerned with studying the fatigue behaviour of cold-formed steel members in transmission towers,

an essential requirement was producing friction type connections during cyclic loading. As such, the third type of nonlinearity (joint flexibility and slippage) was not accounted for in the finite element formulation. Both material and geometric nonlinearities are discussed in the following subsections.

5.4.1   Material nonlinearity

Material nonlinearity encompasses problems in which the stresses are not linearly proportional to the strains. In the finite element formulation, the ANSYS program has the capability of simulating two types of stress-strain relationships; plasticity, and nonlinear elasticity. In that regard, an incremental procedure based on the Newton-Raphson method was adopted where a series of nonlinear iterations converge to the actual nonlinear solution. The stiffness matrix was updated at each equilibrium iteration to form the tangent stiffness matrix.

The Newton-Raphson equation can be written as:

$$[K_T] \{\Delta u\} = \{F^a\} - \{F^{nr}\} \qquad (5.1)$$

where,

$$[K_T] = \text{tangent stiffness matrix}$$

$$\{\Delta u\} = \text{nodal displacement increment vector}$$

$$\{F^a\} = \text{vector of applied loads}$$

245

$$\{F^{nr}\} \quad = \quad \text{vector of restoring loads corresponding}$$

to the element internal loads

Figure 5.2 illustrates the incremental Newton-Raphson procedure adopted in the present study. The procedure utilizes a combination of the incremental and iterative schemes.

The fully reversed load cycle shown in Figure 5.3 was divided into three load steps. The first load step was from zero load to maximum tensile load. The second was from maximum tensile load to maximum compressive load, and the final load step was from maximum compressive load back to zero load.

The load was applied in an incremental (ramped) sequence following the triangular wave form shown in Figure 5.3. Each load step was divided into a series of sub-steps where successive equilibrium iterations were performed until convergence of the solution was achieved.

Apparently, the incremental Newton-Raphson method yields higher accuracy compared to iterative procedures. Furthermore, the additional computational effort could be justified by the fact that the iterative part of the procedure permits one to access the quality of the approximate equilibrium at each stage.

5.4.2 Geometric nonlinearity

Geometric nonlinearities result from the continuous change in the geometry of the structure as it deflect. At each equilibrium iteration, the tangent stiffness matrix $[K_T]$ is updated to account for the modified stiffness of the deformed geometry. In the current study, geometric nonlinear effects were accounted for by using the large deflection concept. This concept assumes that the rotations are large but the mechanical strains (that cause stresses) are small.

5.5 Finite Element Modeling

The finite element model adopted in the present study can be clearly described based on three standpoints: (1) the cross sectional dimensions and the material properties of the test specimen, (2) the discretization process, and (3) the selection of the displacement models (boundary conditions), and the location of the applied loads. These three points are discussed in the following subsections.

5.5.1 Cross sectional dimensions and material properties

In modeling the 90°-angle section (BA), the average recorded cross sectional dimensions of all test specimens were used. The angle had an average flat width of 63.281

mm, an average base metal thickness of 3.95 mm, and an average inner radius of 4.0 mm as illustrated in Figure 5.4.

The average measured hole diameter was 17.385 mm. Moreover, the average horizontal distance measured from the centerline of the hole to the edge of the angle was 35.135 mm. At each end of the member, two bolts were used to connect one leg of the angle with the gusset plate. The vertical edge distance and bolt spacing were 24.457 mm and 50.0 mm respectively. The total length of the angle was 1500 mm. However, due to symmetry about the mid-height plane of the member, only half the length (750 mm) was considered in the finite element modeling.

In the finite element analysis, the steel type used was ASTM A715 Grade 60 with minimum specified yield stress of $F_y \simeq 415\,MPa$. All material properties were extracted from results of standard tension coupon tests performed at room temperature ($\simeq 25^\circ C$). Furthermore, these properties were representative of those obtained from tension tests performed on ungalvanized coupons cut from flat portions of the 90°-angle section (BA). Material properties employed in the finite element analysis are shown in Figure 5.4.

5.5.2 Discretization process

The discretization process involves subdividing the structure into an equivalent system of finite elements. Obviously, the accuracy of a finite element solution can be improved by refining the mesh. However, computational limitations require that only significant portions of the structure need mesh refinement. On that basis, the 90°-angle member was divided into 45 areas as shown in Figure 5.5. The objective here was to produce an efficient finite element model of the specimen by specifying appropriate element size for each area.

A computer-generated plot of the finite element model is shown in Figure 5.6. The angle member was discretized into a total of 1790 shell elements with six degrees of freedom at each node. Of these, 1637 elements were quadrilateral, and 153 elements were triangular. Mesh refinement could be observed for areas surrounding the holes (stress concentration zones), and near the mid-height section (location of symmetry boundary conditions). The X, Y, Z directions shown in Figure 5.6 are in the global coordinate system.

5.5.3 Boundary conditions and location of applied loads

The plane of symmetry for the angle member was at the mid-height section. As such, three degrees of freedom were restrained for all nodes at that section. These include,

the translations in the longitudinal direction ($U_z = 0$), and the rotations about both the X and Y axes in the global coordinate system ($Rot_x = 0$, and $Rot_y = 0$).

Of special interest in the analysis were the areas surrounding the holes (washer areas). These areas were continuously subjected to out-of-plane pressure resulting from the action of the tensile force in the 15.875 mm (5/8") ASTM A490 structural bolts. In the analysis, a value of 103 kN/bolt was assumed (CAN/CSA-S16.1-M94, 1995). This out-of-plane force was distributed over the washer area surrounding each hole. The area has an outer diameter of 31.50 mm, and an inner diameter of 17.385 mm. Moreover, the applied pressure on each washer produced the friction type connection required for cyclic loading. In that regard, the nodes at the edge of the holes were assumed to be totally restrained except for one degree of freedom, and that was the translation in the longitudinal direction ($U_z \neq 0$).

Fully reversed fatigue loads were applied in the sequence shown in Figure 5.3. As only two bolts were used in connecting the angle member to the gusset plate, the end bolt was assumed to transfer 67% of the alternating fatigue load, whereas, 33% of the load was transferred by the second bolt. Moreover, the nodal points used to transfer the loads in both tension and compression cycles are illustrated in Figures 5.7(a) and 5.7(b) respectively. These nodes were chosen to simulate actual load locations observed during the experimental program.

5.6 Comparisons with the Experimental Results

Results obtained from the finite element analysis were compared to those recorded in the experimental program. The objective was to ascertain the adequacy of the finite element model to simulate actual behaviour of 90°-angle members used in constructing transmission towers.

Typical deformed configurations of the finite element model for the angle member are shown in Figures 5.8 and 5.9 for cases of eccentric compression and tension loads respectively. As evident from these figures, maximum lateral translations were found to occur at the mid-height section of the member. The maximum computed translations at this section occurred for the connected leg. These values were compared to those recorded in the experimental program as illustrated in Figure 5.10.

As illustrated in Figure 5.11, under eccentric compression loads, maximum translations at the mid-height section were at the free edge of the connected leg. However, for eccentric tension loads, the corner of the angle showed the most significant lateral displacement value. The maximum values of the computed translations

were in very good agreement with those recorded in the experimental program (error = 5% to 8%). Computed and recorded translations at the mid-height section of the angle are given in Table 5.1. Moreover, computer generated plots of translations in the global Y direction under eccentric compression and tension loads are given in Figures 5.12 and 5.13.

Longitudinal residual stress distribution for the inner and outer surfaces of the 90°-angle section (BA) are shown in Figure 5.14. Due to the irregular distribution, these stresses were not accounted for in the finite element analysis. Typical stress distribution at the mid-height section of the angle member is shown in Figure 5.15. In addition, stress contours in the longitudinal direction are given in Figure 5.16. As evident from these plots, regions surrounding the holes were characterized by the presence of high localized stress concentrations. A close-up view showing the longitudinal stress contours (σ_z) surrounding the end hole zone is shown in Figure 5.17.

The strain gauge pattern used for the 90°-angle specimen is illustrated in Figure 3.23. The exact location of the gauges were used in computing the strains by the finite element method. When the actual location was found between any two nodal points, the strain value was obtained by direct interpolation. The differ-

252

ence between computed and recorded strain readings were within an error band of ± 20%. Such difference was more pronounced for Gauge #1 which was located inside the stress concentration zone. The presence of high residual tensile stresses at the end hole zone is believed to be the major factor causing the noticeable difference in strain values at that location.

Under eccentric tension loads, the finite element model over estimated the strain values by 17%. For compression loads the difference between theoretical and experimental strain readings did not exceed 20%. In general, the predicted strains tend to over estimate the actual measured strains only in the region of high stress concentration. At the mid-height section, no pronounced difference was observed between theoretical and experimental strain values.

5.7 Cumulative Fatigue Damage

Transmission towers are subjected to a large number of repetitive loads of variable magnitudes resulting mainly from the action of wind gusts. These structures are therefore subjected to irregular load histories that generally occur in a random sequence. The cumulative effect of these loading events eventually produces fatigue failure. However, techniques of analysis and of testing have been developed

to predict whether such loads will produce acceptable or unacceptable fatigue lives.

In all cases, solution techniques used for analyzing irregular load histories are based on data obtained from constant amplitude fatigue tests. Moreover, both simple and complicated solution techniques are available. Simple analysis methods are based on nominal stresses and the assumption that fatigue damage (deterioration of the metal during cyclic straining) is linear with the number of cycles. However, more complicated analysis approaches deal with the total fatigue life of a component as a summation of both initiation and propagation lives. In that regard, a notch strain approach is adopted during the crack initiation stage, whereas, a crack growth analysis is used for later stages of the fatigue life.

In evaluating the fatigue life for various types of steel bridge members under variable amplitude loading, Schilling et al., (1978) acquired fatigue data on welded bridge members under variable-amplitude random-sequence stress spectrum. In their study, the effective stress range concept was used to relate variable amplitude fatigue data to constant amplitude data. Three different methods for calculating the effective stress range were discussed. These were: (1) the Rayleigh distribution method, (2) the root mean square technique (RMS), and (3) the Palmgren-Miner's rule for cumulative damage. The results obtained indicated that the transformed variable-amplitude test data points were within a scatter band bounded by the

95% confidence limits of the constant amplitude test data. Furthermore, there was no statistically significant difference between constant amplitude data and the transformed variable amplitude data.

5.7.1 Fatigue life prediction

Numerous methods for the prediction of fatigue life of a component under non-uniform load cycles have been presented by Osgood, (1982). Moreover, both linear and nonlinear methods of fatigue life prediction were discussed in detail. All the methods utilize the concept of gradual accumulation of damage that takes place during cyclic loading. In general, methods of fatigue life prediction under non-uniform load cycles can be classified under the following three categories:

1. Linear cumulative damage based on specific S-N data for each specimen type.

2. Nonlinear cumulative damage based on S-N data for each specimen type.

3. Linear or nonlinear cumulative damage based on damage boundaries or modified S-N curves.

Of special interest in the present study was to utilize the stress concentration method (falls under category 3 above) for predicting the fatigue life of the 90°-angle section. This method was coupled with Palmgren-Miner's rule for cumulative

damage. Moreover, stress concentration factors were determined from a refined stress analysis using the ANSYS finite element program.

The stress concentration factor (K_t) is defined as the ratio of the peak stress at the discontinuity region to the nominal stress. Figure 5.18 shows a typical distribution of the longitudinal stress (σ_z) at the discontinuity region of the angle (end hole region). In that Figure, the x-axis represents a horizontal distance of D measured from the edge of the end hole towards the free edge of the angle, where, D is the diameter of the end hole. The stress distribution path (direction) was chosen based on stress contour plots developed by the ANSYS program. From these plots, the nodal path that yielded the highest stress values was clearly identified. The computed nominal stress (membrane stress) for the chosen path is also illustrated in Figure 5.18. Depending on both the level of the applied load, and the distance from the edge of the hole, the computed stress concentration factors for the angle section ranged from 2.8 to 6.0.

In order to compare the computed stress concentration factors for the angle member with some theoretical values, a uni-axially stressed plate with two circular holes was assumed for the analogy. Considering a plate width of 63.3 mm (equals to the flat width of the angle section), hole spacing of 50 mm, and a hole diameter of 17.385 mm, the stress concentration factor as presented by Peterson, (1974) was

256

approximately 2.32. This value was obtained for the case of uni-axially stressed plate

with an infinite row of circular holes (Schulz, 1942). However, the difference between

the computed stress concentration factors based on the finite element analysis and

the theoretical value of $K_t = 2.32$ is mainly attributed to the fact that the ideal

uni-axial stress condition of a plate is not satisfied for the case of an eccentrically

loaded angle.

For fatigue life prediction, the stress concentration factors can be utilized in two

different ways:

1. To define the peak stress at the region of the discontinuity, and to determine

   the allowable number of cycles based on the approximate S-N curve for the

   new unnotched material.

2. To select an appropriate S-N curve from a graded set of notched specimens.

   In that case, the S-N curve is considered to be the damage boundary of the

   design.

In the present study, fatigue design curves were considered those corresponding to

the lower 95% confidence limit. These curves were based on 2.0 standard deviations

below the mean regression line fitted through the test data. The Palmgren-Miner's

rule for cumulative fatigue damage was adopted by the ANSYS finite element pro-

gram. Inspite of the tendency of the rule to overestimate the fatigue life (Osgood,

1982), it is still used extensively not only for its simplicity, but also because more sophisticated values are not generally applicable to all types of service loading.

Palmgren-Miner's rule is based on the assumption that the phenomenon of cumulative damage under cyclic stressing is related to the net work absorbed by the specimen. In that regard, the number of applied stress cycles expressed as a percentage of the number to failure at the given stress range level would be the portion of the useful life expended. Consequently, the fatigue specimen would fail when the total damage reaches 100% (usage factor = 1). The fatigue damage sustained under one cycle of loading can be expressed as:

$$\text{Fatigue Damage} \quad = \quad \frac{1}{N} \tag{5.2}$$

where, N is the fatigue life to fracture under uniform load cycles. Predicted cumulative fatigue damage curves for the 90°-angle member are shown in Figure 5.19. Several values of stress concentration factors in the longitudinal direction were considered as illustrated in Figure 5.19(a). In addition, the combined effect of both longitudinal and transverse stress concentration factors on the fatigue life of the member is demonstrated in Figure 5.19(b). The curves were developed for a surface point at the edge of the end hole. Fatigue calculations executed by the ANSYS program are explained in the following subsection.

5.7.2 Fatigue Damage Calculations

The ANSYS fatigue calculations rely on the ASME Boiler and Pressure Vessel Code, (1989), Section III, Division 1, and Section VIII, Division 2. The fatigue module used combines the effect of stress cycling over many cycles involving all stress components at a point in the structure. The program automatically calculates all possible stress ranges and keeps track of their number of occurrences using the rain-flow counting method proposed by Stasuiski and Endo in 1968. The failure criterion assumed for fatigue calculations is based on the maximum shear theory. Moreover, fatigue calculations are based on the assumption of fully reversed stress cycles.

The procedure can be summarized by the following main steps:

1. Selecting the nodal locations of interest in the fatigue evaluation. Usually these are points where fatigue crack initiation would most likely occur (at the stress concentration zones).

2. Identifying the material fatigue properties for the specimen. This includes defining an S-N curve for the unnotched specimen to be used as a damage boundary for the design.

3. Defining the elastic-plastic parameters m and n^* (strain hardening exponents).

These parameters are obtained from the ASME Boiler and Pressure Vessel Code, (1989).

4. Storing stresses obtained from all three load steps (Figure 5.3) at the selected nodal locations.

5. Defining the number of repetitions for the loading event (three load steps), and assigning scale factors for the stored stresses.

At this stage, as the nodal locations, stresses, and material parameters are all specified, fatigue calculations can be activated at any selected location as explained by the following steps:

1. Computing the maximum alternating shear stress by comparing stresses obtained from different load steps. A vector of stress differences is first computed as:

$$\{\sigma\}_{ij} \; = \; \{\sigma\}_i \; - \; \{\sigma\}_j \qquad\qquad (5.3)$$

where,

$$\{\sigma\}_i \; = \; \text{stress vector for loading } l_i$$

$$\{\sigma\}_j \; = \; \text{stress vector for loading } l_j$$

A stress intensity σ_I is then computed based on principal stresses (σ_1, σ_2, and σ_3)

calculated at the specified location. The stress intensity σ_I is given as:

$$\sigma_I(i,j) \;=\; \text{Maximum of } \left(\,|\sigma_1 - \sigma_2|\,,\,|\sigma_1 - \sigma_3|\,,\,|\sigma_2 - \sigma_3|\,\right) \qquad (5.4)$$

The alternating shear stress is calculated as:

$$\sigma_{i,j}^{a} \;=\; \frac{\sigma_I(i,j)}{2} \qquad (5.5)$$

The maximum alternating shear stress as calculated by the ANSYS program can be expressed as:

$$\sigma_{i,j}^{c} \;=\; K_e \;\; \sigma_{i,j}^{a} \qquad (5.6)$$

where, K_e is a strain distribution factor used in the elastic-plastic fatigue calculations. The factor could be defined based on the ASME Boiler and Pressure Vessel Code, (1989). A value of $K_e = 1$ is considered for elastic analysis based on peak stresses.

2. The total number of load combinations is given as:

$$\text{Number of load combinations} \;=\; \frac{LS\,(LS - 1)}{2} \qquad (5.7)$$

where, LS is the number of load steps in each loading event (in the current study LS = 3). The loadings are then sorted with the highest value of $\sigma_{i,j}^{c}$ first.

3. The usage factor (f_u) for each nodal location is calculated based on Palmgren-

Miner's rule for cumulative fatigue damage.

$$f_u = \frac{N_{used}}{N_{allowable}} \tag{5.8}$$

where,

N_{used} = specified number of repetitions for a particular loading event

$N_{allowable}$ = number of allowable cycles calculated by the program for the

given stress amplitude level

4. Step 3 is repeated using the next highest value of $\sigma_{i,j}^c$ until all the $\sigma_{i,j}^c$

values are exhausted. The number of times this process is repeated is either equal

to, or less than the number of loading events.

Table 5.1 [*]

Experimental and Theoretical Lateral Displacement Values at the Mid-Height Section.
($90°$-angle section connected through one leg at room temp. $= 25°C$)

Load (kN)	a (mm)		b (mm)		c (mm)		d (mm)	
	Exp.	Theor.	Exp.	Theor.	Exp.	Theor.	Exp.	Theor.
90	2.095	1.310	4.029	3.654	0.534	0.505	1.371	2.066
- 90	19.768	19.962	10.979	10.703	0.244	0.801	6.845	8.960
80	2.076	1.282	3.679	3.298	0.461	0.431	1.080	1.783
- 80	14.603	13.568	8.806	7.910	0.483	0.409	4.700	5.562
70	2.084	1.287	3.304	2.943	0.391	0.356	0.824	1.461
- 70	10.582	9.390	6.995	6.057	0.658	0.193	3.055	3.313
60	2.002	1.166	2.906	2.544	0.325	0.293	0.603	1.225
- 60	7.533	6.555	5.494	4.712	0.768	0.068	1.823	1.858
50	1.694	1.077	2.484	2.147	0.262	0.230	0.416	0.950
- 50	5.283	4.588	4.249	3.663	0.813	-0.001	0.940	0.955
40	1.459	0.961	2.039	1.733	0.203	0.171	0.264	0.682
- 40	3.661	3.152	3.206	2.789	0.794	-0.036	0.346	0.397
20	0.691	0.762	0.817	1.076	0.032	0.189	0.164	0.121
- 20	1.233	1.256	1.130	1.370	0.011	0.388	0.024	0.046

[*] To be Used in Conjunction with Figure 5.11.
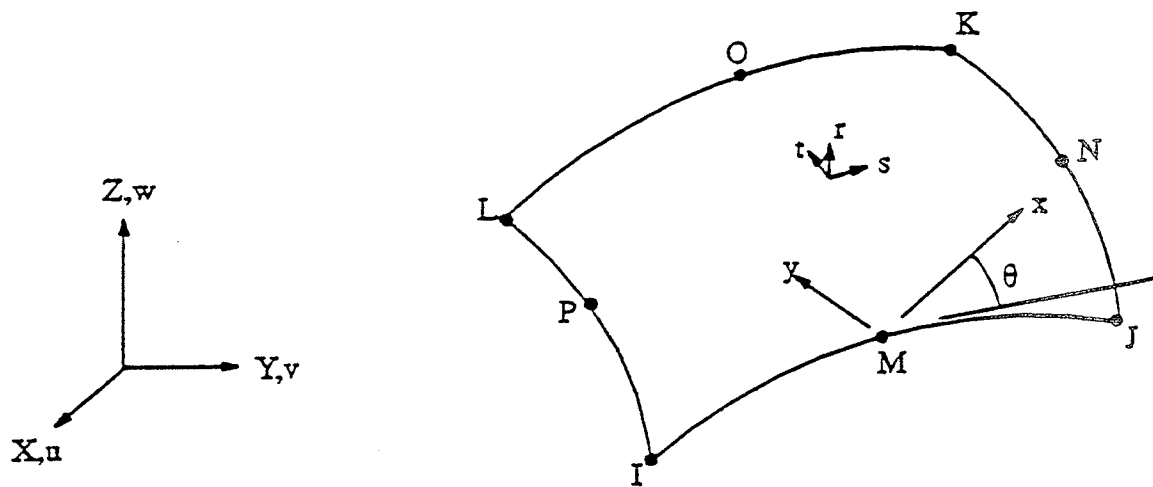
(a)   Quadrilateral Shell Element.
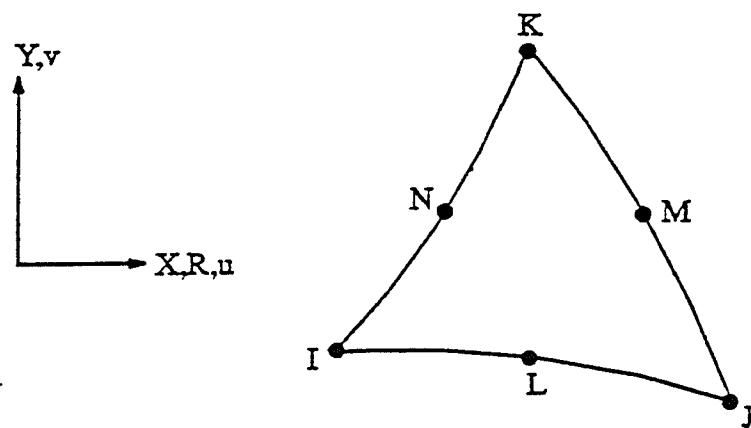
(b)   Triangular Shell Element.

Figure 5.1: Shell Elements Adopted in the Finite Element Analysis.
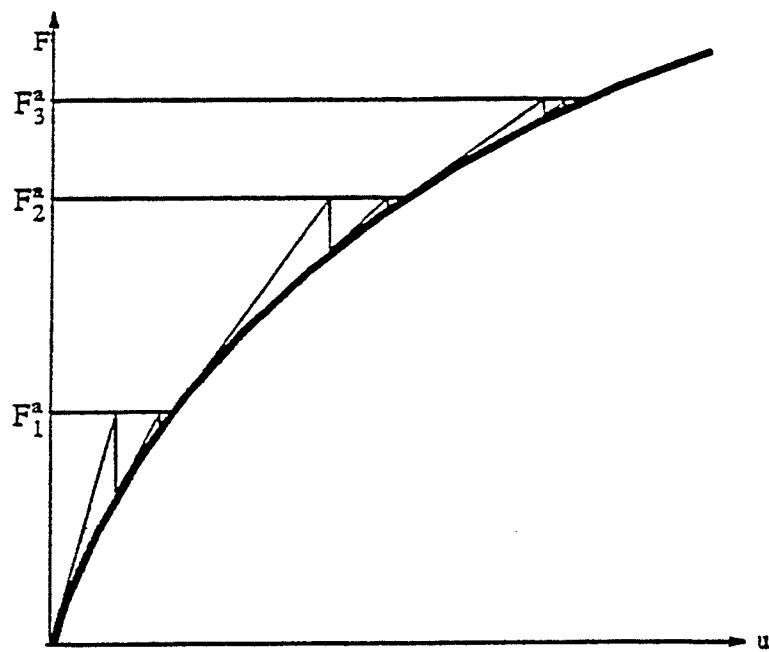
Figure 5.2: Incremental Newton-Raphson Procedure.
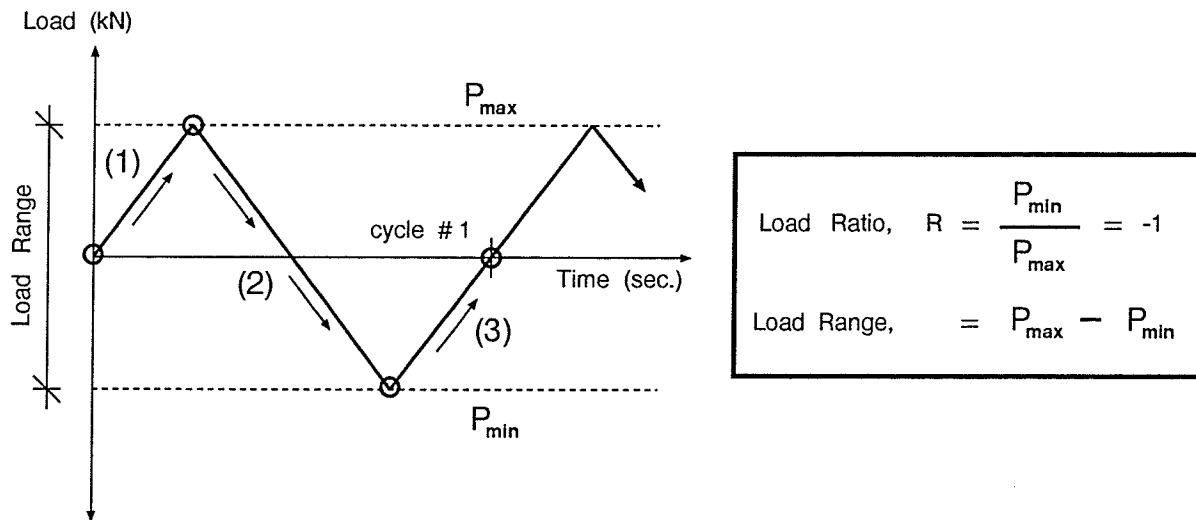
Figure 5.3: Loading Cycle and Load Steps.
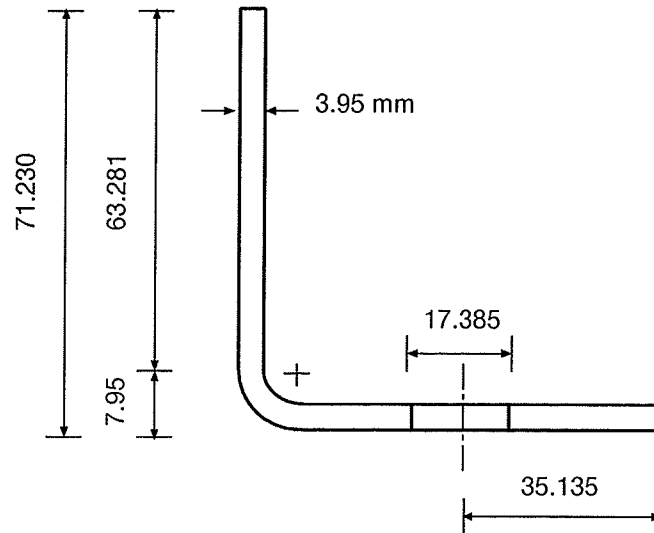
BA - section

Material Properties

$E = 212000$ MPa

$F_y = 434$ MPa

$F_u = 526$ MPa

$\mu = 0.26$

Figure 5.4: Average Cross Sectional Dimensions of the Finite Element Model
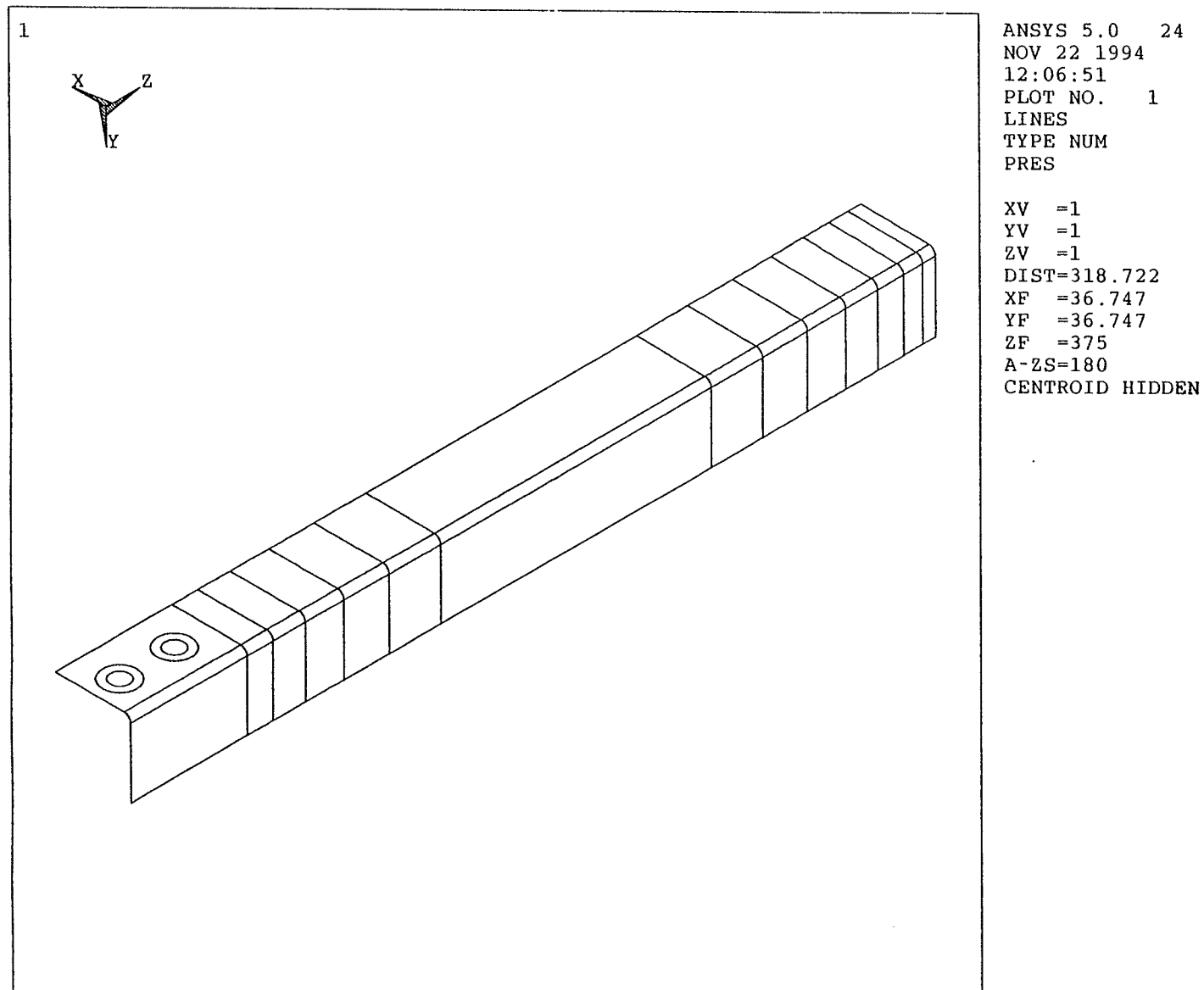
Figure 5.5 :   Discretizing the Finite Element Model into 45 Areas.

ANSYS 5.0   24
NOV 22 1994
12:07:47
PLOT NO.   2
ELEMENTS
TYPE NUM
PRES

XV   =1
YV   =1
ZV   =1
DIST=318.722
XF   =36.747
YF   =36.747
ZF   =375
A-ZS=180
CENTROID HIDDEN
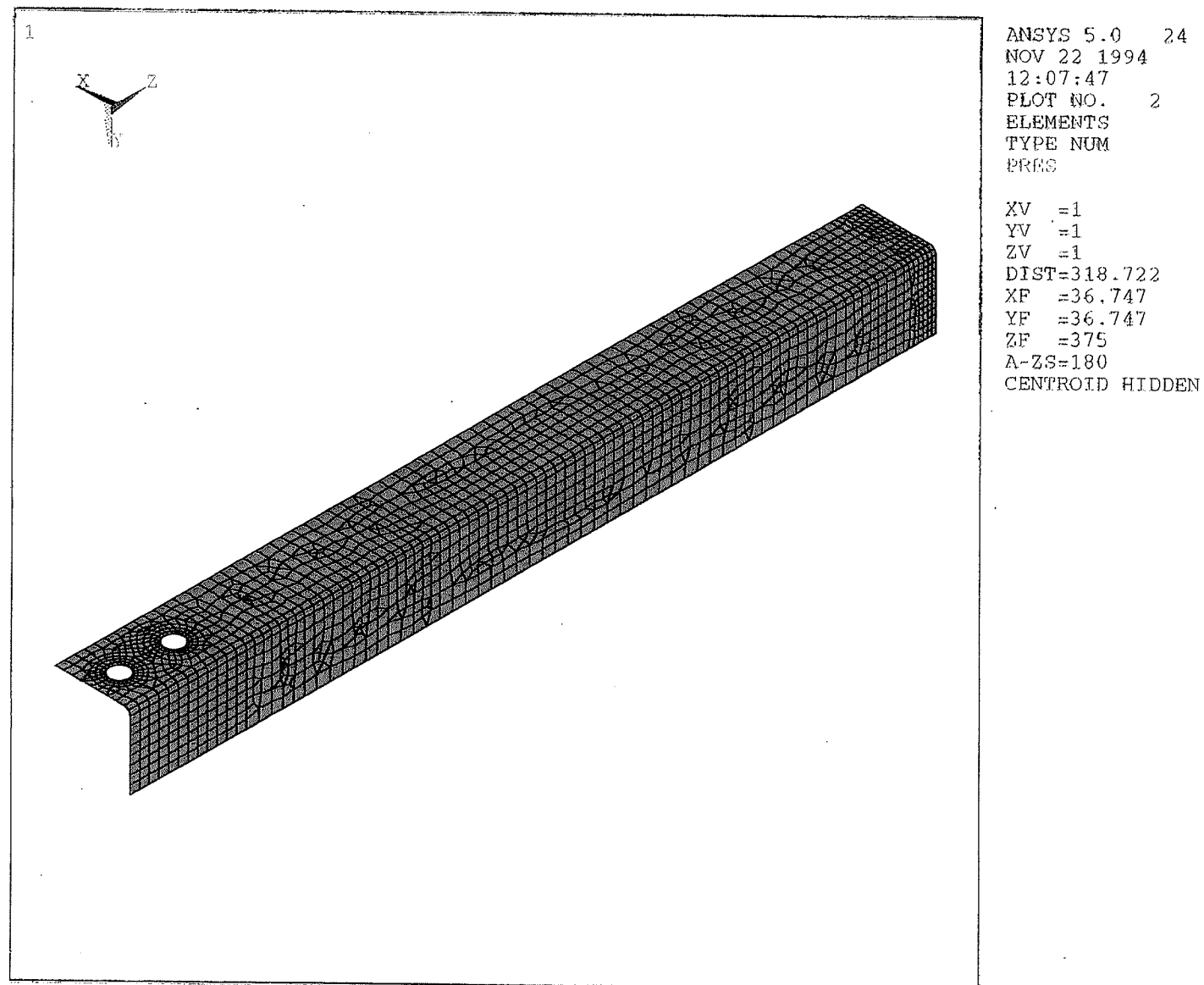
Figure 5.6:   Finite Element Mesh for the 90°-angle Member.
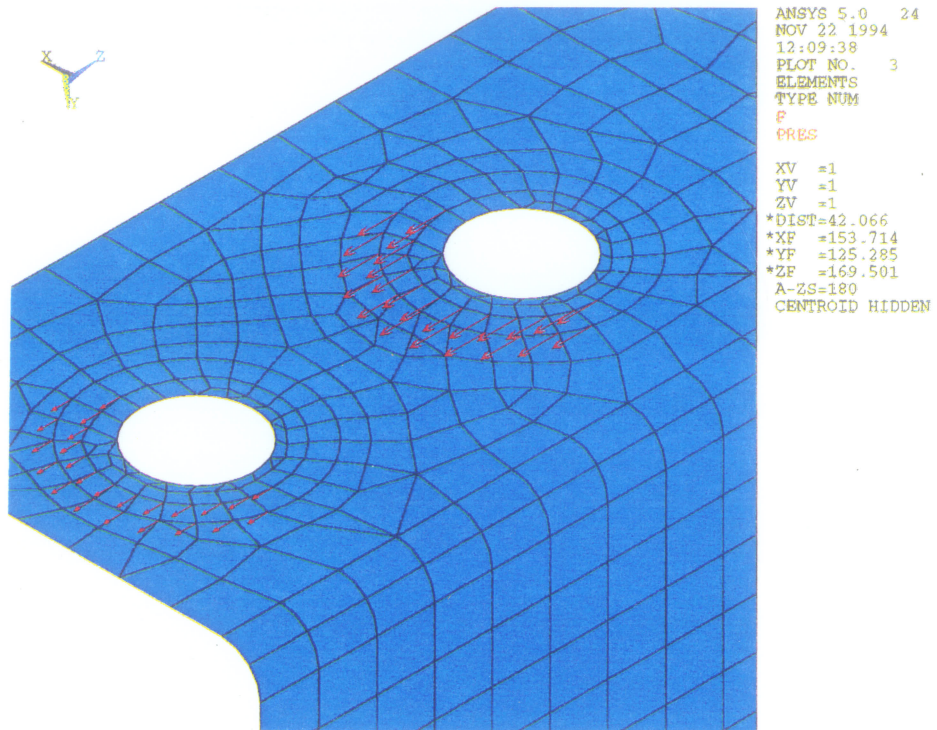
(a)   Tension Cycle.
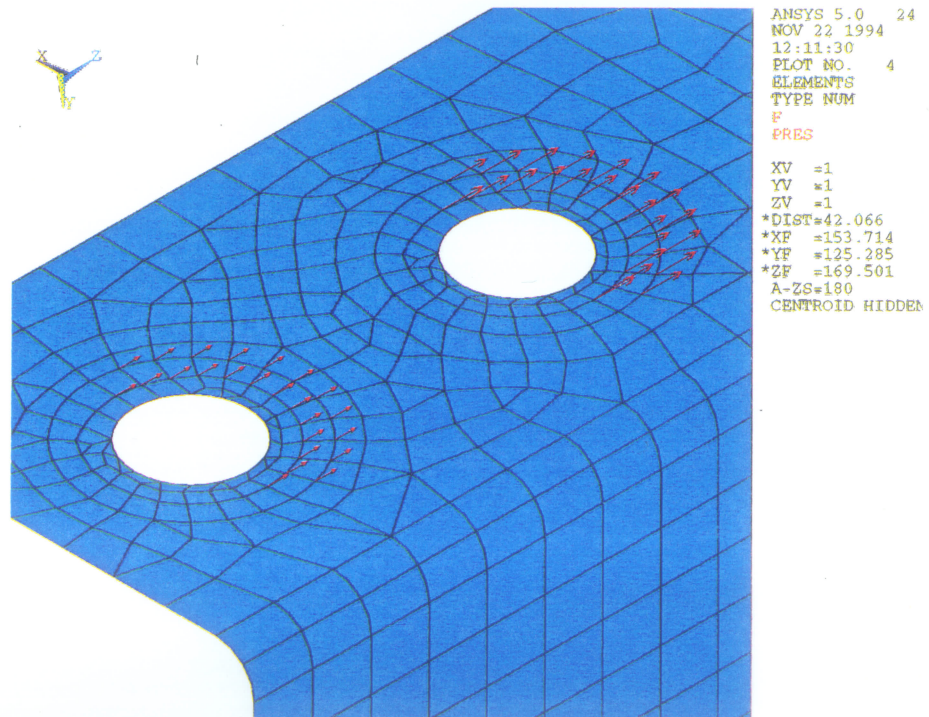
(b)   Compression Cycle.

Figure 5.7: Longitudinal Loads Applied to the Finite Element Model.

ANSYS 5.0   24
NOV 22 1994
12:14:05
PLOT NO.   5
DISPLACEMENT
STEP=2
SUB =4
TIME=0.75
RSYS=0
DMX =19.963
PRES

*DSCA=4
XV =1
YV =1
ZV =1
DIST=333.545
XF =19.118
YF =53.598
ZF =374.156
A-ZS=180
CENTROID HIDDEN
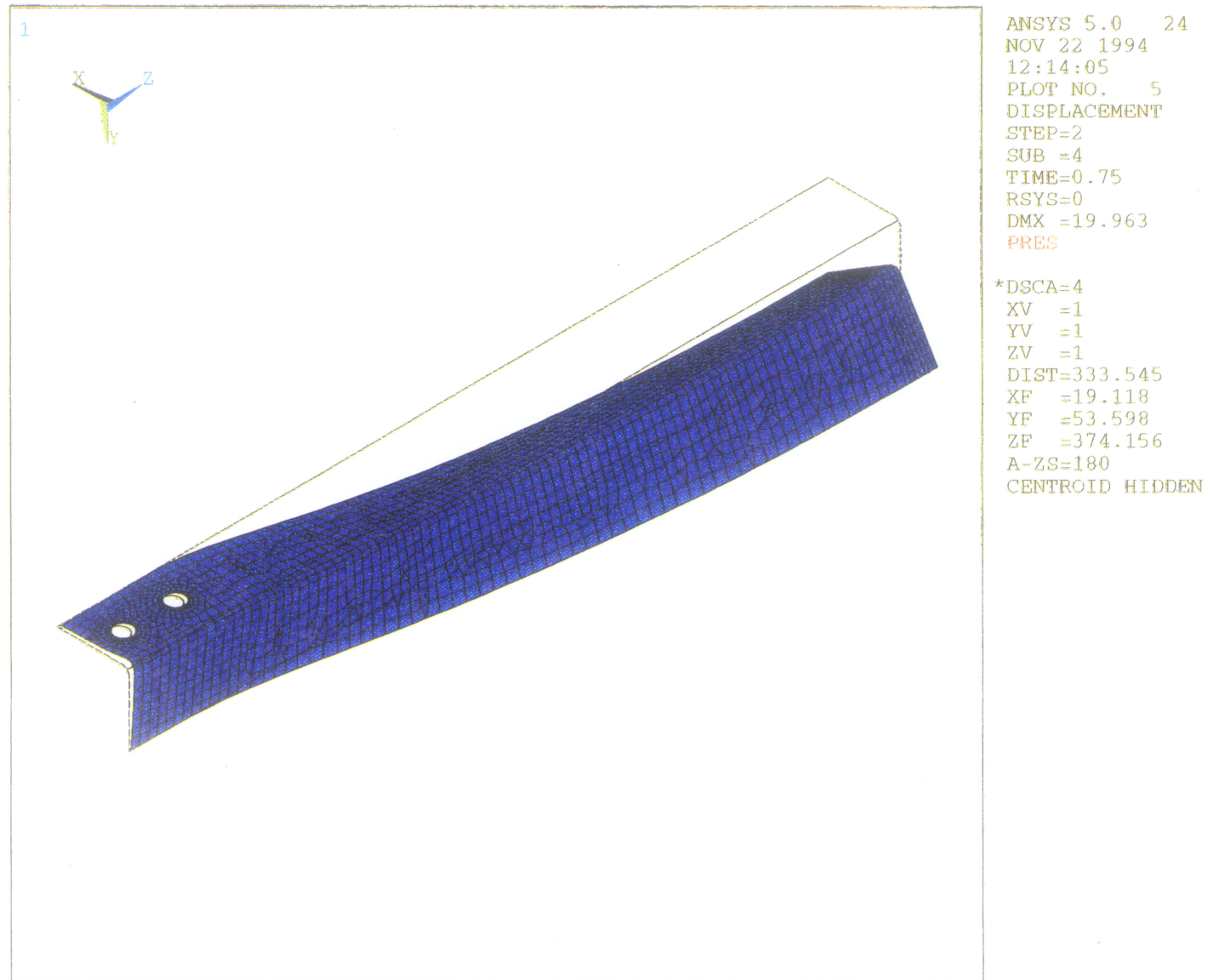
Figure 5.8:   Deformed Configuration of the Finite Element Model in a Compression Cycle.
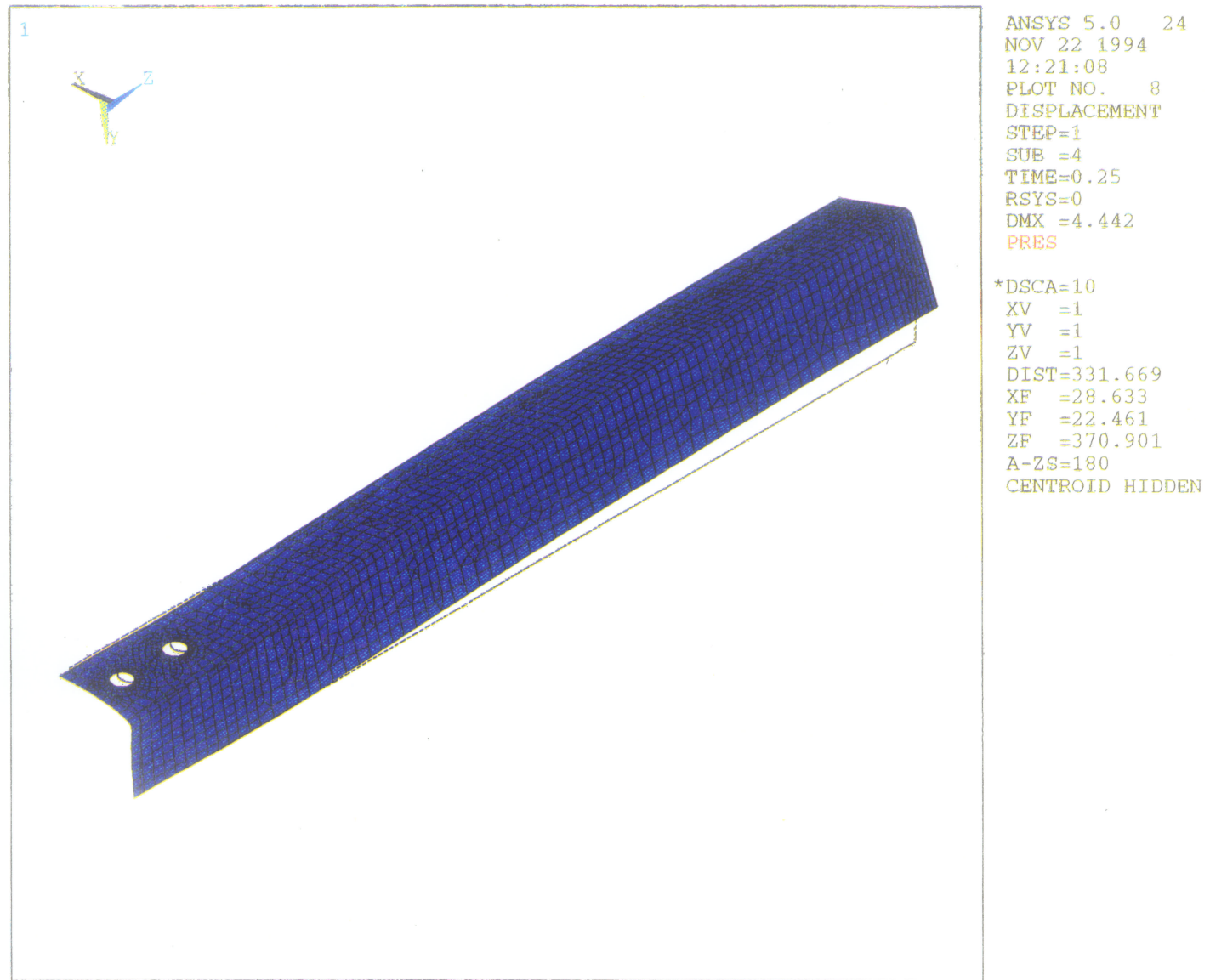
Figure 5.9: Deformed Configuration of the Finite Element Model in a Tension Cycle.
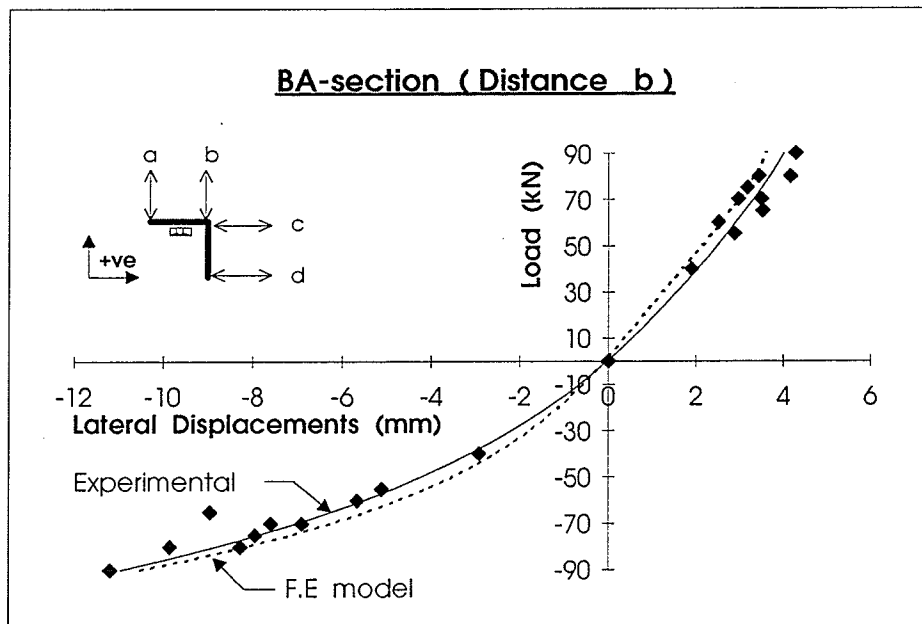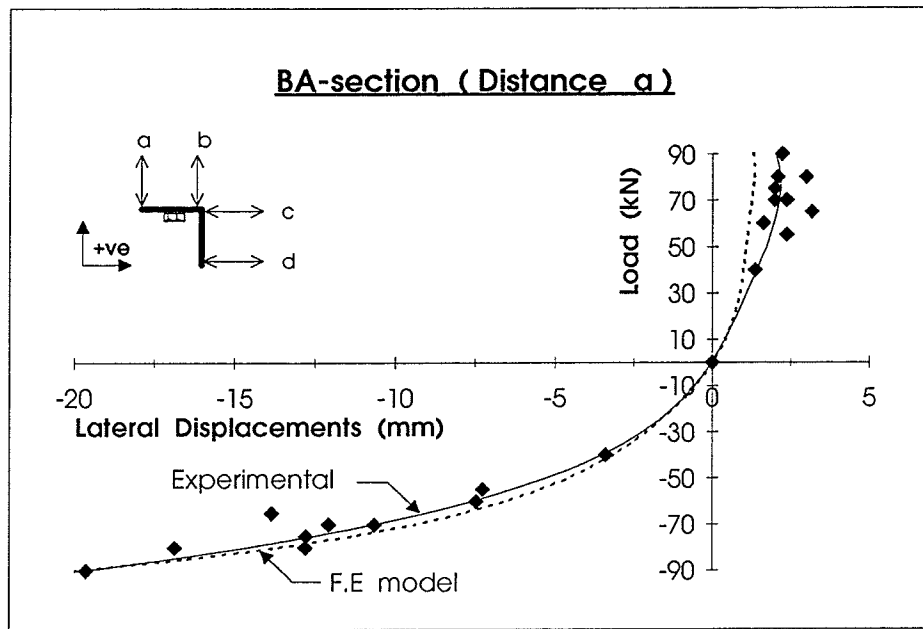
Figure 5.10: Lateral Mid-Height Translations for the Connected Leg of the 90°-angle Section.

272

Global X

Global Y

c

a

b

Tension Cycle

d

c

a

b

Compression Cycle

d
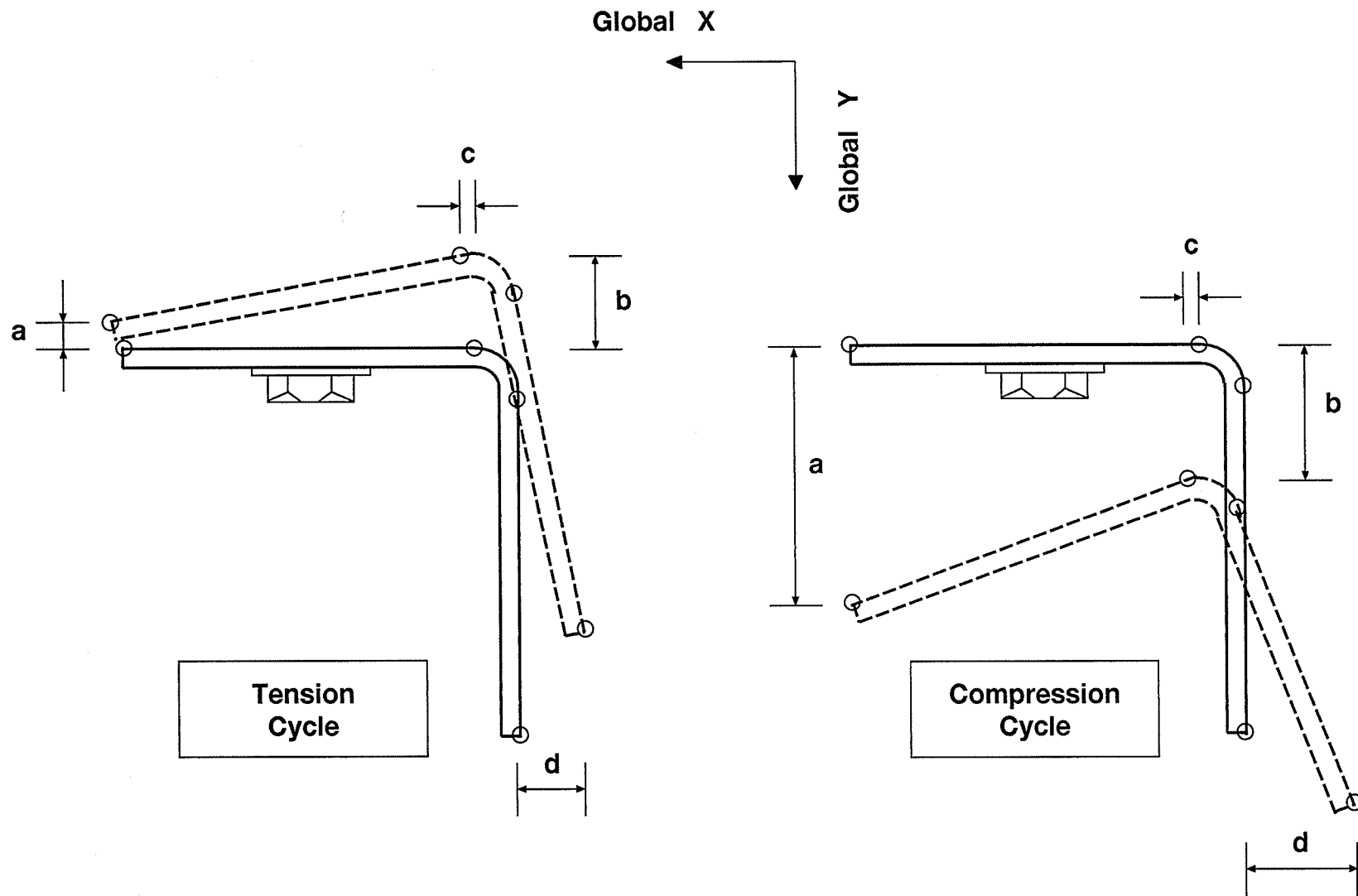
Figure 5.11: Mid-Height Translations in Tension and Compression Cycles.
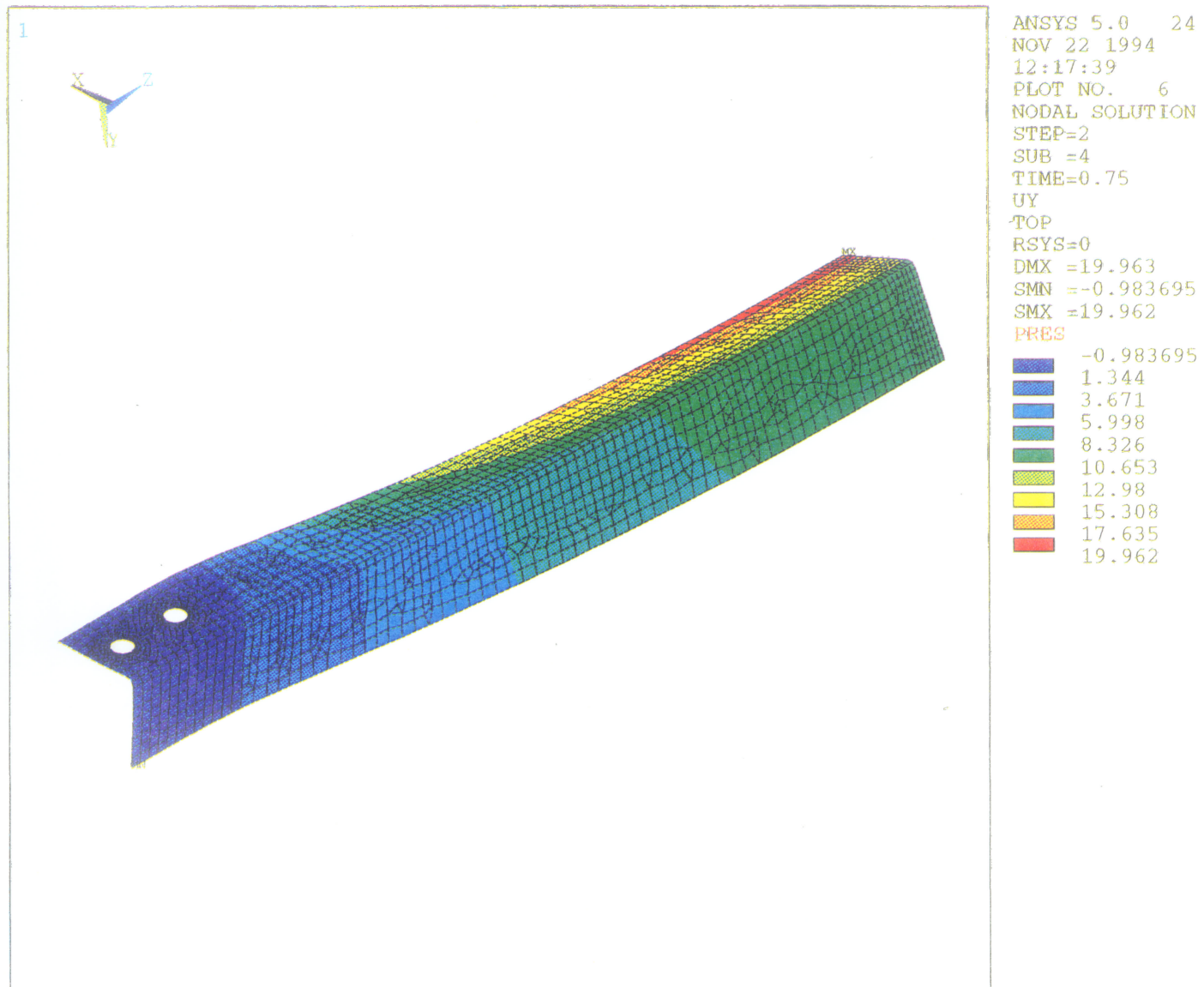
Figure 5.12 : Translations in the Global Y Direction (Compression Cycle).
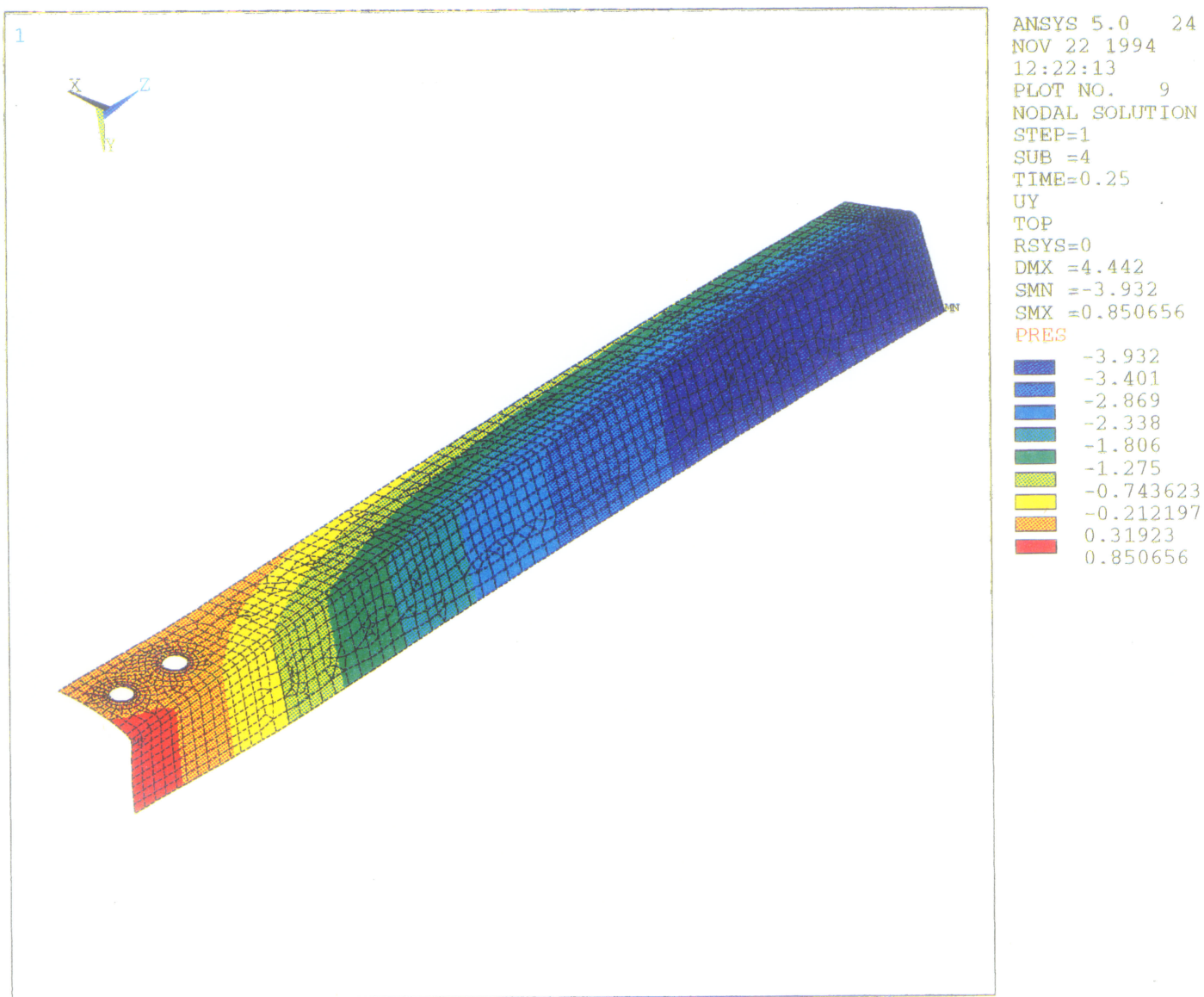
Figure 5.13 : Translations in the Global Y Direction (Tension Cycle).
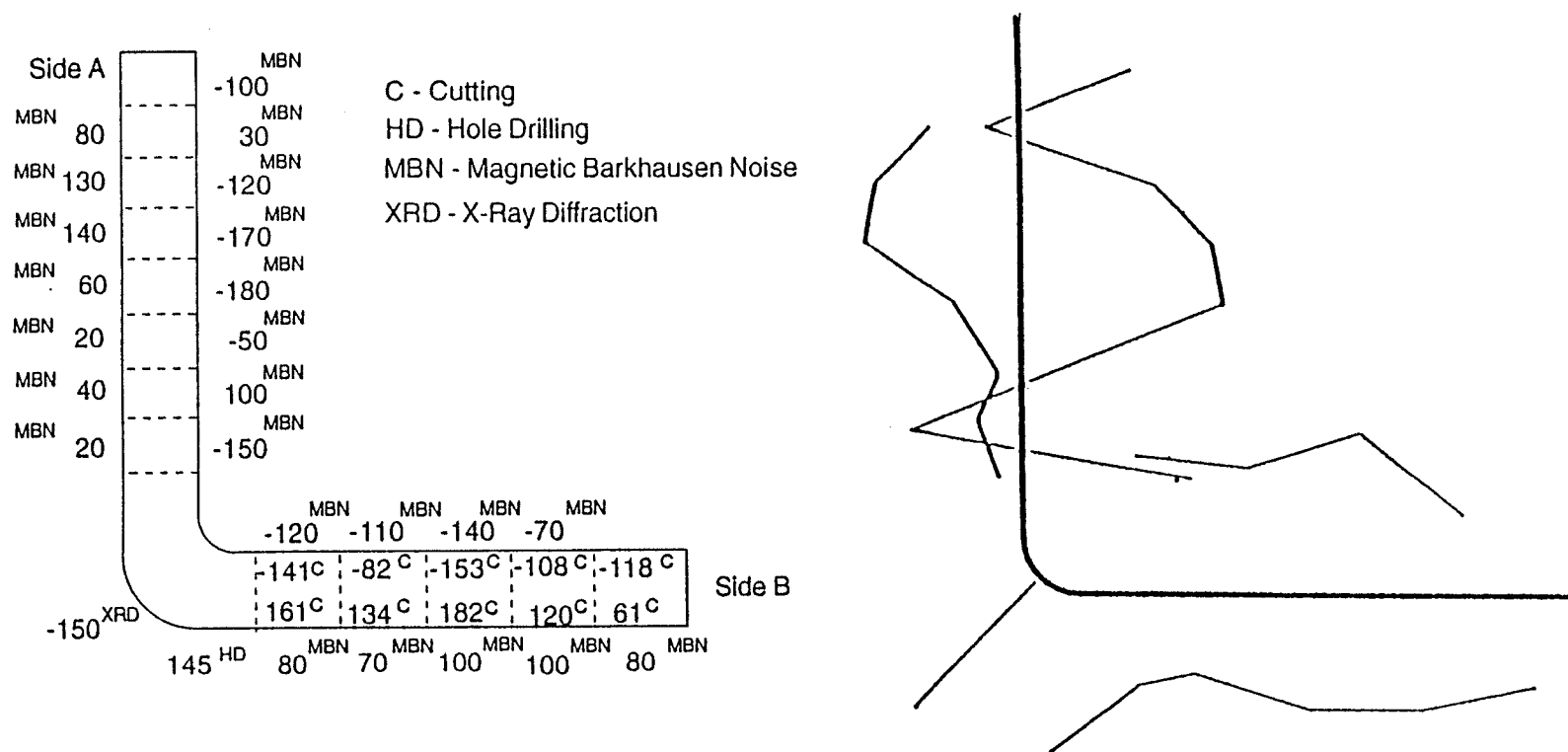
Figure 5.14 : Surface Residual Stresses in the Longitudinal Direction of the 90°-angle Section (Steel Type ASTM A715 Grade 60).

Global X

Global Y

(+)

(+)

(-)

(-)

(+)

(a) Tension Cycle.

(b) Compression Cycle.
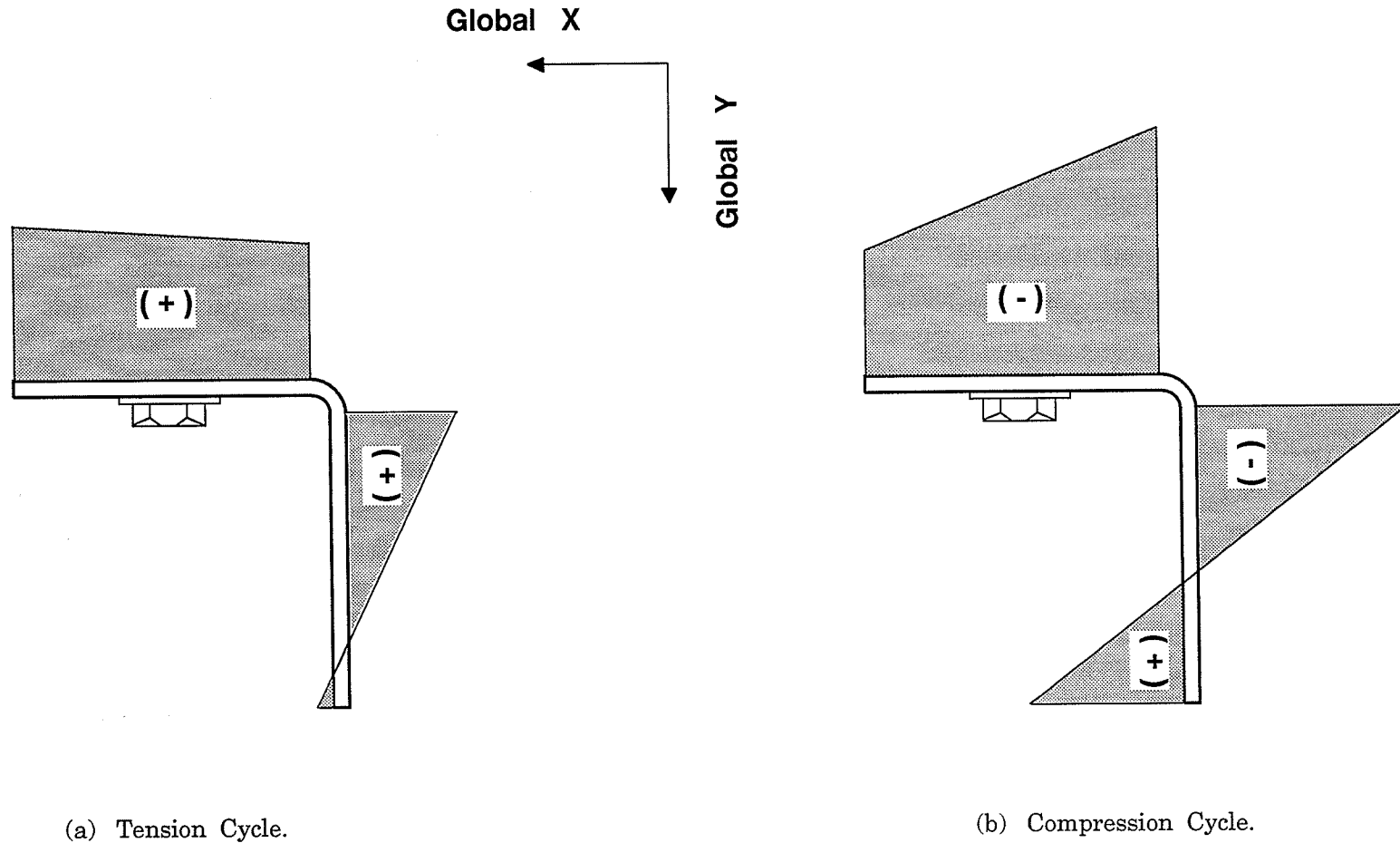
Figure 5.15 : Stress Distribution at the Mid-Height Section.
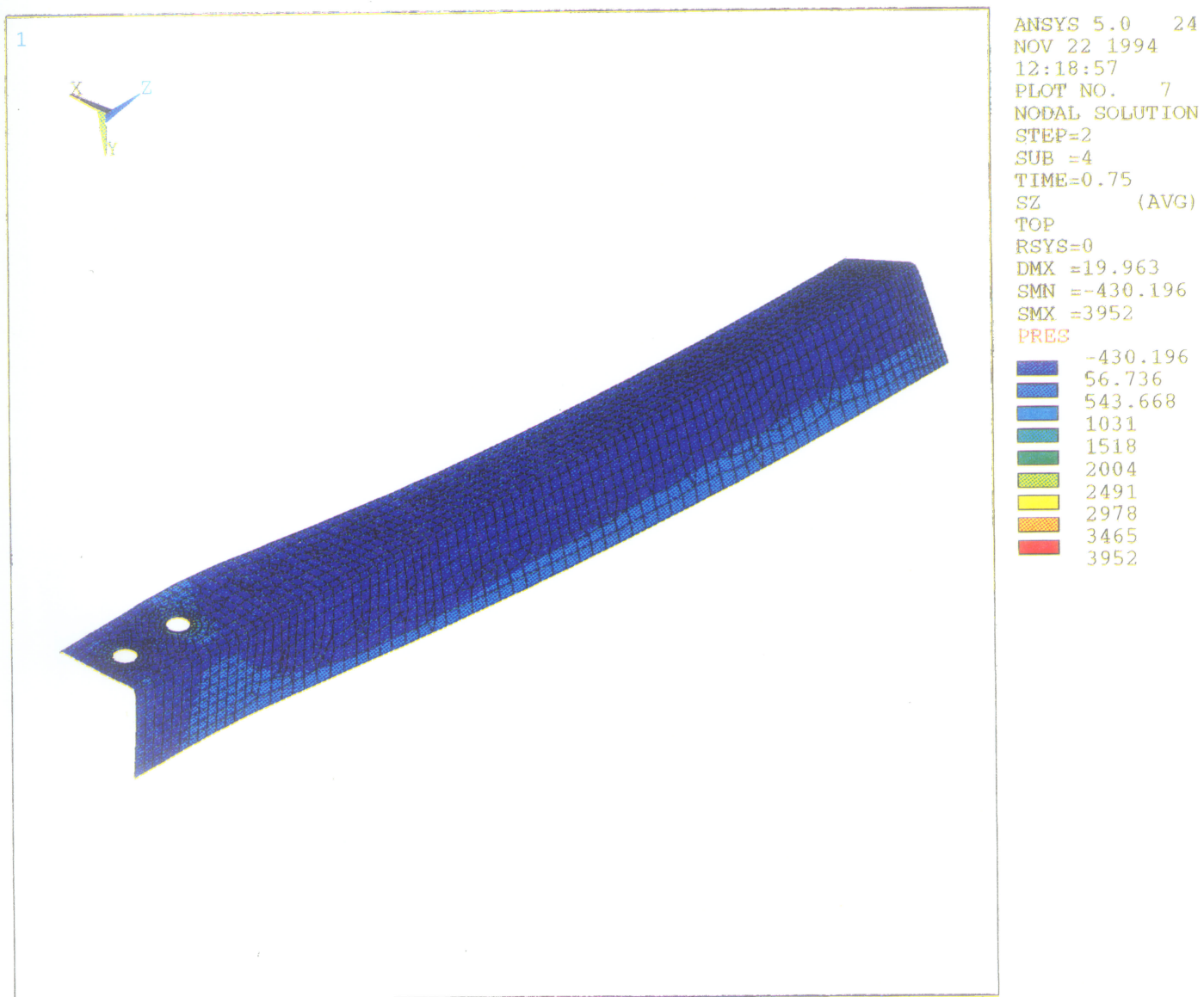
Figure 5.16 : Stress Contours in the Longitudinal Direction.
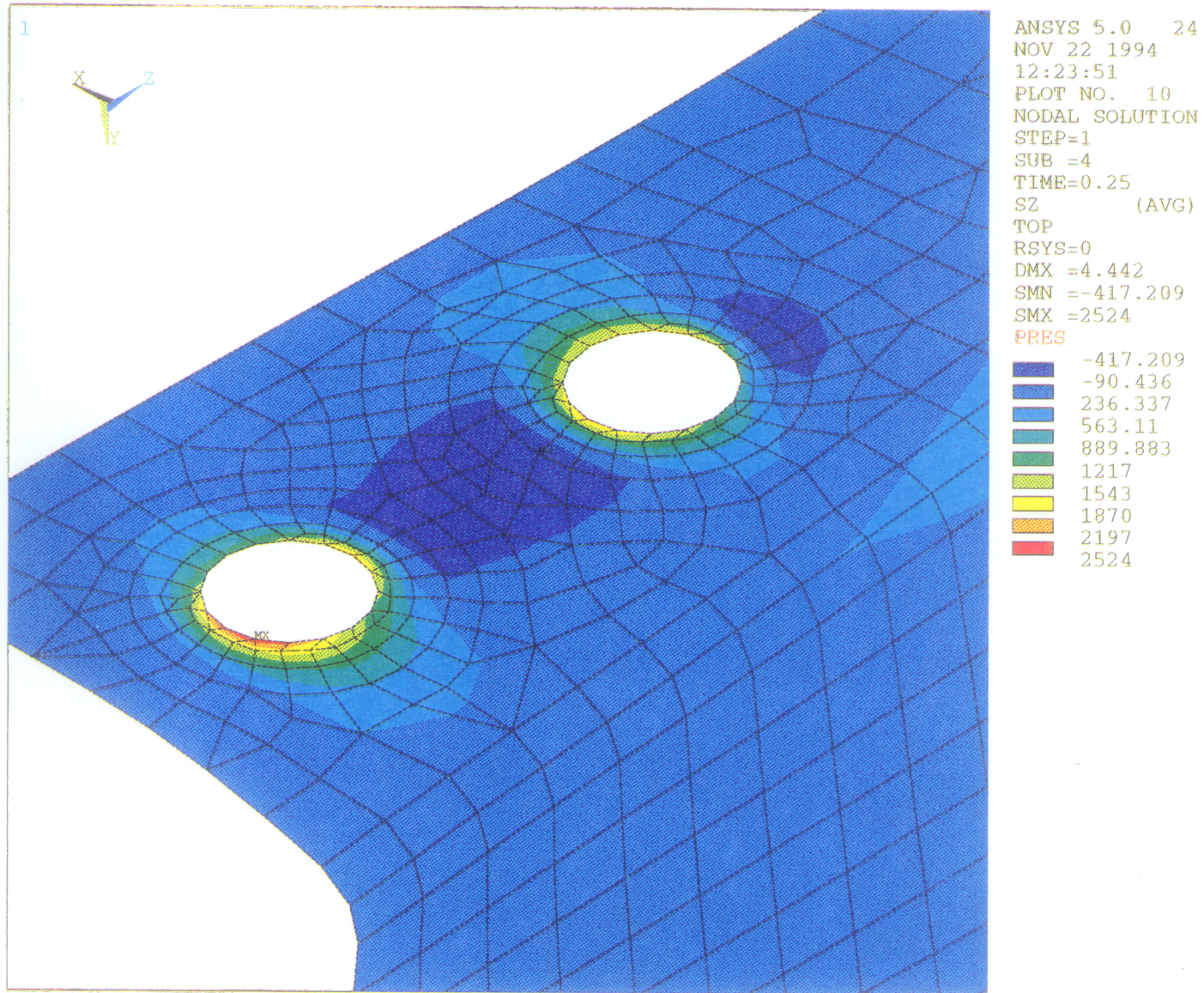
Figure 5.17 : Longitudinal Stress Contours at the End Hole Zone.
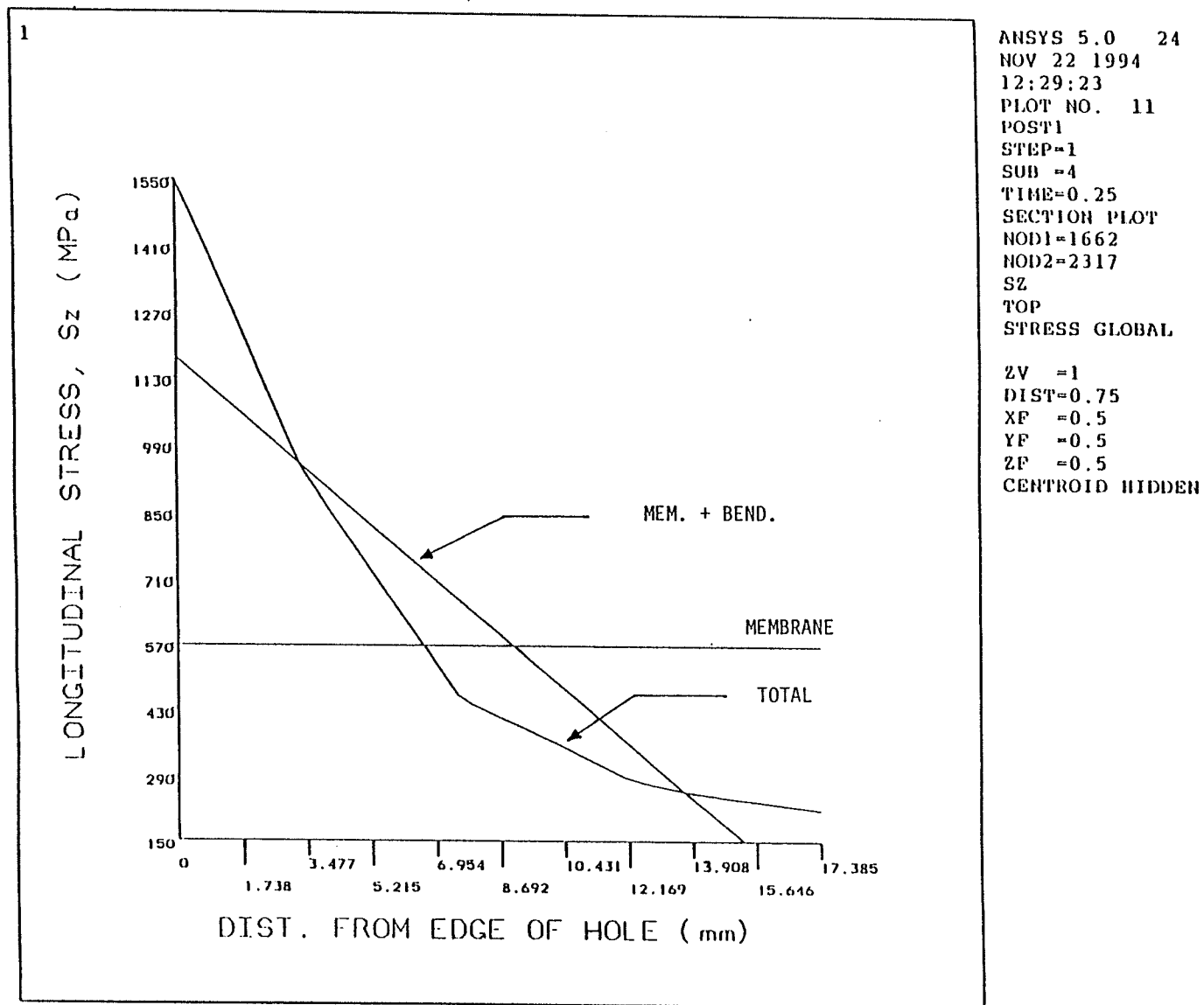
Figure 5.18 : Stress Concentration at the End Hole Zone of the 90°-angle Member.
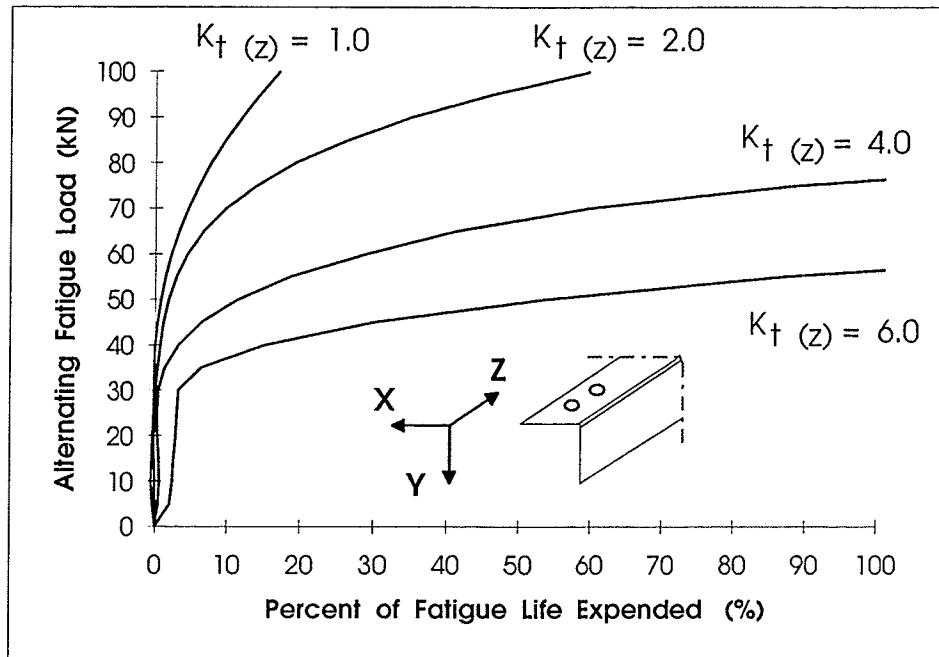
(a) Stress Concentration Factors in the Longitudinal Direction.
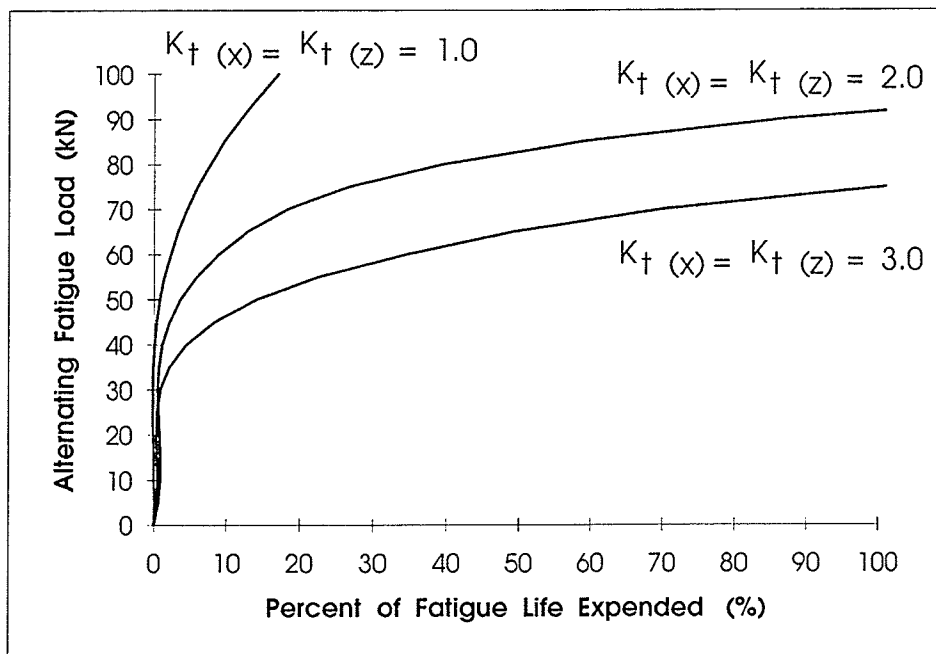
(b) Stress Concentration Factors in both Longitudinal and Transverse Directions.

Figure 5.19: Predicted Cumulative Fatigue Damage Curves.

CHAPTER 6

Conclusions and Recommendations

6.1   General

The conclusions in this chapter are based on the evaluation of the test data

for 52 full-size cold-formed steel members tested under constant amplitude axial

fatigue loads.

1. The stress range was the dominant stress variable influencing the fatigue

   behaviour of cold-formed steel sections tested during this study. Other stress

   variables, such as minimum stress, maximum stress, and the stress ratio did

   not appear to have a significant effect on the sections.

2. Most failures occurred at the extremity of the end hole of the tested specimens.

   However, the 60°-angle section (BC) witnessed several gross section failures.

   In addition, at high stress range levels, a limited number of block-shear failures

were observed for the 90°-angle section (BA) connected through a single leg.

3. For each test series, a log-log linear relationship between the stress range and the number of cycles was given. Moreover, similar relationships were defined for the alternating fatigue loads and the total fatigue life for different cross sectional shapes, temperatures, and type of steel involved in this study.

4. The log-transformation of both the S-N and the Load-N curves resulted in a normal distribution of the test data at all levels of stress range and load.

5. The mean regression line for S-N curves of steel type ASTM-A715 Grade 60 had an average negative slope of approximately 4.5. The corresponding value for steel type CAN/CSA-G40.21-M 300W was 3.61.

6.2   Crack Initiation and Growth

1. Initiation and growth of fatigue cracks were observed to occur in areas subjected to high tensile stress range caused by the presence of initial flaws or discontinuities. These specified locations were characterized by the presence of high stress concentrations which provided a favourable condition for crack growth.

2. Fatigue cracks were observed in both tension and compression cycles. However, the continued progressive crack growth was only pronounced in tension cycles.

3. Fatigue cracks causing net section failure initiated at one or more points in the stress concentration zone surrounding the end hole of the specimen. These cracks propagated in a direction perpendicular to the principal tensile stresses at that particular location.

4. As the fatigue crack grew out of the stress concentration zone, a noticeable change in its direction was observed. This was attributed to the change in the direction of principal tensile stresses between the region of high stress concentration (end hole zone), and the surrounding region.

5. For the 60°-angle section (BC), gross section failures were observed to occur at a horizontal plane 60 mm apart from the mid-height section of the member. These cracks originated from a stress concentration spot caused by the presence of an engraved letter at the back side of one leg.

6.3   Cyclic Behaviour

1. Cycle-dependent softening was observed for all tested specimens, that was evidenced by the exponential increase of strains and the formation of large irrecoverable plastic strains.

2. Fatigue tests performed at a temperature of -50°C indicated that crack initiation process covered almost the entire low temperature fatigue life. Fractures associated with very short crack sizes were attributed to large reductions in fracture toughness and ductility associated with low temperatures.

3. In comparing the hysteresis behaviour (load-stroke curves) of singly symmetric sections connected through both legs to corresponding specimens connected through one leg, it was observed that the average increase in stiffness was 29% for the 90°-angle section (BA), 26% for the 60°-angle section (BC), and 13% for the lipped angle section (BB).

4. Connecting singly symmetric sections through both legs significantly reduced the recorded lateral translations at the mid-height section of the members. Such reductions were highly pronounced in compression cycles.

6.4   Fatigue Strength Curves

- **BA, BC, and BB sections tested at 25°C (one leg connected)**

1. In comparing the fatigue performance of the sections, it was observed that for a given number of cycles, the 90°-angle section (BA) can withstand 4.5% higher stress range than the 60°-angle section (BC) and 30% higher than the lipped angle section (BB).

2. Considering alternating fatigue loads, the lipped angle section (BB) sustained 36% higher load than the 60°-angle section (BC), and 60% higher than the 90°-angle section (BA).

- **BA, BC, and BB sections tested at 25°C (both legs connected)**

1. Better fatigue performance was observed for the sections connected through both legs compared to similar specimens connected only through one leg. For a given number of cycles, the average increase of stress range was 25% for the 90°-angle section (BA), 15% for the 60°-angle section (BC), and 12% for the lipped angle section (BB).

2. Except for the 60°-angle section (BC) which witnessed some gross section failures, a significant increase in the fatigue strength of the 90°-angle (BA), and the lipped angle (BB) sections was noticed at long fatigue lives.

- **T-shaped section (BG) tested at 25°C**

1. The S-N curve for the section had approximately the same negative slope value as the 90°-angle section (BA) connected through one leg. However, for a given number of cycles, the fatigue strength was 5% lower than that of the BA-section connected through one leg.

2. The fatigue limit for the section was obtained by extrapolating the log-log relationships to the level of $N = 10^6$ cycles. Stress range and the corresponding alternating fatigue load at that limit were 276 MPa and $\pm$ 131 kN.

- **Back-to-back channel sections**
  BN and HBN sections at 25°C, and HBN section at -50°C

1. Difference in steel types of BN and HBN sections resulted in a noticeable change of slopes for both S-N and Load-N curves for these groups.

2. Fatigue tests performed on HBN sections at a temperature of $-50°C$ showed 11.5% increase in the stress range level compared to similar specimens tested at room temperature.

6.5   Finite Element Analysis

1. Computed strains and translations based on the finite element analysis were found to be in good agreement with those recorded in the experimental program.

2. Stress concentration factors obtained from the finite element stress analysis ranged from 2.8 to 6.0. These factors were computed at the discontinuity region (end hole zone).

6.6 Recommendations

In the present study, the proposed recommendations could be classified into two parts: (1) general design recommendations for the purpose of establishing fatigue design provisions for cold-formed steel sections, and improving the present situation in the field, and (2) recommendations for future research.

6.6.1 General design recommendations

Although all design details have not been evaluated during the study, the basic framework has been developed and the critical design parameters have been defined. Based on the analysis and evaluation of the test data, the following recommendations are made:

1. Design criteria are recommended on the basis of fatigue life and stress range. Table 4.9 gives the exponential model relating stress range to cycle life for the various cross sections involved in the investigation.

2. It is recommended that fatigue design curves be based on the lower confidence limit obtained from statistical analysis of the test results. This provides a rational means of selecting stress values and takes into consideration the variability of the test data and the size of the sample tested.

288

3. In order to perform a least-square regression analysis for the fatigue test data, the ASTM Committee E-9 on fatigue recommends at least four replicates at each stress range level. Furthermore, due to the considerable scatter of the fatigue test data, it appears reasonable to recommend a log-normal distribution of fatigue life at a given stress range level.

4. Although wind loads are of dynamic nature, however, enormous identifiable methods are available for predicting fatigue lives under non-uniform load cycles. For fatigue damage calculations, it is recommended to use the linear rule of Palmgren and Miner. Inspite of the known tendency of the rule to overestimate the fatigue life, it is still used extensively, first, on account of its simplicity, and secondly, because more sophisticated techniques of fatigue life prediction are not generally applicable to all types of service loading.

5. For the purpose of providing a universal picture for the fatigue behaviour of cold-formed steel members, axial fatigue tests are recommended to be performed on test coupons for various grades of cold-formed steel for identifying the material fatigue properties. These properties include fatigue strength and ductility coefficients (σ_f' and ϵ_f'), and the strain hardening exponent (n^*) of the material.

6. A stress analysis is essential for determining accurate values of the stress concentration factors at the region of discontinuity. Coupling these factors

with Palmgren-Miner's rule for cumulative damage would yield reasonable fatigue life estimates for the specimen under consideration.

7. Field measurements on existing transmission towers are highly recommended to obtain a realistic figure of the number of alternating wind applications acting on tower members. In addition, field measurements of nominal stresses should be available. These recorded stresses should be far enough from a critical detail or surface irregularity in order to eliminate the effect of local stress concentrations.

8. In transmission tower structures, when bolted connections are required, high strength bolts should be used for connecting cold-formed steel members subject to the possibility of repeated cyclic loads in order to ensure slip-resistant connections. The Turn-of-Nut-Tightening method is recommended as it provides more uniform tension in the bolts than does torque-controlled methods.

9. For welded connections, due care must be given to ensure that all fillet welds be made by automatic submerged-arc process if possible. Stop-start welding positions should be avoided. Any defects that are visually apparent should be identified and rewelded.

10. Since most fatigue cracks initiate at the surface, therefore, surface treatments and manufacturing effects are of significant importance in the design process.

6.6.2 Recommendations for future research

The work presented herein investigated the fatigue performance of a wide range of cold-formed steel sections used for constructing transmission towers. However, except for a limited number of specimens, the experimental program did not include repetition of test data at the same stress range level. This was mainly due to financial constraints and the costly process of testing full-scale members under fatigue loads. Consequently, further tests on other cross sectional shapes are recommended in order to make more definitive conclusions about the variables examined. Fields of future research suggested by the present study are as follows:

1. Studies are needed to compare and contrast the fatigue strength of cold-formed steel members when punched holes (rather than drilled holes) are used for bolted connections.

2. Time dependent environmental effects are of prime importance in considering fatigue failures. As such, research would be desirable to establish fatigue strength relationships for cold-formed steel members tested in a corrosive environment.

3. Research on the effect of variable-amplitude loading on the fatigue performance of cold-formed steel sections is recommended. In that regard, load histories with and without sequence effect need to be investigated.

4. Additional work is needed to incorporate the effect of mean stresses on the fatigue behaviour of the sections. Investigating the influence of the tensile mean stress on the long-life fatigue strength of cold-formed steel members is highly recommended.

5. Since fatigue properties are very sensitive to surface conditions, future studies are required to investigate the effect surface roughness or other stress raisers at the surface on the fatigue strength of test coupons extracted from various grades of cold-formed steel material.

REFERENCES

AASHTO Specifications (1989). *"AASHTO Standard Specifications for High-way Bridges,"* American Association of State Highway and Transportation Officials, 14th Edition.

Abdel-Rahim, A.B., and Polyzois, D. (1994). *"Effect of Galvanizing, Cold-Forming and Subfreezing Temperature on the Mechanical Properties of Cold-Formed Steel,"* CSCE Proceedings, Annual Conference, June 1994, Winnipeg, Manitoba, pp. 157-166.

Abdel-Rahim, A.B. (1993). *"Effect of Galvanizing, Cold-Forming and Subfreezing Temperature on the Mechanical Properties of Cold-Formed Steel,"* Technical Report, Department of Civil and Geological Engineering, The University of Manitoba, Winnipeg, Manitoba, Canada.

Adluri, S.M.R., Madugula, M.K.S., and Monforton, G.R. (1991). *"Finite Element Failure Analysis of Schifflerized Angles,"* Journal of Computer and Structures, Vol. 41, No. 5, pp. 1087-1093.

AISI Specifications (1991). *"Cold-Formed Steel Design Manual."* American Iron and Steel Institute, Washington, D.C.

Albrecht, C.O. (1962). *"Statistical Evaluation of a Limited Number of Fatigue Test Specimens, Including a Factor of Safety Approach,"* Symposium on Fatigue

of Aircraft Structures, ASTM, STP No. 338.

American Hot Dip Galvanizing Association and Zinc Institute, (AGA, 1986). *"The Design and Fabrication of Galvanized Products,"* Manual.

American Society for Testing and Materials (1987). *ASTM E 290-87 Standard Test Method for Semi-Guided Bend Test for Ductility of Metallic Materials,"* Philadelphia.

American Society for Testing and Materials (1991). *"ASTM E 23-91 Notched Bar Impact Testing of Metallic Materials,"* Philadelphia.

ANSI/ASCE 10-90 (1992). *"Design of Latticed Steel Transmission Structures,"* ASCE, New York, New York.

ASME Boiler and Pressure Vessel Code. (1989). *"An American National Standard,"* The American Society of Mechanical Engineers, New York N.Y.

Baker, K.A., and Kulak, G.L. (1984). *"Fatigue Strength of a Groove Weld on Steel Backing,"* Canadian Journal of Civil Engineering, Vol. 11, pp. 692-700.

Bannantine, J.A., Comer, J.J., and Handrock, J.L. (1990). *"Fundamentals of Metal Fatigue Analysis,"* Prentice Hall, Englewood Cliffs, New Jersey.

Berger, P. (1982). *"Fatigue Testing of Welded Beams,"* Proceedings IABSE Colloquium - Lausanne, Fatigue of Steel and Concrete Structures, pp. 323-330.

Boone, W.D., and Wishart, H.B. (1935). *"High Speed Fatigue Tests of Several Ferrous and Non-Ferrous Metals at Low Temperatures,"* Proceedings ASTM, Vol. 35, pp. 147-152.

Boyer, H.E. (Editor), (1986). *"Atlas of Fatigue Curves,"* American Society of Metals, Metals Park, Ohio.

CAN/CSA-S136-M94 (1995). *"Cold Formed Steel Structural Members,"* Canadian Standards Association, Rexdale, Ontario.

CAN/CSA-S16.1-M94, (1995). *"Steel Structures for Building - Limit States Design,"* Canadian Standards Association, Rexdale, Ontario.

CAN/CSA-S37-M94 (1995). *"Antennas, Towers, and Antenna-Supporting Structures,"* Canadian Standards Association, Rexdale, Ontario.

Catenacci, A., Finzi, M., and Zavelani, R.A. (1989). *"New Outlines for 500-kV Transmission Towers Using Cold-Formed Shapes: The Experimental Line of the American Electric Power Research Institute,"* ASCE Proceedings, Seventh Structures Congress, San Fransisco, California, pp. 278-287.

CEA Report 340 T 844 (1994). *"Use of Cold-Formed Steel Sections for Transmission Towers in Canada,"* Canadian Electrical Association, Montreal, Quebec.

Chuenmei, Guo. (1984). *"Elastoplastic Buckling of Single Angle Columns,"* Journal of Structural Engineering, ASCE, Vol. 110, pp. 1391-1395.

Comeau, M.P., and Kulak, G.L. (1979). "*Fatigue Strength of Welded Steel Elements,*" Technical Report 79, University of Alberta, Edmonton, Alberta.

Davenport, A.G. (1961). "*The Application of Statistical Concepts to the Wind Loading of Structures,*" Proceedings, Institution of Civil Engineers, London, Vol. 19, pp. 449-471.

Davenport, A.G. (1962). "*The Response of Slender Line-Like Structures to a Gusty Wind,*" Proceedings, Institution of Civil Engineers, London, Vol. 23, pp. 389-408.

Davenport, A.G. (1967). "*Gust Loading Factors,*" Journal of Struct. Div., ASCE, Vol. 93, No. ST3, June 1967, pp. 11-34.

Dionne, M., and Davenport, A.G. (1988). "*A Simple Relationship Between the Gust Response Factor and Fatigue Damage,*" Journal of Wind Engineering and Industrial Aerodynamics, Vol. 30, pp. 45-54.

ECCS Recommendations (1985). "*Recommendations for the Fatigue Design of Structures,*" Committee TC6 Fatigue, First Edition, European Convention for Constructional Steelwork.

European Convention for Constructional Steelwork (1985). "*Recommendations for Angles in Lattice Transmission Towers,*" ECCS - Technical Committee

8 - Structural Stability Technical Working Group 8.1 - Components, First Edition 1985, No. 39, Brussels, Belgium.

Federal Aviation Agency (1959). *"Civil Aeronautics Manual No. 6,"* Appendix A, Supt. of Documents, Whashington, D.C.

Fisher, J.W., Frank, K.H., Hirt, M.A., and McNamee, B.M. (1970). *"Effects of Weldments on the Fatigue Strength of Steel Beams,"* National Cooperative Highway Research Program Report 102, Transportation Research Board, National Academy of Sciences, Washington, D.C.

Fisher, J.W., Albrecht, P.A., Yen. B.T., Klingerman, D.J., and McNamee, B.M. (1974). *"Fatigue Strength of Steel Beams With Welded Stiffeners and Attachments,"* National Cooperative Highway Research Program Report 147, Transportation Research Board, National Academy of Sciences, Washington, D.C.

Fisher, J.W. (1974). *"Guide to 1974 AASHTO Fatigue Specifications,"* AISC, New York, N.Y.

Fisher, J.W., Jin, J., Wagner, D.C., and Yen, B.T. (1990). *"Distortion-Induced Fatigue Cracking in Steel Bridges,"* National Cooperative Highway Research Program Report 336, Transportation Research Board, National Academy of Sciences, Washington, D.C.

Forrest, P.G. (1963). *"Fatigue of Metals,"* Pergamon Press, Elmsford, New York.

Fuchs, H.O., and R.I. Stephens, R.I. (1980). *"Metal Fatigue in Engineering,"* Wiley-Interscience, Newyork.

Gidlund, J.I., Pettersson, A.R., Ruritz, R., Soderberg, L., and Jansson, R. (1988). *"Swedish State Power Board Adopts the T-Tower Design for 420-kV Lines,"* Vattenfall, Stockholm, Sweden.

Goel, A.P. (1994). *"Fatigue Problems in Power Transmission Lines,"* Canadian Civil Engineer, CSCE, February 1994, pp. 6-7.

Gough, H.J. (1924). *"The Fatigue of Metals,"* Scott, Greenwood and Son, London.

Griffith, A.A. (1920). *"The Phenomena of Rupture and Flow in Solids,"* Trans. R. Soc., Vol. A221, London, p.163.

Haaijer, G., Carskaddan, P.S., and Grubb, M.A. (1981). *"Eccentric Load Test of Angle Column Simulated with MSC/NASTRAN Finite Element Program,"* Paper Presented at the Annual Meeting of Structural Stability Research Council, Chicago, Illinois.

Haigh, B.P. (1930). *"The Relative Safety of Mild and High-Tensile Alloy Steels Under Alternating and Pulsating Stresses,"* Proceedings, Inst. Automb. Eng., Vol. 24, p.320.

Hirmatsu, K., and Akagi, H. (1988). *"The Response of Latticed Steel Towers Due to the Action of Wind,"* Journal of Wind Engineering and Industrial Aerodynamics, Vol. 30, pp. 7-16.

Hirt, M.A., and Crisinel, M. (1975). *"La Resistance à la Fatigue des Poutres en ame Pleine Composées - soudées: Effect des Plaquettes et Groussels soudés à l'aile."* ICOM 017, Swiss Fedral Institute, Lausanne, Switzerland.

Hoppe, O. (1896). *"Alberts Versuche und Erfindungen,"* Stalbu Eisen, Vol. 16, p. 437.

Huber, H.W., and Beedle, L.S. (1954). *"Residual Stress and the Compressive Strength of Steel,"* Welding Journal, No. 33, December 1954, pp. 589-614.

Irwin, G.R. (1957). *"Analysis of Stresses and Strains Near the End of a Crack Traversing a Plate,"* Trans. ASME, Journal of Appl. Mech., Vol. 24, p.361.

Jensen, J.J., and Folkestad, G. (1984). *"Dynamic Behaviour of Transmission Towers: Field Measurements,"* Eng. Struct., Vol. 6, October 1984, pp. 288-296.

Keating, P.B., and Fisher, J.W. (1986). *"Evaluation of Fatigue Tests and Design Criteria on Welded Details,"* National Cooperative Highway Research Program Report 286, Transportation Research Board, National Academy of Sciences, Washington, D.C.

Kennedy, J.B., and Neville, A.M. (1976). *"Basic Statistical Methods for Engineers and Scientists,"* Second Edition, Harper and Row, New York, N.Y.

Kenneford, A.S., and Nichols, R.W. (1960). *"The Fatigue Properties at Low Temperatures of a Low Carbon and an Alloy Steel,"* Journal of Iron and Steel.

Klippstein, K.H. (1981). *"Fatigue Behaviour of Sheet Steel Fabrication Details,"* Soc. Automotive Engineers, Paper No. 810436.

Lambert, M.J., Ogle, M.H., and Smith, B.W. (1988). *" Investigation of Wind-Induced Fatigue in Tall Guyed Steel Masts,"* Journal of Wind Engineering and Industrial Aerodynamics, Vol. 30, pp. 55-65.

Libertini, G.Z., Topper, T.H., and Leis, B.N. (1977). *"The Effect of Large Prestrain on Fatigue,"* Experimental Mechanics, Feb. 1977.

Little, R.E., and Jebe, E.H. (1975). *"Statistical Design of Fatigue Experiments,"* Applied Science Publishers Ltd., Essex, England.

Load and Resistance Factor Design (1988). *"Specification for Structural Joints Using ASTM A325 or A490 Bolts,"* American Institute of Steel Construction (AISC), Chicago, Illinois.

LRFD Manual of Steel Construction (1993). *"Load and Resistance Factor Design,"* American Institue of Steel Construction, (AISC), Chicago, Illinois.

Mackey, S., Ko, P.K., and Lam, L.C. (1974). *"Response of a 180-ft Latticed Tower to High Winds,"* Proceedings of the Second U.S.A.- Japan Research Seminar on Wind Effects on Structures, edited by Hatsuo, I., and Arthur, N., pp. 199-207.

Maddox, S.J. (1982). *"Improving the Fatigue Lives of Fillet Welds by Shot Peening,"* Proceedings IABSE Colloquium - Lausanne, Fatigue of Steel and Concrete Structures, pp. 377-384.

Madugula, M. (1990). *"Report for the Canadian Electrical Association (CEA No. ST-340),"* University of Windsor, Windsor, Ontario.

Manson, S.S. (1962). *"Discussion of Reference by Tavernelli, J.F. and Coffin, L.F. (1962),"* Trans. ASME Journal of Basic Eng., Vol. 84, No. 4, December 1962, p.537.

Mehta, K.C. (1984). *"Wind Induced Damage Observations and their Implications For Design Practice,"* Eng. Struct., Vol. 6, October 1984, pp. 242-247.

Mikukawa, M., Jono, M., Kamato, T., and Nakano, T. (1970). *""Low Cycle Fatigue Properties of Steels at Low Temperatures,"* Proceedings 13th Jap. Congr. Mater. Res., p. 69.

Miner, A.A. (1945). *"Cumulative Damage in Fatigue,"* Trans. ASME, Journal of Appl. Mech., Vol. 67, p. A159.

Minner, H.H., and Seeger, T. (1982). *"Improvement of Fatigue Life of Welded Beams by TIG-Dressing,"* Proceedings IABSE Colloquium - Lausanne, Fatigue of Steel and Concrete Structures, pp. 385-392.

Mohamedien, M.A., and Polyzois, D. (1994). *"Effect of Protective Coatings on the Strength of the Cold-Formed Steel Sections,"* CSCE Proceedings, Annual Conference, June 1994, Winnipeg, Manitoba, pp. 187-194.

Moore, H.F., and Kommers, J.B. (1927). *"The Fatigue of Metals,"* McGraw-Hill Book Co., New York.

Nachtigal, A.J. (1974). *"Strain-Cycling Fatigue Behaviour of Ten Structural Metals Tested in Liquid Helium (4 K), in Liquid Nitrogen (78 K), and in Ambient Air (300 K),"* NASA TN D-7532, Feb. 1974.

Neuber, H. (1937). *"Theory of Notches,"* Kerbspannungslehre, Springer-Verlag Berlin, (in German); Edward, J.W., Ann Arbor, Mi., 1946.

Odaisky, D. (1994). *" Cold-Formed Steel Sections for Transmission Towers,"* M.Sc. Thesis, Department of Civil and Geological Engineering, The University of Manitoba, Winnipeg, Manitoba, Canada.

ORE Report D 86 (1971). *"Bending Tests of Structure Consisting of Two Beams Welded at Right Angles,"* Office of Research and Experiments of the International Union of Railways.

302

ORE   Report D 130 (1974 - 1979). *"Fatigue Phenomena in Welded Connections of Bridges and Cranes,"* (Reports D 130/RP 1/E through D 130/RP 10/E) Office of Research and Experiments of the International Union of Railways.

Osgood, C. (1982). *"Fatigue Design,"* Pergamon Press, Cranbury, New Jersey.

Palmgren, A. (1924). *"Die Lebensdauer von Kugellagren,"* (in German), ZDVDI, Vol. 68, No.14, 1924, p.339.

Paris, P.C. and Erdogan, F. (1963). *"A Critical Analysis of Crack Propagation Law,"* Trans. ASME Jornal of Basic Eng., Vol. 85, No. 4, p.528.

Patel, K., and Freathy, P. (1984). *"A simplified Method for Assessing Wind-Induced Fatigue Damage,"* Eng. Struct., Vol. 6, October 1984, pp. 268-273.

Peterson, R.E. (1974). *"Stress Concentration Factors,"* John Wiley and Sons, New York N.Y.

Polák, J., and Klesnil, M. (1976). *"The Dynamics of Cyclic Plastic Deformation and Fatigue Life of Low Carbon Steel at Low Temperatures,"* Mater. Sci. Eng., Vol. 26, No. 2, Dec. 1976, p.157.

Polyzois, D., Charnvarnichborikarn, P., Rizkalla, S., and Wong, C.K. (1990). *"Effect of Temperature and Galvanization on the Compression Strength of Cold-Formed Angles,"* Canadian Journal of Civil Engineering, Vol. 17, pp. 440-451.

Rankin, C.C., and Brogan, F.A. (1986). "*An Element Independent Corotational Procedure for the Treatment of Large Rotations,*" Journal of Pressure Vessel Technology, Vol. 108, pp. 165-174.

Read, N.G. (1972). "*The Effects of Low Temperature on the Fracture and Fatigue of Materials,*" M.Sc. Thesis, Mechanical Engineering Department, The University of Manitoba, Winnipeg, Manitoba.

Roy, G., Mohamedien, M.A., and Polyzois, D. (1994). "*Residual Stresses in Cold-Formed Steel Sections,*" Twelfth International Specialty Conference on Cold-Formed Steel Structures, St. Louis, Missouri, October 1994, pp. 691-703.

Schilling, C.G., Klippstein, K.H., Barsom, J.M., and Blake, G.T. (1978). "*Fatigue of Welded Steel Bridge Members Under Variable-Amplitude Loadings,*" National Cooperative Highway Research Program Report 188, Transportation Research Board, National Academy of Sciences, Washington, D.C.

Schulz, K.J. (1942). "*On the State of Stress in Perforated Strips and Plates,*" Proceedings, Netherlands Royal Academy of Science, Amesterdam, Vol. 45, p. 233, 341, 457, 524.

Serrette, R., Rizkalla, S.H., and Polyzois, D. (1987). "*Buckling Behaviour of Cold-Formed Angles,*" Report, Winnipeg, Manitoba, Department of Civil Engineering, The University of Manitoba.

Smith, I.F.C., Bremen, U., and Hirt, M.A. (1984). *"Fatigue Thresholds and Improvement of Welded Connections,"* ICOM I25, Swiss Fedral Institute, Lausanne, Switzerland.

Spretnak, J.W., Fontana, M.G., and Brooks, H.E. (1951). *"Notched and Unnotched Tensile and Fatigue Properties of Ten Alloys at $25°C$ and $-196°C$,"* Trans., ASME, Vol. 43, p. 547.

Stasuiski, M., and Endo, T. (1968). *"The Fatigue Life of Materials Subjected to Random Strains,"* Society of Mechanical Engineering, Japan.

Stephens, R.I. (Editor), (1983). *"Symposium of Fatigue at Low Temperatures,"* ASTM Committees E-9 on Fatigue and E-24 on Fracture Testing, Louisville, KY.

Swanson Analysis Systems Inc., (1992). *"Ansys User's Manual for Revision 5.0 Volumes I to IV,"* Houston, PA.

Sweeting, T.J. (1992). *"A Method for the Construction of Safe S-N curves,"* Fatigue Fract. Engng Mater. Struct., Vol. 15, No. 4, pp. 391-398.

Tavernelli, J.F. and Coffin, L.F. (1962). *"Experimental Support for Generalized Equation Predicting Low Cycle Fatigue,"* Trans. ASME, Journal of Basic Eng., Vol. 84, No. 4, December 1962, p.533.

Tebedge, N., Alpsten, G.A., and Tall, L. (1973). *"Residual Stress Measurement by the Sectioning Method,"* Exp. Mech., February 1973, pp. 88-96.

Teed, P.L. (1950). *"The Properties of Mettalic Materials at Low Temperatures,"* Chapman and Hall.

Thrasher, W.J. (1984). *"Halt Redundant Member Failure on 765-kV Towers,"* Transmission and Distribution, May 1984, pp. 66-70.

Troughton, A.J., and McStay, J. (1963). *"Theory and Practice in Fail-Safe Wing Design,"* Current Aeronautical Fatigue Problems, (ICAF - AGARD Symposium at Rome, 1963), ed. by Schijve et al., Pergamon Press, New York, N.Y., 1965.

TRRL (1979). *"Fatigue Behaviour of Intermittent Fillet Welds,"* Technical Report LF860, Transport and Road Research Laboratory.

Wilhoite, G.M. (chairman), (1988). *"Guide for Design of Steel Transmission Towers,"* ASCE Manuals and Reports on Engineering Practice No. 52, Second Edition, American Society of Civil Engineers, New York.

Wöhler, A. (1867). *"Wöhler's Experiments on the Strength of Metals,"* Engineering , August 1867, p.160.

Wyatt, T.A. (1984). *"An Assessment of the Sensitivity of Lattice Towers to Fatigue Induced by Wind Gusts,"* Eng. Struct., Vol. 6, October, 1984, pp.

262-267.

Yamada, K., and Hirt, M.A. (1982). *"Fatigue Life Estimation Using Fracture Mechanics,"* Proceedings IABSE Colloquium - Lausanne, Fatigue of Steel and Concrete Structures, pp. 361-368.

Yang, C.H., Beedle, L.S., and Johnston, B.G. (1952). *"Residual Stress and the Yield Strength of Steel Beams,"* Welding Journal, No. 31, April 1954, pp. 205-229.

Appendix A

Regression Analysis of Test Data

(Tables)

Table A.1

Regression Analysis for the Effect of Stress Range
(BA-section Connected Through One Leg at Room Temperature)

	σ_r (MPa)	N	Log σ_r (x)	Log N (y)	x^2	x y	y^2	$(x - \bar{x})^2$	$\hat{y}$	$(y - \hat{y})^2$
BA-109-1	334.8081	650000	2.524796	5.8129134	6.3745946	14.67642	33.789962	0.0580776	5.7976114	0.0002341
BA-109-6	515.0209	105960	2.7118249	5.0251419	7.353994	13.627305	25.252052	0.0029121	5.0097929	0.0002356
BA-109-7	496.7852	90200	2.6961686	4.9552065	7.2693254	13.360073	24.554072	0.004847	5.0757413	0.0145286
BA-109-5	589.2696	62700	2.770314	4.7972675	7.6746399	13.289938	23.013776	2.048E-05	4.76342	0.0011457
BA-109-3	611.3042	60000	2.7862574	4.7781513	7.7632302	13.313159	22.830729	0.000419	4.6962621	0.0067058
BA-109-4	653.2346	32000	2.8150692	4.50515	7.9246145	12.682309	20.296376	0.0024285	4.5748987	0.0048649
BA-109-2	673.5571	31000	2.8283744	4.4913617	7.9997019	12.703253	20.17233	0.0039169	4.5188533	0.0007558
BA-109-9	706.7313	30580	2.8492543	4.4854375	8.1182502	12.780152	20.119149	0.0069665	4.4309012	0.0029742
BA-109-8	812.9023	15550	2.9100384	4.1917304	8.4683232	12.198096	17.570604	0.0208079	4.1748617	0.0002846

Sum	24.892097	43.04236	68.946674	118.6307	207.59905	0.100396	43.042342	0.0317293
Mean	2.7657886	4.7824845						

b = -4.137255

a = 16.225258

t = 19.471055

S_e = 0.0673257

Table A.2

Regression Analysis for the Effect of Stress Range
(BC-section Connected Through One Leg at Room Temperature)

	σ_r (MPa)	N	Log σ_r (x)	Log N (y)	x^2	x y	y^2	$(x - \bar{x})^2$	$\hat{y}$	$(y - \hat{y})^2$
BC-81-10	290.5506	1200000	2.4632218	6.0791812	6.0674615	14.974372	36.956445	0.0355955	6.008396	0.0050105
BC-81-9	336.0537	500000	2.5264087	5.69897	6.3827408	14.397927	32.478259	0.0157455	5.7282228	0.0008557
BC-81-8	351.117	339600	2.5454519	5.5309677	6.4793252	14.078812	30.591603	0.011329	5.6437846	0.0127277
BC-81-4	433.8593	218590	2.6373489	5.3396303	6.9556093	14.082468	28.511652	0.0002114	5.2363095	0.0106752
BC-81-7	455.1293	102073	2.6581348	5.0089109	7.0656806	13.31436	25.089188	3.9E-05	5.144144	0.018288
BC-81-1	514.5573	78000	2.7114337	4.8920946	7.3518729	13.26459	23.93259	0.0035455	4.9078144	0.0002471
BC-81-5	545.5645	72000	2.7368461	4.8573325	7.4903266	13.293772	23.593679	0.0072176	4.795135	0.0038685
BC-81-6	603.3284	43760	2.7805538	4.6410773	7.7314793	12.904765	21.539599	0.0165545	4.6013335	0.0015796
BC-81-3	642.1063	31500	2.8076069	4.4983106	7.8826567	12.629488	20.234798	0.0242479	4.4813787	0.0002867

Sum			23.867007	46.546475	63.407153	122.94055	242.92781	0.1144859	46.546519	0.053539
Mean			2.6518896	5.1718306						

b = -4.328567
a = 16.650713

t = 16.746881

S_e = 0.0874553

Table A.3

Regression Analysis for the Effect of Stress Range
(BB-section Connected Through One Leg at Room Temperature)

	σ_r (MPa)	N	Log σ_r (x)	Log N (y)	x^2	x y	y^2	$(x - \bar{x})^2$	$\hat{y}$	$(y - \hat{y})^2$
BB-70-2	206.334	1050000	2.3145708	6.0211893	5.357238	13.936469	36.254721	0.0392976	6.110289	0.0079388
BB-70-1	255.8119	600150	2.4079207	5.7782598	5.7980823	13.913592	33.388286	0.0110011	5.7354363	0.0018339
BB-70-3	305.0116	270000	2.4843164	5.4313638	6.1718278	13.493226	29.499712	0.0008117	5.4286648	7.284E-06
BB-70-4	381.4753	136900	2.5814664	5.1364034	6.6639689	13.259453	26.38264	0.0047141	5.0385524	0.0095748
BB-70-5	596.7055	16000	2.77576	4.20412	7.7048438	11.669628	17.674625	0.0691444	4.2583539	0.0029413

		x	y						
Sum		12.564034	26.571336	31.695961	66.272368	143.19998	0.1249689	26.571296	0.022296
Mean		2.5128069	5.3142673						

b = -3.97114
a = 15.292974

t = 16.284066

S_e = 0.0862091

Table A.4

Regression Analysis for the Effect of Stress Range
(BA-section Connected Through Both Legs at Room Temperature)

	σ_r (MPa)	N	Log σ_r (x)	Log N (y)	x^2	x y	y^2	$(x - \bar{x})^2$	$\hat{y}$	$(y - \hat{y})^2$
BA-109-11	488.8102	355188	2.6891403	5.5504583	7.2314753	14.925961	30.807587	0.0110829	5.56412	0.0001866
BA-109-12	641.6726	75000	2.8073135	4.8750613	7.8810091	13.685825	23.766222	0.0001664	4.8440476	0.0009618
BA-109-13	770.536	22000	2.8867929	4.3424227	8.3335734	12.535675	18.856635	0.0085336	4.3597506	0.0003003

Sum	8.3832467	14.767942	23.446058	41.147461	73.430444	0.0197828	14.767918	0.0014487
Mean	2.7944156	4.9226474						

b = -6.081355
a = 21.91648

t = 22.472357

S_e = 0.0380624

Table A.5

Regression Analysis for the Effect of Stress Range
(BC-section Connected Through Both Legs at Room Temperature)

	σ_r (MPa)	N	Log σ_r (x)	Log N (y)	x^2	x y	y^2	$(x - \bar{x})^2$	$\hat{y}$	$(y - \hat{y})^2$
BC-81-12	352	624000	2.5465427	5.7951846	6.4848795	14.757685	33.584164	0.0192306	5.8020374	4.696E-05
BC-81-11	510.4	145000	2.7079107	5.161368	7.3327802	13.976523	26.63972	0.000515	5.1439082	0.0003048
BC-81-13	632.7	56600	2.8011978	4.7528164	7.8467093	13.313579	22.589264	0.0134515	4.7634425	0.0001129

Sum	8.0556512	15.709369	21.664369	42.047787	82.813148	0.0331971	15.709388	0.0004647
Mean	2.6852171	5.2364563						

b = -4.074999
a = 16.178713

t = 34.441636

S_e = 0.0215573

312

Table A.6

Regression Analysis for the Effect of Stress Range
(BB-section Connected Through Both Legs at Room Temperature)

	σ_r (MPa)	N	Log σ_r (x)	Log N (y)	x^2	x y	y^2	$(x - \bar{x})^2$	$\hat{y}$	$(y - \hat{y})^2$
BB-70-6	565.692	26500	2.75258	4.4232459	7.5766969	12.175338	19.565104	0.0147773	4.4361336	0.0001661
BB-70-7	469.6213	70000	2.6717478	4.845098	7.1382362	12.94488	23.474975	0.0016589	4.8265389	0.0003444
BB-70-8	294.257	633000	2.4687268	5.8014037	6.094612	14.322081	33.656285	0.0263385	5.807094	3.238E-05

Sum	7.8930546	15.069748	20.809545	39.442299	76.696364	0.0427747	15.069767	0.0005429
Mean	2.6310182	5.0232492						

b = -4.827186

a = 17.723663

t = 42.84716

S_e = 0.0233005

313

Table A.7

Regression Analysis for the Effect of Stress Range
(BG-section at Room Temperature)

	σ_r (MPa)	N	Log σ_r (x)	Log N (y)	x^2	x y	y^2	$(x - \bar{x})^2$	$\hat{y}$	$(y - \hat{y})^2$
BG-36-3	316.5	600000	2.5003737	5.7781513	6.2518687	14.447538	33.387032	0.0056405	5.7634875	0.000215
BG-36-1	379.8	253000	2.579555	5.4031205	6.6541038	13.937646	29.193711	1.663E-05	5.4454139	0.0017887
BG-36-2	443.1	160000	2.6465018	5.20412	7.0039715	13.772713	27.082865	0.0050445	5.1764865	0.0007636

Sum	7.7264304	16.385392	19.909944	42.157896	89.663608	0.0107016	16.385388	0.0027674
Mean	2.5754768	5.4617973						

b = -3.952659
a = 15.64178

t = 7.7728717

S_e = 0.0526058

Table A.8

Regression Analysis for the Effect of Stress Range
(BN-section at Room Temperature)

	σ_r (MPa)	N	Log σ_r (x)	Log N (y)	x^2	x y	y^2	$(x - \bar{x})^2$	$\hat{y}$	$(y - \hat{y})^2$
BN-36-4	183.702	1528000	2.2641139	6.1841234	5.1262117	14.00156	38.243382	0.0160846	6.1990597	0.0002231
BN-36-1	219.287	660000	2.3410129	5.8195439	5.4803413	13.623627	33.867092	0.0024926	5.8191708	1.392E-07
BN-36-2	257.014	336000	2.4099568	5.5263393	5.8078917	13.318239	30.540426	0.0003617	5.478581	0.0022809
BN-36-5	285.853	160100	2.4561428	5.2043913	6.0326372	12.782728	27.085689	0.0042515	5.2504176	0.0021184
BN-36-3	304.417	134352	2.4834689	5.1282441	6.1676178	12.735835	26.298888	0.0085618	5.1154237	0.0001644

		Log σ_r (x)	Log N (y)	x^2	x y	y^2	$(x - \bar{x})^2$	$\hat{y}$	$(y - \hat{y})^2$
Sum		11.954695	27.862642	28.6147	66.461989	156.03548	0.0317522	27.862653	0.0047869
Mean		2.390939	5.5725284						

b = -4.431426
a = 16.19138
t = 19.76812
S_e = 0.0399452

Table A.9

Regression Analysis for the Effect of Stress Range
(HBN-section at Room Temperature)

	σ_r (MPa)	N	Log σ_r (x)	Log N (y)	x^2	x y	y^2	$(x - \bar{x})^2$	$\hat{y}$	$(y - \hat{y})^2$
HBN-37-4	137.145	1290000	2.13718	6.1105897	4.5675383	13.05943	37.339307	0.0413674	6.138607	0.000785
HBN-37-1	181.814	450000	2.2596273	5.6532125	5.1059156	12.774153	31.958812	0.0065517	5.690589	0.001397
HBN-37-2	229.801	258000	2.3613519	5.4116197	5.5759829	12.778739	29.285628	0.0004319	5.3183927	0.0086913
HBN-37-3	271.487	120000	2.433749	5.0791812	5.9231344	12.361452	25.798082	0.0086824	5.0535016	0.0006594
HBN-37-5	324.295	52185	2.5109403	4.7175457	6.304821	11.845475	22.255237	0.0290261	4.7710696	0.0028648

Sum	11.702849	26.972149	27.477392	62.81925	146.63707	0.0860595	26.97216	0.0143975
Mean	2.3405697	5.3944298						

b = -3.613136

a = 13.851228

t = 15.300334

S_e = 0.069276

Table A.10

Regression Analysis for the Effect of Stress Range
(HBN-section at Temperature of - 50 C)

	σ_r (MPa)	N	Log σ_r (x)	Log N (y)	x^2	x y	y^2	$(x - \bar{x})^2$	$\hat{y}$	$(y - \hat{y})^2$
HBN-37-6	151.435	1306275	2.1802263	6.1160346	4.7533866	13.334339	37.405879	0.019135	6.1083763	5.865E-05
HBN-37-7	180.06	590000	2.2554172	5.770852	5.086907	13.015679	33.302733	0.0039864	5.8335845	0.0039354
HBN-37-8	208.074	452000	2.3182178	5.6551384	5.3741338	13.109843	31.980591	1.14E-07	5.6040746	0.0026075
HBN-37-9	248.504	223000	2.3953334	5.3483049	5.737622	12.810973	28.604365	0.0058949	5.3222493	0.0006789
HBN-37-10	277.704	133000	2.4435821	5.1238516	5.9710937	12.520552	26.253856	0.0156317	5.1459203	0.000487

Sum	11.592777	28.014182	26.923143	64.791387	157.54742	0.044648	28.014205	0.0077674
Mean	2.3185554	5.6028363						

b = -3.606977
a = 13.965812

t = 14.97842

S_e = 0.0508837

Table A.11

Regression Analysis for the Effect of Alternating Fatigue Load
(BA-section Connected Through One Leg at Room Temperature)

	P (kN)	N	Log P (x)	Log N (y)	x^2	x y	y^2	$(x - \bar{x})^2$	$\hat{y}$	$(y - \hat{y})^2$
BA-109-1	40	650000	1.60206	5.8129134	2.5665962	9.3126359	33.789962	0.0491622	5.7651514	0.0022812
BA-109-6	55	105960	1.7403627	5.0251419	3.0288623	8.7455696	25.252052	0.0069594	5.1522108	0.0161465
BA-109-7	60	90200	1.7781513	4.9552065	3.1618219	8.8111067	24.554072	0.0020825	4.9847365	0.000872
BA-109-5	65	62700	1.8129134	4.7972675	3.2866548	8.6970304	23.013776	0.0001182	4.8306751	0.0011161
BA-109-3	70	60000	1.845098	4.7781513	3.4043868	8.8161575	22.830729	0.0004542	4.6880365	0.0081207
BA-109-4	75	32000	1.8750613	4.50515	3.5158547	8.4474322	20.296376	0.0026292	4.5552432	0.0025093
BA-109-2	80	31000	1.90309	4.4913617	3.6217515	8.5474655	20.17233	0.0062892	4.4310233	0.0036407
BA-109-9	80	30580	1.90309	4.4854375	3.6217515	8.5361912	20.119149	0.0062892	4.4310233	0.0029609
BA-109-8	90	15550	1.9542425	4.1917304	3.8190638	8.1916577	17.570604	0.017019	4.2043216	0.0001585

Sum		16.414069	43.04236	30.026744	78.105247	207.59905	0.0910031	43.042422	0.0378059
Mean		1.8237855	4.7824845						

b = -4.338134

a = 12.69431   t = 17.807385 S_e = 0.0734905

Table A.12

Regression Analysis for the Effect of Alternating Fatigue Load
(BC-section Connected Through One Leg at Room Temperature)

	P (kN)	N	Log P (x)	Log N (y)	x^2	xy	y^2	$(x - \bar{x})^2$	$\hat{y}$	$(y - \hat{y})^2$
BC-81-10	40	1200000	1.60206	6.0791812	2.5665962	9.7392131	36.956445	0.0369745	6.0038413	0.0056761
BC-81-9	45	500000	1.6532125	5.69897	2.7331116	9.4216085	32.478259	0.0199191	5.7825091	0.0069788
BC-81-8	50	339600	1.69897	5.5309677	2.8864991	9.3969482	30.591603	0.0090969	5.5845208	0.0028679
BC-81-4	60	218590	1.7781513	5.3396303	3.1618219	9.4946703	28.511652	0.0002623	5.2419109	0.0095491
BC-81-7	65	102073	1.8129134	5.0089109	3.2866548	9.0807214	25.089188	0.0003447	5.0914985	0.0068207
BC-81-1	70	78000	1.845098	4.8920946	3.4043868	9.0263942	23.93259	0.0025756	4.9522384	0.0036173
BC-81-5	75	72000	1.8750613	4.8573325	3.5158547	9.107796	23.593679	0.0065147	4.8225904	0.001207
BC-81-6	85	43760	1.9294189	4.6410773	3.7226574	8.9545824	21.539599	0.0182443	4.5873898	0.0028823
BC-81-3	90	31500	1.9542425	4.4983106	3.8190638	8.7907897	20.234798	0.0255664	4.4799805	0.000336

Sum	16.149128	46.546475	29.096646	83.012724	242.92781	0.1194985	46.54648	0.0399353
Mean	1.7943475	5.1718306						

b = -4.249671

a = 12.797218

t = 19.44945

S_e = 0.0755317

Table A.13

Regression Analysis for the Effect of Alternating Fatigue Load
(BB-section Connected Through One Leg at Room Temperature)

	P (kN)	N	Log P (x)	Log N (y)	x^2	x y	y^2	$(x - \bar{x})^2$	$\hat{y}$	$(y - \hat{y})^2$
BB-70-2	50	1050000	1.69897	6.0211893	2.8864991	10.22982	36.254721	0.0366878	6.1021592	0.0065561
BB-70-1	60	600150	1.7781513	5.7782598	3.1618219	10.27462	33.388286	0.0126246	5.7764485	3.281E-06
BB-70-3	75	270000	1.8750613	5.4313638	3.5158547	10.18414	29.499712	0.0002387	5.3778108	0.0028679
BB-70-4	90	136900	1.9542425	5.1364034	3.8190638	10.037778	26.38264	0.0040618	5.0521002	0.007107
BB-70-5	140	16000	2.146128	4.20412	4.6058655	9.0225798	17.674625	0.0653403	4.2627823	0.0034413

Sum	9.4525531	26.571336	17.989105	49.748937	143.19998	0.1189531	26.571301	0.0199756
Mean	1.8905106	5.3142673						

b = -4.072661

a = 13.013677

t = 17.213791

S_e = 0.0815999

Table A.14

Regression Analysis for the Effect of Alternating Fatigue Load
(BA-section Connected Through Both Legs at Room Temperature)

	P (kN)	N	Log P (x)	Log N (y)	x^2	$x\,y$	y^2	$(x - \bar{x})^2$	$\hat{y}$	$(y - \hat{y})^2$
BA-109-11	66.5	355188	1.8228216	5.5504583	3.3226788	10.117496	30.807587	0.0136105	5.5653059	0.0002205
BA-109-12	90	75000	1.9542425	4.8750613	3.8190638	9.527052	23.766222	0.0002178	4.8413437	0.0011369
BA-109-13	110	22000	2.0413927	4.3424227	4.1672841	8.8645899	18.856635	0.0103851	4.3612568	0.0003547

Sum	5.8184568	14.767942	11.309027	28.509137	73.430444	0.0242133	14.767906	0.0017121
Mean	1.9394856	4.9226474						

b = -5.495911
a = 15.581888   t = 20.668472 S_e = 0.0413769

Table A.15

Regression Analysis for the Effect of Alternating Fatigue Load
(BC-section Connected Through Both Legs at Room Temperature)

	P (kN)	N	Log P (x)	Log N (y)	x^2	x y	y^2	$(x - \bar{x})^2$	$\hat{y}$	$(y - \hat{y})^2$
BC-81-12	50	624000	1.69897	5.7951846	2.8864991	9.8458448	33.584164	0.0192877	5.8016285	4.152E-05
BC-81-11	72.5	145000	1.860338	5.161368	3.4608575	9.6018891	26.63972	0.0005057	5.1449483	0.0002696
BC-81-13	90	56600	1.9542425	4.7528164	3.8190638	9.2881559	22.589264	0.0135472	4.7628079	9.983E-05

Sum	5.5135505	15.709369	10.16642	28.73589	82.813148	0.0333406	15.709385	0.000411		
Mean	1.8378502	5.2364563								

b = -4.066421
a = 12.709928

t = 36.626779

S_e = 0.0202722

Table A.16

Regression Analysis for the Effect of Alternating Fatigue Load
(BB-section Connected Through Both Legs at Room Temperature)

	P (kN)	N	Log P (x)	Log N (y)	x^2	xy	y^2	$(x - \bar{x})^2$	$\hat{y}$	$(y - \hat{y})^2$
BB-70-6	144	26500	2.1583625	4.4232459	4.6585286	9.546968	19.565104	0.0145993	4.4392784	0.000257
BB-70-7	120	70000	2.0791812	4.845098	4.3229947	10.073837	23.474975	0.0017344	4.8219592	0.0005354
BB-70-8	75	633000	1.8750613	5.8014037	3.5158547	10.877987	33.656285	0.0263977	5.8084655	4.987E-05

Sum	6.112605	15.069748	12.497378	30.498792	76.696364	0.0427314	15.069703	0.0008423
Mean	2.037535	5.0232492						

b = -4.828905
a = 14.862312

t = 34.394147

S_e = 0.0290227

Table A.17

Regression Analysis for the Effect of Alternating Fatigue Load
(BG-section at Room Temperature)

	P (kN)	N	Log P (x)	Log N (y)	x^2	xy	y^2	$(x-\bar{x})^2$	$\hat{y}$	$(y-\hat{y})^2$
BG-36-3	150	600000	2.1760913	5.7781513	4.7353732	12.573784	33.387032	0.0056405	5.7634875	0.000215
BG-36-1	180	253000	2.2552725	5.4031205	5.0862541	12.185509	29.193711	1.663E-05	5.4454139	0.0017887
BG-36-2	210	160000	2.3222193	5.20412	5.3927025	12.085108	27.082865	0.0050445	5.1764865	0.0007636

Sum		6.7535831	16.385392	15.21433	36.844401	89.663608	0.0107016	16.385388	0.0027674
Mean		2.2511944	5.4617973						

b = -3.952659
a = 14.360001

t = 7.7728717

S_e = 0.0526058

Table A.18

Regression Analysis for the Effect of Alternating Fatigue Load
(BN-section at Room Temperature)

	P (kN)	N	Log P (x)	Log N (y)	x^2	$x\,y$	y^2	$(x - \bar{x})^2$	$\hat{y}$	$(y - \hat{y})^2$
BN-36-4	225	1528000	2.3521825	6.1841234	5.5327626	14.546187	38.243382	0.0170363	6.2126949	0.0008163
BN-36-1	270	660000	2.4313638	5.8195439	5.9115298	14.149428	33.867092	0.002636	5.8243497	2.31E-05
BN-36-2	325	336000	2.5118834	5.5263393	6.309558	13.88152	30.540426	0.0008513	5.4294406	0.0093893
BN-36-5	350	160100	2.544068	5.2043913	6.4722822	13.240326	27.085689	0.0037653	5.2715906	0.0045157
BN-36-3	375	134352	2.5740313	5.1282441	6.625637	13.200261	26.298888	0.0083403	5.1246357	1.302E-05

Sum			12.413529	27.862642	30.85177	69.017721	156.03548	0.0326293	27.862711	0.0147575
Mean			2.4827058	5.5725284						

$b = -4.812282$

$a = 17.520009$

$t = 12.393926$

$S_e = 0.0701368$

Table A.19

Regression Analysis for the Effect of Alternating Fatigue Load
(HBN-section at Room Temperature)

	P (kN)	N	Log P (x)	Log N (y)	x^2	x y	y^2	$(x - \bar{x})^2$	$\hat{y}$	$(y - \hat{y})^2$
HBN-37-4	150	1290000	2.1760913	6.1105897	4.7353732	13.297201	37.339307	0.0412735	6.1452718	0.0012028
HBN-37-1	200	450000	2.30103	5.6532125	5.294739	13.008212	31.958812	0.0061184	5.6835156	0.0009183
HBN-37-2	250	258000	2.39794	5.4116197	5.7501163	12.976739	29.285628	0.0003493	5.3253498	0.0074425
HBN-37-3	300	120000	2.4771213	5.0791812	6.1361297	12.581748	25.798082	0.0095788	5.032707	0.0021599
HBN-37-5	350	52185	2.544068	4.7175457	6.4722822	12.001757	22.255237	0.027165	4.785281	0.0045881

Sum	11.896251	26.972149	28.38864	63.865657	146.63707	0.0844849	26.972125	0.0163116
Mean	2.3792501	5.3944298						

b = -3.643624

a = 14.063523

t = 14.362703

S_e = 0.0737373

Table A.20

Regression Analysis for the Effect of Alternating Fatigue Load
(HBN-section at Temperature of - 50 C)

	P (kN)	N	Log P (x)	Log N (y)	x^2	xy	y^2	$(x - \bar{x})^2$	$\hat{y}$	$(y - \hat{y})^2$
HBN-37-6	170	1306275	2.2304489	6.1160346	4.9749024	13.641503	37.405879	0.018979	6.1067063	8.702E-05
HBN-37-7	200	590000	2.30103	5.770852	5.294739	13.278904	33.302733	0.0045136	5.848561	0.0060387
HBN-37-8	235	452000	2.3710679	5.6551384	5.6219628	13.408717	31.980591	8.149E-06	5.5924023	0.0039358
HBN-37-9	280	223000	2.447158	5.3483049	5.9885824	13.088147	28.604365	0.0062323	5.3141078	0.0011694
HBN-37-10	310	133000	2.4913617	5.1238516	6.2068831	12.765368	26.253856	0.0151655	5.152436	0.0008171

		Log P (x)	Log N (y)	x^2	xy	y^2	$(x - \bar{x})^2$	$\hat{y}$	$(y - \hat{y})^2$
Sum		11.841067	28.014182	28.08707	66.182638	157.54742	0.0448986	28.014213	0.012048
Mean		2.3682133	5.6028363						

b = -3.584059
a = 14.090652

t = 11.98379

S_e = 0.063372

Appendix B

Regression Analysis of Test Data

(S-N and Load-N Plots)
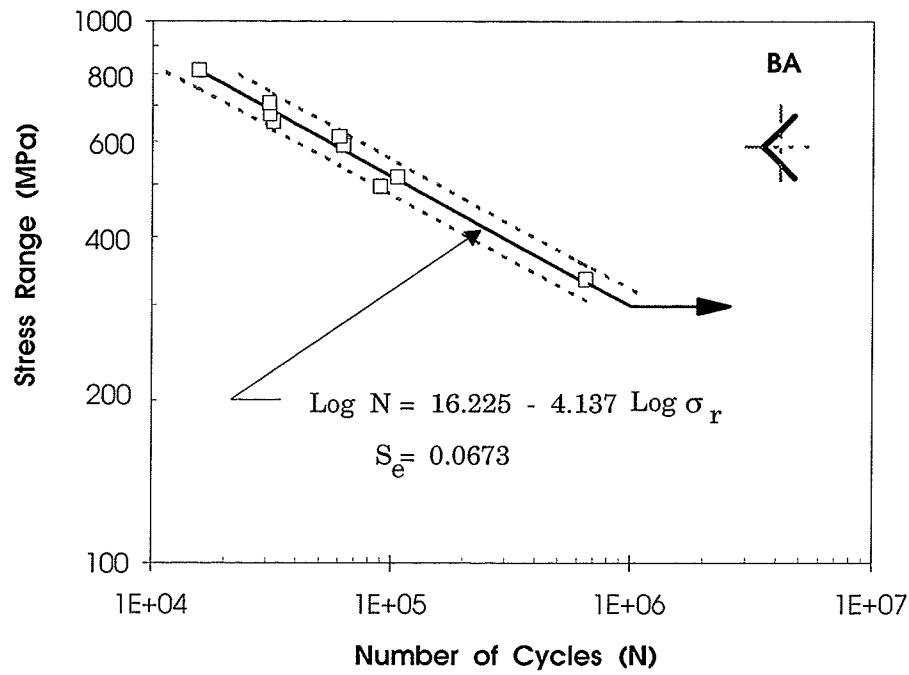
Figure B. 1: S-N Plot for $90°$-angle section Connected Through One Leg. ASTM A715 Grade 60 Steel (Temperature = 25 C)
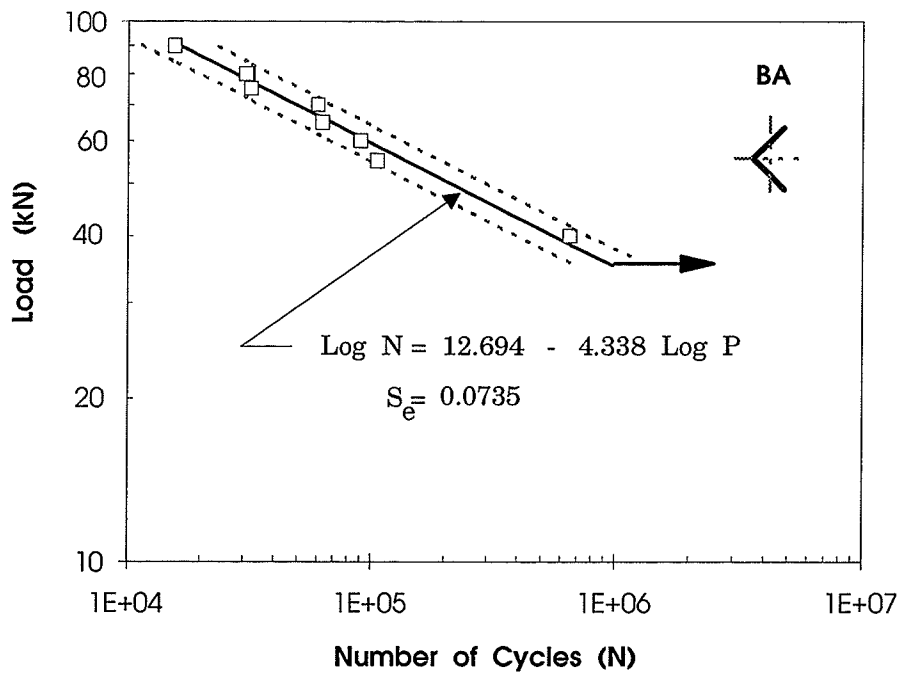
Figure B. 2: Load-N Plot for $90°$-angle section Connected Through One Leg. ASTM A715 Grade 60 Steel (Temperature = 25 C)
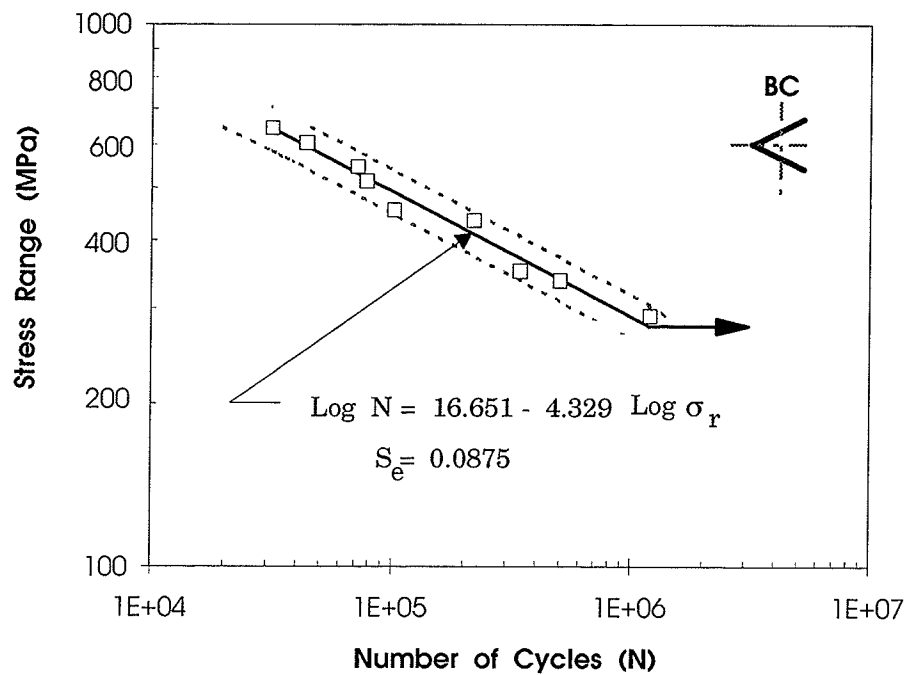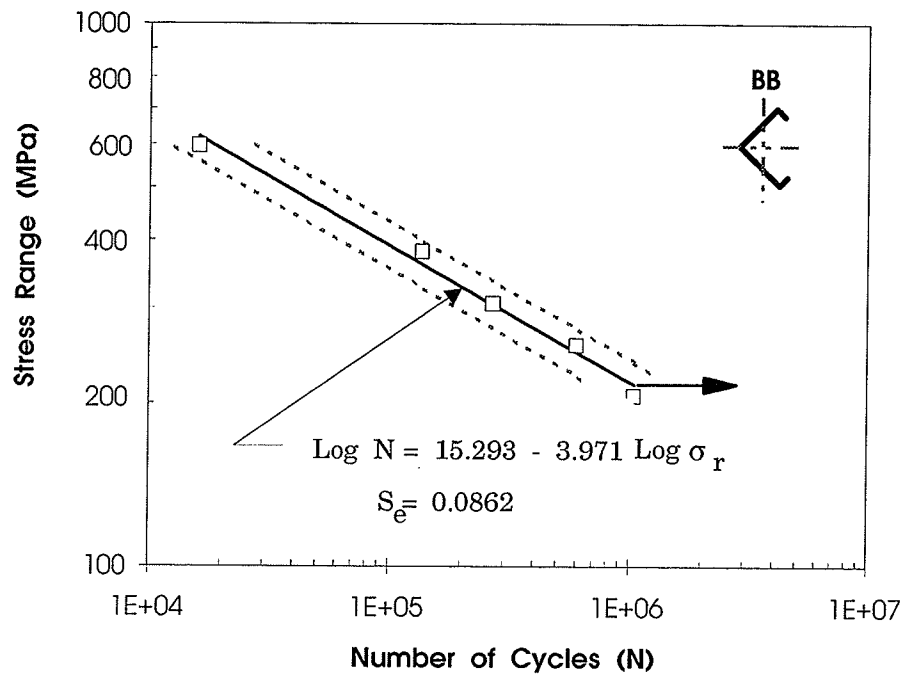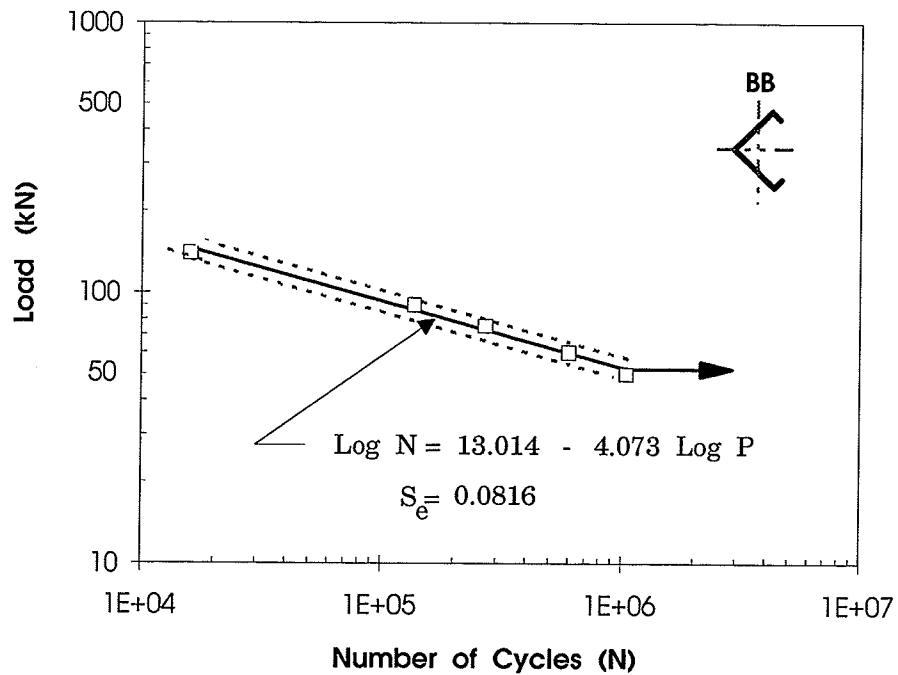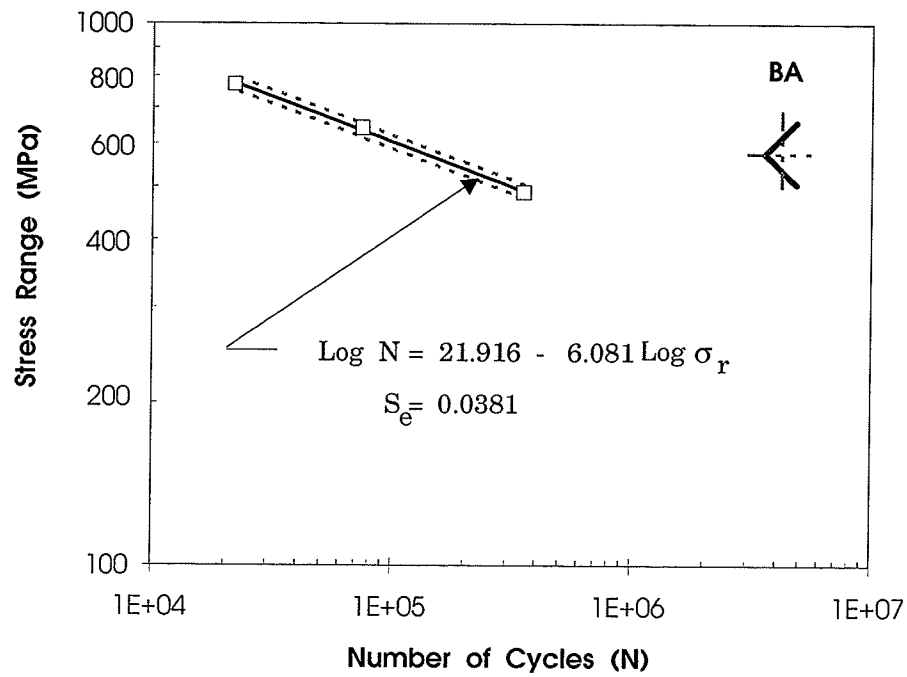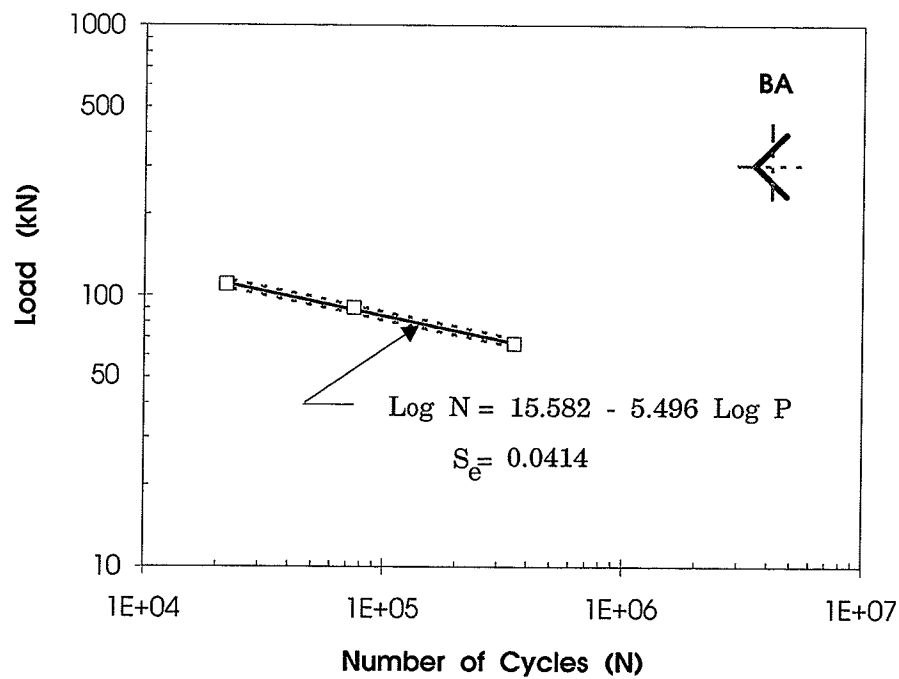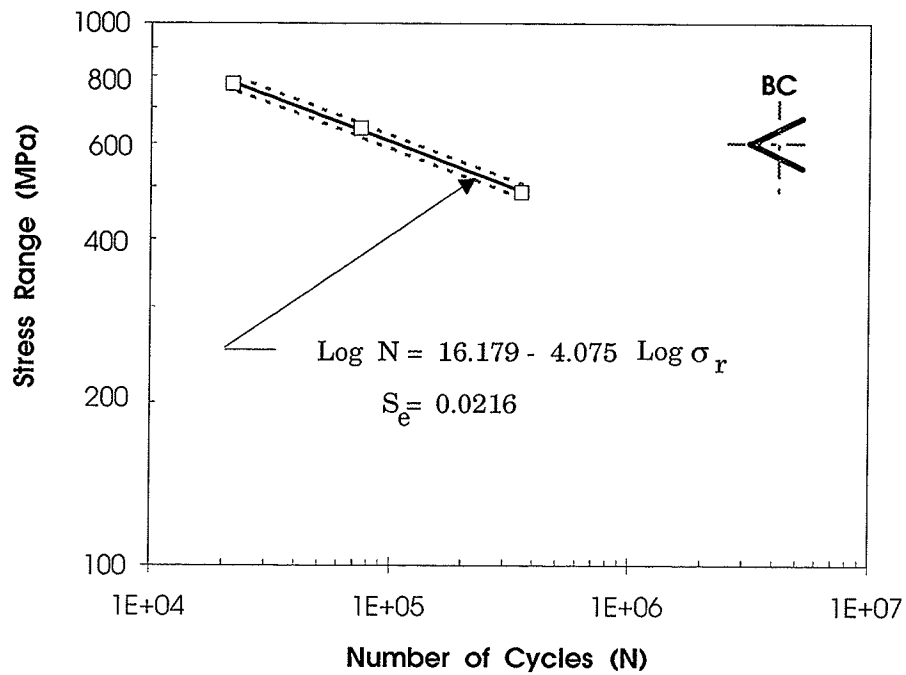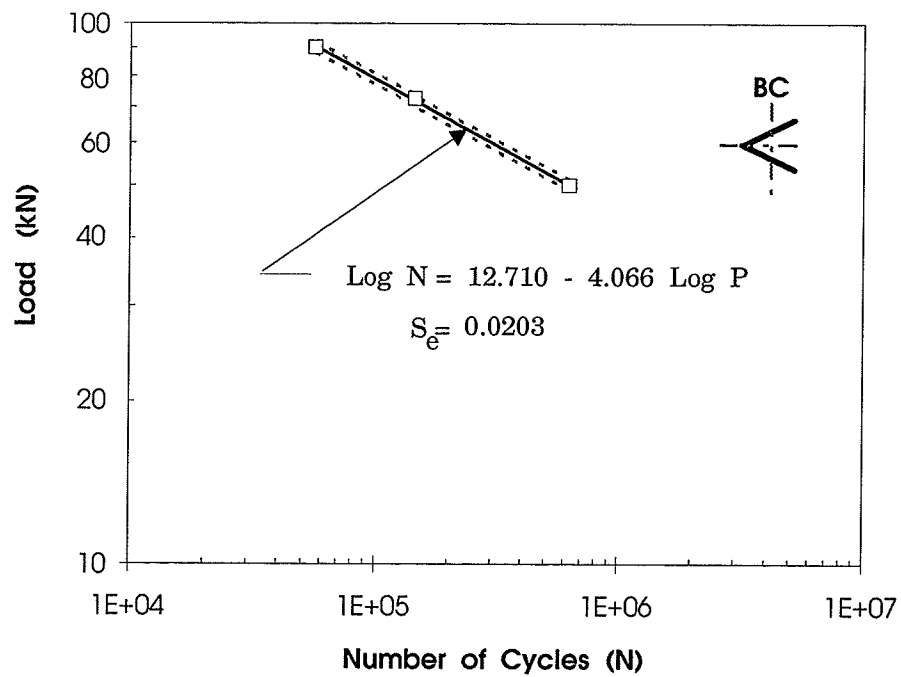
Figure B. 3: S-N Plot for 60°-angle section Connected Through One Leg. ASTM A715 Grade 60 Steel (Temperature = 25 C)

The equation shown in the figure:
$$\text{Log } N = 16.651 - 4.329 \text{ Log } \sigma_r$$
$$S_e = 0.0875$$
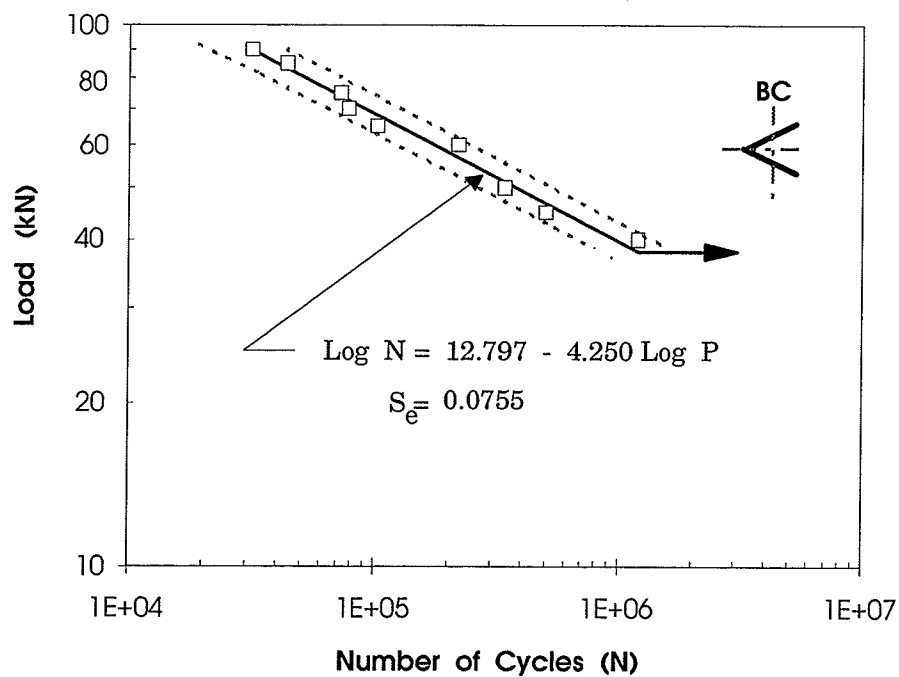
Figure B. 4: Load-N Plot for 60°-angle section Connected Through One Leg. ASTM A715 Grade 60 Steel (Temperature = 25 C)

The equation shown in the figure:
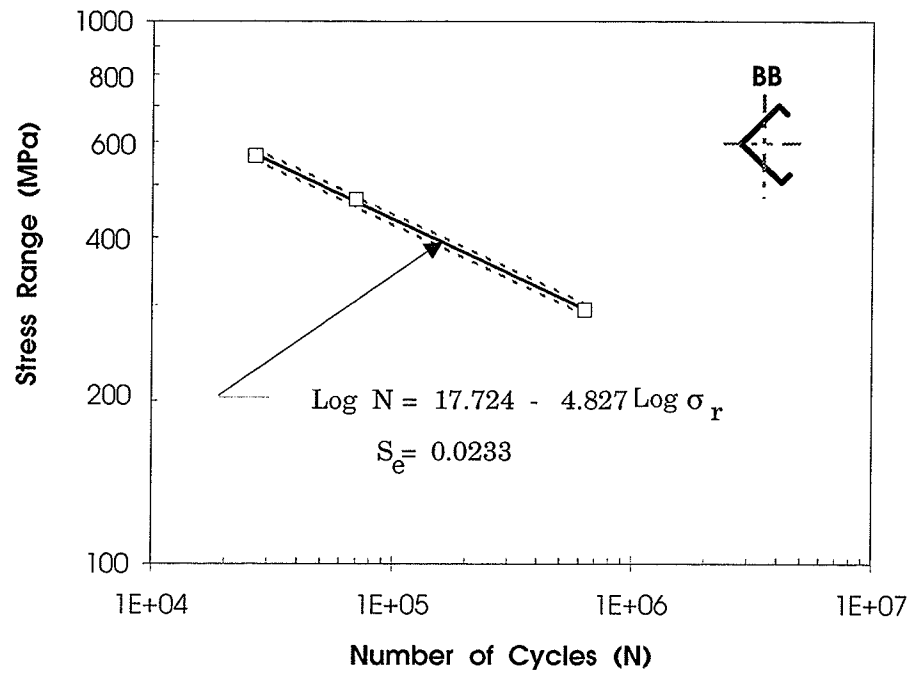$$\text{Log } N = 12.797 - 4.250 \text{ Log } P$$
$$S_e = 0.0755$$

329

Figure B. 5: S-N Plot for Lipped-angle section Connected Through One Leg. ASTM A715 Grade 60 Steel (Temperature = 25 C)
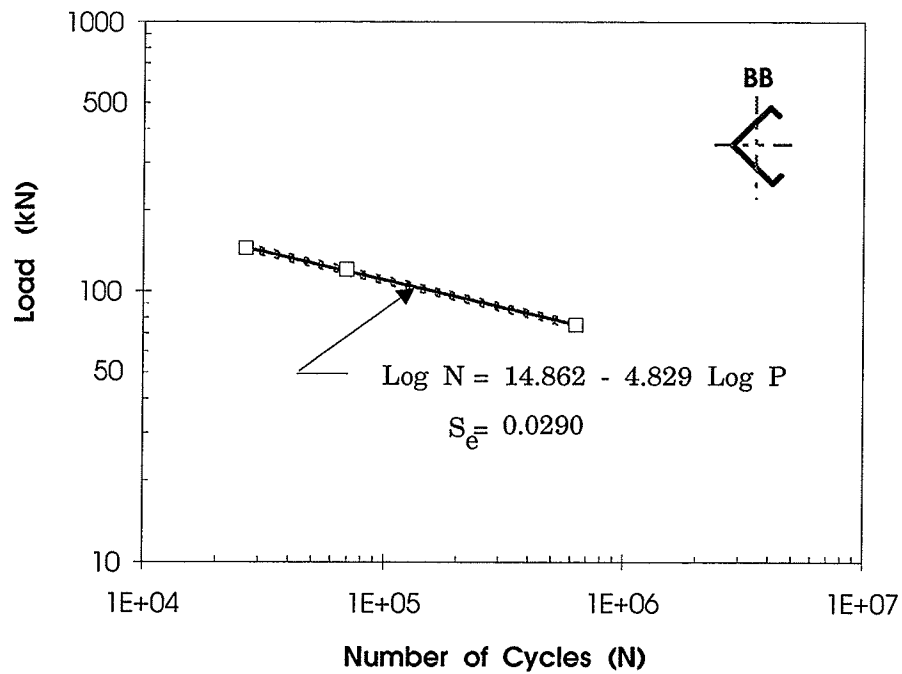

Figure B. 6: Load-N Plot for Lipped-angle section Connected Through One Leg. ASTM A715 Grade 60 Steel (Temperature = 25 C)

330

Figure B. 7: S-N Plot for $90°$-angle section Connected Through Both Legs
ASTM A715 Grade 60 Steel (Temperature = 25 C)

Figure B. 8: Load-N Plot for $90°$-angle section Connected Through Both Legs.
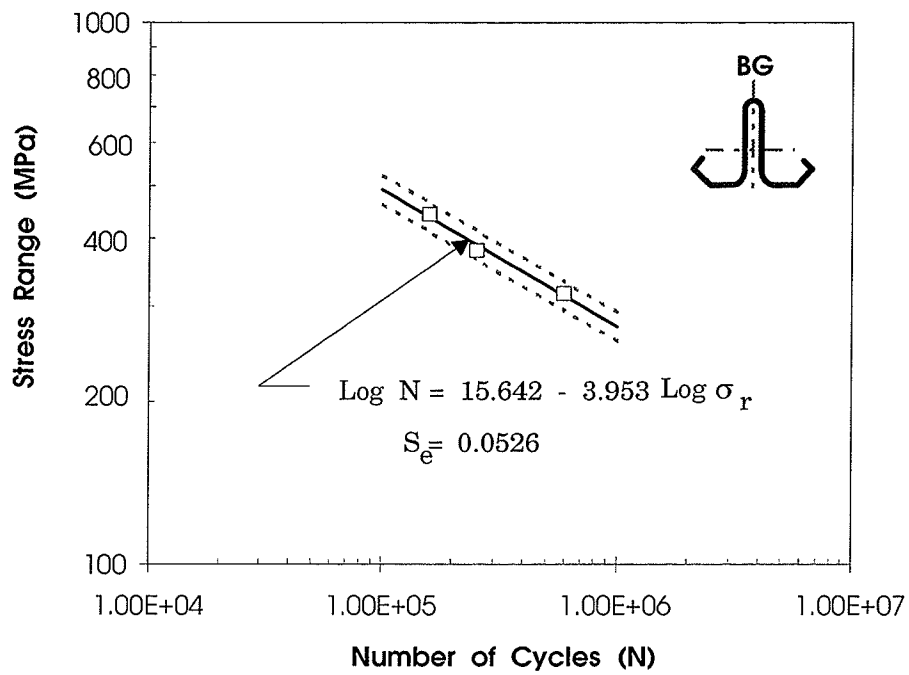ASTM A715 Grade 60 Steel (Temperature = 25 C)

Figure B. 9: S-N Plot for 60°-angle section Connected Through Both Legs
ASTM A715 Grade 60 Steel (Temperature = 25 C)

$$\text{Log } N = 16.179 - 4.075 \text{ Log } \sigma_r$$
$$S_e = 0.0216$$

Figure B.10: Load-N Plot for 60°-angle section Connected Through Both Legs.
ASTM A715 Grade 60 Steel (Temperature = 25 C)

$$\text{Log } N = 12.710 - 4.066 \text{ Log } P$$
$$S_e = 0.0203$$

Figure B.11: S-N Plot for Lipped-angle section Connected Through Both Legs
ASTM A715 Grade 60 Steel (Temperature = 25 C)

The equation shown in the plot:

$$\text{Log } N = 17.724 - 4.827 \text{ Log } \sigma_r$$
$$S_e = 0.0233$$

Figure B.12: Load-N Plot for Lipped-angle section Connected Through Both Legs.
ASTM A715 Grade 60 Steel (Temperature = 25 C)

The equation shown in the plot:

$$\text{Log } N = 14.862 - 4.829 \text{ Log } P$$
$$S_e = 0.0290$$

Figure B. 13: S-N Plot for T-shaped section (Temperature = 25 C). ASTM A715 Grade 60 Steel
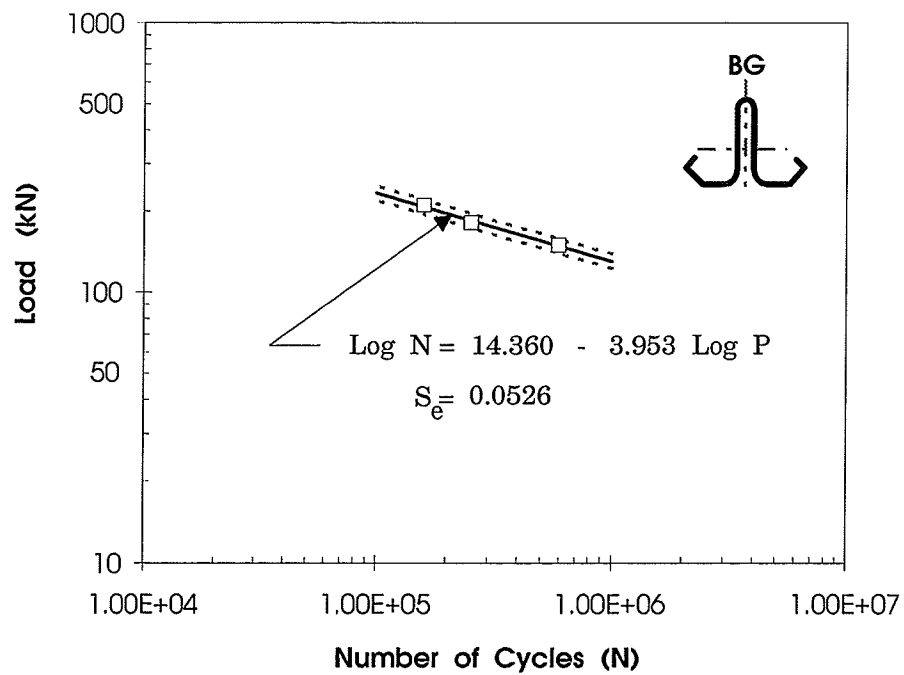
Figure B. 14: Load-N Plot for T-shaped section (Temperature = 25 C). ASTM A715 Grade 60 Steel
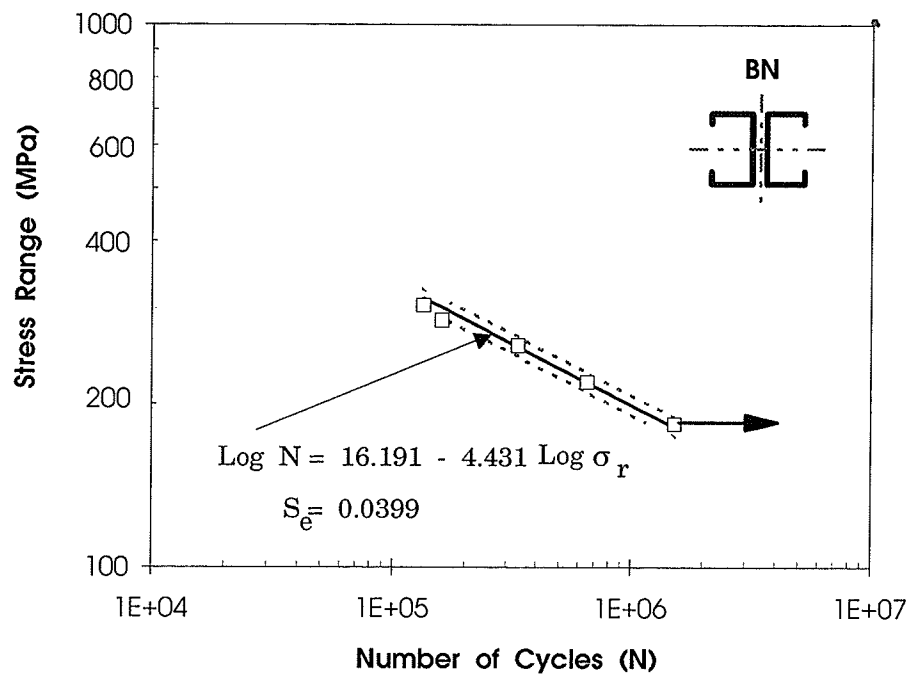
Figure B. 15: S-N Plot for Back-to-Back Channel section.
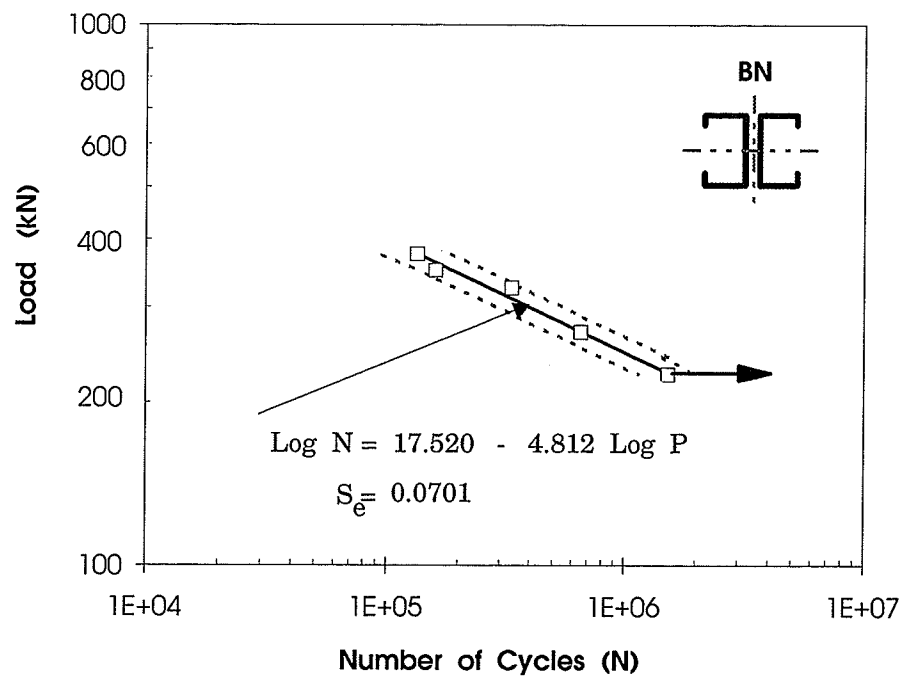ASTM A715 Grade 60 Steel. (Temperature = 25 C)

Figure B. 16: Load-N Plot for Back-to-Back Channel section.
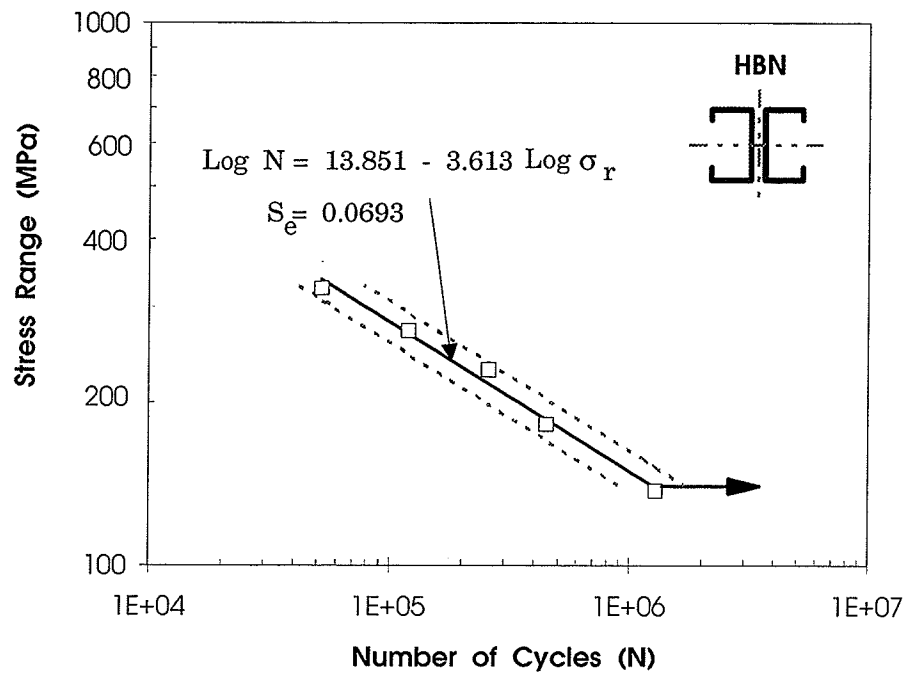ASTM A715 Grade 60 Steel. (Temperature = 25 C)

Figure B. 17: S-N Plot for Back-to-Back Channel section.
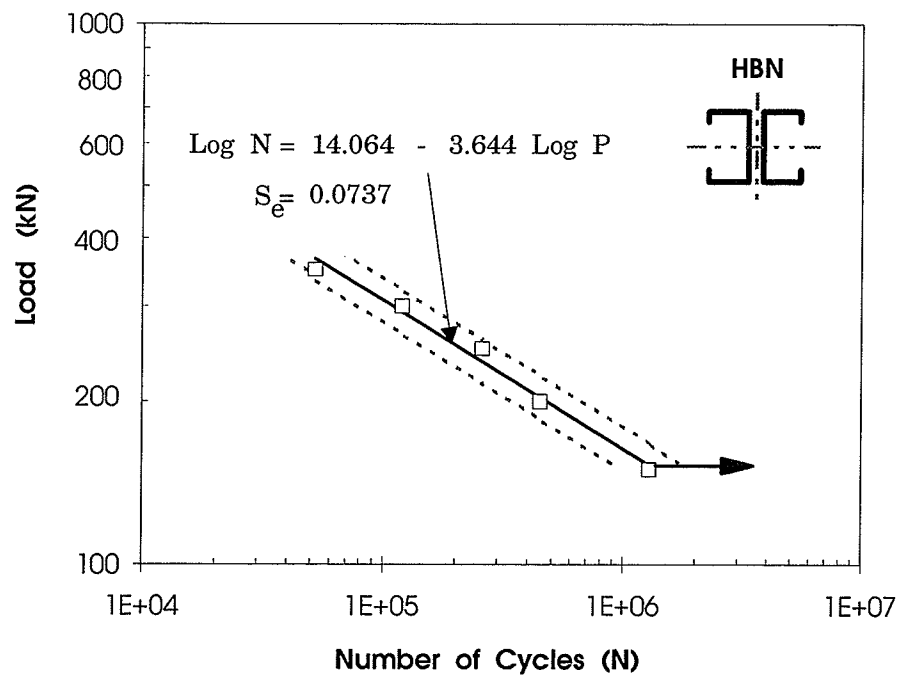CAN/CSA G40.21-M 300W Steel. (Temperature = 25 C)

Figure B. 18: Load-N Plot for Back-to-Back Channel section.
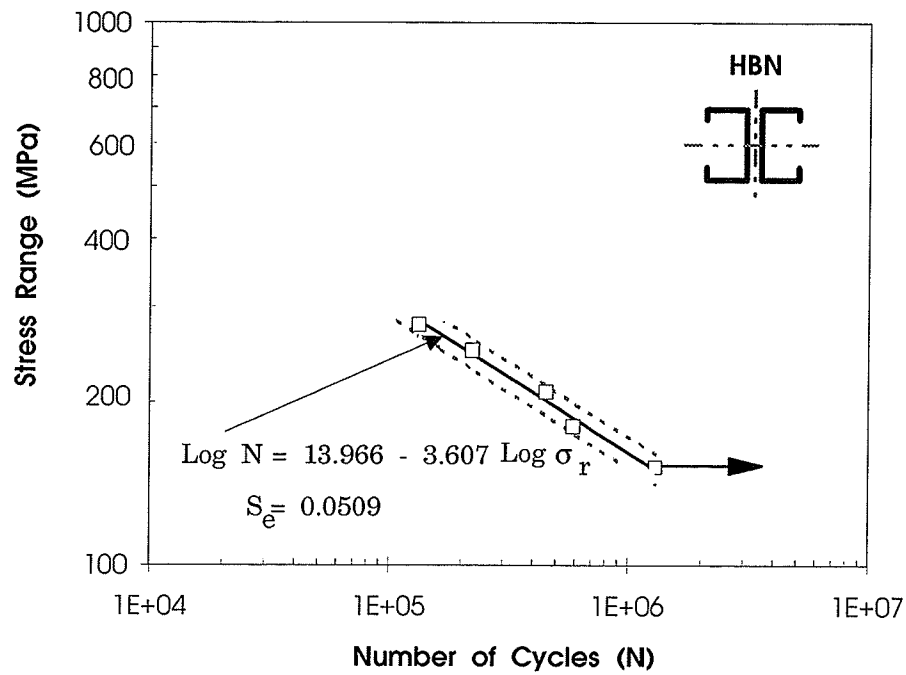CAN/CSA G40.21-M 300W Steel. (Temperature = 25 C)

336

Figure B. 19: S-N Plot for Back-to-Back Channel section.
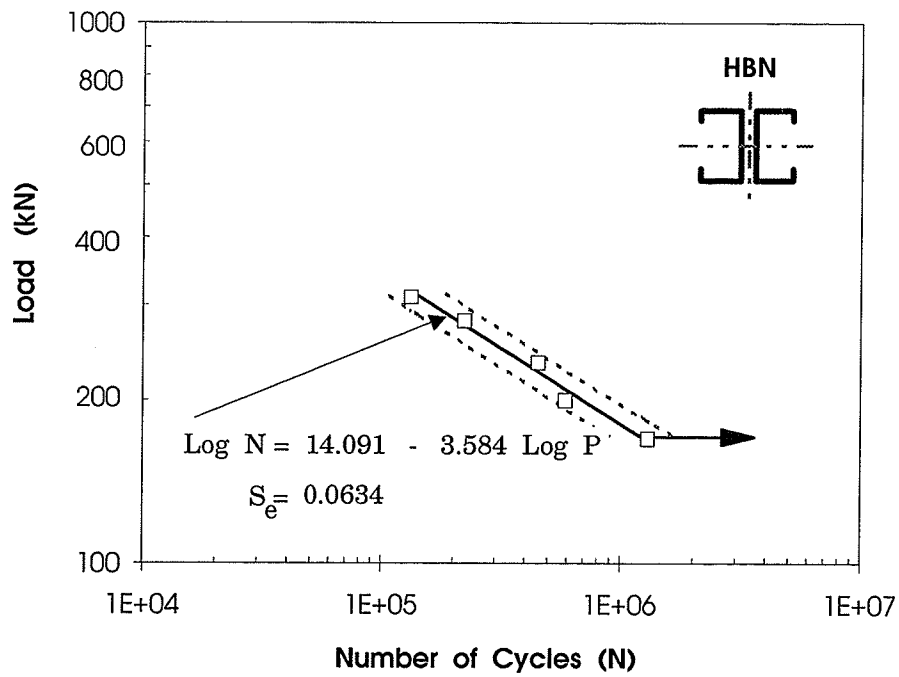CAN/CSA G40.21-M 300W Steel. (Temperature = - 50 C)

Figure B. 20: Load-N Plot for Back-to-Back Channel section.
CAN/CSA G40.21-M 300W Steel. (Temperature = - 50 C)